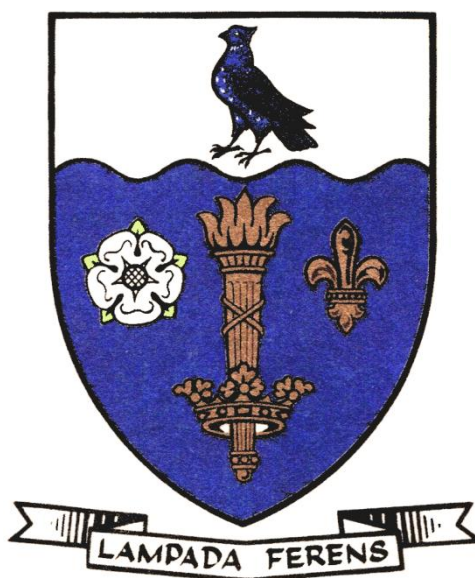


THE UNIVERSITY OF HULL



‘UNDERSTANDING AND OPTIMISATION OF
NON-CONVENTIONAL EMULSIONS’

being a Thesis submitted for the Degree of

Doctor of Philosophy
at the University of Hull

by

Michael Andrew Thompson, B.Sc.

August, 2012

ACKNOWLEDGEMENTS

I have had the most memorable and enjoyable times in Hull which has come with help from a lot of people, without whom the experience would not have been half as much rewarding. Therefore, I take great enjoyment in having the chance to show my appreciation to all those who have helped.

I would like to give genuine thanks to both my supervisors, Profs. B.P. Binks and P.D.I. Fletcher. Whom, I will always be grateful, not only for the opportunity to work with them in the Surfactant and Colloid Group, but for their guidance, patience and excellent supervision.

Thanks also go to GlaxoSmithKline at Barnard Castle, especially Dr. R.P. Elliott and Mr. A.D. Mounter for encouragement and support both financially and academically.

I have had the privilege to work with two undergraduate groups who I must thank for working with great enthusiasm towards some of the results presented in this thesis. Many technical staff also deserve thanks for their assistance throughout my three years. I owe a very big thanks to all members of the Surfactant and Colloid Group, both staff and students, past and present. There is always someone within the group who is willing and would be patient, friendly and give knowledgeable support. Sincere thanks go to; Josef Borovička, Shwan Hamad, Ben Holt, Andrew Johnson, Adam Law, Rob Machen, Baghali Mathapa, Karl Reed, Anaïs Rocher, Marius Rutkevičius, Ibrahim Salama, Emma Hope, Mark Ward and many more I've missed. Special thanks go to all fellow members of the C107 club; it is truly a great lab to work in and an experience that I will miss for a very long time.

Finally, but most importantly, I would like to thank my family and friends for being supportive throughout this section of my life. I will never forget the support. Particular thanks go to my parents and grandparents for instilling in me the attitude to do what I love. Included in this is my fiancée Lauren, who has now put up with me for 6 years, without her this would have been a lot harder – thank you.

For those whose names I have not mentioned here, I offer my apologies, but know those who have made this experience unique will never be forgotten.

For my family and friends with special thanks to my beautiful fiancée Lauren, without whom none of this would have been possible.

'There are in fact two things, science and opinion; the former begets knowledge, the latter ignorance.'

Hippocrates, Law (460 BC - 377 BC)

'The scientist is not a person who gives the right answers; he's one who asks the right questions.'

Claude Lévi-Strauss, *Le Cru et le cuit* (1964)

PUBLICATIONS AND PRESENTATIONS

The work from this thesis has been presented by the author at the following events:

1. Poster: ‘Emulsion phase inversion with glycols’, 24th Conference of European Colloid and Interface Society, 5 – 10th September 2010, Prague, Czech Republic.
2. Talk: ‘Effect of added glycols on the emulsion properties of oil, water and surfactant mixtures’, University of Hull Research Colloquia, 11th July 2011, Hull, UK.
3. Talk: ‘Understanding and Optimisation of Non-conventional Emulsions’, GlaxoSmithKline Learning Forum, 18th July 2011, Barnard Castle, UK.

The work from this thesis has contributed to the following publications:

1. B.P. Binks, P.D.I. Fletcher, M.A. Thompson and R.P. Elliott, ‘Effect of added diols (glycols) on the emulsion properties of oil, water and surfactant mixtures’, *Colloids and Surfaces A*, **360**, 67 – 73 (2011).
2. B.P. Binks, P.D.I. Fletcher, M.A. Thompson and R.P. Elliott, ‘Influence of propylene glycol on aqueous silica dispersions and particle-stabilised emulsions’, awaiting submission after patent application.

ABSTRACT

This thesis is concerned with understanding the effect of diols on emulsion properties and to use knowledge gained to optimise emulsions containing them. The project was sponsored by GlaxoSmithKline, a world leading pharmaceutical company, whose interest is in using the knowledge to help in research and development of new products and optimising existing products during manufacture. For this reason pharmaceutical ingredients were used throughout unless additional knowledge could be gained from using non-pharmaceutical ingredients. Systems studied included emulsions with water, diols and paraffin liquid stabilised by surfactants and particles using various techniques from microscopy, conductivity, surface tension, rheology, light scattering, stability analysis, differential scanning calorimetry and nuclear magnetic resonance.

The thesis will examine three aspects of emulsion non-conventionality; addition of diol to both surfactant and particle-stabilised emulsions and the effect of crystallisation in diol containing emulsions stabilised solely by surfactant. Surfactant and particle-stabilised systems will be discussed in terms of phase inversion where it will be shown that inversion of emulsions can be controlled by addition of diol within both systems. For phase inversion in water, diol, paraffin liquid and non-ionic surfactant systems it will be argued that the phase inversion witnessed is due to the change in preferred surfactant monolayer curvature. This will be shown by examining the structurally and isomeric nature of the diols as well as their surface activity. Also considered and compared will be the well established experimental facts that occur in related systems at phase inversion including initial droplet diameter, emulsion stability, temperature variation and surfactant structure change. Results will show that for all traits examined at phase inversion diol addition follows all well known facts regarding a change of preferred surfactant monolayer curvature from negative to positive values.

Emulsions stabilised by particles will be shown to phase invert from w/o to o/w emulsions with the addition of diol and changing particle hydrophobicity at fixed hydrophobicity and fixed diol content respectively. This will be contributed to the surface energies of each system and therefore a decrease in contact angle θ with increasing diol addition and changing hydrophobicity. Included will be a comparison between calculated and measured phase inversion of a number of diol containing series which shows good correlation. Systematic studies will also include the effect of this

phase inversion on droplet diameter, stability and emulsion type. These will be explained in terms of existing theory regarding particle stabilised emulsions. Diol effect on the *in situ* contact angle will also be shown in water/diol–air mixtures. Investigations will include the immersion times of fumed silica powders of varying wettability in water-propane-1,2-diol mixtures and from theory the contact angles of particles at the air-polar phase interface will be determined. The materials formed upon aerating these samples will also be described in terms of the wettability of the particles *in situ*. Again the result will indicate that diol increase the inherent hydrophilicity of the system and therefore change the materials formed upon aeration.

The final chapter of the thesis will discuss the effects of crystallisation in emulsions containing diol stabilised solely by surfactant. Crystallisation with surfactant stabilised systems will be discussed in terms of changing temperature and varying droplet diameter of emulsions. It will be shown that droplet diameter has an effect on the crystallisation of dispersed oil droplets and linked to stability. Systemic investigations using differential scanning calorimetry, rheology and nuclear magnetic resonance will show the crystallisation effect of a model system and attempts to link such findings to stability and the crystallisation mechanism. Microscopy of an additional model system containing high amounts of diol will show the ability of such systems to produce ‘dumbbell’ droplets when the systems temperature is decreased. Additional discussion on the formation of dumbbells and the effect on stability in diol containing emulsions will also be considered.

CONTENTS

Chapter 1. Introduction	12
1.1 Industrial relevance of current research	12
1.2 Colloid dispersions	12
1.3 Surfactants	13
1.3.1 Types of surfactant	13
1.4 Micelle formation in aqueous surfactant solutions	14
1.5 Micelle formation in oil/surfactant solutions	16
1.6 Microemulsions (water/oil/surfactant systems)	17
1.7 Phase inversion	20
1.7.1 Phase inversion temperature (PIT)	20
1.7.2 Effect of surfactant type and structure on phase inversion	21
1.7.3 Effect of oil type on phase inversion	22
1.7.4 Effect of electrolyte concentration on phase inversion	23
1.8 Phase inversion method	23
1.9 Relationship between micro and macroemulsions	26
1.10 Macroemulsions	27
1.10.1 Stability	28
1.10.1.1 DLVO theory	29
1.10.1.1.1 Attractive forces (van der Waals)	29
1.10.1.1.2 Repulsion forces (electrical double layer)	30
1.10.1.1.3 Total interaction energy	31
1.10.1.2 Creaming	33
1.10.1.3 Flocculation	33
1.10.1.4 Coalescence	34
1.10.1.5 Ostwald ripening	34
1.10.1.6 Instability mechanisms	35
1.10.1.6.1 Oriented wedge theory	35
1.11 Particle-stabilised emulsions	37
1.12 Non-aqueous polar phase emulsions	41
1.13 Presentation of thesis	42
1.14 References	43
Chapter 2. Experimental	46

2.1	<i>Materials</i> -----	46
2.1.1	Water-----	46
2.1.2	Oils and non-aqueous solvent-----	46
2.1.3	Surfactants-----	47
2.1.4	Silica particles-----	48
2.1.5	Glassware-----	50
2.2	<i>Methods</i> -----	50
2.2.1	Solubility and phase diagram determination-----	50
2.2.2	Emulsion preparation-----	51
2.2.2.1	<i>Surfactant-stabilised</i> -----	51
2.2.2.2	<i>Particle-stabilised</i> -----	52
2.2.3	Emulsion characterisation-----	52
2.2.3.1	<i>Drop test</i> -----	52
2.2.3.2	<i>Conductivity</i> -----	52
2.2.3.3	<i>Initial droplet size</i> -----	52
2.2.3.3.1	Light scattering-----	53
2.2.3.3.2	Microscopy-----	54
2.2.3.3.3	Freeze fracture cryo-scanning electron microscopy of emulsions---	54
2.2.4	Emulsion stability-----	55
2.2.5	Tension measurements-----	56
2.2.6	Mixtures of air, silica particles and aqueous propane-1,2-diol-----	59
2.2.7	Rheology-----	59
2.2.8	Differential scanning calorimetry-----	61
2.2.9	Nuclear magnetic resonance-----	62
2.3	<i>References</i> -----	64
	Chapter 3. Effect of adding diol into surfactant stabilised emulsions-----	65
3.1	<i>Introduction</i> -----	65
3.2	<i>Diol partitioning and solubilities</i> -----	69
3.3	<i>Effect of diol addition on emulsion type and phase inversion</i> -----	71
3.3.1	Effect of surfactant structure and emulsion preparation temperature-----	81
3.4	<i>Effect of diol addition on emulsion drop size</i> -----	86
3.5	<i>Effect of diol addition on emulsion stability</i> -----	91
3.6	<i>Conclusions</i> -----	97
3.7	<i>References</i> -----	98

Chapter 4. Effect of diol addition on particle dispersions and particle-stabilised emulsions	100
4.1 Introduction	100
4.2 Effect of diol on water-propane-1,2-diol-silica-air systems	101
4.2.1 Effect of aeration	107
4.3 Emulsions formed in water-propane-1,2-diol-silica-paraffin liquid systems	112
4.3.1 Experimental findings	112
4.3.1.1 Increasing particle hydrophobicity (fixed aqueous phase ratio)	112
4.3.1.1.1 Addition of propane-1,2-diol to the aqueous phase	117
4.3.1.2 Increasing propane-1,2-diol in the emulsion (fixed particle hydrophobicity)	121
4.3.1.3 Summary of quaternary silica-water-paraffin liquid-propane-1,2-diol systems	126
4.3.2 Theoretical approach of determining phase inversion by contact angle of fumed silica at the water/propane-1,2-diol-paraffin liquid interface	128
4.4 Conclusions	133
4.5 References	133
Chapter 5. Effect of crystallisation in diol containing emulsions	135
5.1 Introduction	135
5.1.1 Aims	140
5.2 Effect of homogeniser conditions on droplet diameter of model system	140
5.2.1 Universal graph of droplet diameter vs. shear rate	140
5.2.2 Droplet diameter versus shear rate ⁻¹	144
5.2.3 Varying homogenisation time and volume	146
5.3 Stability with varying droplet diameter	148
5.4 Crystallisation with varying droplet diameter	152
5.4.1 Differential scanning calorimetry	153
5.4.2 Rheology	156
5.4.2.1 Shear rate	156
5.4.2.2 Pre-shear and temperature cycle	158
5.4.2.2.1 Thermal cycling (small droplets)	158
5.4.2.2.2 Thermal cycling (large droplets)	161
5.4.2.2.3 Pre-shear time	164
5.4.2.3 Cooling rates	164

5.4.2.4	<i>Comparison between large and small droplet diameters</i>	166
5.4.3	Nuclear magnetic resonance	168
5.5	<i>Possible mechanism of instability in diol containing emulsions – dumbbell droplets</i>	175
5.6	<i>Conclusions</i>	181
5.7	<i>References</i>	182
	Summary and conclusions	184
	Future work	187

CHAPTER 1. INTRODUCTION

1.1 Industrial relevance of current research

The research project is solely funded by GlaxoSmithKline (GSK) in Barnard Castle, UK. GSK is one of the world's leading research based pharmaceutical companies, as well as the fourth largest in terms of revenue. GSK has therapeutic areas including respiratory, gastro-intestinal/metabolic, central nervous system, vaccines and anti-infectives. In addition the company has a consumer healthcare section which produces some of the world leading nutritional drinks and counter medicines. They also formulate and manufacture a wide range of pharmaceutical creams for consumer and therapeutic uses, such as cold sores and skin diseases. The area of creams and ointments within GSK is growing with the acquisition of a leading dermatological pharmaceutical company Stiefel in July 2009.

GSK's interest in the Ph.D. presented here is to acquire an understanding of the characteristics of emulsions which are classed as "non-conventional". The two aspects of non-conventionality of interest are emulsions containing high amounts of diol (glycols) used for various therapeutic and aesthetic reasons (higher pharmaceutical active solubility and better skin feel), and the process of crystallisation in such emulsions and its links to stability. To-date, very little is known about the characteristic effects both types of "non-conventionality" have on emulsions, and therefore the aim of this thesis is to investigate such effects and potentially use them for industrial gains, such as lower production costs and higher stability. The knowledge from the results presented in this thesis will then be used to develop existing and future products within the creams and ointments section of the company. To maintain the academic-industrial collaboration, surfactants, oils and diols commonly used in the pharmaceutical industry are utilised in the following investigations.

1.2 Colloid dispersions

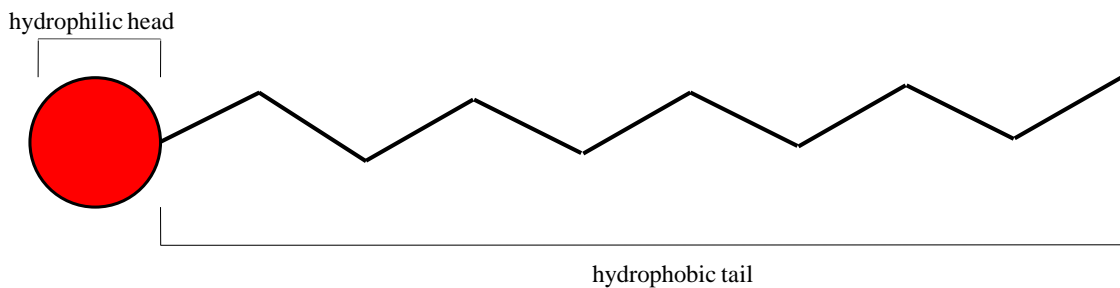
A colloidal dispersion is a heterogeneous system in which particles of solid, liquid or gaseous droplets, with dimensions of 10 μm or less, are dispersed in either solid, liquid and gas.[1] These dispersions are seen in a wide variety of systems including consumer products (paints, inks and pharmaceuticals) and food products (milk, butter and ice cream). The colloidal dispersion used and characterised throughout this project is

mainly liquid-in-liquid or in some cases semi-solid-in-liquid which are termed emulsions. Emulsions are generally stabilised by either surfactant or particles. The surfactant or particle stabilisers adsorb at the liquid-liquid interface, acting as a protective layer between dispersed phase droplets to prevent coalescence. For this reason the background behind these concepts is discussed in this chapter.

1.3 Surfactants

A surface-active agent or surfactant is a molecule that contains a hydrophilic head (water liking) and a hydrophobic tail (water hating); the structure is known as amphiphilic, Figure 1.1, with a typical length of 1.5 nm.

Figure 1.1. Schematic representation of the structure of a surfactant showing the hydrophobic tail group and hydrophilic head group.



The amphiphilic nature of surfactants leads to two useful properties;

- The ability for monomers to adsorb at an interface.
- The ability to form aggregates known as micelles above a critical concentration.

1.3.1 Types of surfactant

The hydrophobic (tail) group of the surfactant is generally a long alkyl chain which can be branched or straight chained (chain lengths normally vary between 8 and 20 carbon atoms (C₈-C₂₀)). Surfactants can also have varying numbers of head groups, of which there are four main types. It is from these head groups that surfactant molecules are classified (in all examples R represents an alkyl tail group):

1. Anionic – the surfactant head group has a negative charge, for example sodium lauryl sulphate $R(SO_4^- Na^+)$.
2. Cationic – the head group of the surfactant has a positive charge, for example a quaternary ammonium chloride $(RN(CH_3)_3^+ Cl^-)$.

3. Non-ionic – the surfactant head group has no charge, for example monoglyceride of long chain fatty acid ($\text{RCOOCH}_2\text{CHOHC}_2\text{OH}$).
4. Zwitterionic – positive and negative charges are on the head group, for example long chain amino acids ($\text{R}^+\text{NH}_2\text{CH}_2\text{COO}^-$).

1.4 Micelle formation in aqueous surfactant solutions

When a surfactant is added to a system containing pure water there is a negative entropy change generated by putting a hydrophobic group into water. Therefore, the hydrophobic tail wants to be removed from water and does so by adsorbing at the water-air interface. At low concentrations (below the critical micelle concentration, $< \text{cmc}$) a surfactant dissolved in water will be present as monomers, as shown in Figure 1.2(a).[2] However, as the temperature is increased the solubility of the surfactant increases dramatically at a point known as the Krafft point.[2] The concentration at which increased solubility occurs is known as the critical micelle concentration (cmc), where the surfactant molecules spontaneously aggregate to form micelles, Figure 1.2(b) and Figure 1.3. Micelles maybe spherical aggregates made of a hydrophobic core of disordered tail groups and an outer hydrophilic part containing the head groups, the structure of which facilitates an increase in solubility.

Figure 1.2. Schematic representation of aqueous surfactant solution (a) below and (b) above the cmc.

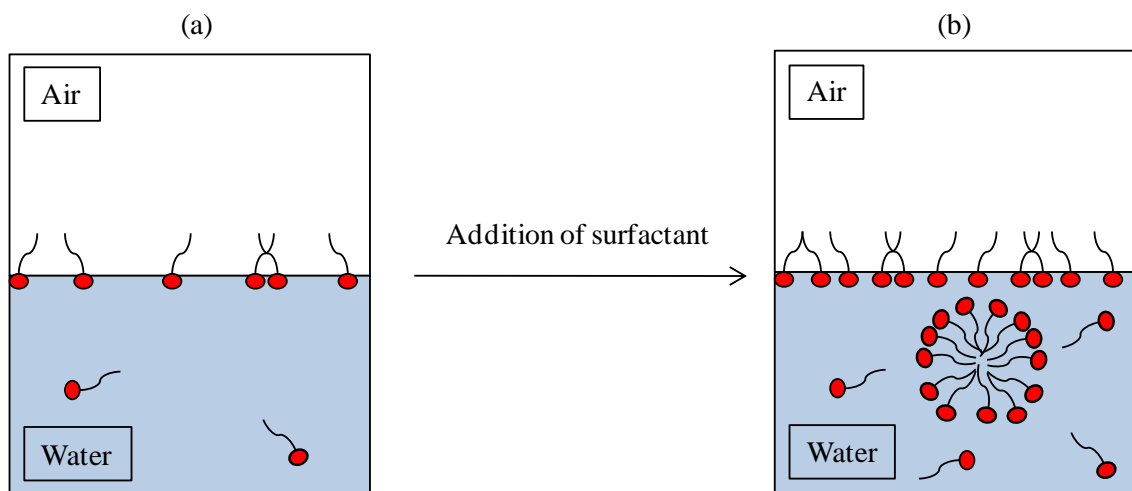
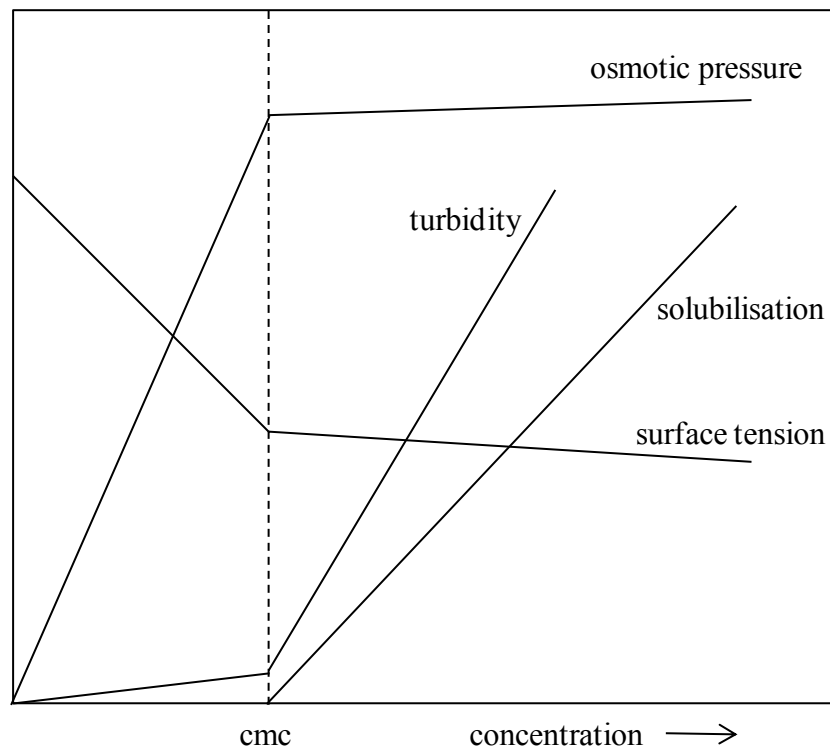


Figure 1.3. Cross-sectional view of a micelle with the hydrophilic head groups on the outside and the “liquid like” hydrophobic core made up of the tail groups.[3]



Micelles with low aggregation numbers are generally spherical, and as the aggregation numbers increase from increasing the surfactant concentration or by adding salt, the micelle will adapt to a rod or disc shape.[4] The point at which micelles form can be measured using various techniques which detect a change in bulk properties of the system which results from the formation of the micelle aggregates. The cross sectional structural appearance of a micelle formed in water, “normal micelle”, is shown in Figure 1.3. Due to the small size of the micelle, a few nm (normally twice the size of the tail group), micelle solutions appear transparent as micelles scatter light very weakly. Examples of micelle formation detection techniques include surface tension (the amount of energy require to form unit area of interface), where the surface tension remains relatively constant when the cmc is reached, and light scattering, where the formation of micelles above the cmc will cause an increase in turbidity, other examples of techniques used to detect a surfactants cmc are shown in Figure 1.4.[2]

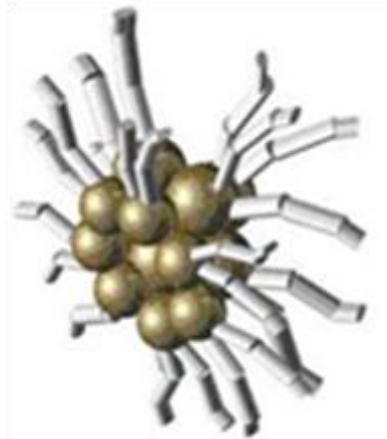
Figure 1.4. Physical properties of a surfactant aqueous solution with increasing surfactant concentration and the response to micelle formation (>cmc). Re-drawn from [5].



1.5 *Micelle formation in oil/surfactant solutions*

Due to their amphiphilic structure, some surfactants are not just soluble in aqueous systems but also in oils. Much like in aqueous-surfactant solutions, a critical concentration is also reached within an oil-surfactant system. However, in the oil-surfactant system, reverse micelles are formed, where the hydrophilic head groups form the inner part of the micelle and the hydrophobic tail groups form the outer part, as shown in Figure 1.5. However, unlike the cmc value which can be defined precisely for surfactant/water systems, the concentration of surfactant required to form reversed micelles is much broader or very low due to the low aggregation number.[2]

Figure 1.5. Schematic representation of a reverse micelle showing the core of head groups and the exterior tail groups.[3]

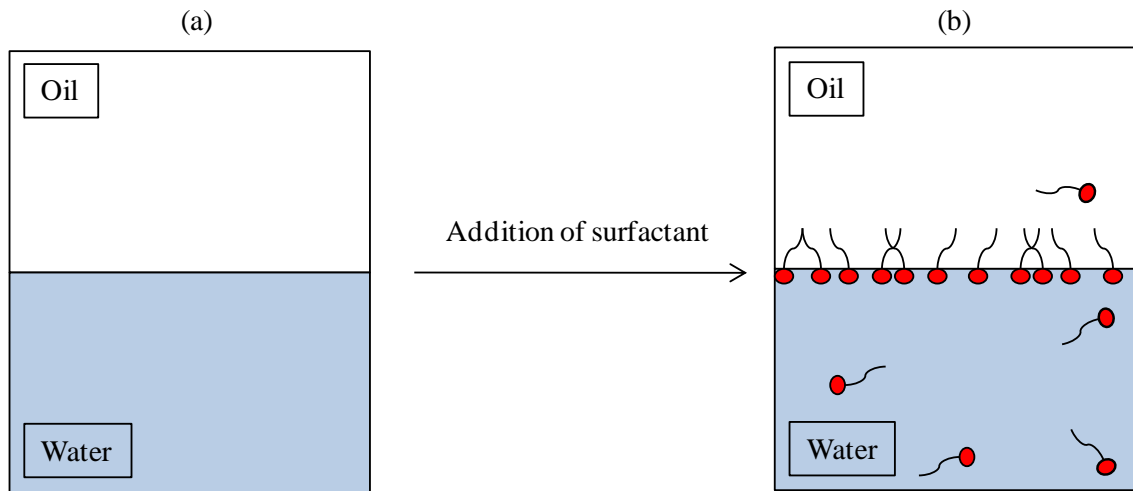


1.6 Microemulsions (water/oil/surfactant systems)

Due to the immiscibility of most oils with water, if the two are mixed via shaking or mechanical methods they will quickly separate into the original oil and water phases. An absorbing surfactant or particle at the oil-water interface is required to create stabilisation of an emulsion. However, if certain surfactants are added to a mixture of separated water and oil, systems known as microemulsions are spontaneously formed. Microemulsions are thermodynamically stable mixtures of oil, water and surfactant.[1, 2, 6, 7] The amphiphilic nature of a surfactant again allows for adsorption at the water-oil interface, much like in the water/air systems discussed earlier.

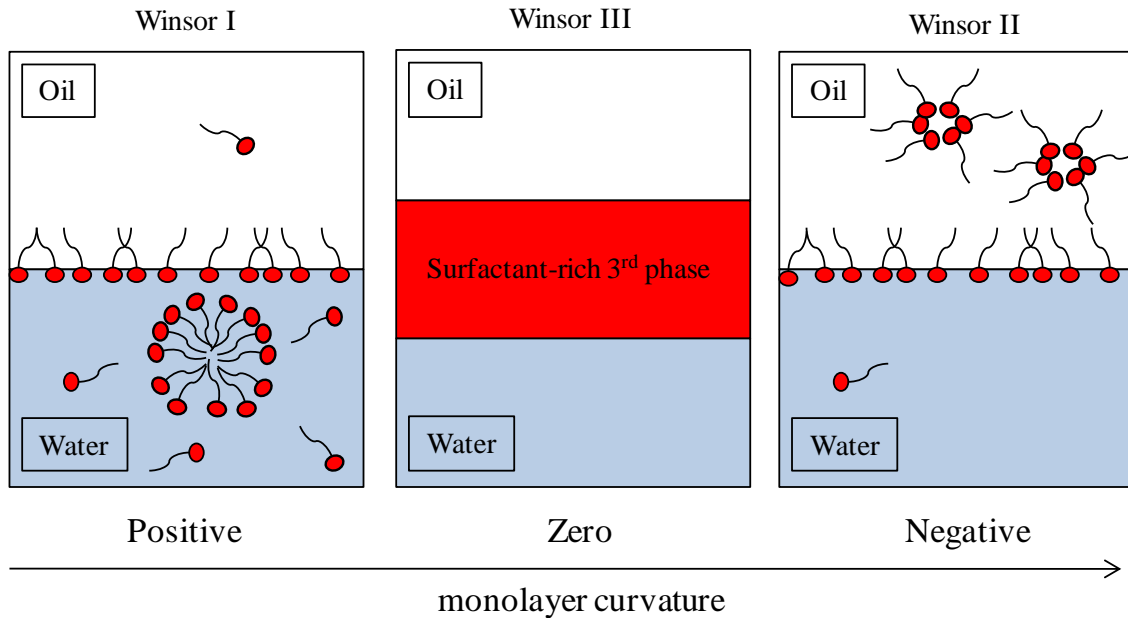
Figure 1.6 shows a 50/50 mixture of oil and water with the concentration of surfactant below a critical aggregation concentration (cac), where surfactant monomers are present in water and oil but at a concentration too low to form microemulsions.

Figure 1.6. Illustration of the addition of surfactant at concentration lower than the cac to a two phase system containing 50/50 water and oil, (a) no surfactant and (b) surfactant concentration < cac.



Above the cac the surfactant begins to aggregate and form microemulsion aggregates in either water, oil or a third phase. One of three microemulsion systems known as Winsor systems (Winsor I, II and III) can form.[2] The structure of each system is shown schematically in Figure 1.7. In the case of a Winsor I system, oil-in-water (o/w) microemulsion aggregates (swollen micelles) consist of spherical droplets of oil coated by a monolayer of surfactant in water with excess oil. Winsor II systems are the opposite, swollen reverse micelles, with water droplets surrounded by surfactant in oil and excess water. Winsor III systems contain both an excess water and oil phase with an additional third phase which is described as a bicontinuous phase or a lamellar liquid crystal that is surfactant-rich.[8-11]

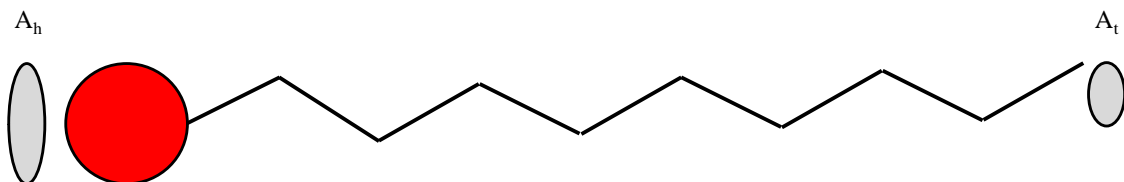
Figure 1.7. Illustration of Winsor systems: Winsor I containing excess oil with o/w microemulsion, Winsor II containing excess water with water-in-oil (w/o) microemulsion, and Winsor III containing a bicontinuous or lamellar liquid crystal phase and excess oil and water.



The microemulsion formed depends on the preferred monolayer curvature of the oil-water interface. The preferred curvature is determined *inter alia* from the packing parameter of the surfactant. The packing parameter P is defined as the ratio of the area of the tail group A_t to that of the head group A_h , where both the head and tail group areas are effective cross-sectional areas *in situ*. [12, 13]

$$P = \frac{A_t}{A_h} \quad (1.1)$$

Figure 1.8. Schematic representation of surfactant molecule showing the cross sectional areas A_h and A_t .



At a fixed packing parameter above the cac , the surfactant molecules will aggregate to form micelles corresponding to the preferred curvature. Values of P , >1 , promote w/o microemulsions (Winsor II) formation and values, <1 , promote o/w microemulsions (Winsor I). Values of P at approximately zero preferred curvature result in the

surfactant-rich Winsor III system, as shown in Figure 1.7. P values are also determined by prevailing conditions such as oil type, temperature and salt concentration as well as the inherent structure of the surfactant. The way in which these conditions effect P will be discussed in detail later.

1.7 Phase inversion

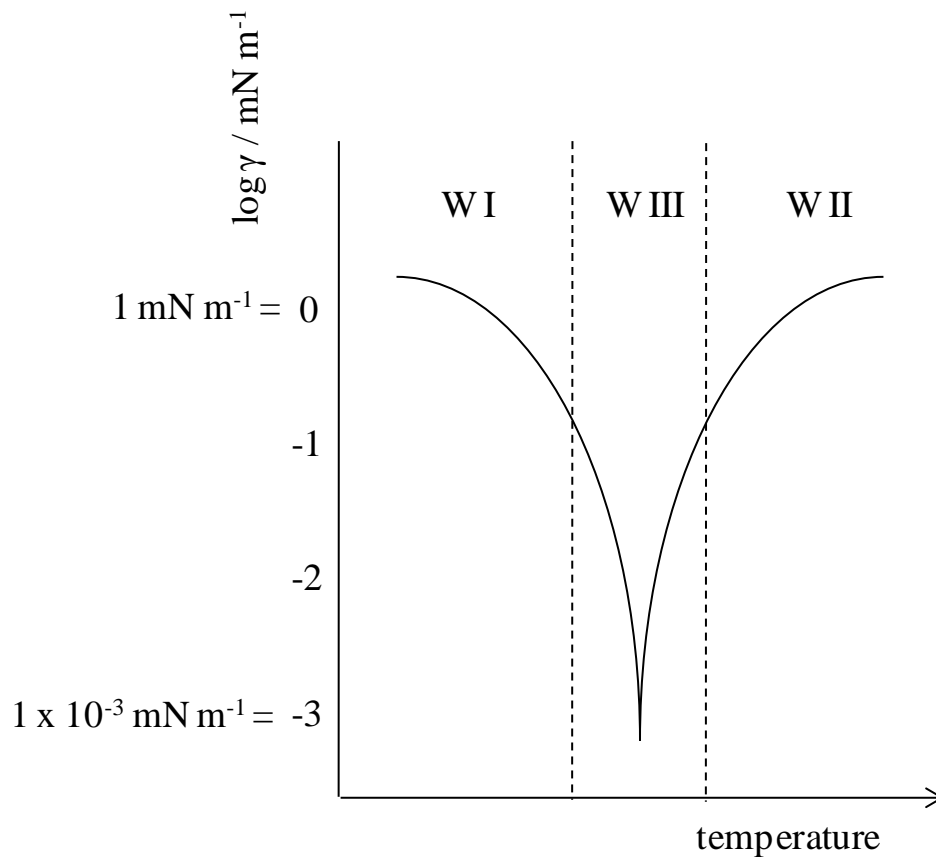
Manipulation of the preferred surfactant monolayer curvature of a system can be achieved by changing the ratio of the head and tail areas, therefore causing the corresponding emulsion phase inversion. Phase inversion in emulsions is divided into two scenarios; transitional and catastrophic. Catastrophic phase inversion is induced through changing the oil:water ratio before emulsification, alternatively transitional phase inversion is induced by changing the preferred monolayer curvature of the surfactant with equal volumes of oil and water.[1] Effects which are known to be able to change the preferred monolayer curvature are temperature, surfactant type, surfactant structure, co-surfactant addition, oil type and salt concentration.

1.7.1 Phase inversion temperature (PIT)

The effect of temperature on the inversion of Winsor systems, and therefore the corresponding emulsions was first investigated by Shinoda *et al.* between 1964 and 1969, demonstrating the ability to progress through Winsor systems by changing non-ionic surfactant affinity by varying temperature.[14, 15] They discovered that by increasing the temperature resulted in an increase in the affinity of the non-ionic surfactant for the oil. Therefore, if the initial surfactant at low temperature had affinity for the water phase, it would form Winsor I microemulsions (o/w). However, if the temperature was increased the corresponding microemulsion would go through each Winsor state in a predictable way, Winsor I > III > II. Shinoda *et al.* concluded that a non-ionic surfactant with an affinity for water (low temperatures), would bend the monolayer towards water (positive curvature), but at high temperatures the same surfactant had an affinity for oil and therefore the monolayer would bend towards it (negative curvature). By changing the curvature the same surfactant would produce different microemulsions and therefore different macroemulsions. The temperature at which any surfactant in a specific system goes through zero curvature (changing microemulsion Winsor system) with increasing temperature is known as the phase inversion temperature (PIT).

The effect witnessed by Shinoda *et al.* was attributed to the de-hydration of the surfactant head group with increasing temperature, resulting in the reduction of A_h and therefore an increase in the packing parameter, P . As the preferred monolayer curvature reaches approximately zero the interfacial tension, which is the energy required to form unit area of interface, is a minimum.[8, 16-18] In many cases the interfacial tension can be a factor of 10 times lower than the equivalent Winsor I and II systems with typical values between $1 - 10^{-3} \text{ mN m}^{-1}$. Figure 1.9 illustrates a generic profile of interfacial tension in a microemulsion system containing a non-ionic surfactant.

Figure 1.9. Illustrated example of the effect of temperature on the interfacial tension (γ) and the relationship between this and changing monolayer curvature from positive through zero to negative (Winsor I – III – II) with non-ionic surfactant.



1.7.2 Effect of surfactant type and structure on phase inversion

An indication of the preferred monolayer curvature can be gained using the classification system called the hydrophilic-lipophilic balance number of the surfactant (HLB), indicating how hydrophobic or hydrophilic a surfactant is. Surfactants are given

a HLB number normally between 0 – 20, where low HLB numbers (4 - 6) give w/o emulsions (negative preferred curvature), and are hydrophobic in nature. High HLB numbers (8-18) give o/w emulsions (positive preferred curvature), and are hydrophilic in nature.[13]

HLB numbers are described and calculated by the balance of the size and strength of the two opposing groups of a surfactant at 20 °C.[19] First described by Griffin in 1949, as an alternative to the Bancroft rule, that stated the phase which the surfactant partitioned in more became the continuous phase of the emulsion.[20, 21] Griffin determined HLB numbers for a number of industrial non-ionic surfactants using a trial and error methodology based on the balance of head and tail groups and the type of emulsion formed. Leading on from this work Griffin developed a calculation method based on the molecular weight of the hydrophobic and hydrophilic part of the surfactant to determine the HLB number providing a more accurate way to predict non-ionic surfactant HLB numbers than the previous trial and error investigations.[20] An example of the predictive nature of such a system was given when Griffin clearly stated that petrolatum and paraffin oil both require a surfactant HLB number of ≈ 4 to form w/o emulsions, which was proven correct.[20]

Both of the above predictive methods described were later shown to have limitations when compared to the arguments of preferred surfactant monolayer curvature discussed in the PIT model, such as an exclusion of the effect of temperature and the primary focus on the number of atoms of the head and tails, rather than the whole structure.[13, 22-24] However, the underlying importance of the HLB number system is that it gives a rough idea of the preferred monolayer curvature of a surfactant. For example, changing the HLB number of a surfactant by changing the hydrophilic and hydrophobic parts of the surfactant, *i.e.* the size of head or tail groups, can give an idea of the preferred surfactant monolayer curvature.

1.7.3 Effect of oil type on phase inversion

Oil molecules can penetrate the surfactant monolayer, and therefore change the ratio A_t/A_h , or dissolve in the core of a micelle. The relative hydrophobicity and hydrophilicity of the oil affects the action the oil will take. In a microemulsion system containing hydrophilic non-ionic surfactants (positive preferred curvature), the more

hydrophobic the oil the higher the PIT will be.[18, 25] For oil types which are alkanes, the shorter the chain length the lower the PIT due to the higher extent of penetration of the smaller chains into the surfactant tails therefore increasing A_t . [12]

1.7.4 Effect of electrolyte concentration on phase inversion

For systems containing non-ionic and ionic surfactants an increase in salt concentration will cause lower A_h and therefore the monolayer will have an affinity for the oil phase.[13, 26] For ionic surfactants, the salt screens the head group charge and reduces the repulsion between them, whereas for non-ionic surfactant a high salt concentration can salt out the head group causing shrinkage. In both cases, A_h will decrease and result in negative curvature and therefore formation of w/o microemulsions is preferred and consequently w/o emulsions upon emulsification.

1.8 Phase inversion method

As the relationship between microemulsion Winsor systems and the type of macroemulsions is well understood, along with insight into how external and internal parameters of these systems affect preferred curvature, the manipulation of these characteristics has been used in emulsion formation; this is known as the phase inversion method.

The main traits of the phase inversion method are four-fold: [22, 27-31]

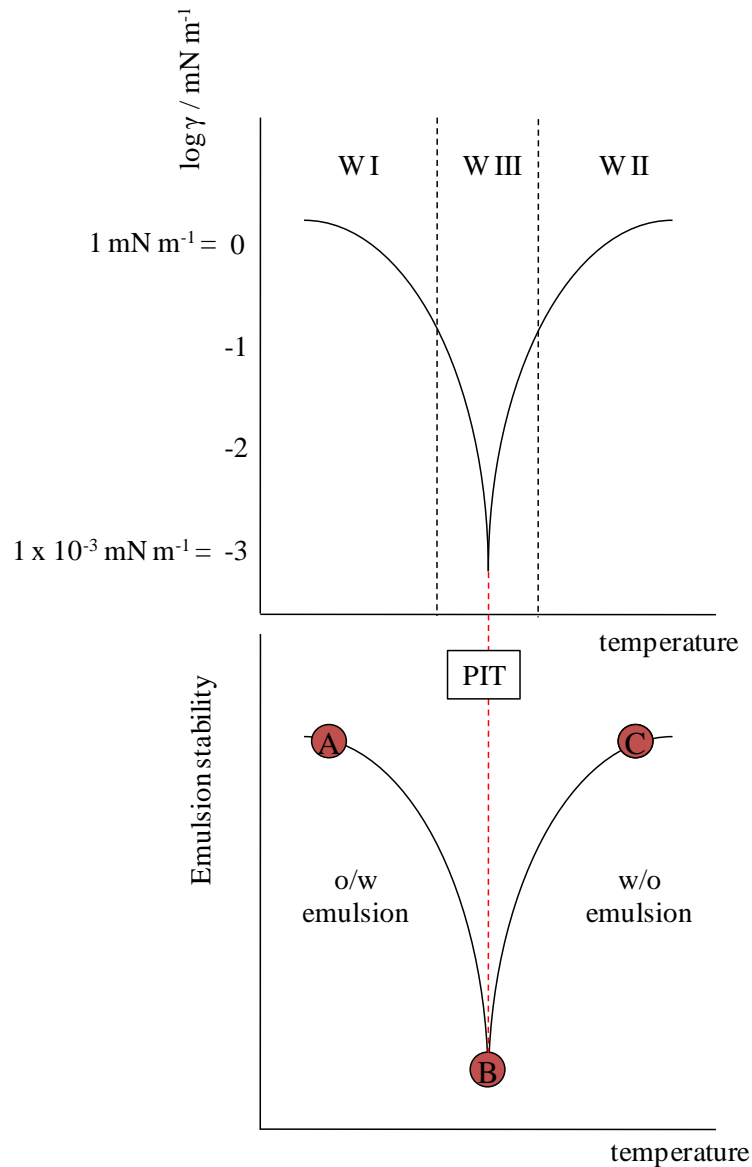
- Emulsification of a system with overall surfactant concentration $< c_{ac}$ does not produce a stable emulsion owing to less than maximum surfactant adsorption at the droplet surfaces and the increased oil-water tension.
- For systems where the overall surfactant concentration is $> c_{ac}$ containing equal volumes of oil and aqueous phases, emulsification of a WI system always gives an o/w emulsion and a WII system always produces a w/o emulsion. Emulsification of a three-phase WIII system can produce a variety of multiple emulsions.
- Since emulsion formation increases the amount of oil-water interface, the energy cost is proportional to the oil-water interfacial tension. Hence, when emulsions are formed using a constant energy input, minimum emulsion drop size (maximum oil-water interface created) is observed under conditions

corresponding to microemulsion phase inversion when the interfacial energy is a minimum.

- Emulsion stability with respect to drop coalescence is generally high under conditions far from microemulsion phase inversion and low close to microemulsion phase inversion.

The phase inversion method uses all the above traits for successful formulation of stable emulsions. Experiments can be performed to change the parameters of the microemulsion systems and hence the preferred curvature of the surfactant monolayer; allowing the identification of the Winsor III region (zero preferred curvature). Emulsions of the required type, either o/w or w/o, can be formed by emulsifying either side of the pre-determined phase inversion point. Due to the minimum interfacial tension around phase inversion, extremely small droplets $<1 \mu\text{m}$ can be formed.[32-34] Figure 1.10 illustrates the relationship between microemulsion interfacial tensions and corresponding macroemulsion stability. The minimum interfacial tension at phase inversion is the cause of the corresponding macroemulsion instability, arising from the ultra low interfacial tension, enabling instability mechanisms to occur at a higher rate, according to literature, where coalescence is thought to be the major contribution to the instability.[35]

Figure 1.10. Interfacial tension of Winsor systems containing non-ionic surfactant, corresponding to the macroemulsion counterpart stability, with varying temperature. A represents a stable o/w emulsion, B represents a stable w/o emulsion, and C represents an unstable w/o or o/w emulsion.



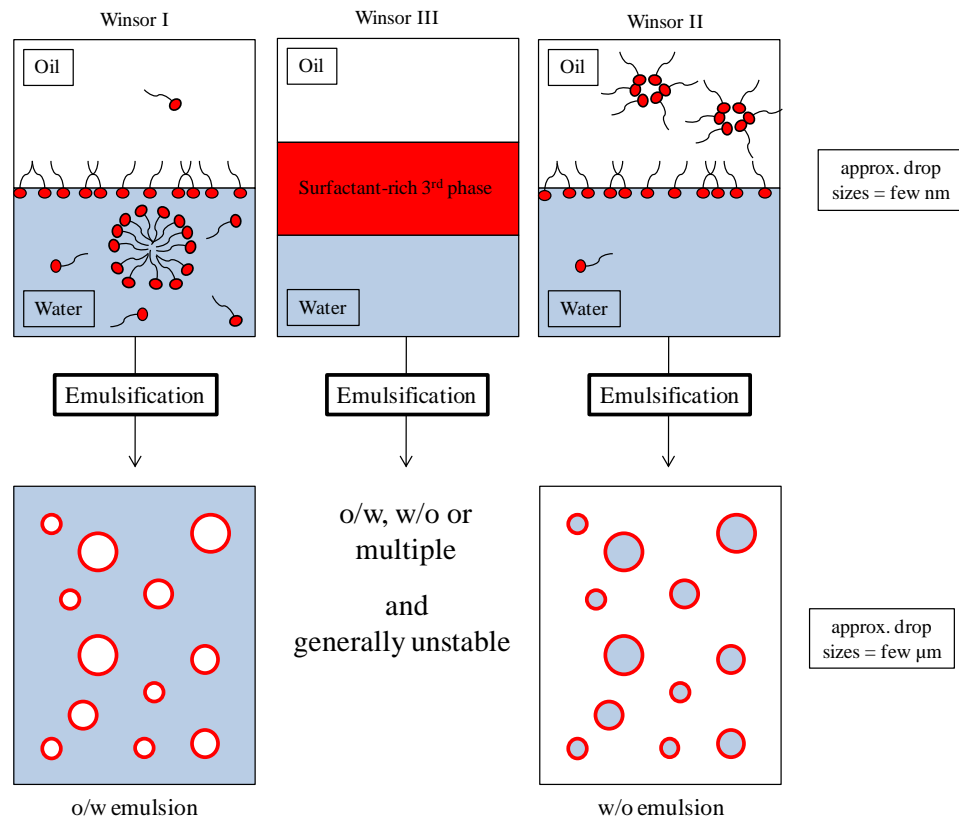
The small droplets produced around phase inversion are an advantage as it has been shown that smaller droplets are more stable to coalescence in emulsions than larger droplets.[36] However, if conditions are kept constant, *i.e.* at phase inversion point, it has been shown that the extremely low interfacial tension causes instability. The theory behind this instability is discussed in more detail in section 1.10.1.6.1 on page 35. Friberg *et al.* produced a method to make stable o/w macroemulsions from microemulsions close to the PIT in 1976.[37] The emulsion formed around the PIT is rapidly cooled to keep the smaller droplets that were able to be obtained during

emulsification due to the ultra low interfacial tension. These small droplets are in a more stable state with respect to coalescence once cooled due to the increase in interfacial tension.[38] This method of emulsion formulation ensures less energy input needed to obtain small droplets upon emulsification and a more stable final emulsion after a system change from the phase inversion point. The PIT method has been used in academia and industry in the preparation of stable emulsions ever since, where it has also been used in the preparation of so called nanoemulsions with droplets smaller than 100 nm, that are transparent due to the lack of ability to scatter light strongly.[39-41]

1.9 Relationship between micro and macroemulsions

Immiscible water and oil can be mixed to form an unstable mixture of one within another, known as a macroemulsion or emulsion. These macroemulsions can be made kinetically stable with the addition of surface-active ingredients, surfactant or particles. The relationship between microemulsions and macroemulsions in a system of equal volumes of oil, water and fixed surfactant concentration above the cac is that the resulting macroemulsion will be of the same type as the corresponding microemulsion.[13, 42] For example, if a Winsor I microemulsion containing o/w micelles with excess oil is emulsified it produces an o/w macroemulsion. Likewise, when a Winsor II microemulsion containing w/o micelles and excess water is emulsified a w/o macroemulsion is created. Figure 1.11 illustrates the relationship between micro- and macroemulsions. Theory relating to the formation and stability of macroemulsions will be discussed in greater detail in section 1.10.

Figure 1.11. Schematic representation of the relationship between microemulsions and macroemulsions with changing Winsor systems (preferred surfactant monolayer curvature positive to negative from left to right).



1.10 Macroemulsions

Macroemulsion (or emulsions) are described as opaque dispersions of droplets of one liquid phase in another with which it is completely immiscible.[7] Emulsions that contain dispersions of oil droplets in water are called oil-in-water (o/w) emulsions, whereas water drops dispersed in oil are called water-in-oil (w/o) emulsions. The size of the dispersed phase droplets generally ranges from 0.1 μm – 10 μm and they scatter visible light, which is the cause of their opaque appearance. Other emulsions, known as multiple emulsions can also be formed when the drops are dispersed in other drops. These can either be water-in-oil-in-water (w/o/w) or oil-in-water-in-oil (o/w/o) emulsions.

Macroemulsions are thermodynamically unstable and without the addition of surfactants will phase separate very rapidly. However, with the addition of surfactants, the dispersed drops can be protected from coalescence and flocculation and produce a

stable emulsion. Stability is achieved through charge (electrostatic) and steric stabilisation, where charged drops repel each other because of electrostatic interactions, and the bulky head or tail group of a surfactant acts as a steric repulsion. Due to this, macroemulsions can be made kinetically stable over a time scale which can range from a few minutes to years. The fact that emulsions require energy input to be formed (non-spontaneous) can be explained thermodynamically. The free energy of formation of an emulsion from bulk phases is given by,[43]

$$\Delta G = \Delta A\gamma - T\Delta S \quad (1.2)$$

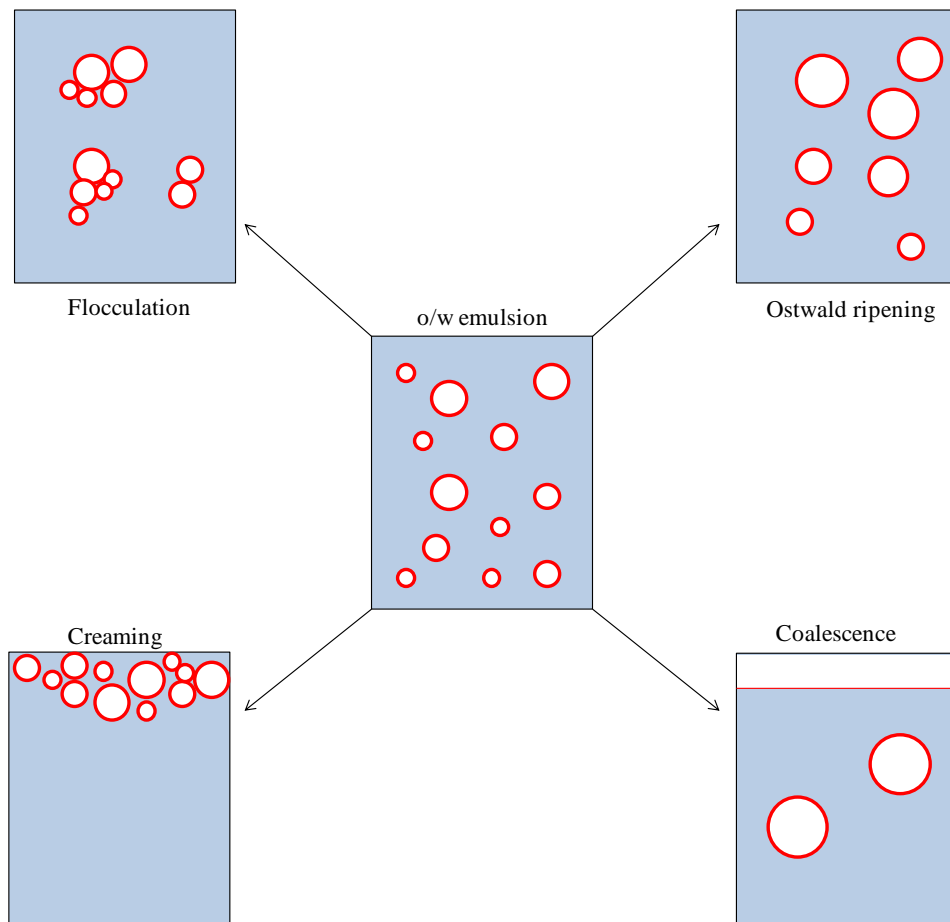
where ΔA is the increase in the interfacial area, γ is the interfacial tension and ΔS is the change of entropy in the system at temperature T . The interfacial energy term $\Delta A\gamma$ is larger than the entropy contribution $T\Delta S$ in macroemulsions, hence, the overall free energy change is positive ($\Delta G > 0$), *i.e.* the change is thermodynamically non-spontaneous. Thus, macroemulsions require energy to form, normally from high sheer homogenisers. The spontaneous formation of microemulsions, which are thermodynamic stable (discussed earlier in section 1.6), can be explained using the same principles, where the reduced interfacial tension and increased entropy causes the free energy of formation to be zero or negative ($\Delta G \leq 0$).

The type of emulsion formed (o/w or w/o) is dependent on various factors: the volume fraction of the dispersed phase, viscosity of the two phases, the structure/type and concentration of the surfactant in the system. Emulsion type can be simply determined by adding the emulsion to the aqueous or oil phases separately: this test is known as the drop test. Emulsions of type o/w will disperse in the aqueous phase, whereas w/o emulsions would sediment. The opposite is true when the oil phase is used in the drop test. A second technique is to determine the conductivity of the emulsion. In this case o/w emulsions would normally have high conductivity, whereas w/o emulsions would have low conductivity because the continuous phase has low conductivity.

1.10.1 Stability

There are four instability mechanisms in emulsions: creaming (or sedimentation), coalescence, flocculation and Ostwald ripening. Some or all of these instabilities can occur in a single emulsion and they are inter-dependent processes. A schematic of the major emulsion breakdown processes is shown in Figure 1.12.

Figure 1.12. Schematic representation of emulsion instability breakdown processes. In this case oil is less dense than the water.



Before discussing these in more detail, the forces between colloidal particles/emulsion drops should be examined, known as the DLVO theory.

1.10.1.1 DLVO theory

A useful approach to understanding the stability of colloids is the Derjaguin-Landau-Verwey-Overbeek (DLVO) theory, which quantitatively explains the mechanism of stability in suspensions or emulsions by considering the attractive and repulsive forces, van der Waals and electrical double layer respectively, present in colloidal systems.[44]

1.10.1.1.1 Attractive forces (van der Waals)

van der Waals forces are the attractive force resulting from interactions between the electric dipoles of molecules. The term was introduced in 1873 by van der Waals to explain the non-ideal properties of gases and liquids. Colloid particles have attractive van der Waals forces arising from the interactions of molecules on an uncharged

particle inducing dipoles in other particles. The dipole created causes a long range attractive force (V_A) between two spherical particles of radius r , having an interparticle separation, h , ($h < r$). The attractive energy between the two particles is:[44]

$$V_A = -\frac{Ar}{12h} \quad (1.3)$$

Where A is the Hamaker constant

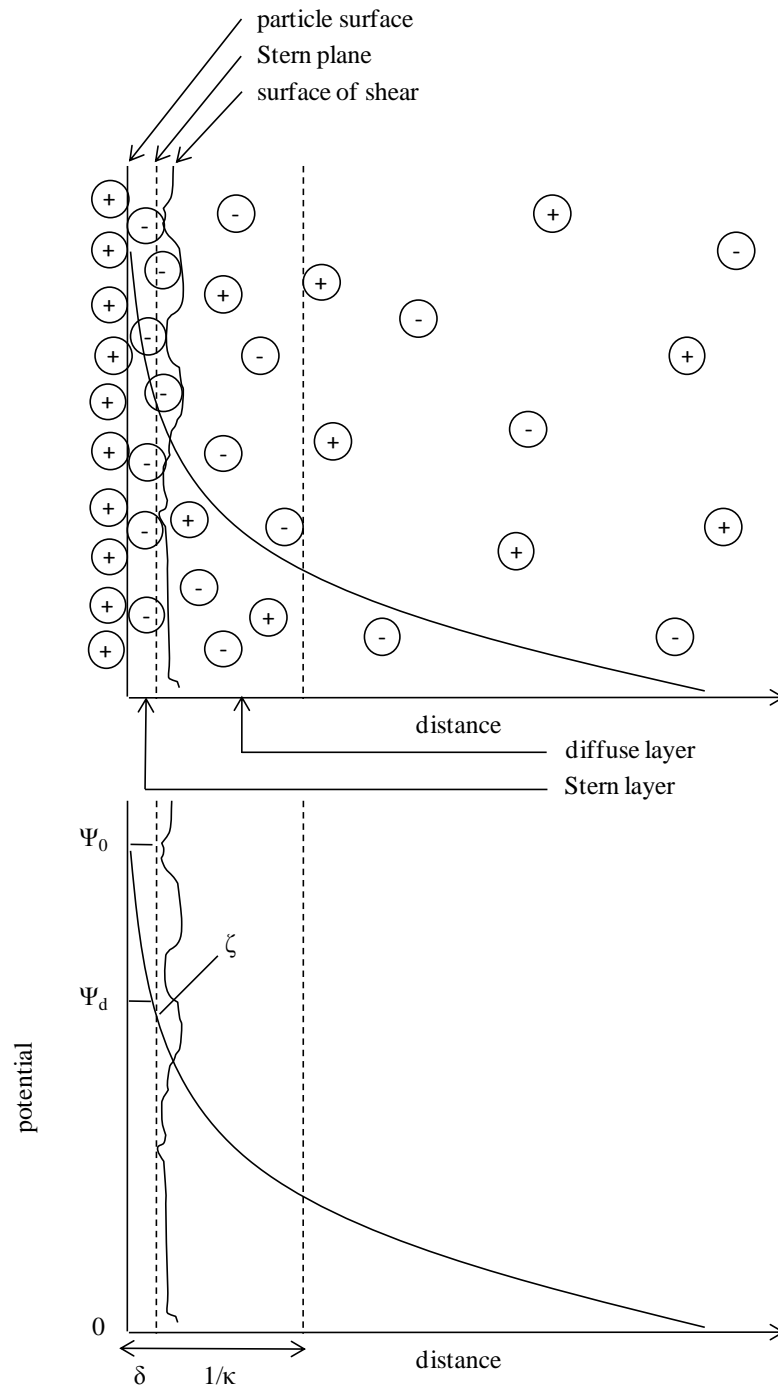
1.10.1.1.2 Repulsion forces (electrical double layer)

The repulsion force present in colloidal systems is due to the electrical double layer which results from an electrical charge on the surface of the colloid. The charges develop from ionisation of chemical groups at the surface or from the adsorption of ions from the solution of the system. An electrical double layer forms which consists of dissolved ions at the surface of the colloid and the equivalent amount of ionic charge distributed uniformly. The electrostatic interactions are screened by dissolved ions and it is found that the Coulomb interaction exponentially decays with distance from the colloid (Figure 1.13).[6] The repulsive energy (V_R) that occurs from the electrical double layer of two spherical particles of identical radius r at separation h is given by:[44]

$$V_R = \frac{\epsilon r \Psi_0^2}{2} \ln(1 + \exp^{-\kappa h}) \quad (1.4)$$

where Ψ is the surface potential, ϵ is the permittivity of free space and κ is the inverse Debye length. This equation can only be used if the double layer thickness is smaller than the particle radius ($\kappa r > 1$).

Figure 1.13. Schematic representation detailing the structure of the electric double layer. Re-drawn from [4].



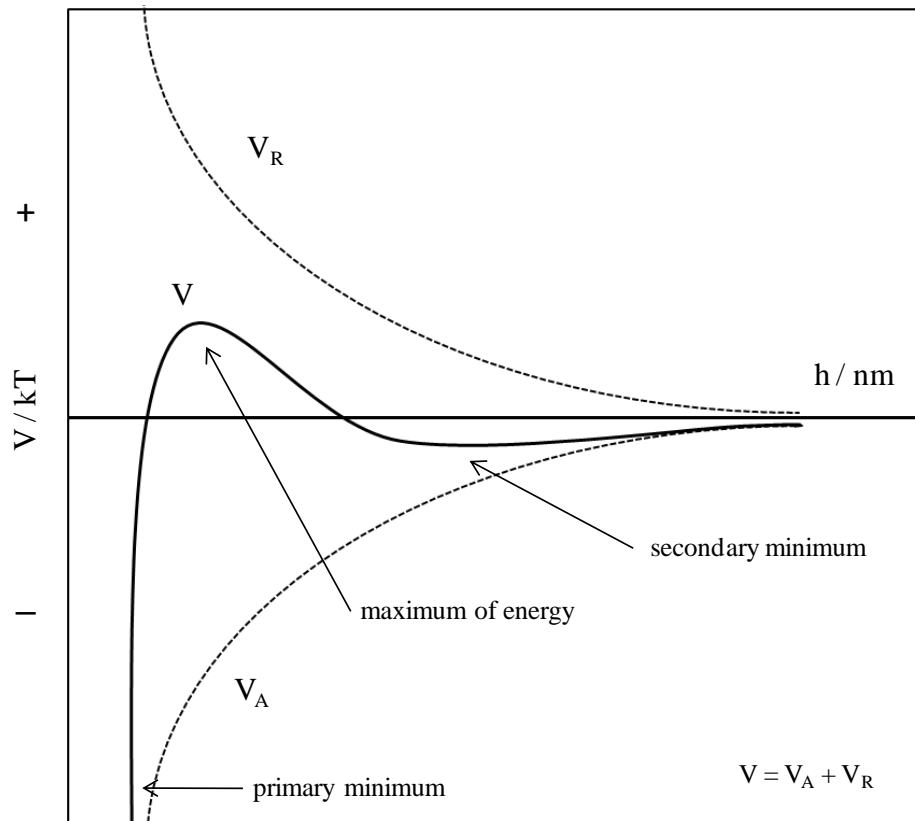
1.10.1.1.3 Total interaction energy

The total interaction energy (V) of a colloidal system, assumed to be the sum of the repulsion and attractive forces discussed in the previous two sections, is explained quantitatively by the DLVO theory:[44]

$$V = V_A + V_R \quad (1.5)$$

The total interaction energy (V) between two spherical particles can be represented as a function of inter-drop separation h (Figure 1.14).

Figure 1.14. Schematic of interaction energy (V) between two spherical particles of identical size with varying distance (h), according to the DLVO theory.



The DLVO theory shows four interesting aspects. The first is the repulsive force (V_R) which shows an exponential decay relative to the thickness of the double layer. Secondly, the attractive force (V_A) shows a decrease with inverse power of the distance between the colloids.[44] Also, at very small distances between the colloids, there is a large negative in total interaction energy (V), indicating that the dominant force is the attractive force. Finally, at intermediate separation there is a maximum in total interaction energy, which shows that the repulsive force dominates.

From these observations the DLVO theory can explain the stability of suspensions or emulsion systems. For example, the primary minimum relates to the coalescence or coagulation of emulsion droplets and particles respectively and is irreversible. The secondary minimum relates to the flocculation of droplets or particles, and is generally

reversible. The DLVO theory is slightly restricted to o/w emulsions with ionic surfactants due to the theory being related to electric charge on surfaces, however similar repulsions for steric reasons can occur with non-ionic surfactants.

1.10.1.2 Creaming

Creaming in emulsions is due to the movement of oil/water drops under gravity to form a oil-rich or water-rich layer in o/w or w/o emulsions respectively, with no accompanying change in the droplet diameter. It is a reversible process, by which shaking can restore the emulsion to its previous state.[6, 13] In w/o emulsions the process is called sedimentation. In dilute emulsions the speed v_s of an isolated, spherical drop of radius r moving through a medium of density ρ_o and Newtonian shear viscosity η_o , is given by Stokes' law, where g is the acceleration due to gravity and ρ is the density of the dispersed phase:[45]

$$v_s = \frac{2r^2(\rho_o - \rho)}{9\eta_o} \quad (1.6)$$

If no flocculation is assumed, Stokes' law is a good indicator for understanding some of the critical processes which can affect the rate at which creaming occurs. An increase in droplet diameter or a decrease in viscosity of the continuous phase dramatically increases the speed of creaming. Therefore, reducing and increasing both parameters respectively would cause an increase in the stability to creaming. However, the law is based on the following assumptions:

1. Droplets are perfect spherical spheres throughout the whole process and the drop interface must be immobile.
2. Brownian motion (random movement due to thermal energy) does not disturb the movement of drops.
3. The continuous phase is Newtonian liquid (viscosity is not changed with shear rate) and no attractive interactions occur between the droplets.

1.10.1.3 Flocculation

Flocculation is when emulsion drops aggregate without rupture of the stabilising layers at their interfaces, and arises if the pair interaction free energy becomes considerably

negative at a droplet/particle separation. Flocculation can be either weak (reversible) or strong (irreversible) depending on the strength of the inter-drop forces.

Flocculation will lead to enhanced creaming rates due to the increase in apparent size of the drops. Flocculation can be enhanced if an emulsion is polydisperse (wide range of droplet diameters) because the different creaming rates will result in more collisions between droplets, resulting in an increased chance of flocculation.

1.10.1.4 Coalescence

Coalescence is the process where two droplets come together to form a single bigger droplet. This process is irreversible and over a time period (dependant on the system) will cause irreversible emulsion breaking into two phases. Coalescence occurs when the interfacial film between two dispersed droplets becomes sufficiently thin that film rupture becomes more likely. Coalescence can be caused by random surface fluctuations, for example ripples on the surfaces, or differences in thickness of the interfacial film.[2] An additional point to add is that the probability of coalescence occurring can be greatly increased by the presence of particles/crystals in the dispersed phase. In some cases the rate of coalescence can increase by a factor of 10^6 when semi-crystalline fat is located at the oil-water boundary.[46, 47]

1.10.1.5 Ostwald ripening

Ostwald ripening is a spontaneous process that is driven by the greater solubility of the smaller droplets, giving rise to bigger droplets as material moves from smaller droplets to larger droplets, in turn initiating advances in creaming and final emulsion break down. [48] This spontaneous process is described by the Kelvin equation stated below,[49]

$$c(r) = c_{\infty} \exp\left(\frac{2\gamma V_m}{rRT}\right) \quad (1.7)$$

where $c(r)$ is the aqueous phase solubility of the oil contained within a droplet of radius r , $c(\infty)$ is the solubility in a system with only a planar interface (*i.e.* infinitely large drop) and V_m is the molar volume of the oil. As the solubility in the smaller droplets in the dispersed phase increases, oil diffuses through the continuous phase into the larger droplets with lower solubility in the dispersed phase, a process driven by the differential

pressures on the variable droplets generated from the Laplace pressure. Therefore, small droplets have higher pressure and higher solubility in the continuous phase. From this theory, monodisperse emulsions would not exhibit Ostwald ripening.

1.10.1.6 Instability mechanisms

The four instability processes discussed above and shown in Figure 1.12 occur simultaneously and are inter-dependent. For example, increased rates of flocculation could lead to increased rates of creaming, which could then lead to coalescence and emulsion breakdown. The complication of this process means that there is not one theory which can explain the overall process. However, it is known that emulsion breakdown is a multi-step process:[6]

- Two dispersed emulsion droplets come together and are separated by a thin layer of the continuous phase.
- Thinning of the continuous phase layer promotes the formation of a planar bilayer which consists of two surfactant monolayers from two separate droplets separated by a distance of < 100 nm.
- Fluctuations in the surfactant monolayer cause an unstable region or hole to form.
- Enlargement or prohibition of the unstable region causes the emulsion droplets to coalesce or stabilise.

1.10.1.6.1 Oriented wedge theory

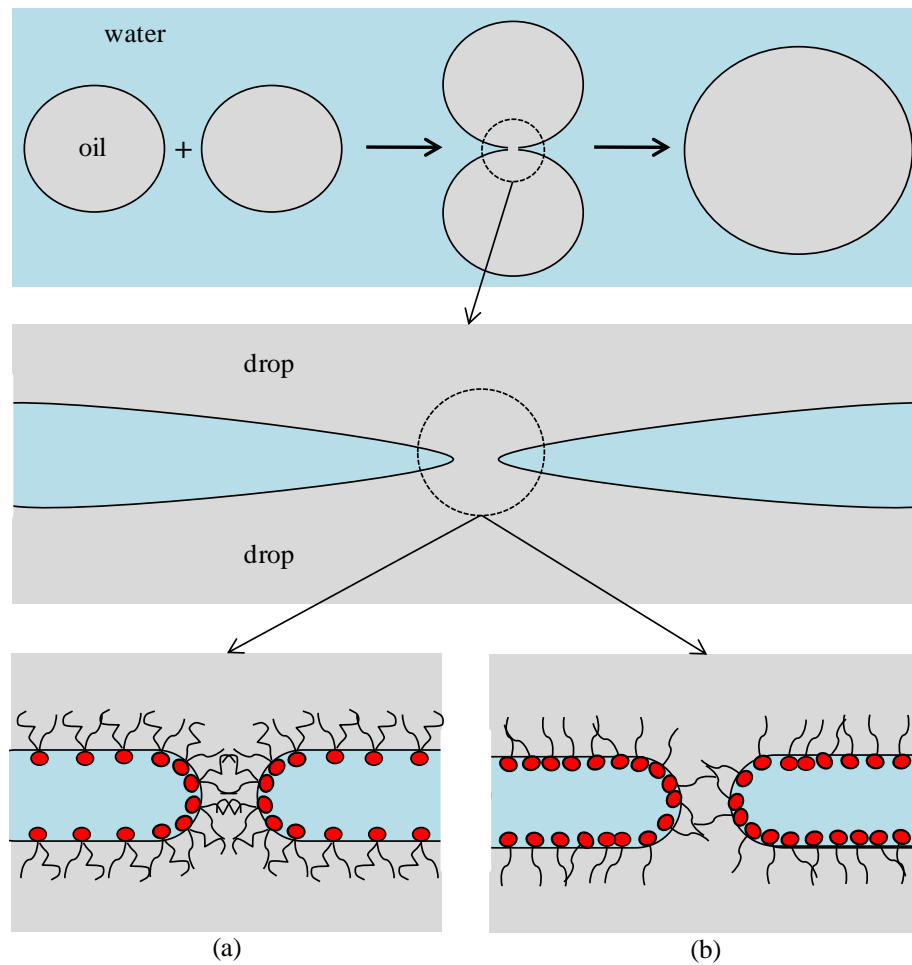
The oriented wedge theory is an explanation of the process of coalescence by Kabalnov and Wennerström through instability or holes in the surfactant monolayer, adapted from the earlier work of Harkins *et al.* and Langmuir, who used the theory to explain how the type of emulsion is dependent on the surfactant monolayer structure.[35, 50, 51] According to the revisited theory of Kabalnov and Wennerström, the final stage of coalescence occurs when two emulsion droplets make contact with each other to form a hole or neck through the continuous phase. At this point the surfactant monolayer is highly curved in the region of the hole, and planar in the remaining monolayer, due to the emulsion droplet size being in the μm region and the surfactant in the nm region. It is hypothesised that the tension at the edge of the hole is different from the planar film, due to the monolayer frustration at the edge. The radius of the hole in the thin film and

the thickness of the aqueous phase are adjusted to minimise the free energy of the hole, which can lead to growth of the hole (coalescence) or stabilisation of the hole (no coalescence). The monolayer “frustration energy”, discussed above, therefore plays an important role with the preferred curvature of the surfactant monolayer playing a major role in coalescence, shown in Figure 1.15.

The total energy of formation of the hole W can be described by three terms; the interfacial free energy, due to the change of interfacial area caused by the formation of the hole (W_1); the mean curvature energy accounting for the extra interfacial tension of the curved interface in the hole region relative to the planar one (W_2) and the Gaussian curvature contribution (W_3) that is independent of the film orientation, *i.e.* the same for both o/w/o and w/o/w films.

The energy arguments discussed above allow for explanation of the heightened instability witnessed around the phase inversion point, where the surfactant monolayer curvature is approximately zero. It has been shown that the mean curvature energy has a large influence on the energetics of neck growth.[52] For example, for emulsions containing non-ionic surfactant ($C_{12}E_5$), water and octane at a temperature far away from the PIT, the energy barrier to coalescence could be as high as 40 kT. If the system was close to the PIT, an increase in the film instability is predicted and the energy barrier to coalescence approaches zero.

Figure 1.15. Schematic representation of the Kabalnov and Wennerström oriented wedge theory model; upper schematic, the process of coalescence of two oil droplets in a water continuous phase, middle schematic shows the formation of a hole in the thin film between the oil droplets caused by chance or fluctuations in the oil-water interface and the lower schematics show the effect of preferred surfactant monolayer curvature on the stability of the hole. If the preferred curvature of the surfactant monolayer fits the neck, the hole will grow without a significant barrier (a), in the opposite case the growth of the hole is suppressed (b). Re-drawn from [38].

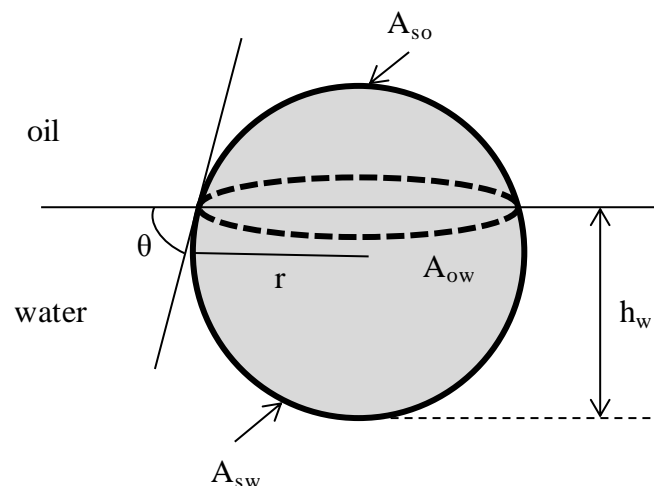


1.11 Particle-stabilised emulsions

Emulsions have been discussed in detail with surfactants adsorbed at the oil-water interface being the stabiliser against instability mechanisms. Recently the use of particles as stabilisers has been shown and investigated in detail.[53-55] Particles such as silica, carbon, minerals, metals and oxides have been shown to stabilise emulsions by adsorbing at the water-oil interface and protect against coalescence.[55] The adsorption at the water-oil interface occurs by partial wetting of the particle by both the polar and non-polar phases.

The phenomenon of particles adsorbing at a water-oil interface was first recognised by Pickering who showed that they could be used to stabilise o/w emulsions, leading to particle-stabilised emulsions named as “Pickering emulsions” in the literature.[56] However, the interfacial activity of colloidal particles was shown 4 years earlier by Ramsden who described the formation of a membrane of solid particles enveloping air bubbles in water and oil drops in water.[57] Finkle *et al.* showed how the emulsion type is linked to the wettability of particles, by showing that either oil or water could wet the particles differently, with the phase that wets the particles most becoming the continuous phase. For example, hydrophilic particles (water wetting) such as silica will form o/w emulsions and hydrophobic particles (oil wetting) such as carbon black will form w/o emulsions.[58] The results demonstrated by Finkle *et al.* were further established by Schulman and Leja who concluded that the contact angle θ of the particle at the water-oil interface was a measurement of the wettability of particles.[59] For contact angles (measured through the aqueous phase) $< 90^\circ$, particles would stabilise o/w emulsions, and for values $> 90^\circ$, particles would stabilise w/o emulsions (Figure 1.16). Particles which are classed as too hydrophilic or hydrophobic remain dispersed in the water or oil phase respectively and form unstable emulsions due to lack of adsorption at the water-oil interface.

Figure 1.16. Schematic representation of a spherical solid particle of radius r at a water-oil interface. Contact angle θ is measured through the water phase and h_w is the depth of the immersion in the water phase. A_{so} and A_{sw} are the areas of the particle in contact with oil and water, with A_{ow} being the area the adsorbed particle displaces at the oil-water interface.



Assuming that a spherical particle of radius r has the same density as the oil and water and that gravitational forces are negligible, the particle will be partly immersed in both liquids and the equilibrium contact angle at the planar water-oil interface can be calculated from the Young equation;[55]

$$\gamma_{so} - \gamma_{sw} = \gamma_{ow} \cos \theta \quad (1.8)$$

However, the gravitational pull on the particle is expected to displace the particle from the interface until the net force of the interfacial tension is equal to the gravitational force.[60]

The strength at which the particle is held at a water-oil interface is related not only to the contact angle but also to the interfacial tension γ_{ow} . [61] A single particle of radius r at the water-oil interface with a contact angle θ (measured through the aqueous phase) denotes the depth of immersion h_w into the water using $r(1 + \cos\theta)$. The area between the water and particle can be calculated by $A_{sw} = 2\pi r^2(1 + \cos\theta)$. The planar area of the water-oil interface eliminated by the presence of the particle is:

$$A_{ow} = \pi r^2 \sin^2 \theta = \pi r^2 (1 - \cos^2 \theta) \quad (1.9)$$

Again assuming that the particle is not affected by gravitational forces and that the water-oil interface remains planar up to the contact line of the particle, the energy required E to remove the particle from the interface to the oil is,

$$\Delta E = 2\pi r^2 (1 + \cos\theta)(\gamma_{so} - \gamma_{sw}) + \pi r^2 (1 - \cos^2\theta)\gamma_{ow} \quad (1.10)$$

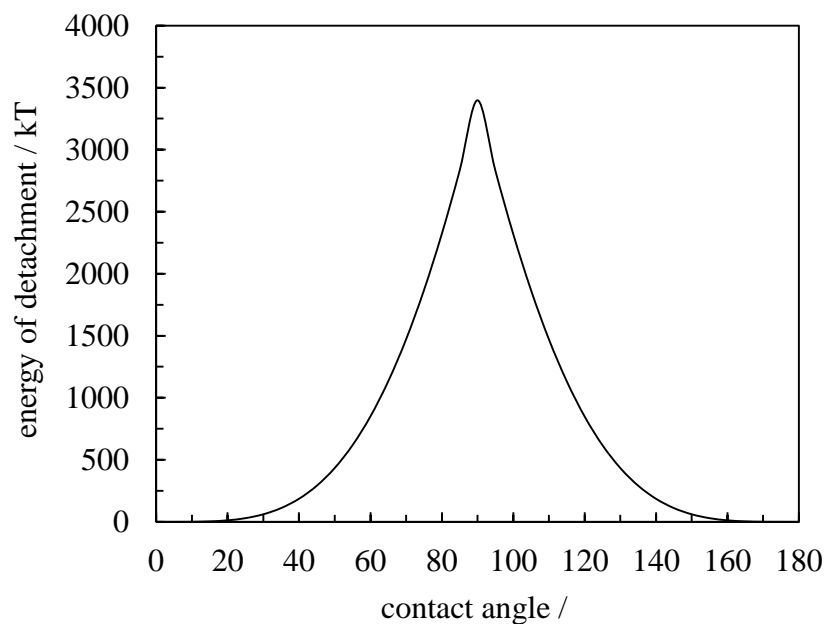
where γ refers to the relevant interfacial tension and the subscripts s , o , w represent solid, oil and water. Substituting the Young equation (1.8) into (1.10) the change in free energy for the desorption of a spherical particle from the oil-water interface to the oil phase is,[62]

$$\Delta E = \pi r^2 \gamma_{ow} (1 + \cos\theta)^2 \quad (1.11)$$

where r is the particle radius and γ_{ow} is the bare oil-water interfacial tension; the plus sign refers to desorption of the particle into oil and a minus sign would refer to desorption into water. As the free energy is always positive, the particle at the water-oil interface is thermodynamically stable.[55] Figure 1.17 shows the energy of detachment

versus the contact angle of a system used in this project, where the water-oil interfacial tension is equal to 0.044 N m^{-1} and the particle radius is $1 \times 10^{-8} \text{ m}$. Figure 1.17 also shows that the particle is strongly held at a contact angle of 90° ; at either side of 90° , the energy decreases dramatically, *i.e.* for contact angles at very high and low values, the energy is as little $<10 \text{ kT}$. Such values indicate that particles can be easily removed from the interface and therefore the ability to form emulsion with shear would reduce.

Figure 1.17. Energy of detachment for a spherical silica particle of radius $r = 1 \times 10^{-8} \text{ m}$ at a planar paraffin liquid-water interface of interfacial tension $\gamma_{ow} = 0.044 \text{ N m}^{-1}$ versus the contact angle θ the particle makes at the interface measured through the aqueous phase at 298 K.



The important implication of these calculations and theory is that the high energy of detachment around 90° shows that the energy of detachment is so high that the particles are effectively thermodynamically stable. In contrast, in surfactant stabilised emulsions the surfactants are always in dynamic equilibrium with the interface. As a result, heightened stability in particle-stabilised emulsions at approximately 90° contact angle is achieved.

Since the discovery of particle-stabilised emulsions in the early 20th century, intense investigations have regenerated interest, not only in emulsions which are very stable to instability mechanisms due to effective thermodynamically attached particles, but also in developing applications such as colloidosomes and self assembly structures, with each application using the ability of solid particles to adsorb at interfaces.[63]

1.12 Non-aqueous polar phase emulsions

The non-conventional component added to the emulsions of interest in this project is a non-aqueous polar phase. Little research has been conducted over the years involving non-aqueous polar phases in emulsions, compared to that of emulsions with only an aqueous polar phase. However, there have been exceptions.[16, 26, 32, 42, 64-66] The normal reasons for the presence of a non-aqueous polar phase in emulsions include better solubility of active drugs, used as a skin penetrator and improved aesthetic feel. For example, Zovirax cream was shown to have a dose response proportional to the amount of propane-1,2-diol with an induced optimum between 30 and 40% v/v propane-1,2-diol.[65]

In 1984 Fletcher *et al.* studied the difference between water in n-heptane and non-aqueous glycerol dispersed in n-heptane stabilised by Aerosol-OT (AOT) in equilibrated microemulsion systems.[16] The study showed that droplet size was independent of temperature and primarily depends on the glycerol to AOT molar ratio (R) and when dispersed in n-heptane. AOT occupies $\approx 20\%$ less area on glycerol than on water drops.

More recently, Sakthivel *et al.* looked at the possibility of making emulsions with formamide replacing water, as they believed it was the closest polar solvent which may be able to replace water in emulsions.[64] They used formamide at 20, 25 and 33% v/v, with various low molecular weight oils and non-ionic surfactants (polysorbate 20, 40, 60 and 80). It was found that the polar component increased the cmc by many orders of magnitude compared to water. It was also stressed that addition of water to these hydrocarbon/formamide systems did not destabilise them.

Seguin *et al.* studied adsorption and aggregation properties of model non-ionic surfactants with mixtures of water/ethane-1,2-diol and water/propane-1,2-diol. Total replacement of water as the continuous phase with ethane-1,2-diol and propane-1,2-diol was also investigated.[66] The study concluded the cac dramatically increased with the addition of the polar non-aqueous solvents. Upon the addition of water to these emulsions the adsorption and aggregation properties of the surfactant were preserved. The authors suggest that these types of systems could possibly be used for systems that will be subjected to high dilution with water. In addition, they suggest a procedure to make emulsions from water and the two glycols that could be used in solubilisation or

delivery of hydrophobic materials, such as, flavours, dyes and pharma-active ingredients/molecules.

In 1997 Imhof investigated the stability of non-aqueous emulsions.[32] Many polar solvents were examined with non-ionic surfactants (polyoxyethylene alkyls) including formamide, N-methylformamide, N,N'-dimethylformamide, dimethylsulfoxide, methanol and acetonitrile. Using large triblock copolymers it was found that indefinitely stable non-aqueous emulsions were formed for formamide and dimethylsulfoxide in water. Whereas formamide could be stabilised by polyoxyethylene alkyl phenols for 2-3 days when using a optimum surfactant HLB number of 12. It was suggested that hydrogen bonding was a major aspect in forming the stable emulsions. Ostwald ripening was also demonstrated to play a more major role in the stability because of increased solubility of the oil in the continuous phase. To overcome the increased instability to Ostwald ripening, 1% w/w of the oil was dissolved in the aqueous phase, after which stable emulsions were formed with Ostwald ripening being significantly slowed down.

In conclusion, little research involving non-aqueous polar phases has been conducted and the existing literature indicates that various water-miscible solvents can produce microemulsion and macroemulsion but the cac and cmc can increase greatly.[26, 42] Also, Ostwald ripening can increase due the solubility of the oil in the less polar aqueous phase.

1.13 Presentation of thesis

The objective of this project is to understand the effect of two “non-conventional” aspects of emulsions, meaning the presence of diol replacing water and the effect of oil crystallisation on such emulsions. For this reason the thesis is conveniently presented in two parts. Chapters 3 and 4 are concerned with the effect of added diols on emulsions stabilised by either surfactant or particles respectively. In Chapter 5 the effect of crystallisation in oil dispersed phases is discussed in emulsions containing high amounts of diol.

Chapter 3 describes the effect of adding diols in place of water to emulsions containing non-ionic surfactants, water and paraffin liquid. The results are discussed in terms of phase inversion of the emulsions, and directly linked to the surface activity of the diols and consequently how they affect the preferred curvature of the surfactant monolayer.

Results are rationalised by investigating known traits of emulsions around phase inversion, including coalescence stability, droplet diameter, water-oil tensions and surfactant/diol structure.

The effect of diol addition on particle-stabilised aqueous dispersions and emulsions containing water, paraffin liquid and fumed silica particles of varying wettability are examined in Chapter 4. Phase inversion is again used as a technique to monitor the effect of diols on the wettability of solid particles at the aqueous-oil interface. The importance of the addition of diols to such systems will be discussed in terms of a known model, where the effect of diol addition will be shown to be predictable by using surface energy arguments.

Chapter 5 investigates the solidification of the dispersed oil phase within a model o/w emulsion containing a high amount of diol, with the varying factor of droplet diameter. Results indicate that droplet diameter plays a role in the crystallisation process, and is explained using techniques including rheology, differential scanning calorimetry (DSC) and nuclear magnetic resonance (NMR).

A summary of conclusions and suggestions for future work are described at the end of this thesis.

1.14 References

-
1. F. Leal-Calderon, J. Bibette and V. Schmitt, *Emulsion Science - Basic Principles*, Springer, New York (2007).
 2. M. J. Rosen, *Surfactants and Interfacial Phenomena*, John Wiley & Sons, New York (1978).
 3. *Micelle Pictures*, <http://lamp.tu-graz.ac.at/~hadley/nanoscience/week4/micelles.jpg>.
 4. D. J. Shaw, *Introduction to Colloid & Surface Chemistry*, Butterworth Heinemann, Oxford (1992).
 5. T. F. Tadros, *Applied Surfactants*, Wiley-VCH, Weinheim (2005).
 6. E. Dickinson, *An Introduction to Food Colloids*, Oxford University Press, Oxford (1992).
 7. R. M. Pashley and M. E. Karaman, *Applied Colloid and Surface Chemistry*, Wiley, London (2004).
 8. R. Aveyard, B. P. Binks, T. A. Lawless and J. Mead, *J. Chem. Soc. Faraday Trans.*, **81**, 2155 (1985).
 9. K. Shinoda and B. Lindman, *Langmuir*, **3**, 135 (1987).

10. R. Aveyard, B. P. Binks, S. Clark and P. D. I. Fletcher, *J. Chem. Soc., Faraday Trans.*, **86**, 3111 (1990).
11. R. Strey, *Colloid Polym. Sci.*, **272**, 1005 (1994).
12. R. Aveyard, B. P. Binks, P. Cooper and P. D. I. Fletcher, *Adv. Colloid Interface Sci.*, **33**, 59 (1990).
13. R. Aveyard, B. P. Binks, P. D. I. Fletcher, X. Ye and J. R. Lu, in *Nato Adv Sci I C-Mat*, Ch.7, J. Sjöblom (ed.), Kluwer Academic Publishers, Dordrecht (1992).
14. K. Shinoda and H. Arai, *J. Phys. Chem.*, **68**, 3485 (1964).
15. K. Shinoda and H. Arai, *J. Colloid Sci.*, **20**, 93 (1965).
16. P. D. I. Fletcher, M. F. Galal and B. H. Robinson, *J. Chem. Soc. Faraday Trans.*, **80**, 3307 (1984).
17. P. D. I. Fletcher and D. I. Horsup, *J. Chem. Soc. Faraday Trans.*, **88**, 855 (1992).
18. T. Sottmann and R. Strey, *J. Chem. Phys.*, **106**, 8606 (1997).
19. W. C. Griffin, *J. Soc. Cosmetic Chemists*, **1**, 311 (1949).
20. W. C. Griffin, *J. Soc. Cosmetic Chemists*, **5**, 249 (1954).
21. W. D. Bancroft, *J. Phys. Chem.*, **17**, 501 (1913).
22. B. P. Binks, *Langmuir*, **9**, 25 (1993).
23. H. T. Davis, *Colloids Surf. A*, **91**, 81 (1994).
24. K. Shinoda and S. Friberg, *Emulsions and Solubilization*, Wiley, New York (1986).
25. R. Aveyard, B. P. Binks and P. D. I. Fletcher, *Langmuir*, **5**, 1210 (1989).
26. R. Aveyard, B. P. Binks, P. D. I. Fletcher, A. J. Kirk and P. Swansbury, *Langmuir*, **9**, 523 (1993).
27. K. Shinoda and H. Saito, *J. Colloid Interface Sci.*, **30**, 258 (1969).
28. H. Wennerström, O. Söderman, U. Olsson and B. Lindman, *Colloids Surf. A*, **123-124**, 13 (1997).
29. J.-L. Salager, L. Márquez, A. A. Peña, M. Rondón, F. Silva and E. Tyrode, *Ind. Eng. Chem. Res.*, **39**, 2665 (2000).
30. D. H. Smith, S. N. Nwosu, G. K. Johnson and K. H. Lim, *Langmuir*, **8**, 1076 (1992).
31. K.-H. Lim, W. Zhang, G. A. Smith and D. H. Smith, *Colloids Surf. A*, **264**, 43 (2005).
32. A. Imhof and D. J. Pine, *J. Colloid Interface Sci.*, **192**, 368 (1997).
33. K. Shinoda and H. Saito, *J. Colloid Interface Sci.*, **30**, 258 (1969).
34. B. P. Binks, W. G. Cho, P. D. I. Fletcher and D. N. Petsev, *Langmuir*, **16**, 1025 (2000).
35. A. Kabalnov and H. Wennerström, *Langmuir*, **12**, 276 (1996).
36. J.-L. Salager, in *Emulsions and Emulsion Stability*, Ch.4, J. Sjöblom (ed.), CRC Press, Boca Raton (2006).
37. S. Friberg, I. Lapczynska and G. Gillberg, *J. Colloid Interface Sci.*, **56**, 19 (1976).
38. B. P. Binks (ed.), *Modern Aspects of Emulsion Science*, The Royal Society of Chemistry, Cambridge (1998).
39. S. L. Ee, X. Duan, J. Liew and Q. D. Nguyen, *Chem. Eng. J.*, **140**, 626 (2008).
40. P. Fernandez, V. Andre, J. Rieger and A. Kuhnle, *Colloids Surf. A*, **251**, 53 (2004).
41. C. Solans, P. Izquierdo, J. Nolla, N. Azemar and M. J. Garcia-Celma, *Curr. Opin. Colloid Interface Sci.*, **10**, 102 (2005).
42. B. P. Binks, P. D. I. Fletcher and D. I. Horsup, *Colloids Surf.*, **61**, 291 (1991).

43. T. Tadros, P. Izquierdo, J. Esquena and C. Solans, *Adv. Colloid Interface Sci.*, **108-109**, 303 (2004).
44. H. Ohshima and K. Furusawa, in *Electrical Phenomena at Interfaces, Second Edition, Fundamentals: Measurements, and Applications*, Ch.5, Taylor and Francis, New York (1998).
45. P. D. I. Fletcher, in *Drops and Bubbles in Interfacial Research*, Ch.12, D. Möbius and R. Miller (eds.), Elsevier, Oxford (1998).
46. A. G. Marangoni, *Fat Crystal Networks*, Marcel Dekker, New York (2005).
47. F. Thivilliers, E. Laurichesse, H. Saadaoui, F. Leal-Calderon and V. Schmitt, *Langmuir*, **24**, 13364 (2008).
48. A. S. Kabalnov, *Langmuir*, **10**, 680 (1994).
49. W. Thomson, *Proc. Roy. Soc. Edinburgh*, **7**, 63 (1871).
50. W. D. Harkins, E. C. H. Davies and G. L. Clark, *J. Am. Chem. Soc.*, **39**, 541 (1917).
51. I. Langmuir, *J. Am. Chem. Soc.*, **39** (1917).
52. A. Kabalnov and J. Weers, *Langmuir*, **12**, 1931 (1996).
53. B. P. Binks, *Curr. Opin. Colloid Interface Sci.*, **7**, 21 (2002).
54. B. P. Binks and J. H. Clint, *Langmuir*, **18**, 1270 (2002).
55. B. P. Binks and T. S. Horozov (eds.), *Colloid Particles and Liquid Interfaces*, Cambridge University Press, Cambridge (2006).
56. S. U. Pickering, *J. Chem. Soc.*, **91**, 2001 (1907).
57. W. Ramsden, *Proc. Roy. Soc.*, **72**, 156 (1903).
58. P. Finkle, H. D. Draper and J. H. Hildebrand, *J. Am. Chem. Soc.*, **45**, 2780 (1923).
59. J. H. Schulman, *Trans. Faraday Soc.*, **50**, 598 (1954).
60. P. Becher (ed.), *Encyclopedia of Emulsion Technology*, Marcel Dekker, New York (1983).
61. S. Levine, B. D. Bowen and S. J. Partridge, *Colloids Surf.*, **38**, 325 (1989).
62. B. P. Binks and S. O. Lumsdon, *Langmuir*, **16**, 8622 (2000).
63. A. D. Dinsmore, M. F. Hsu, M. G. Nikolaidis, M. Marquez, A. R. Bausch and D. A. Weitz, *Science*, **298**, 1006 (2002).
64. T. Sakthivel, V. Jaitely, N. V. Patel and A. T. Florence, *Int. J. Pharm.*, **214**, 43 (2001).
65. L. Trottet, H. Owen, P. Holme, J. Heylings, I. P. Collin, A. P. Breen, M. N. Siyad, R. S. Nandra and A. F. Davis, *Int. J. Pharm.*, **304**, 63 (2005).
66. C. Seguin, J. Eastoe, R. Clapperton, R. K. Heenan and I. Grillo, *Colloids Surf. A*, **282**, 134 (2006).

CHAPTER 2. EXPERIMENTAL

This chapter contains descriptions of materials and methods used throughout investigations in this project. The preparation of emulsions with both surfactant and particle stabilisers is described as well as techniques used to investigate emulsion properties and characteristics. The methodologies include microscopy, rheology, differential scanning calorimetry (DSC), nuclear magnetic resonance (NMR), and surface tension measurements.

2.1 *Materials*

2.1.1 Water

Water was purified by an Elga Prima reverse osmosis unit and treated with a Milli-Q reagent water system. The water obtained was considered ultra pure with a resistivity of 18 M Ω cm; in good correlation with the specification of ultra pure water of 18.2 M Ω cm at 25 °C.[1] The conductivity of Milli-Q water was equal to approximately 1 - 2 μ S cm⁻¹. The surface tension was measured to be 71.8 mN m⁻¹ at 25 °C, again in excellent agreement with the literature value.[2]

2.1.2 Oils and non-aqueous solvent

Table 2.1 lists the oils and solvents used, and their suppliers. When stated, oils were purified by column chromatography through alumina (activated basic) in order to remove polar impurities.

Table 2.1. Suppliers and purities of oils and diols.

<u>Material</u>	<u>Supplier</u>	<u>Purity / %</u>
White soft paraffin	FUCHS	blend ^a
Paraffin liquid	Total	blend ^b
Ethane-1,2-diol	Sigma	>99
Propane-1,3-diol	Sigma	98
Propane-1,2-diol	Dow Corning	98
Butane-1,2-diol	Sigma	>98
Butane-1,3-diol	Sigma	99
Butane-1,4-diol	Sigma	99
Pentane-1,5-diol	Sigma	>97
Dimethicone	Dow Corning	blend ^c

^aWhite soft paraffin is a mixture of linear and branched alkanes/alkenes with varying chain length of $\approx 16 - 26$ carbon atoms. Density = 0.8961 g/cm^3 .

^bParaffin liquid is a mixture of linear and branched alkanes with varying chain length of $\approx 12 - 20$ carbon atoms. Density = 0.8593 g/cm^3 .

^cDimethicone is a medium chain linear polydimethylsiloxane with a molecular formula $(\text{C}_2\text{H}_6\text{OSi})_n$. This particular grade represents a range of $n \approx 30 - 36$.

2.1.3 Surfactants

Table 2.2 shows the surfactants and their purities; suppliers are listed accordingly.

Surfactants used throughout the project consisted of industrial surfactants used in many of GSK's formulations. These included;

- Pluronic F127 is a non-ionic surfactant which is triblock copolymer consisting of a central hydrophobic block of polypropylene glycol flanked by two hydrophilic blocks of polyethylene glycol acting as the tail and head respectively.
- Arlacel 165 is a mixture of non-ionic surfactants glyceryl stearate and PEG-100 stearate; glyceryl stearate is a glycerol ester of stearic acid where the glycerol ester acts as the head group and steric acid acts as the tail group. PEG-100 stearate is polymeric non-ionic surfactant with a hydrophilic head of polyethylene glycol and again contains a steric acid hydrophobic tail group.

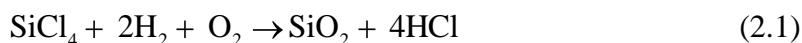
- Cetostearyl alcohol is a mixture of fatty alcohols, consisting predominantly of cetyl (C₁₈) and stearyl (C₁₆) alcohols, where the alcohol acts as the hydrophilic head group and the alkyl chain acts as the hydrophobic tail group.
- Sodium lauryl sulphate is an anionic surfactant salt consisting of a hydrophilic anionic organosulfate head group and a 12-carbon hydrophobic tail group attached to a sulphate group.
- O_nG_n are non-ionic surfactants made from glycerol and oleic acid. Glycerol becomes the hydrophilic head group and oleic acid becomes the C₁₈ hydrophobic tail group. Subscript n on both the O and G represents the average of each group by weight, *i.e.* if n=1 then there would be 1 glycerol head group and 1 C₁₈ alkyl tail group.

Table 2.2. Surfactants structures, suppliers and purities.

<u>Surfactant</u>	<u>Structure</u>	<u>Supplier</u>	<u>Purity / %</u>
Pluronic F127		BASF	>95
Arlacel 165		Croda International	>94
Cetostearyl alcohol		Cognis	>96
Sodium lauryl sulphate		Huntsman	>96
O _n G _n (O ₂ G ₁ shown)		Croda	blend

2.1.4 Silica particles

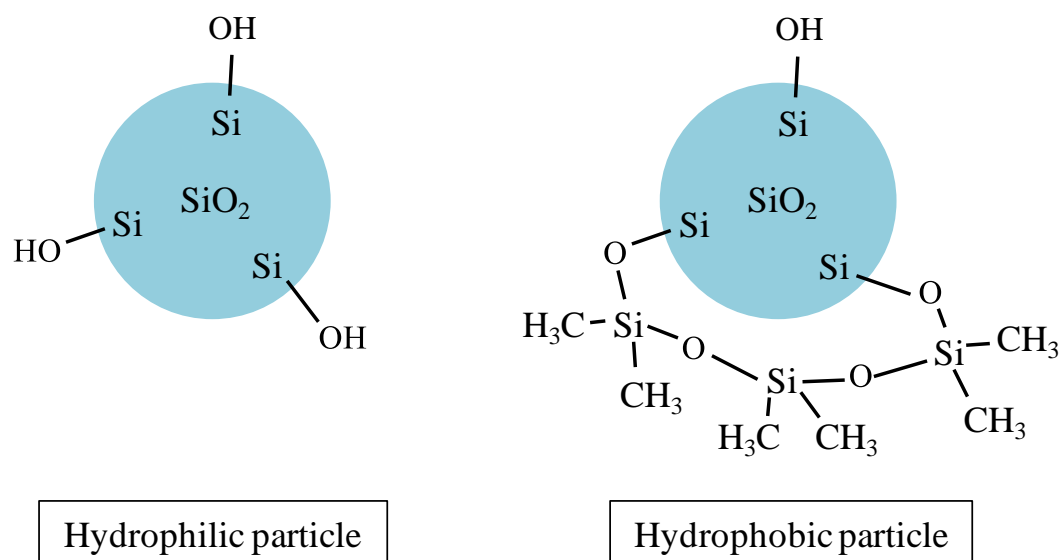
Silica particles with varying hydrophobicities were produced by high temperature hydrolysis of silicon tetrachloride in an oxygen-hydrogen flame provided by Wacker-Chemie in Burghausen, Germany.[3]



Throughout the flame process particles of SiO_2 collide and coalesce to give primary silica particles of 10 – 30 nm in diameter. Once cooled the primary particles form aggregates of 100 – 500 nm through collision and fusion. These silica particles are hydrophilic due to silanol (SiOH) groups present at the surface.[4]

Hydrophobic silica can be formed by modifying the silanol groups on the surface of the silica particles by reacting it with dichlorodimethylsilane vapour in the presence of molar amounts of water, followed by drying at 300 °C for 1 hour. This reaction results in the formation of dimethylsiloxy groups on the particle surface.[4, 5] Figure 2.1 shows the schematic representation of both hydrophobic and hydrophilic particles.

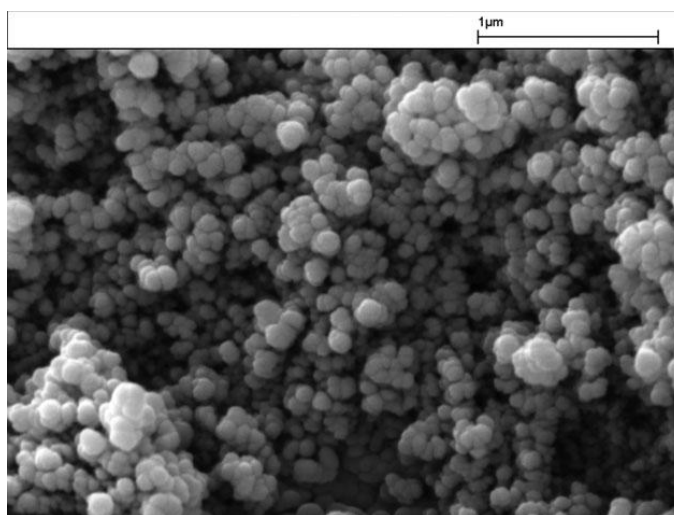
Figure 2.1. Schematic representation of both hydrophilic (before treatment with dichlorodimethylsilane) and hydrophobic (after treatment with dichlorodimethylsilane) silica particles.



Using the preparation discussed above the percentage of surface coverage of silanol groups can be varied from 100% SiOH (untreated with dichlorodimethylsilane) to a minimum of 14% SiOH (treated with dichlorodimethylsilane) by varying the reaction time and reactant concentration. The percent silanol content are measured using acid-base titration with sodium hydroxide and relative contents of silanol groups, after surface modification, were determined by dividing the silanol content of hydrophobic silica by the silanol content of initial hydrophilic silica (100% SiOH).[4]

The raw silica particles used during the silanisation process was a specific surface area of $200 \text{ m}^2 \text{ g}^{-1}$, and the density of silanol groups varied from 2 SiOH per nm^2 (100% SiOH) to 0.5 SiOH per nm^2 for the highly hydrophobic particles.[3] Figure 2.2 shows an SEM image of 20% SiOH silica primary particles and aggregates.

Figure 2.2. Scanning electron microscope image of fumed silica primary particles and aggregates with 20% SiOH surface chemistry as a dry powder.[6]



2.1.5 Glassware

All glassware was cleaned using a solution of 10 % w/w of KOH in ethanol, washed afterwards with copious amounts of Milli-Q water and dried in an oven at $45 \text{ }^\circ\text{C}$.

2.2 Methods

2.2.1 Solubility and phase diagram determination

The solubilities of the diols in oil phases were determined as follows. 5 mL of oil was accurately weighed into a thermostated and stirred sample tube. Small amounts of diol were then added sequentially using a $50 \text{ }\mu\text{L}$ syringe until phase separation was observed visually. The maximum amount of diol which could be added before phase separation was taken to be equal to the solubility of the diol in the oil. This was repeated at different temperatures, normally 20 and $70 \text{ }^\circ\text{C}$.

In addition to determining the solubility of diols in paraffin liquid, the solubility/partitioning of mixtures of water, diol and paraffin liquid were determined in the form of a ternary phase diagram. This was completed using the same process as the solubility determinations above, but with varying compositions of the three different

components; water, propane-1,2-diol and paraffin liquid at varying temperature of 20 and 70 °C.

2.2.2 Emulsion preparation

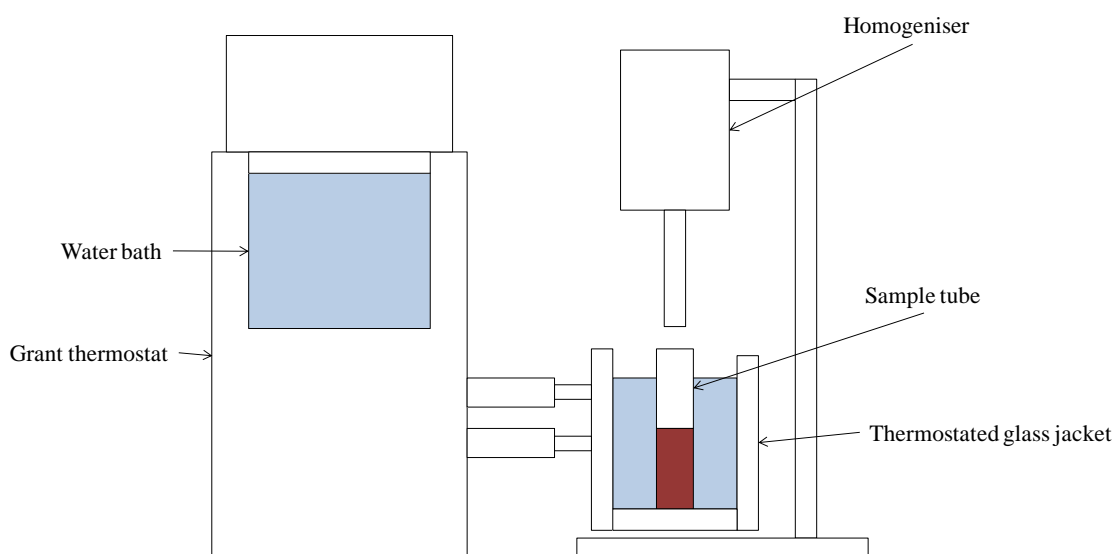
2.2.2.1 Surfactant-stabilised

The required amount of oil, water and/or diol was added in a one pot process with the required amount of surfactant. The rule was to half fill the vessel with the densest phase followed by the less dense phase and then finally add the surfactant. The sample was then left for 30 minutes to reach equilibrium at the appropriate temperature of interest.

The oil and aqueous phase plus surfactant were then emulsified using an IKA Ultra-Turrax T25 homogeniser with a rotor-stator head size varying from 8 or 18 mm. In some investigations a Silverson homogeniser was used. In all cases the homogeniser head was totally immersed in the mixture and homogenisation takes place for an appropriate amount of time at varying rpm. A batch process was employed, with 4 mM NaCl added to water or diol, or mixtures of the two. This was to ensure a trace amount of salt to identify a more abrupt change in conductivity which is discussed in emulsion characterisation.

A schematic representation of the experimental setup of the homogeniser and water bath and jacket is shown below in Figure 2.3.

Figure 2.3. Schematic representation of experimental setup used for the preparation of emulsion samples.



2.2.2.2 *Particle-stabilised*

As with the emulsion preparation in the surfactant systems, the appropriate amount of water/diol (containing 4 mM NaCl) and oil phase are calculated. Required amounts of particles (fumed silica with varying % SiOH) are added between the two phases as a powder, known as the powdered particle method. The systems are then emulsified using an IKA Ultra-Turrax T25 homogeniser (18 mm rotor stator head) at 13000 rpm for 5 minutes at a controlled temperature of interest.

2.2.3 Emulsion characterisation

2.2.3.1 *Drop test*

The continuous phase of the emulsion was determined by observing if a drop of emulsion dispersed or sedimented when added to either pure oil or aqueous phase of the corresponding emulsion. Emulsions with the aqueous phase as the continuous phase (o/w emulsions) tended to remain as drops in the oil and dispersed in the aqueous phase., the opposite being true for emulsions with oil as the continuous phase (w/o emulsions).

2.2.3.2 *Conductivity*

The findings of emulsion type by drop test are corroborated by conductivity measurements of the emulsions using a Jenway 3540 conductivity meter with platinum/platinum black electrodes immediately after homogenisation. The conductivity meter was calibrated using a standard solution of 0.01 M KCl.[7] High conductivity measurements indicate a water/diol continuous emulsion, and low measurements indicate oil continuous emulsions. An example of a high conductivity would be approximately $100 \mu\text{S cm}^{-1}$, whereas low measurements would be approximately $0 \mu\text{S cm}^{-1}$.

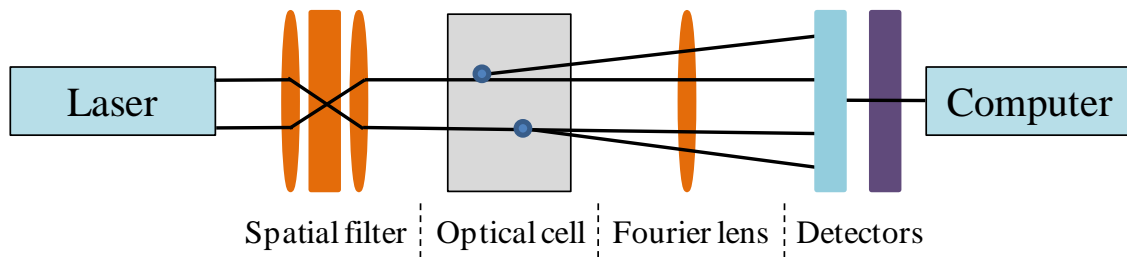
2.2.3.3 *Initial droplet size*

Two methods were used to determine the average droplet diameter of emulsions, and these are discussed below.

2.2.3.3.1 Light scattering

The average droplet diameter was determined by using a Malvern Mastersizer 2000 particle size analyzer from Malvern Instruments. A Helium-Neon laser beam of 633 nm wavelength are spatially filtered and collimated to produce a clean parallel beam of light. This beam is then focused using a Fourier lens to a photosensitive detector. The laser beam then passes through a pinhole at the centre of the detector and falls on a second detector known as the obscuration detector. If no particles are present in the sample port all light from the laser beam hit the obscuration detector. Whereas, if particles are introduced the light scatters at an angle inversely proportional to its size.[8] Scattering of the laser beam generates a scattering pattern of the droplet distribution which is subsequently analysed by the software using Mie light scattering theory.[9] See Figure 2.4.

Figure 2.4. Schematic representation of particle size analyzer (Mastersizer 2000).



Approximately 2 – 4 drops of emulsion sample were placed in the Malvern Mastersizer sample port (Hydro 2000SM), which contains the appropriate continuous phase of the emulsion (≈ 125 ml), approximately 100 – 200 dilution factor. Each sample flowed through the system using a Malvern dispersion unit controller which can be set between 100 - 3000 rpm. Malvern Mastersizer 2000 software then relayed the information of the analysis to the computer software. Producing a graph representing the volume percentage vs. droplet diameter and average values such as volume median diameter ($d(0.5)$), the volume mean diameter ($D[4, 3]$) and uniformity, U . The uniformity is defined as the absolute deviation from the median of a distribution of drops, and was calculated using the equation below,

$$U = \frac{\sum_i X_i |d(0.5) - d_i|}{d(0.5) \sum_i X_i} \quad (2.2)$$

where X_i is the number of drops having a diameter equal to d_i .

Measurements were taken at room temperature unless otherwise stated. The dispersed unit was cleaned between measurements by passing ethanol (approx. 100 ml) through, followed by washing twice with water. The calibration of the instrument was measured using latex particles with a known average diameter of 4 μm .

2.2.3.3.2 Microscopy

The initial droplet diameters determined by microscopy (Olympus BX51M), where the sample was placed on a microscope slide with a cover slip no later than 10 minutes after homogenisation. In certain cases the emulsion was diluted with the appropriate continuous phase, approximately 10 times dilution. The microscope was equipped so that different magnifications (4, 10, 20, 50 and 100x) were observed. Digital micrographs of 1366 x 768 pixels were obtained using a DP70 digital camera (Olympus) mounted on the microscope and represented the overall emulsion.

The mean diameters of the droplets were calculated from at least one hundred individual drop diameters measured using the digital micrographs and ImagePro Plus (Media Cybernetics) software. Calibration was done using a National Physical Laboratory calibration microscope slide, with the software calculating the size (μm) of each pixel. The slides were maintained at the appropriate temperature which varied for different investigations using a stage-mounted strip heater (Linkam CO102). This was placed on the microscope mount with a hole in the middle to allow light to pass through the heater and sample. The temperature of the stage was controlled using the strip heaters corresponding control unit (Linkam).

2.2.3.3.3 Freeze fracture cryo-scanning electron microscopy of emulsions

Freeze fracture cryo-scanning electron microscopy (cryo-SEM) was taken for emulsions containing water-propane-1,2-diol-paraffin liquid and stabilised by silica particle. The amount of propane-1,2-diol present in the aqueous was investigated. Cryo-SEM was achieved by plunging a drop of emulsion in slushed liquid nitrogen, known as plunge-frozen, and transferred to a Gatan Alto-2500 cryo-transfer unit. The sample was fractured and briefly warmed to $-95\text{ }^\circ\text{C}$ before re-cooling, platinum sputtered and transferred to a cold stage in a Hitachi S4500 field-emission scanning electron microscopy (SEM). The sample was maintained at $-160\text{ }^\circ\text{C}$ and imaged at an

accelerating voltage of 12 kV. Digital micrographs were collected using Quartz PCI (version 4.20) software.

2.2.4 Emulsion stability

By measuring the change in height of the clear water-emulsion (h_{aq}) and oil-emulsion (h_o) interface, and the height of the oil-emulsion (h_o) and water-emulsion (h_{aq}) interfaces respectively, the stability of emulsions, either o/w or w/o, to creaming/sedimentation and coalescence over time was determined. The stability was studied at different temperature for different investigations over 1 week to 6 months.

By using Equation (2.3) and (2.4), the fraction of continuous phase resolved (creaming/sedimentation) and dispersed phase resolved (coalescence and sometimes defined as f_d) was calculated over a desired time period of between 1 week and 6 months to assess the stability of emulsion samples,

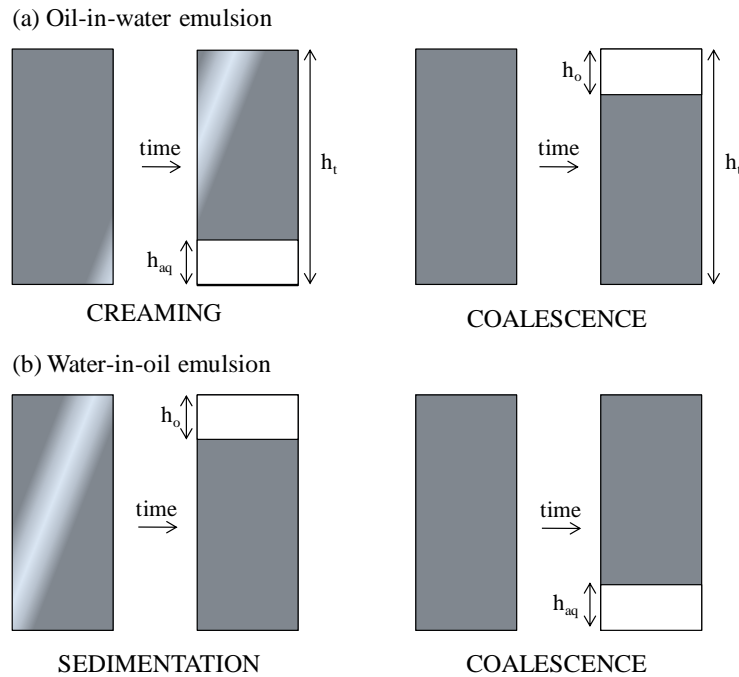
$$f_{\text{continuous phase resolved}} = \frac{h_{aq}}{h_t \times \Phi_{aq}} \quad (2.3)$$

$$f_{\text{dispersed phase resolved}} = \frac{h_o}{h_t \times \Phi_{oil}} \quad (2.4)$$

where h_{aq} is the height of the water-emulsion interface at any appropriate time after emulsification h_o is the height of the oil-emulsion interface at an appropriate time after emulsification and h_t is the total height of the emulsion including the height of the resolved oil and/or water. The fraction of creaming and/or coalescence was calculated relative to the volume fraction of aqueous (Φ_{aq}) and oil (Φ_{oil}) phase present in the emulsion. Depending on the emulsion type h_{aq} and h_o are interchangeable.

From the equations above a value of 1 in either would indicate complete phase separation (CPS) of the emulsion. Figure 2.5 shows the parameters used in the equations shown above.

Figure 2.5. Schematic of emulsion instability according to aqueous and/or oil resolved. It is assumed in this case that the oil phase is less dense than the aqueous phase.

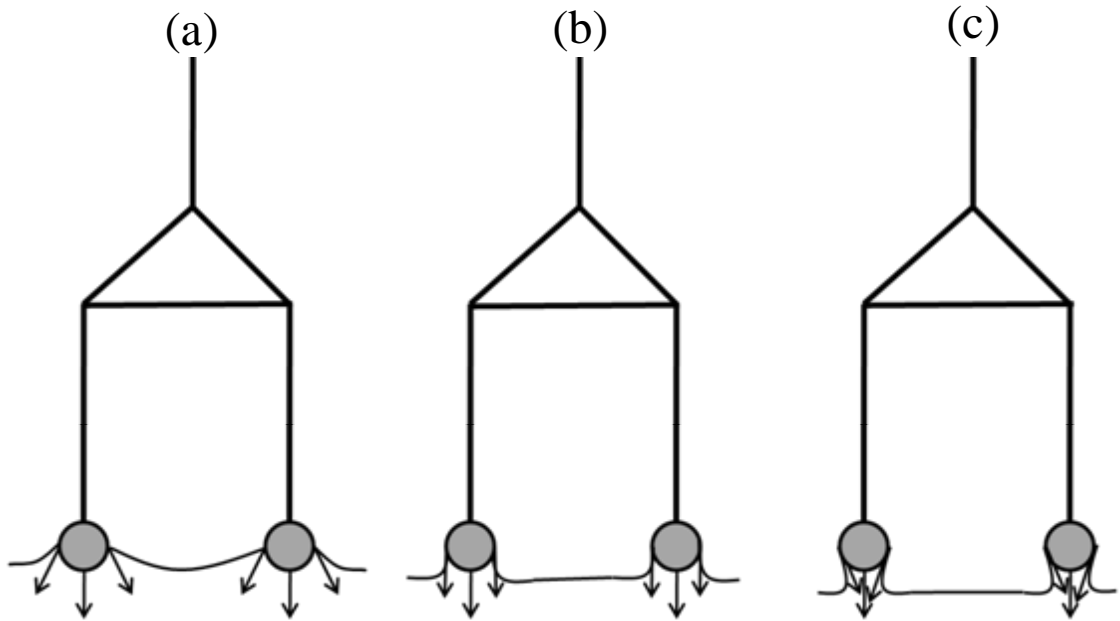


The emulsion samples were also monitored over time using photographs of the vessels taken using a Sony Cyber-shot DSC-S950 SteadyShot digital camera.

2.2.5 Tension measurements

The surface tensions of water, diol, mixtures of water/diol and paraffin liquid were determined as well as interfacial tensions of water/diol and paraffin liquid using the du Noüy ring method and a Krüss K10 digital tensiometer. The ring was made of an alloy of platinum and iridium and attached to a frame made from the same alloy. This was then suspended from a torsion balance horizontally over the surface/interface of the sample, before being submersed in the heavier phase and pulled through the surface or interface. Figure 2.6 shows the forces acting on the ring as it is pulled through a surface or interface.

Figure 2.6. Schematic of various stages during the measurement of surface/interfacial tension when using a du Noüy ring. (a) formation of meniscus, (b) maximum pulling force F , (c) near break down of the meniscus. Force is acting vertically up in all cases.



The maximum pulling force on the ring could be used to calculate the surface/interfacial tension by using the equation below,

$$F_p = Mg = 4\pi R\gamma \quad (2.5)$$

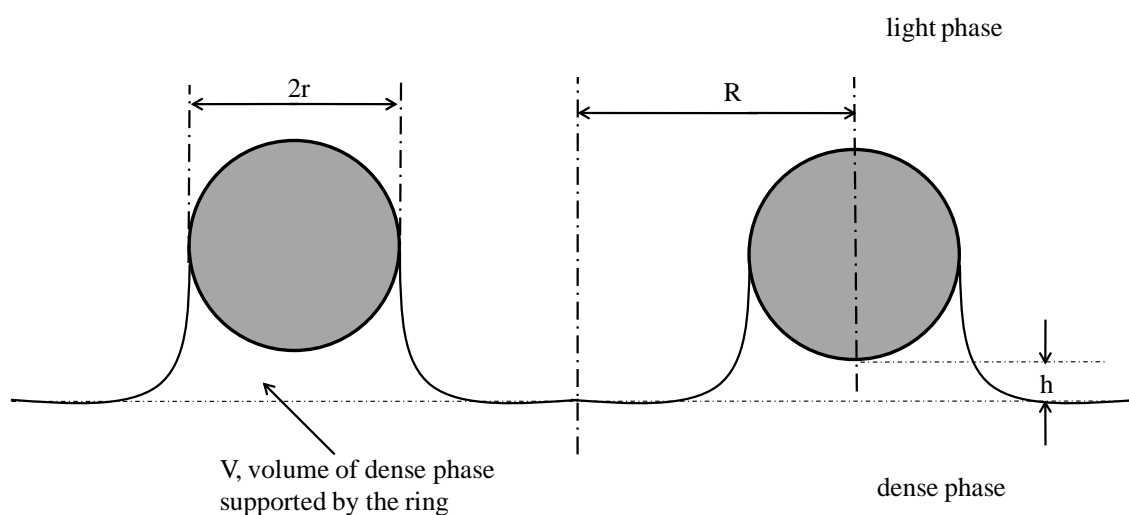
where M is the maximum weight of the liquid raised from the free surface of the liquid, g is the acceleration due to gravity, R is the radius of the du Noüy ring and γ is the surface tension.

However, it was found that the assumption made in equation (2.5) had significant error ($\pm 30\%$) when using the du Noüy ring, as it was shown that the measured value of tension from the du Noüy ring was not completely linear when compared directly to other tension measurement techniques, *e.g.* capillary method and spinning drop technique. Therefore, Harkins and Jordan showed that an alternative factor relating to the shape of the meniscus should be taken into account.[10] Due to this an adapted equation was given for the calculation of surface tension,

$$\gamma = \frac{Mg}{4\pi R} \times \alpha = \frac{\Delta\rho Vg\alpha}{4\pi R} \quad (2.6)$$

where V is the volume of dense phase supported by the ring and $\Delta\rho$ is the density difference between the two phases where the interface is being measured, α is the correction factor and is determined from the parameters of the ring (R^3/V and R/r), which were measured by comparing true values of surface tension measured via the capillary method. Harkins and Jordan tabulated many correction factors for different R/r values and their accuracy was proven to be within $\pm 0.25\%$ by Freud and Freud.[11] Zuidema and Waters later developed alterations for tensions lower than 25 mN m^{-1} . [12] For a schematic representation of the terms shown in equation (2.6) see Figure 2.7.

Figure 2.7. Schematic of cross sectional view of meniscus formed during the measurement of surface/interfacial tension.



The methods developed by Harkins and Jordan and also Zuidema and Waters were used throughout the tension measurements in this thesis, and were complete as follows.

All glassware was cleaned using KOH and washed with plenty of Milli-Q water. The du Noüy ring ($R = 9.545 \text{ mm}$, $r = 0.184 \text{ mm}$, $L(\text{wetted length}) = 11.995 \text{ mm}$) was placed in the lighter phase (air or oil) and zeroed using the tension instrument (Krüss K10). In the case of interfacial tension the ring was then removed and cleaned using a flame until the ring glows and placed in the heavy phase. The light phase (oil) was then placed gently on top of the heavy phase. Alternatively, for surface tension measurements the ring was directly immersed into the heavy phase as it is already clean. Tension was then measured between the light and heavy phase after 15 minutes of equilibration. The maximum pulling force was then measured and corrected using the appropriate factors.[10, 12]

Samples for measurements of interfacial tension, water/diol and paraffin liquid were pre-equilibrated before measurement. This included pre-mixing of the two phases by hand shaking for 30 seconds and then allowed to equilibrate over 48 hours before being separated and used. The samples were also thermostated (Grant LTD6G) at 20 °C during measurements and in all cases the volumes of the aqueous and oil phases were kept constant at a ratio of 1:1.

2.2.6 Mixtures of air, silica particles and aqueous propane-1,2-diol

Immersion time for silica powder in aqueous propane-1,2-diol solutions was determined as a method for showing the effect propane-1,2-diol has on the contact angle of particles at the air-polar phase interface. Immersion tests were achieved by carefully placing 25 mg of powder evenly on the surface of 10 cm³ of solution contained in a glass vessel of diameter 2.7 cm at room temperature. The time taken for all of the powder to enter the liquid was measured (if wetting occurred with 24 hrs).[13] Immersion times were determined for silica powders of different wettability (as defined by % SiOH) in water-propane-1,2-diol mixtures. The same samples were subsequently used to investigate the materials formed from aqueous propane-1,2-diol-silica-air mixtures. This was achieved by hand shaking the vessels for 30 sec. At room temperature and observing whether a dispersion, foam or climbing film formed. In addition, liquid marbles (macroscopic drops coated with particles in air) were formed by rolling a 50 µL drop of aqueous propane-1,2-diol on a bed of hydrophobic silica powder (14% SiOH) in a petri dish.[14]

2.2.7 Rheology

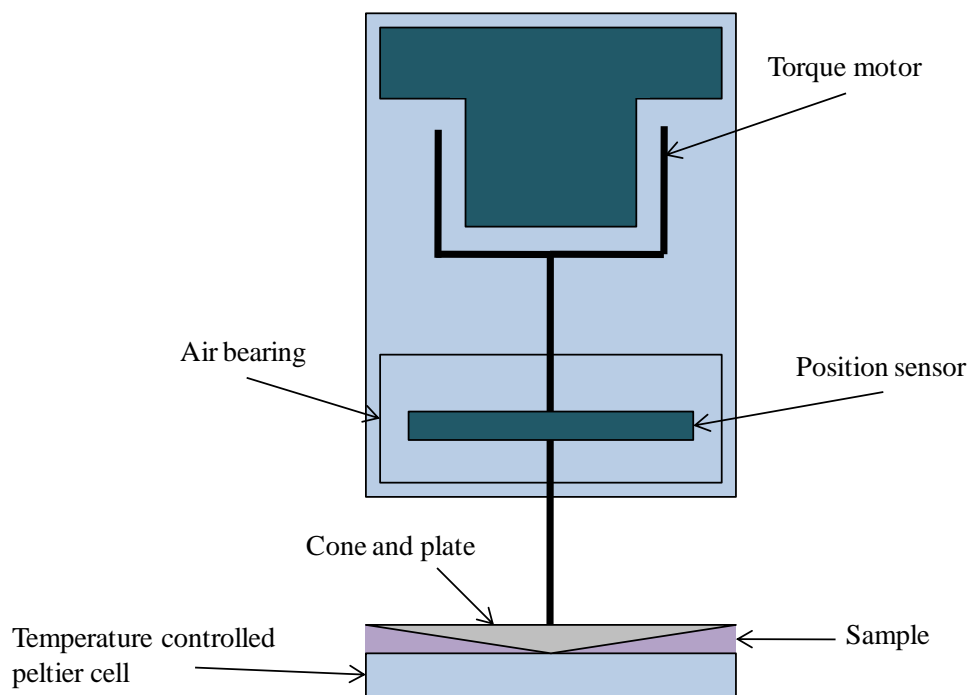
The viscosities of emulsions at various temperatures were determined using a Bohlin CVO rheometer. These measurements were used to identify a change in the viscosity of the emulsions due to crystallisation of the dispersed phase with varying droplet diameters. A schematic of the essential components is shown in Figure 2.8. The rheometer applies a controlled shear rate to the sample and detects the sample deformation as shear strain, which was then converted into shear stress using the cone and plate method.[15] The rheometer has a torque motor which applies a constant torque, and the angular position sensor detects the movement of the system being measured. Displacement of the emulsion sample from the constant torque was measured

using the position sensor and the Bohlin inbuilt software automatically converts the torque to shear stress. Viscosity was then calculated by the Bohlin software using the equation below,

$$\eta = \frac{\sigma}{\dot{\gamma}} \quad (2.7)$$

where σ is the shear stress in Pa and $\dot{\gamma}$ is the shear rate in s^{-1} .

Figure 2.8. Schematic representation of major components used in the Bohlin CVO rheometer.



Approximately 2 ml of emulsion sample was placed on the clean plate of the rheometer and the cone (4/40) was lowered to a gap of 150 μm . The geometry of the cone is described by two numbers, *e.g.* 4/40, where the first number indicates the angle of the cone and the second number showing the diameter of the cone. Any extruding sample from the cone and plate was then removed using a spatula; ensuring constant volume of sample.

Before measurements of viscosity versus temperature were started standard pre-conditions needed to be complete, which include a pre-shear for 30 min. at a shear rate equal to 5 s^{-1} . After which a temperature cycle was then completed ranging from 25 and 0 $^{\circ}\text{C}$, returning to 25 $^{\circ}\text{C}$ at a rate of 0.1 $^{\circ}\text{C min}^{-1}$. Explanation of the pre-conditions

used will be discussed in chapter 5 which relates to the use of the rheometer. The arguments will be based on the emulsion stability and equilibrium conditions.

Viscosity measurements were then taken throughout the procedure creating a plot of viscosity versus temperature. Plots of temperature versus time were generated to ensure the peltier cell had swept through the temperature cycle at the required set rate of 0.1 °C min⁻¹.

2.2.8 Differential scanning calorimetry

Differential scanning calorimetry (DSC) was used to investigate the thermal behaviour of two o/w emulsions with varying droplet diameter to determine the range of temperature that melting occurred, as well as the enthalpy change associated with the melting transition.

The DSC calorimeter records a change in exo- or endo-thermal effect in the sample by eliminating the difference between the sample and a reference sample, normally an empty pan. To record a change in exo- or endo-thermal effect two circuits were used to control the average and differential temperature within the DSC chamber. The first circuit regulates a constant temperature ramp whereas the second detects a thermal change and eliminates the change using the heater current. This double circuit allows the two sample ports to remain at the same temperature, while the difference in the two circuits is directly correlated to the quantity of heat per unit time, dq/dt , and recorded as a function of temperature.

Gray showed that the absorption/evolution of heat by a sample per unit time, dH/dt , are represented by the sum of three components presented in the equation below,[16]

$$\frac{dH}{dt} = -\frac{dq}{dt} + (C_s - C_r) \frac{dT}{dt} - RC_s d^2 \frac{q}{dt^2} \quad (2.8)$$

Where the first component is the recorded heat flux of the sample (*i.e.* the experimental curve), the second component shows the heat capacities of the sample and the reference (C_s and C_r) and the rate of temperature change during heating (dT/dt). Displacement of the baseline from zero is represented by this component. The third component is the gradient of the experiment curve in multiples of constant RC_s , where R is the thermal resistance of the sample.

Calculations from DSC curves were not as simple as indicated by Gray and had significant error, *i.e.* dq/dt is not the real heat flux dH/dt . The error which occurred was that the DSC curves slightly shifted the T_{\max} value to higher values (known as thermal lag), and are proportional to the constant RC_s . It is possible to minimise this error by reducing the thermal resistance (R) using small samples. However, the heat effect relating to the DSC curve had to be corrected using calibration. This is equal to the change in enthalpy of the sample ($\Delta q = -\Delta H$). The calibration uses the coefficient K_H which directly relates the area S of the peak between the DSC curve and the baseline to ΔH .

$$\Delta H = K_H .S \quad (2.9)$$

K_H was determined by calibration using an indium standard.

DSC measurements using the theory discussed above were used in analysis according to the following procedure. A Mettler Toledo DSC-822^e instrument was used where dry nitrogen was used as the purge gas. Emulsion or oil samples (≈ 3 mg) were placed in sealed aluminium pans which were run alongside an empty pan. Temperature scans began with the samples held for 10 min. at 25 °C followed by heating at a particular rate (10 °C/min) to a start temperature of 70 °C. This was immediately followed by cooling at the same rate, with a second heating–cooling cycle subsequently. The results were plotted as heat flow as a function of temperature, and the system software was used to obtain the onset, major peak and end of the melting/solidification transitions, while the associated heats were calculated by standard methods.

2.2.9 Nuclear magnetic resonance

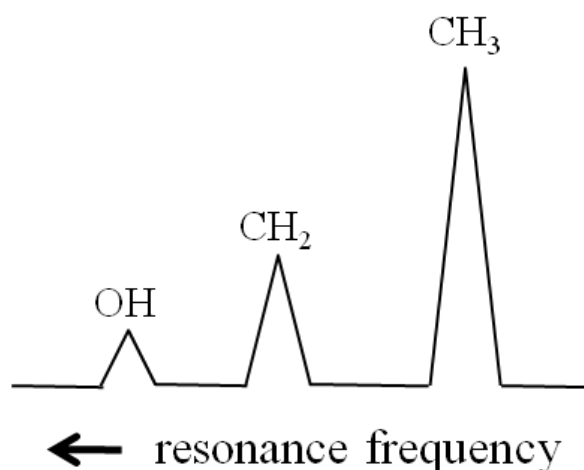
Nuclear magnetic resonance (NMR) was used in the investigation of o/w emulsions with varying droplet diameter. Measurements were performed in a liquid state in a Bruker - AVANCE™ II – 500 MHz instrument. The desired results were to establish crystallisation characteristics using the corresponding spectra of the emulsions with changing temperature. NMR was chosen due to its sensitivity in delicate measurements of nuclear magnetic moments within atomic nuclei with changing physical properties.[17] If a magnetic nucleus is placed into a magnetic field, *e.g.* a nucleus of a hydrogen atom (the proton) it can be present in two orientations, one in the direction of

the field and the other in the opposite direction to the field. These two states are separated by energy, ΔE , which can be measured by applying electromagnetic radiation at a certain frequency, ν . The frequency required to flip the nucleus from the lower state to the upper state is measured, and the energy determined using the resonance condition,

$$\Delta E = h\nu \quad (2.10)$$

where h is Plank's constant. Fortunately, the resonance frequencies of molecules are slightly different for different chemical environments and hence allows for sensitive measurements. This effect is known as chemical shift, see Figure 2.9, and can be used to probe individual atoms within molecules by using well established knowledge of chemical shifts, integration and peak splitting.

Figure 2.9. ^1H NMR spectrum of liquid ethanol, $\text{CH}_3\text{CH}_2\text{OH}$. Re-drawn from [17].



In this project NMR was used to probe the solidification properties of emulsions by using the effect on peak broadening, due to the reduced mobility of molecules as they freeze, *i.e.* liquid samples give good resolution of peaks, whereas solid samples tend to give broad peaks.[18-20] All NMR experiments were carried out on a Bruker - AVANCE™ II – 500 MHz spectrometer using a 10 cm liquid probe operating at frequency of 500.1025 MHz (^1H). Spectra were externally referenced to tetramethylsilane at 0 ppm. Experiments were conducted with a typical $\pi/2$ pulse length of 7 μs and a relaxation delay of 4 s. NMR measurements of approximately 1 ml of emulsion are made at different temperatures, where the temperature of the probe and sample is controlled using the systems built-in software. All investigations started at a

temperature of 60 °C, which decreased to 0 °C and then returned to 60 °C, recording a spectrum every 5 – 2 °C. The temperature gradient was 1 °C min⁻¹. Data processing was complete using Topspin version 1.3 (Bruker Instruments, Karlsruhe, Germany). Analysis of spectra was complete using ACD/LAB NMR processor software (version 12.01), which utilised Gauss+Lorentz theory to predict peak parameters such as full width at half height (FWHH), integration and peak assignment.

2.3 References

1. R. Nagarajan, *Langmuir*, **18**, 31 (2001).
2. D. R. Lide (ed.), *CRC Handbook of Chemistry and Physics 90th Edition*, CRC Press, Boca Raton (2009).
3. Wacker HDK[®] Fumed Silica Product Information, *Wacker-Chemie GmbH* Germany (2000).
4. H. Barthel, *Colloids Surf. A*, **101**, 217 (1995).
5. R. K. Iler, *The Chemistry of Silica*, John Wiley & Sons, New York (1979).
6. B. P. Binks, P. D. I. Fletcher, B. L. Holt, P. Beaussoubre and K. Wong, *Phys. Chem. Chem. Phys.*, **12**, 11954 (2010).
7. Jenway 4310 Conductivity Meter Manual, *Jenway* UK.
8. The Mastersizer family of particle characterisation systems - Brochure MRK 251A, *Malvern Instruments* UK.
9. Principles of Particle Size Analysis - Technical paper MRK034, *Malvern Instruments* UK.
10. W. D. Harkins and H. F. Jordan, *J. Am. Chem. Soc.*, **52**, 1751 (1930).
11. B. B. Freud and H. Z. Freud, *J. Am. Chem. Soc.*, **52**, 1772 (1930).
12. H. Zuidema and G. Waters, *Ind. Eng. Chem. Anal. Ed.*, **13**, 312 (1941).
13. R. Benitez, S. Contreras and J. Goldfarb, *J. Colloid Interface Sci.*, **36**, 146 (1971).
14. P. Aussillous and D. Quéré, *Nature*, **411**, 924 (2001).
15. Bohlin CVO User Manual, *Bohlin Instruments* UK (2001).
16. A. Gray, *Analytical Calorimetry*, Plenum Press, New York (1977).
17. P. J. Hore, *Nuclear Magnetic Resonance*, Oxford University Press, Oxford (1995).
18. E. Andrew, *J. Chem. Phys.*, **18**, 607 (1950).
19. J. Rault, R. Neffati and P. Judeinstein, *Eur. Phys. J. B*, **36**, 627 (2003).
20. P. Apte and B. H. Suits, *NanoStruct. Mater.*, **10**, 917 (1998).

CHAPTER 3. EFFECT OF ADDING DIOL INTO SURFACTANT STABILISED EMULSIONS

3.1 Introduction

Emulsions are thermodynamically unstable dispersions of one liquid in a second immiscible liquid where the two liquids are normally a polar aqueous phase and an apolar oil phase. Emulsions can be made kinetically stable by the addition of a suitable stabiliser which adsorbs on the droplet surfaces and renders them stable with respect to the possible breakdown processes of flocculation, sedimentation or creaming, Ostwald ripening and coalescence.

Stable emulsions are important in a wide range of diverse applications in sectors including the household cleaner, personal care, cosmetics and pharmaceutical fields.

However, within the pharmaceutical industry, the majority of emulsions are designed for drug delivery through skin application and contain not only water, oil, stabilising surfactant and pharmaceutically-active species, but also high concentrations of added polar diol (glycol) species such as propane-1,2-diol (propylene glycol). Diols are added to these products mainly to enhance penetration of active species, improve the solubility of the active species and as anti-microbial preservatives.[1-3] In some cases the addition of diol has been used as a formulation aspect for product design, an example being the preparation of transparent emulsions through refractive index matching.[4]

Although the use of diols in emulsions is high within certain industrial sectors there are a limited number of studies investigating the effect of adding such components to conventional emulsions and for this reason it is not fully understood.[5-9] Therefore, the main aims of the investigations described in this chapter are to understand how the addition of various diols to emulsions containing water, paraffin liquid and non-ionic surfactants effect the characteristic properties of the emulsion and in turn how these can be used to give formulation rationale.

To investigate this, the tendency of emulsions to phase invert with the addition of diols was determined. This allows for understanding of emulsion properties and characteristics to be rationalised in terms of the properties of the equilibrium multi-phase liquid systems from which they are prepared by energy input through the

emulsification process.[10-13] Hence, the findings can be used to understand the effect of adding diol to emulsions and secondly to understand the fundamental principles of diol interactions at the oil-water interface.

To understand the relationship between the equilibrium phase behaviour of equal volumes of oil, water and surfactant and emulsions prepared from them, the behaviour of the equilibrium systems are first summarised. Addition of surfactant at an overall concentration less than a critical value (cac) yields two co-existing liquid phases containing monomeric (non-aggregated) surfactant molecules which distribute between the water and oil phases with distribution coefficient K_{ow} . [14-16]

$$K_{ow} = \frac{[\text{surfactant monomer}]_{oil}}{[\text{surfactant monomer}]_{water}} \quad (3.1)$$

For a system with oil and water volume fractions Φ_{oil} and Φ_{water} , the overall surfactant concentration is

$$[\text{surfactant}]_{ov} = \Phi_{oil}[\text{surfactant}]_{oil} + \Phi_{aq}[\text{surfactant}]_{aq} \quad (3.2)$$

As the overall surfactant concentration is increased, the monomer concentrations in both the oil and aqueous phases increase in the ratio K_{ow} until the critical concentration at which aggregation occurs is reached.

Addition of further surfactant such that $[\text{surfactant}]_{ov} > cac$ produces equilibrium liquid phases which contain monomeric surfactant at concentrations equal to cac_{oil} and cac_{water} in the oil and water phases plus aggregated surfactant in *either* the oil, the water or a third phase.[17-23] A hydrophilic surfactant will form a Winsor I (WI) system consisting of an o/w microemulsion phase coexisting with an excess oil phase. A hydrophobic surfactant will form a Winsor II (WII) system of a w/o microemulsion with a coexisting aqueous phase. A surfactant of the appropriate intermediate hydrophilicity will form a Winsor III (WIII); a three-phase system consisting of excess oil and aqueous phases coexisting with a third phase containing all the aggregated surfactant in the form of either a bicontinuous microemulsion or lamellar liquid crystalline phase.

The oil-water interfacial tension decreases progressively from the value for a “bare” oil-water interface (of the order of 40 mN m^{-1}) down to a value of a few mN m^{-1} or less due

to monomeric surfactant adsorption as $[\text{surfactant}]_{\text{ov}}$ increases from zero to value cac . For $[\text{surfactant}]_{\text{ov}} > cac$, the tension is independent of surfactant concentration at a constant value γ_c since the additional surfactant is in the form of aggregates which are not surface active. If a system condition (e.g. surfactant hydrophilicity, temperature, electrolyte concentration) is altered so that they have the phase sequence WI-WIII-WII, microemulsion phase inversion is observed and the tension, γ_c , will pass through a minimum, which may be ultralow, e.g. $< 10^{-3} \text{ mN m}^{-1}$.

As discussed in chapter 1, the system conditions that affect the phase sequence of Winsor systems, *i.e.*, temperature, surfactant hydrophilicity and electrolyte concentration all related to an effective change in the preferred surfactant monolayer curvature, where by convention, negative values correspond to w/o microemulsions and positive values to o/w microemulsions.

When a Winsor equilibrium multiphase system is emulsified there is a relationship between the properties of the prepared emulsion and the equilibrium system from which it is prepared.[10-13] The main features of this relationship are four-fold:

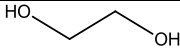
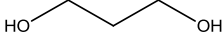
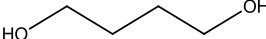
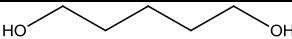
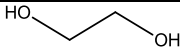
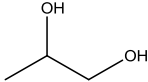
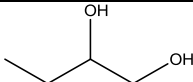
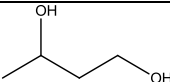
- Emulsification of a system with overall surfactant concentration $< cac$ does not produce a stable emulsion owing to less than maximum surfactant adsorption at the droplet surfaces and the increased oil-water tension.
- For systems with $[\text{surfactant}]_{\text{ov}} > cac$ and containing equal volumes of oil and aqueous phases, emulsification of a WI system always gives an o/w emulsion and a WII system always produces a w/o emulsion. Emulsification of a three-phase WIII system can produce a variety of multiple emulsions.[24, 25]
- Since emulsion formation increases the amount of oil-water interface, the energy cost is proportional to the oil-water interfacial tension. Hence, when emulsions are formed using a constant energy input, minimum emulsion drop size (maximum oil-water interface created) is observed under conditions corresponding to microemulsion phase inversion when γ_c is a minimum.

- Emulsion stability with respect to drop coalescence is generally high under conditions far from microemulsion phase inversion and low close to microemulsion phase inversion.

This chapter describes how the type of emulsion formed, the droplet sizes and emulsion stability vary with the addition of a range of pharmaceutically-relevant diols. The aim is to understand whether the effects of diol addition follow the patterns of behaviour discussed above and thus to establish formulation design principles applicable to these systems.

The emulsion system used to examine these characteristics always contained equal volumes of polar and non-polar components, in this case water/diol, paraffin liquid and non-ionic surfactant as a stabiliser. The diols investigated are discussed in three distinct groups, described here as, 1,2-diols, α,ω -diols and moving alcohol position. Table 3.1 shows the structure relating to each group.

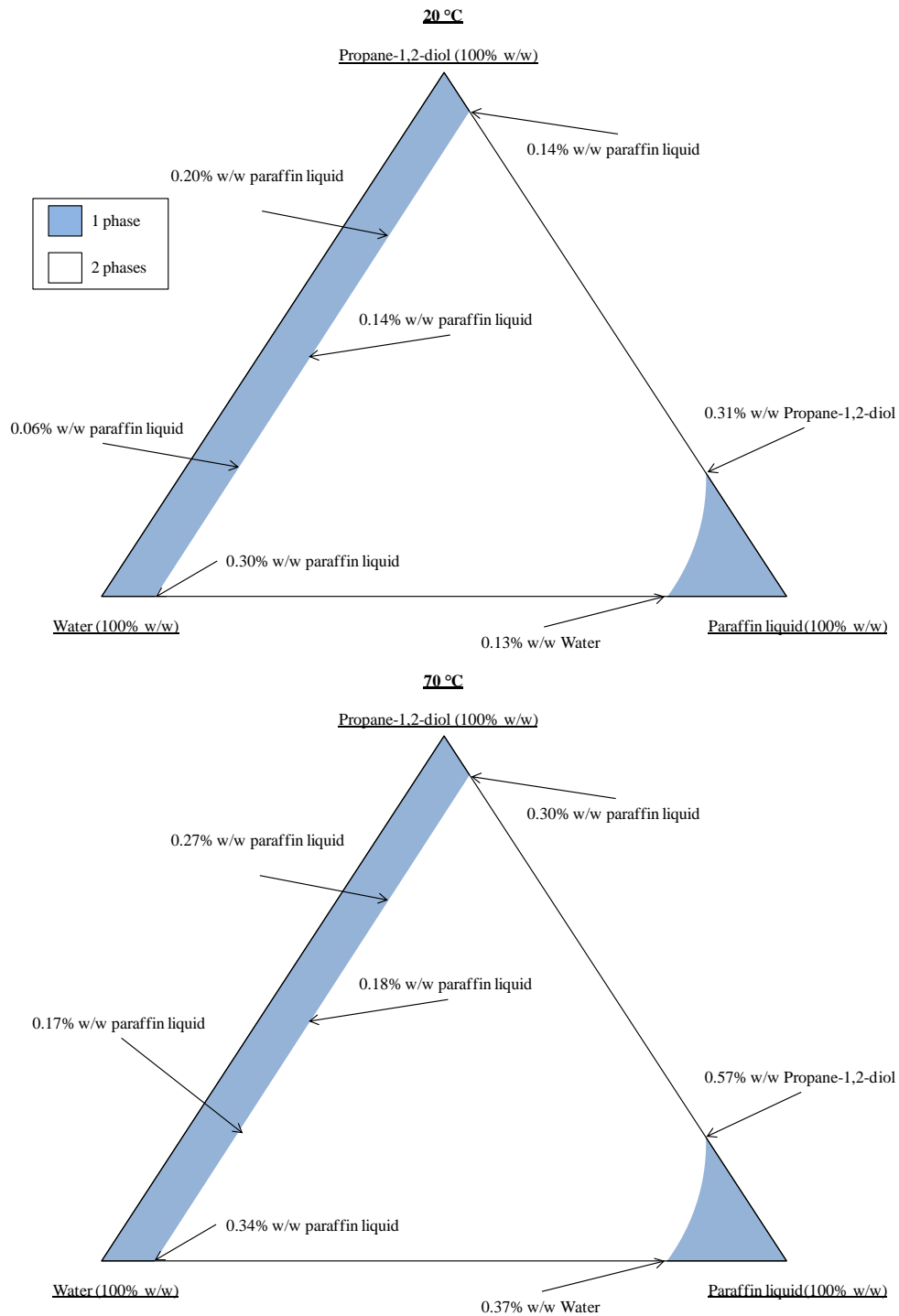
Table 3.1. Structures of diols used, shown in groups of interest.

<u>Diol IUPAC name</u>	<u>Diol structure</u>
<u>α,ω-diols</u>	
Ethane-1,2-diol	
Propane-1,3-diol	
Butane-1,4-diol	
Pentane-1,5-diol	
<u>1,2-diols</u>	
Ethane-1,2-diol	
Propane-1,2-diol	
Butane-1,2-diol	
<u>Moving alcohol position</u>	
Butane-1,3-diol	

3.2 Diol partitioning and solubilities

Before investigations into the emulsion behaviour of water, diol, paraffin liquid and non-ionic surfactants could begin there was a need to understand the partitioning of diol between the water and oil. This was required so that volumes of the immiscible phases (oil and water/diol) were kept constant at emulsification so that the equilibrium multi-phase liquid system properties discussed above are relevant. To establish this, a ternary phase diagram of water, propane-1,2-diol and paraffin liquid was determined at two temperatures of 20 and 70 °C. In addition, the solubilities of the remaining diols in paraffin liquid were determined to establish the extent of diol partitioning between water and oil.

Figure 3.1. A schematic ternary phase diagram of water, propane-1,2-diol and paraffin liquid at 20 °C (upper schematic) and 70 °C (lower schematic). The arrows indicate the actual compositions measured. Raw data available in Appendix.



The ternary phase diagram (Figure 3.1) illustrates that water and propane-1,2-diol are completely miscible and that a small amount of oil is miscible with propane-1,2-diol, water and mixtures of the two. These values range from as little as 0.06 to 0.34% w/w in water/propane-1,2-diol mixtures.

Increasing the temperature from 20 to 70 °C shows a general increase in the partitioning of water/diol mixtures into the oil and a slight increase in the extent of oil partitioning into the water/diol mixtures. However, the amount of partitioning is very limited, $\leq 0.57\%$ w/w for either water/diol into oil or oil into water/diol. Because of the negligible mutual miscibilities of the diol, water and paraffin liquid mixtures it can, to good approximation, be treated that diol can be added in place of water to maintain the equal volumes of aqueous (water+diol) and paraffin liquid in the emulsion samples for investigation and therefore described as a pseudo-ternary system.

For all other diols, it was established first that they were miscible in all proportions with water and the solubilities of all the diols were determined in paraffin liquid to determine the extent of diol-paraffin liquid partitioning. Results from ternary phase diagram and solubility studies indicate that all diol systems can be treated as pseudo-binary.

Table 3.2. Diol solubility in paraffin liquid at 20 °C.

<u>Diol</u>	<u>Diol solubility in paraffin oil/% w/w</u>
Ethane-1,2-diol	0.13 ± 0.03
Propane-1,3-diol	0.24 ± 0.01
Butane-1,4-diol	0.40 ± 0.03
Pentane-1,5-diol	0.47 ± 0.03
Propane-1,2-diol	0.31 ± 0.06
Butane-1,2-diol	0.32 ± 0.03
Butane-1,3-diol	0.34 ± 0.03

3.3 *Effect of diol addition on emulsion type and phase inversion*

The effect of diol addition on the type of emulsion formed was determined by measuring the electrical conductivity of the emulsions immediately after preparation and confirmed using the drop test method. Figure 3.2 shows systems containing equal

volumes of oil and mixed diol + water aqueous phases and 4% w/w of $O_{1.4}G_1$ non-ionic surfactant form w/o emulsions (with low conductivity) with no diol present; on addition of diol the emulsion type switches to o/w (with high conductivity). Figure 3.2 shows that diol addition to an emulsion (in replacement of water) causes the preferred curvature of the adsorbed $O_{1.4}G_1$ surfactant monolayer to change progressively from a negative value producing w/o drops to positive values producing o/w drops.

A similar effect of ethane-1,2-diol substitution for water causing increased positive preferred curvature of the surfactant film has been observed previously for microemulsion systems stabilised by an anionic surfactant.[26] It is shown by Aveyard *et al.* that changing the entire polar phase of a microemulsion system containing AOT (sodium bis(2-ethylhexyl)sulfosuccinate) and equal volumes of oil (toluene) and polar phase from water to ethane-1,2-diol, the required amount of salt to cause microemulsion inversion from WI-WIII-WII is dramatically increased. This shows that the required amount of salt needed to screen the electrostatic repulsion between adjacent heads of the surfactant and hence change the preferred surfactant monolayer curvature to negative is much larger in an ethane-1,2-diol-toluene system than in a water-toluene system. Hence, the addition of diol causes a change in the equilibrium preferred monolayer curvature to more positive.

Figure 3.2. Conductivity of emulsions versus mole fraction of diol in the aqueous phase. Measurements taken immediately after emulsification at 20 ± 2 °C. Sharp increases in conductivity indicate a change in emulsion type from w/o to o/w emulsions. Each system contains 4% w/w $O_{1.4}G_1$, equal volumes paraffin liquid and water/diol. Legend identifies the diol representing each series.

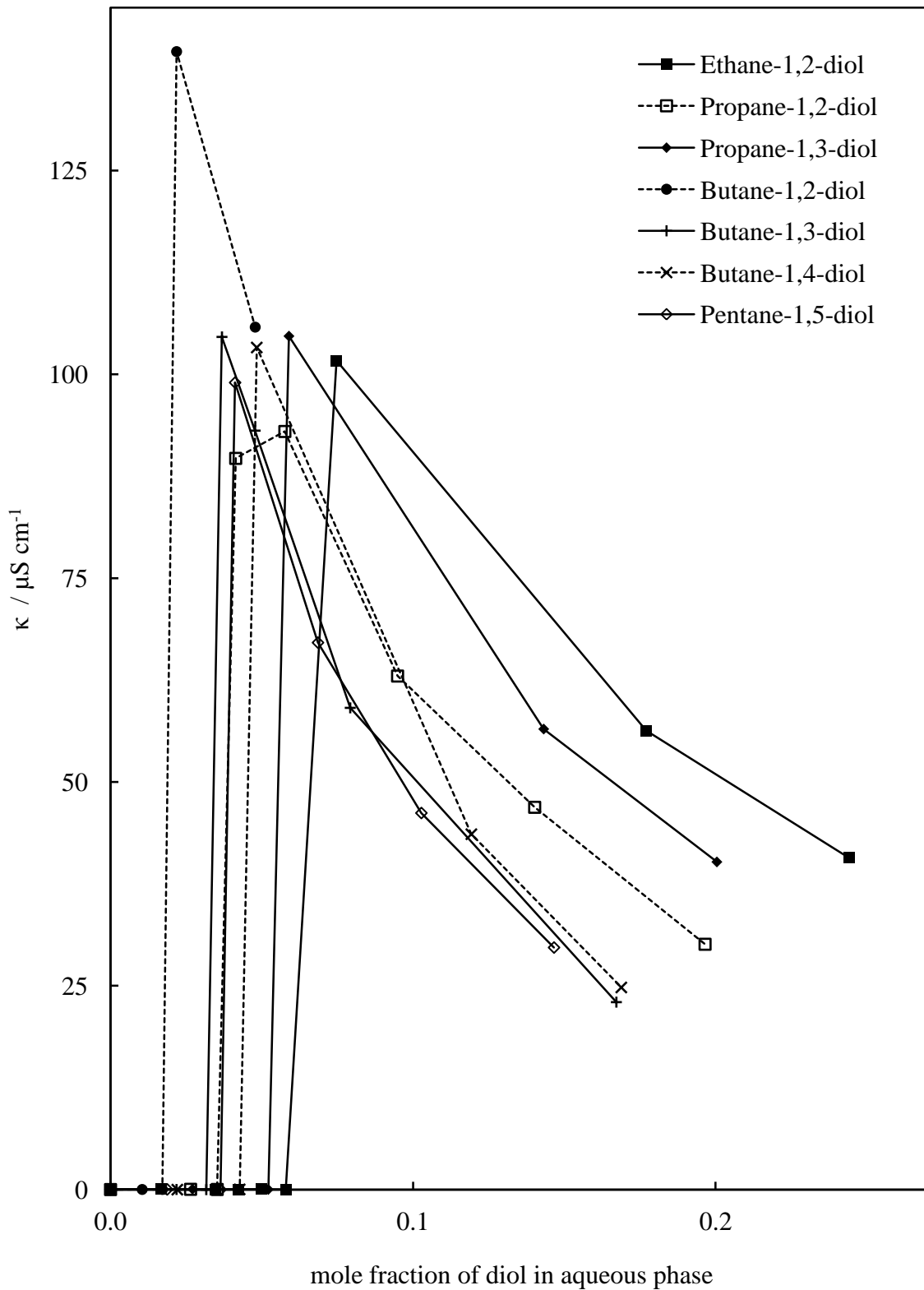


Figure 3.3. Comparison between the amounts of diol required to cause phase inversion versus the number of carbon atoms in diols for emulsions containing equal volumes of (water+diol) and oil phase with 4% w/w O_{1,4}G₁ surfactant at 20 °C.

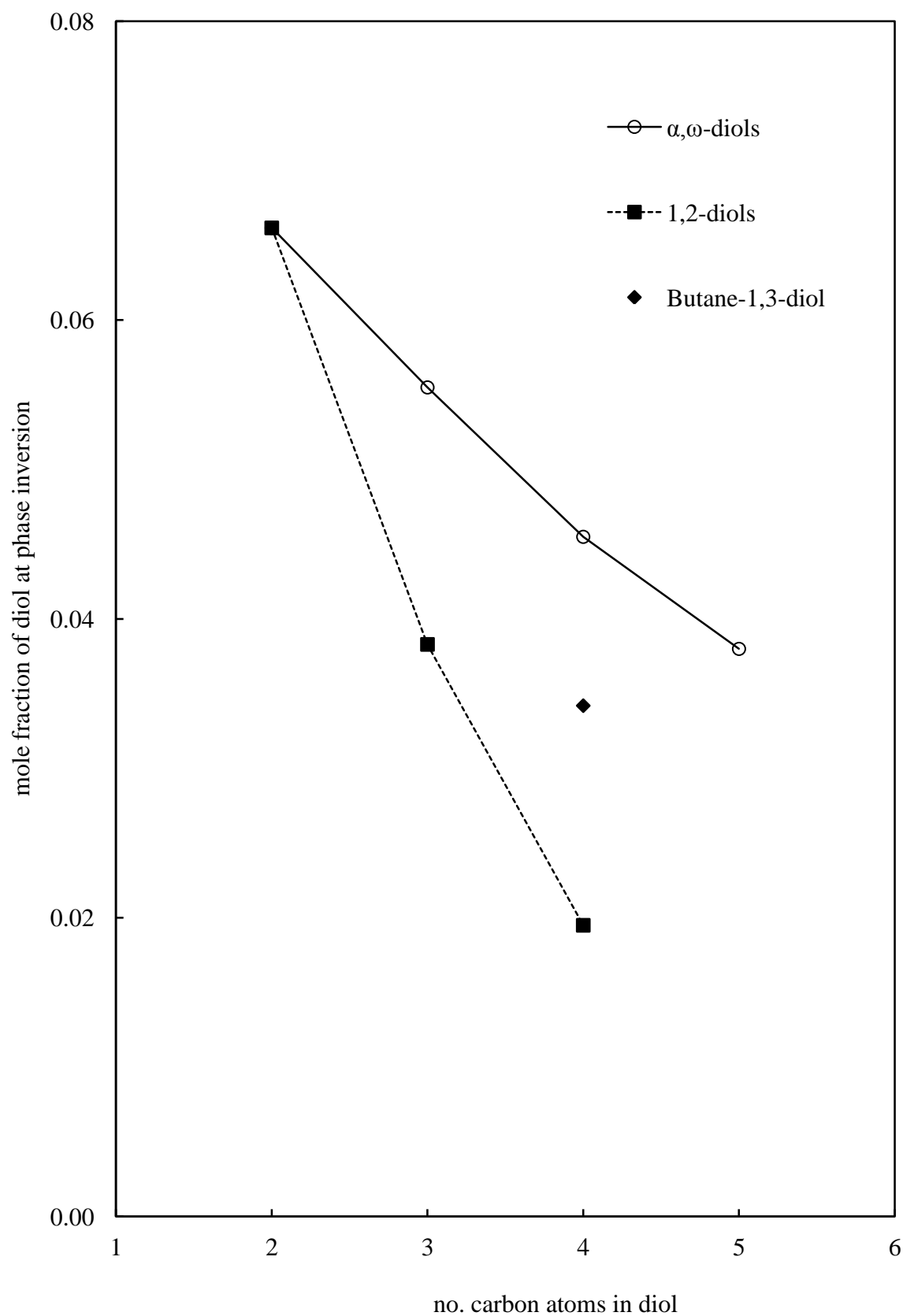


Figure 3.3 compares the variation of diol mole fraction required to cause emulsion phase inversion (X_{pi}) with the number of carbon atoms in the diol for each separate diol series. Diols with higher carbon atom numbers (which are more hydrophobic) cause phase inversion at lower concentrations than more hydrophilic diols. In addition, the series of α,ω -diols and 1,2-diols fall on separate curves with the butane-1,3-diol value lying between the values for butane-1,2-diol and butane-1,4-diol.

The emulsion phase inversion results described above suggest that the diols change the preferred monolayer curvature of the surfactant from negative to positive by co-adsorbing at the oil-water interface in a manner that swells the headgroup region of the main surfactant. To test this explanation, one strategy would be to measure interfacial tension as a function of diol to determine the tendency of the different diols to co-adsorb in the presence of a fixed concentration of $O_{1,4}G_1$ surfactant and observe whether the relative adsorptions of the different diols correlate with the diol concentrations required to achieve phase inversion. However, as noted in the experimental section, the $O_{1,4}G_1$ surfactant used here is a commercial blend containing a distribution of structures around the average structure with the consequence that tension results for these complex mixtures of surfactant species are unlikely to be amenable to analysis in terms of the Gibbs adsorption equation. For this reason, tension measurements as a function of diol concentration to measure their tendency to adsorb to the “bare” oil-water interface in the absence of the $O_{1,4}G_1$ surfactant were measured.

Figure 3.4. Surface pressure versus the mole fraction of diol in the aqueous phase for water – paraffin liquid interface at 20 °C. The interfacial tension of the pure water-paraffin oil interface is 44.5 mN m⁻¹.

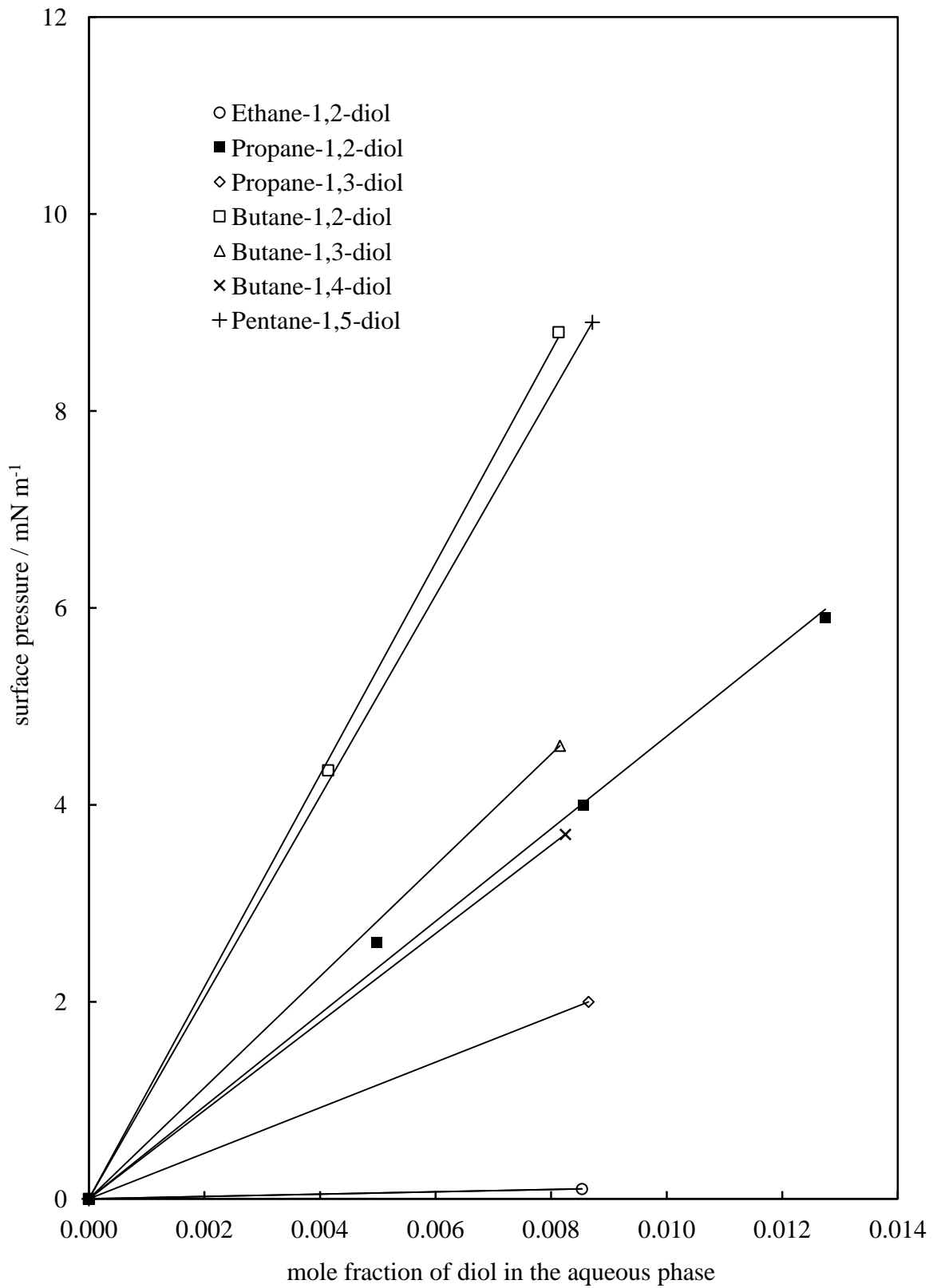


Figure 3.4 shows plots of the variation of surface pressure Π (equal to the difference in oil-water tension in the absence and presence of added diol) with aqueous phase diol mole fraction for adsorption from water to the water-paraffin oil interface. For the low diol concentration range studied the plots are linear and can be used to derive the standard molar Gibbs free energy of adsorption $\Delta G_{\text{ads}}^{\circ}$ for the different diols. Choosing unit mole fraction (behaving ideally) as the solution standard state and a surface pressure of 1 mN m^{-1} (obeying the ideal 2D gas equation) for the surface standard state, $\Delta G_{\text{ads}}^{\circ}$ is given by,[27]

$$\Delta G_{\text{ads}}^{\circ} = -RT \ln(d\Pi/dX)_{X \rightarrow 0} \quad (3.3)$$

where R is the gas constant and T is the absolute temperature. Using the derived $\Delta G_{\text{ads}}^{\circ}$ values determined from the linear trends in Figure 3.4 for each diol at the ‘bare’ oil/water interface Figure 3.5 shows the correlation between X_{pi} and $\Delta G_{\text{ads}}^{\circ}$.

It can be seen that the more strongly adsorbing diols (i.e. those for which $\Delta G_{\text{ads}}^{\circ}$ is large and negative) cause emulsion phase inversion at lower concentrations. However, the data do not all lie on a single curve; the α,ω - and 1,2-diol series remain separated. This lack of a “universal” correlation is probably a consequence of the fact that the $\Delta G_{\text{ads}}^{\circ}$ values measured here reflect the tendency to adsorb to a “bare” oil water interface rather than the tendency of the diols to coadsorb competitively with the $\text{O}_{1.4}\text{G}_1$ surfactant and swell the headgroup region of the $\text{O}_{1.4}\text{G}_1$ adsorbed film.

Figure 3.6 shows a plot of $\Delta G_{\text{ads}}^{\circ}$ versus number of carbon atoms in the diol where it can be seen that, for the same number of carbon atoms, the 1,2-diols are more surface active than the α,ω -diols. The increments in $\Delta G_{\text{ads}}^{\circ}$ per additional carbon atom in the diols are -1.8 and -2.0 kJ mol^{-1} for the α,ω and 1,2 diol series respectively. These values are lower in magnitude than the value of $-3.15 \text{ kJ mol}^{-1}$ per additional methylene group for a homologous series of 1-alkanols adsorbing from aqueous solution to the dodecane-water interface at 20°C [29]. This comparison suggests that, when adsorbed at the oil-water interface, the additional methylene groups of the adsorbed diols are not as fully removed from contact with water as methylene groups in adsorbed n -alkanols. It also indicates that the effect witnessed is sensitive to the positions of the two hydroxyl groups on the diol.

In summary, addition of diols causes emulsion phase inversion from w/o to o/w. Knowledge from literature studies on the relationship between equilibrium (microemulsion) phase behaviour and emulsion type show that this is driven by the preferred curvature of the stabilising surfactant film becoming progressively more positive. It is known that the preferred film curvature, and hence the conditions at which emulsion phase inversion occurs, is also affected by other factors such as, the surfactant structure, temperature, oil type and electrolyte concentration according to established and qualitatively understood principles.[10-13, 17-23] Consequently, changing one of these latter variables affecting preferred film curvature should induce a corresponding change in the concentration of diol required to effect emulsion phase inversion.

Figure 3.5. Relationship between mole fraction of diol require to cause phase inversion and the standard Gibbs free energy of adsorption of the diols at a bare water – paraffin liquid interface at 20 °C. Legend indicates the different isomeric diol series.

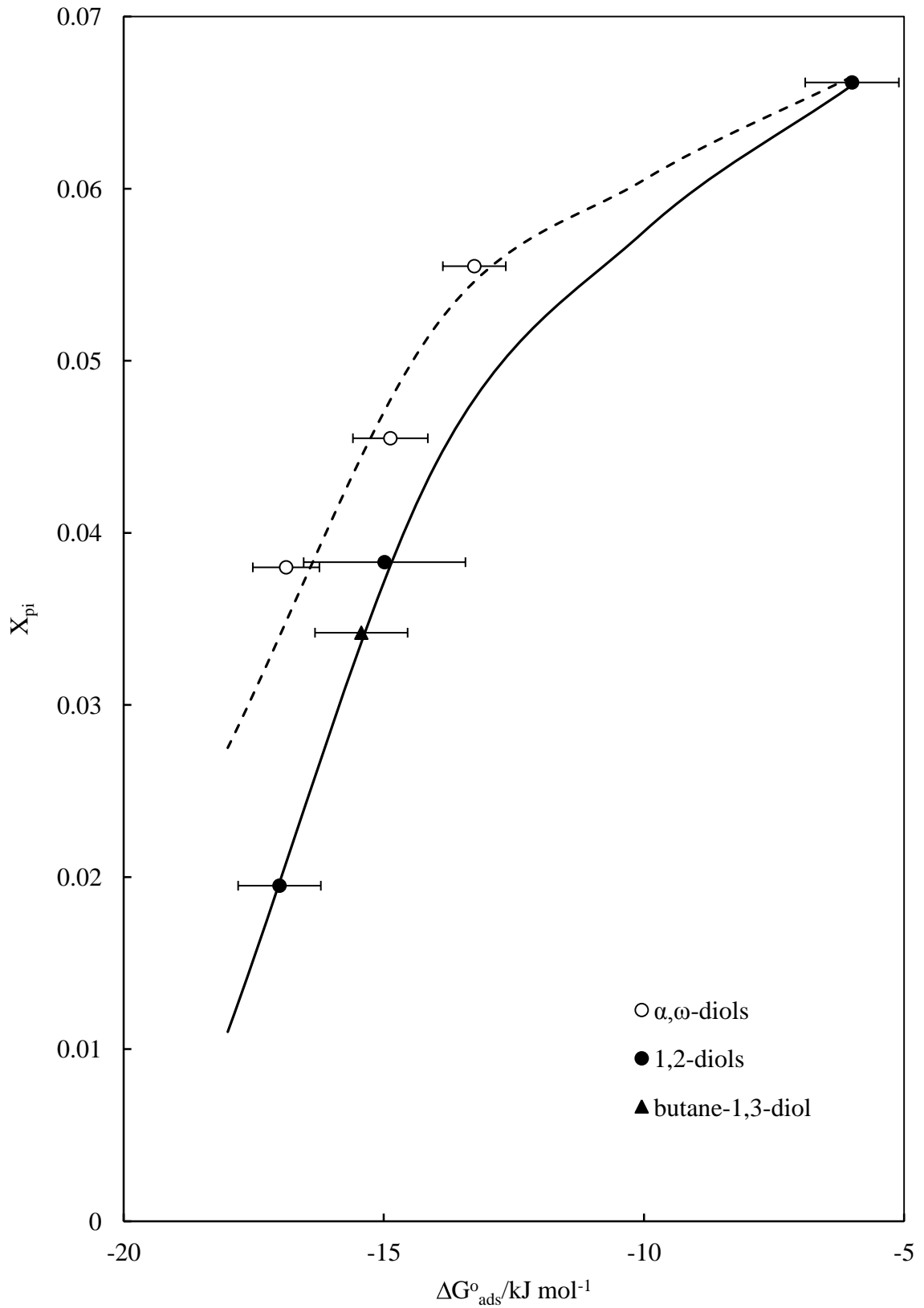
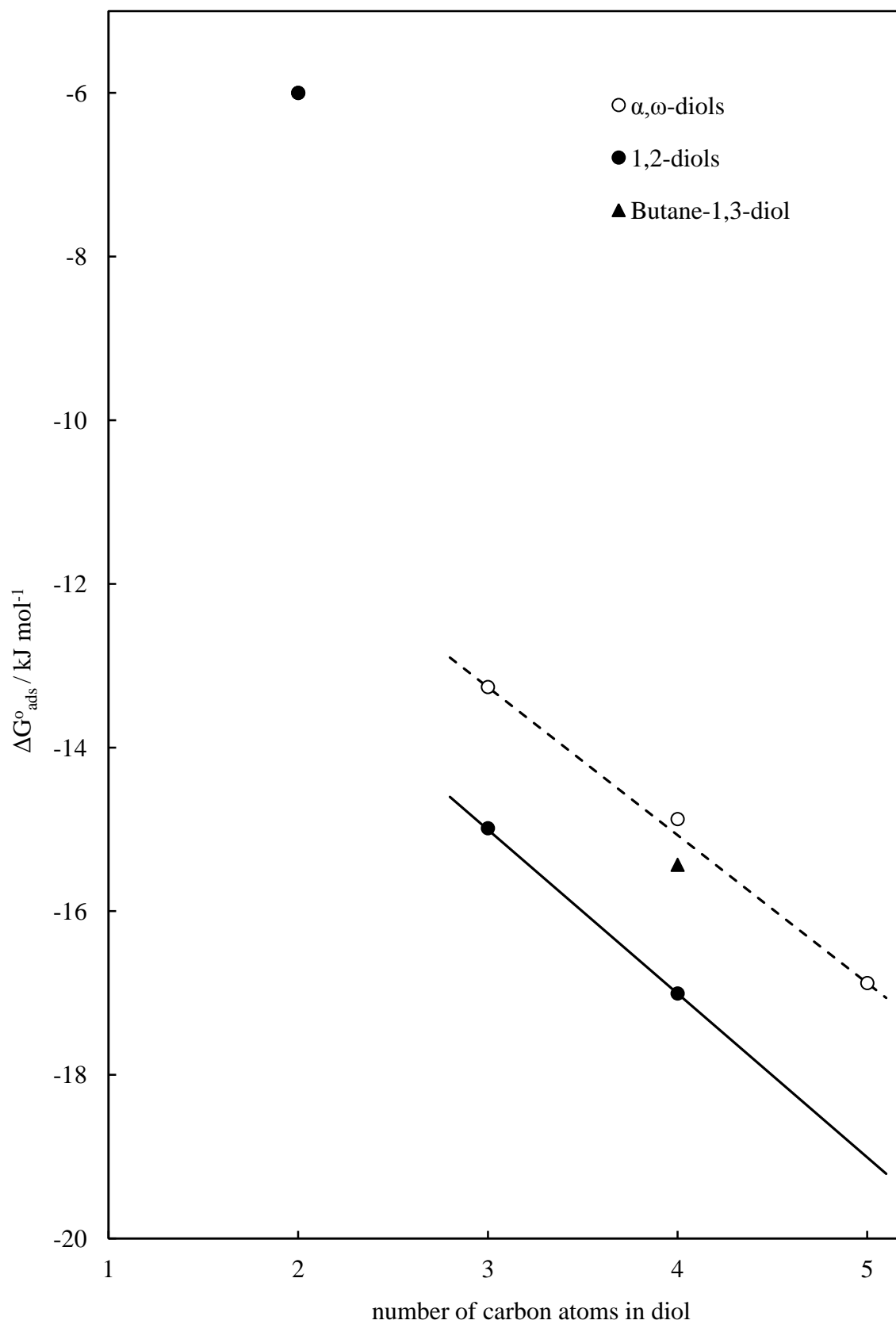


Figure 3.6. Correlation between $\Delta G^{\circ}_{\text{ads}}$ versus number of carbon atoms for the different diols at a water – paraffin liquid interface at 20 °C. Legend indicates the diols in series.



3.3.1 Effect of surfactant structure and emulsion preparation temperature

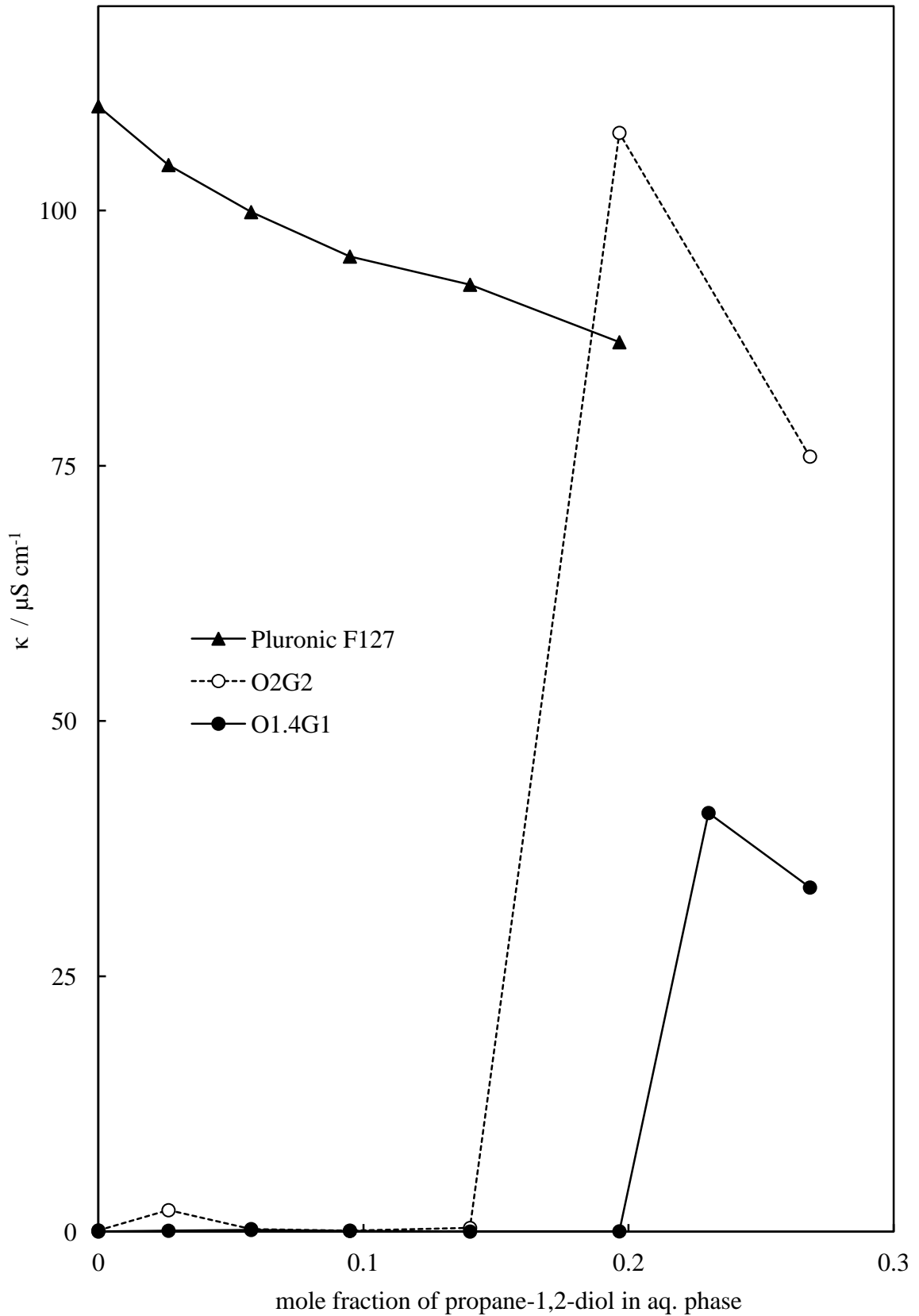
To investigate whether the phase inversion witnessed follows well established trends from other water-oil-surfactant studies, Figure 3.7 compares plots of emulsion conductivity versus propane-1,2-diol addition for three different surfactants at 70 °C, showing how the phase inversion point shifts with the structure of the surfactant. The three surfactants used can be qualitatively ranked in order of decreasing hydrophilicity (i.e. decreasing preference for positive curvature and o/w emulsion formation) using the mass fraction of hydrophilic groups in the molecules to give (most hydrophilic) Pluronic F127 > O₂G₂ > O_{1.4}G₁ (least hydrophilic).

For a surfactant with preferred positive curvature (Pluronic F127) it would be expected that the addition of diol would have little effect on the emulsion type, since the diol would just promote greater positive curvature. As seen in Figure 3.7, Pluronic F127 forms o/w emulsions with no diol present (zero concentration of diol and presumed positive curvature) and further addition causes no change in emulsion type.

For surfactants which would be expected to have negative curvature in the absence of added diol (hydrophobic) it would be assumed that the diol would cause phase inversion in the order of their hydrophilicity. The hydrophobic O₂G₂ and O_{1.4}G₁ surfactants both form w/o emulsions in the absence of diol and are phase inverted to o/w by diol addition. However, it is shown that the less hydrophobic O₂G₂ (as measured by HLB number) requires a lower amount of diol concentration than O_{1.4}G₁ for phase inversion.

Overall, the phase inversion behaviour with diol addition of all three surfactants is consistent with expectations based on their relative hydrophobicities and corresponding preferred monolayer curvature.

Figure 3.7. Conductivity of emulsions containing equal volumes of oil and aqueous phase with 10% w/w O_{1.4}G₁, O₂G₂ or Pluronic F127 surfactant by addition of propane-1,2-diol at 70 °C. Legend designates the surfactants belonging to each data series.



For non-ionic surfactants adsorbed at oil-water interfaces, increasing the temperature causes dehydration of the uncharged hydrophilic headgroup and shrinks the effective headgroup size.[21] This effect causes the preferred curvature of the adsorbed film to become increasingly negative with increasing temperature and hence emulsions stabilised by non-ionic surfactants undergo phase inversion from o/w (WI – positive curvature) to w/o (WII – negative curvature) with increasing temperature. The effect of increasing temperature can be seen in Figure 3.8 for an emulsion containing a fixed diol mole fraction of 0.075 propane-1,2-diol which phase inverts from o/w to w/o with increasing temperature.

For phase inversion by diol addition it is expected that at higher temperatures, more diol would be required to cause phase inversion, due again to the larger difference between initial curvature and curvature at phase inversion. Figure 3.9 illustrates the results where emulsions stabilised by $O_{1.4}G_1$ at 20 °C phase invert from w/o to o/w at a propane-1,2-diol mole fraction of approximately 0.04. Whereas the same system at 70 °C, when the surfactant preferred curvature is more negative, phase inversion from w/o to o/w requires a higher diol mole fraction of approximately 0.12, as expected.

Results at different temperatures again suggest that the diol changes the preferred curvature of the surfactant molecule from negative to positive. Adjusting the temperature to change the curvature, either towards negative or positive, will result in the system requiring more or less diol to cause phase inversion respectively.

Figure 3.8. Phase inversion by increasing the temperature for an emulsion containing a fixed mole fraction of propane-1,2-diol equal to 0.075 in the aqueous phase with equal volumes of both aqueous/oil phase and 4% w/w O_{1,4}G₁.

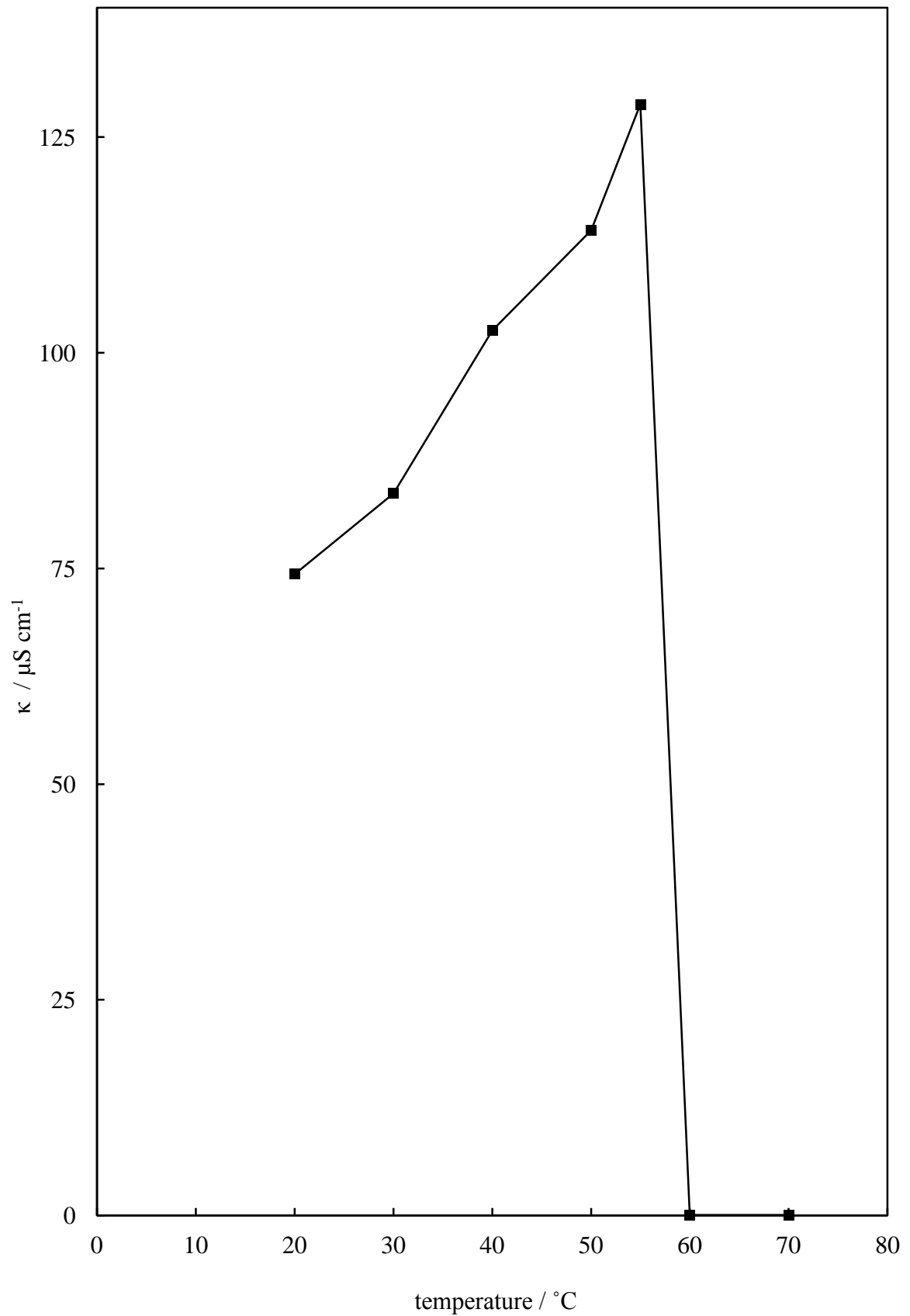
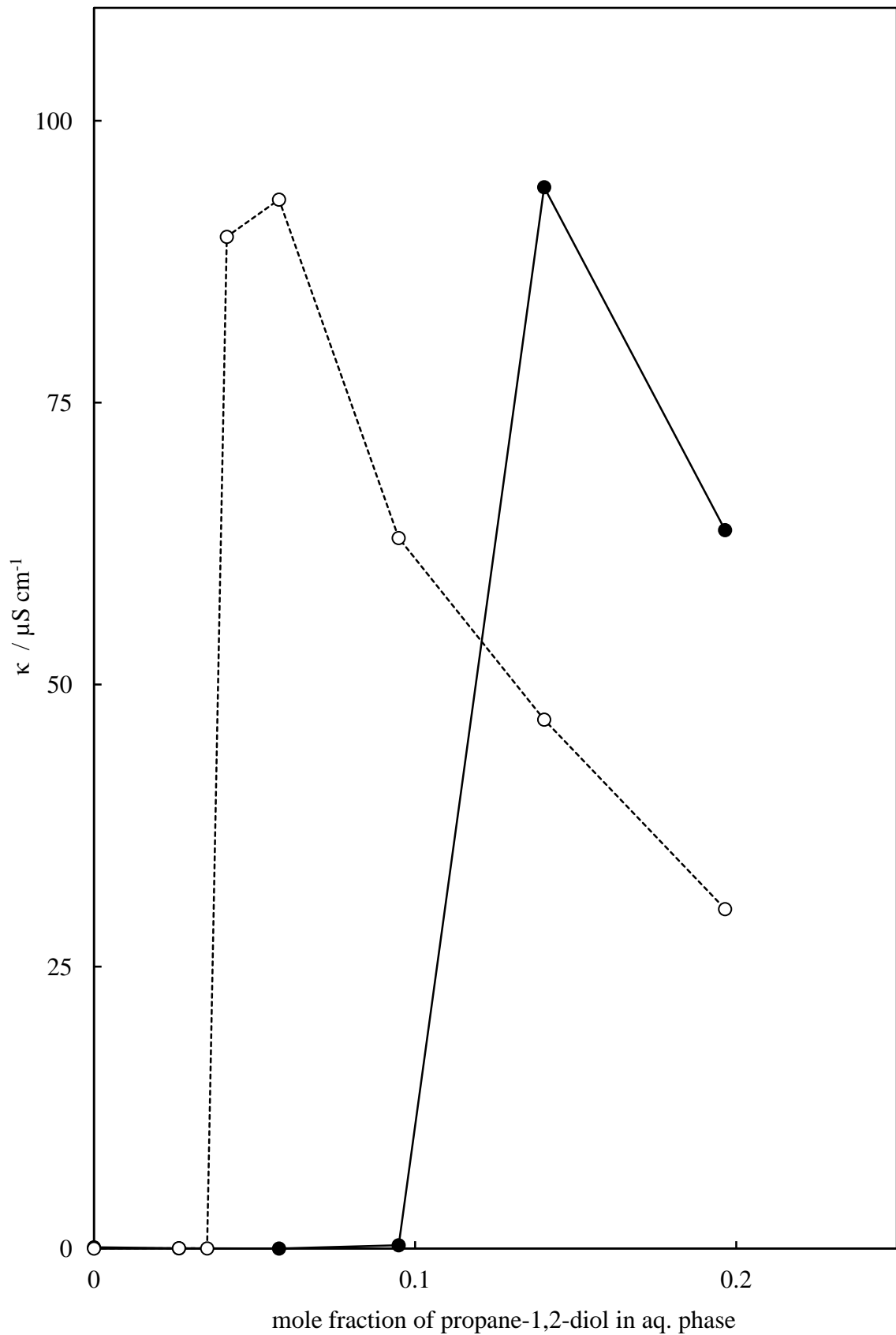


Figure 3.9. Conductivity of emulsions containing equal volumes of oil and aqueous phase with 4% w/w $O_{1.4}G_1$ surfactant by addition of propane-1,2-diol at two temperatures, unfilled points indicate 20 °C and filled points are 70 °C.



3.4 Effect of diol addition on emulsion drop size

How diols affect emulsion type for different surfactants and temperatures has been shown. As shown in chapter 1, the major contribution to the energy required to form an emulsion is the energy needed to create the additional oil-water interfacial area corresponding to the drop surfaces which, in turn, is proportional to the oil-water interfacial tension. When forming a series of emulsions at fixed energy input (*i.e.*, a constant emulsification procedure), small drop diameters corresponding to the creation of large additional oil-water interfacial area is expected when the oil-water tension is low and large drops are expected when the tension is high. For emulsions with equal oil and aqueous phase volumes, the point of emulsion phase inversion corresponds to that at which the corresponding equilibrium liquid phases undergo microemulsion phase inversion. At phase inversion, the post-cac tension γ_c is minimum.[18, 21, 23] It therefore follows that, for emulsions prepared with constant energy input, the initial droplet diameter should be a minimum around the point of emulsion phase inversion.

This expectation has been tested by measuring the average drop diameters for the emulsions stabilised by $O_{1.4}G_1$ and phase inverted by addition of the different diols. These results are plotted in Figure 3.10 in which the drop diameter is plotted versus the diol mole fraction divided by the mole fraction required for phase inversion, X/X_{pi} . Using this normalised scale enables easy visual comparison of all the different diols on a common scale; w/o emulsions are formed for $X/X_{pi} < 1$, o/w emulsions are formed for $X/X_{pi} > 1$ and phase inversion occurs at $X/X_{pi} = 1$. It can be seen that the emulsion drop size does indeed pass through a minimum at approximately the point of phase inversion for all the different diols.

Figure 3.10. Initial average drop diameter (measured from micrograph images) as a function of diol addition through phase inversion for emulsions containing equal volumes of oil and aqueous phase and 4% w/w $O_{1,4}G_1$ at 20 °C. Legend indicates the diols to each series.

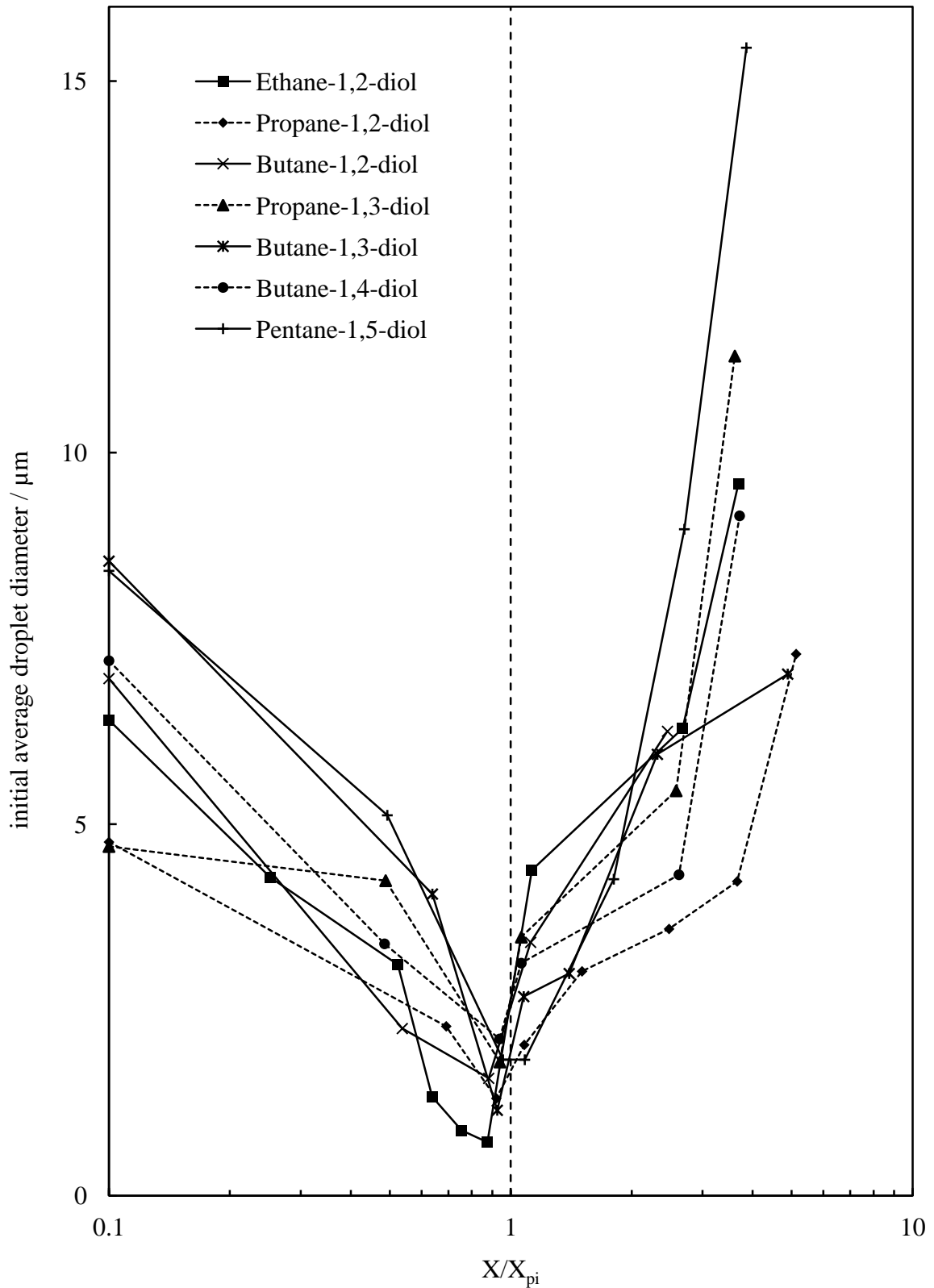


Figure 3.11. Micrographs of emulsions containing 4% w/w O_{1,4}G₁, equal volumes oil and water/pentane-1,5-diol, with increasing pentane-1,5-diol replacing water. a = 0, b = 5, c = 9, d = 10, e = 15, f = 20 and g = 25% v/v pentane-1,5-diol. Phase inversion from w/o to o/w emulsions occurs between (c) and (d). 50x magnification, scale bars = 100 μ m. Pictures taken at room temperature, 22 \pm 3 $^{\circ}$ C.

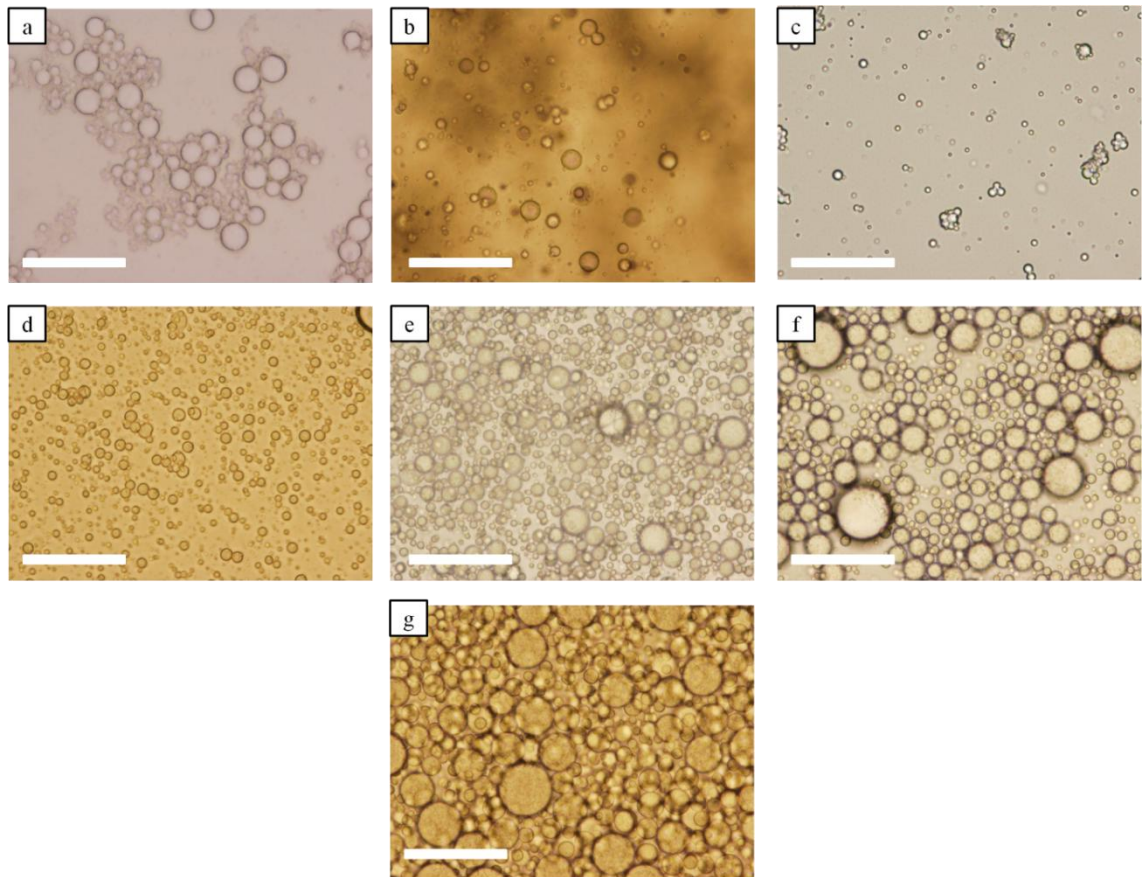
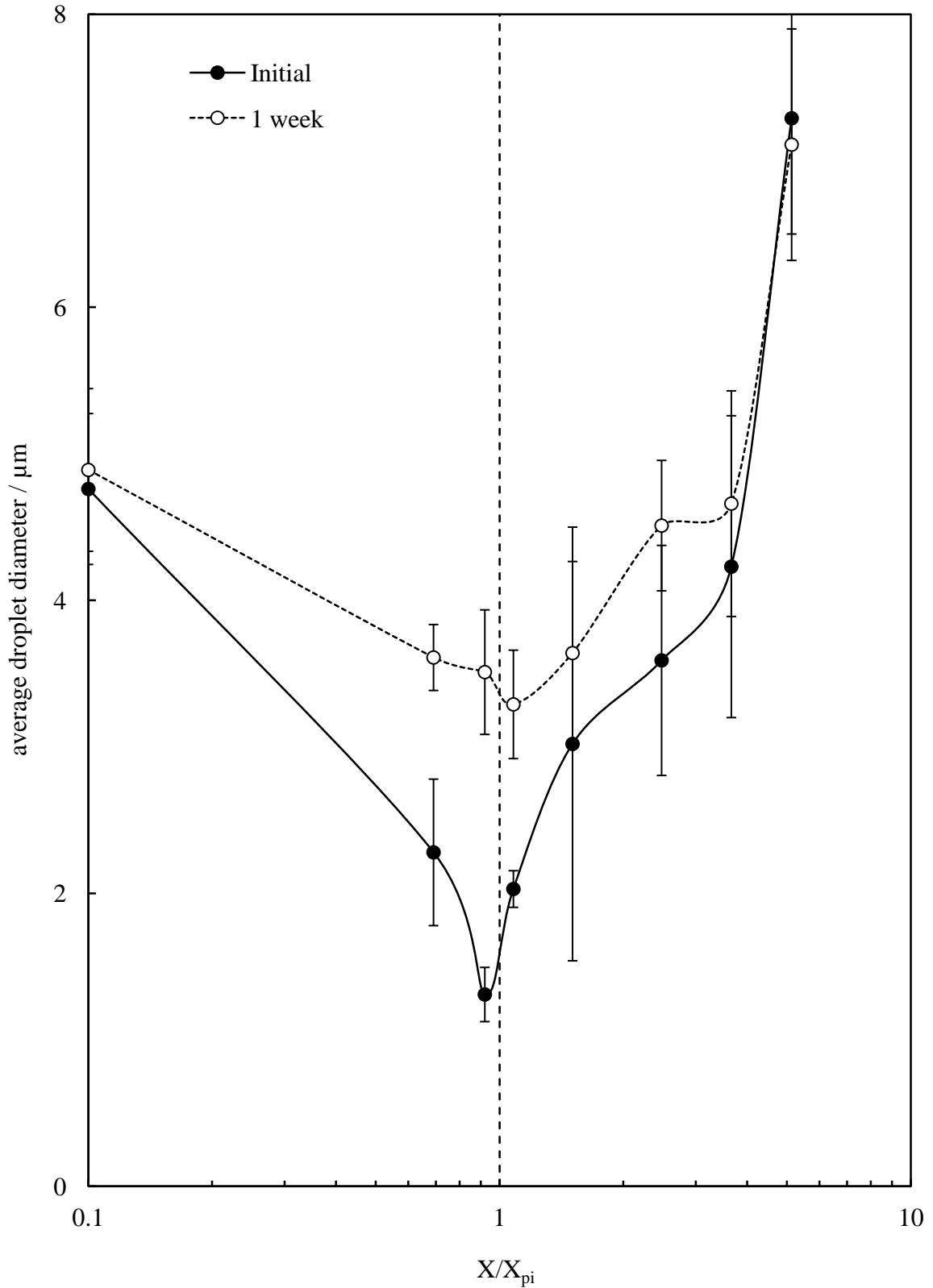


Figure 3.11 shows an example of the appearance of the emulsion droplets with increasing amounts of pentane-1,5-diol being added in replacement of water using microscopy immediately after emulsification. Phase inversion occurs between micrographs c and d where the minimum in droplet diameter discussed earlier can be seen visually.

In addition to the minimum initial droplet diameter plot it is of interest to measure the aged emulsions droplet diameter. As noted earlier, emulsions under conditions corresponding to phase inversion (when the oil-water tension is minimum) are maximally unstable with respect to time to droplet coalescence. Figure 3.12 shows the variation of initial and aged (after 1 week) average droplet diameters against X/X_{pi} . Data are shown only for the propane-1,2-diol system to aid clarity, however, similar behaviour was observed for all the diol systems.

It can be seen that emulsion drop growth over 1 week is largest around phase inversion. Drop growth, presumably (from findings in the literature) due mainly to droplet coalescence, is negligibly small for both o/w or w/o emulsions far from the conditions corresponding to phase inversion.

Figure 3.12. Initial and aged (1 week) average drop diameter (measured from micrograph images) as a function of propane-1,2-diol addition. The emulsions are w/o for $X/X_{pi} < 1$ and o/w for $X/X_{pi} > 1$; the vertical dashed line corresponds to phase inversion at $X/X_{pi} = 1$. Emulsion stored at emulsification condition, *i.e.* 20 ± 4 °C.



3.5 *Effect of diol addition on emulsion stability*

As noted in the previous section, Figure 3.12 shows that $O_{1.4}G_1$ -stabilised emulsion drop growth over 1 week is largest around phase inversion induced by the addition of propane-1,2-diol and similar behaviour is seen for the diol systems. For all the different diol systems, the stability has been characterised systematically by measuring the fraction of the emulsion droplet phase (i.e. aqueous phase from w/o and oil phase from o/w) which has resolved from the emulsion after storage for 1 week at emulsification conditions.

Increased instability thought to be from coalescence should occur around phase inversion for all systems when stored at emulsification conditions. Figure 3.13 shows the appearance of the emulsions after 1 week with increasing diol through phase inversion for a number of systems. Figure 3.14 shows plots of the fractional resolution versus X/X_{pi} for three of the diol systems. The results for the other diols are broadly similar but not shown here to aid the clarity of the figure. Firstly, as expected, the instability with respect to droplet coalescence is generally maximum around the point of emulsion phase inversion, i.e. at approximately $X/X_{pi} = 1$. As noted earlier, emulsion instability around phase inversion is a general phenomenon, irrespective of which variable is adjusted to effect inversion.[10-13]

The second interesting stability feature of these systems was that many of the diol systems (but not all) exhibit complete resolution of the drop phase at the highest diol concentrations investigated, as shown in Figure 3.14.

Figure 3.13. Photograph of some emulsion series discussed showing phase inversion (dotted red line) from w/o to o/w emulsions with the addition diols. Top to bottom, ethane-1,2-diol, propane-1,3-diol, butane-1,4-diol and pentane-1,5-diol. System containing 4% w/w O_{1.4}G₁ non-ionic surfactant and equal volumes of oil/aqueous phase where the diol added replaces a portion of the water. Photograph taken 1 week after homogenisation and stored at room temperature (21 ± 4 °C).

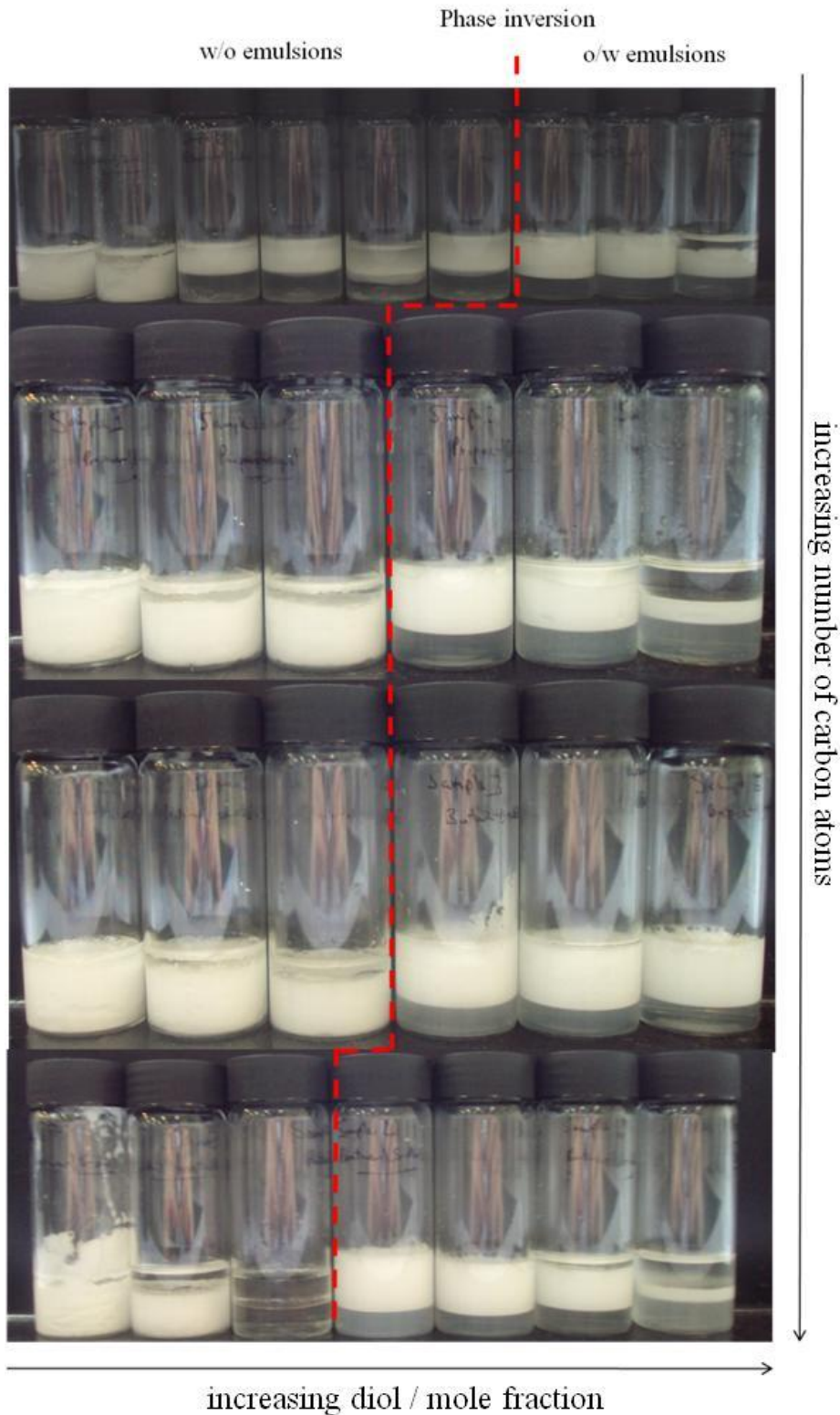
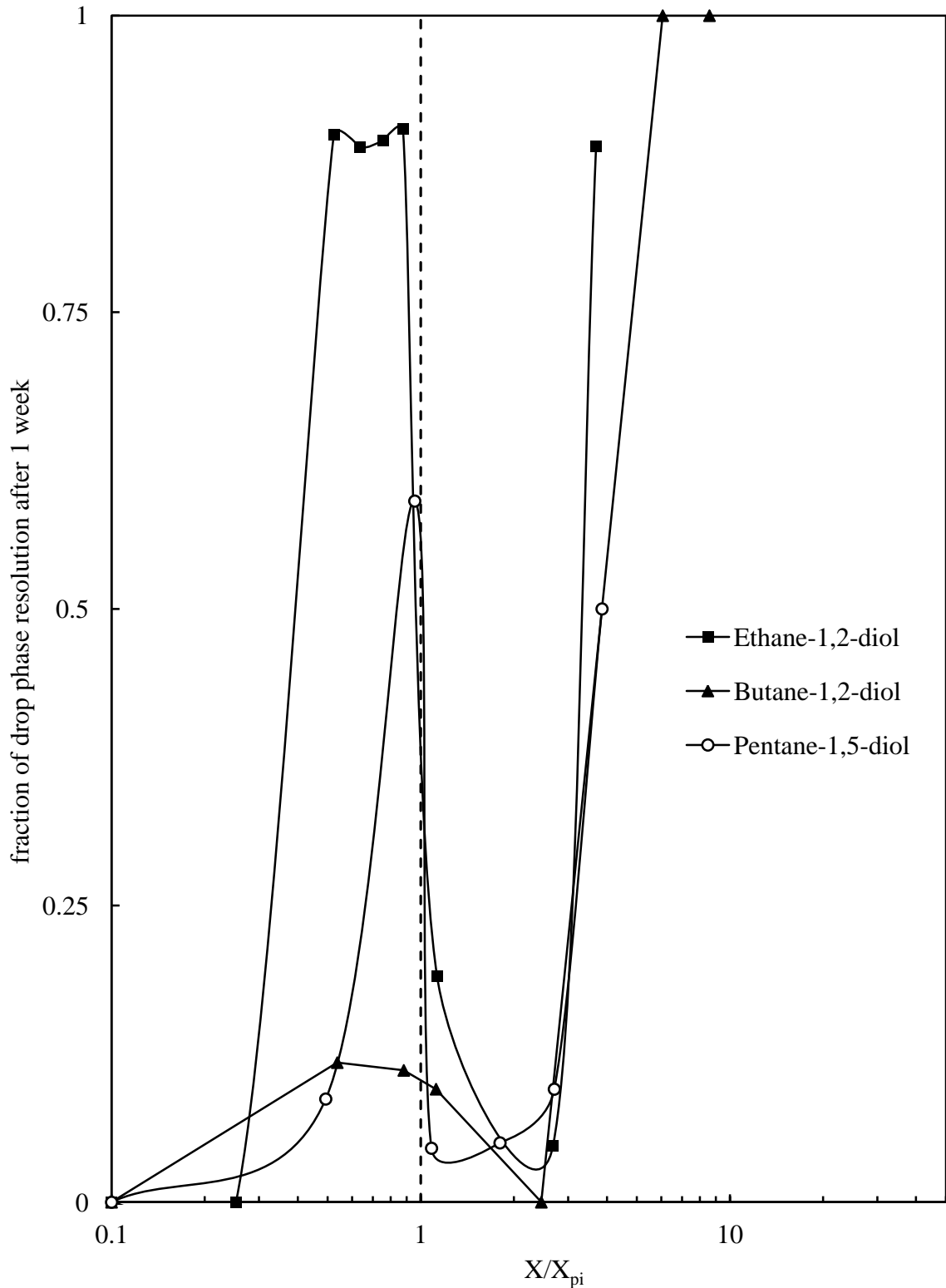


Figure 3.14. Variation of emulsion stability with respect to droplet coalescence on the addition of diols as the phase inversion point is passed. All emulsions contained equal volumes of oil and aqueous phase and 4% w/w $O_{1,4}G_1$ surfactant and the temperature was 20 °C. The emulsions are w/o for $X/X_{pi} < 1$ and o/w for $X/X_{pi} > 1$; the vertical dashed line corresponds to phase inversion at $X/X_{pi} = 1$. Legend indicates the diol in each series.



This second type of instability, occurring of X/X_{pi} greater than 1, can be explained by a mechanism in which the high diol concentration increases the value of the cac of the surfactant in the aqueous phase (cac) and/or K_{ow} such that cac of the system increases to a value which exceeds $[surfactant]_{ov}$. This hypothesis is based on literature showing that diol addition increases the critical aggregation concentrations of different surfactants.[26, 28, 29]

If this hypothesis is correct, it is predicted that for diol concentrations greater than X_{pi} (i.e. when the emulsions are o/w), diol addition should initially decrease the amount of oil drop coalescence/resolution and hence stabilise the emulsions. However, if the system is taken further from the phase inversion condition above a certain diol concentration such that cac exceeds $[surfactant]_{ov}$, further diol concentration should then increase the amount of oil drop coalescence, *i.e.* the emulsion should be destabilised. The diol concentration at which $cac > [surf]_{ov}$ is predicted to increase with increasing $[surf]_{ov}$. Consistent with this idea, Figure 3.15 shows that progressive diol addition initially stabilises and then destabilises o/w emulsions. Furthermore, as expected, Figure 3.16 shows the diol concentration at which this second type of instability occurs does indeed increase with the overall surfactant concentration. Based on these arguments presented, the surfactant concentration at the onset of the 2nd instability (dependent on the diol content) is expected to be approximately equal to the value of cac at the corresponding diol concentration.

Figure 3.15. Variation of oil drop phase resolution after 1 week with aqueous phase mole fraction of propane-1,2-diol for emulsions for o/w emulsions containing equal volumes of oil and aqueous phases and different concentrations (indicated in legend) of O_{1,4}G₁ surfactant at 20°C.

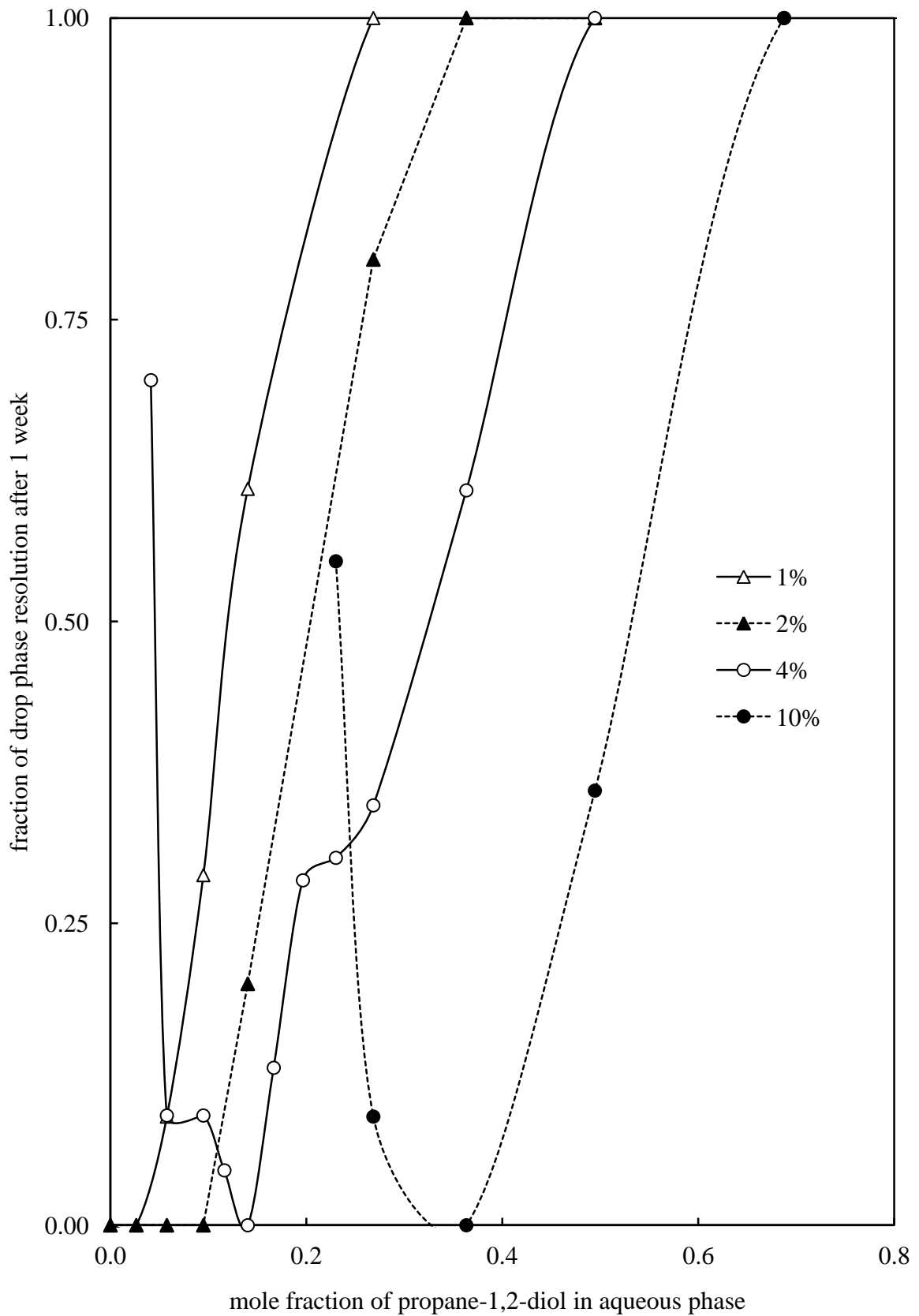
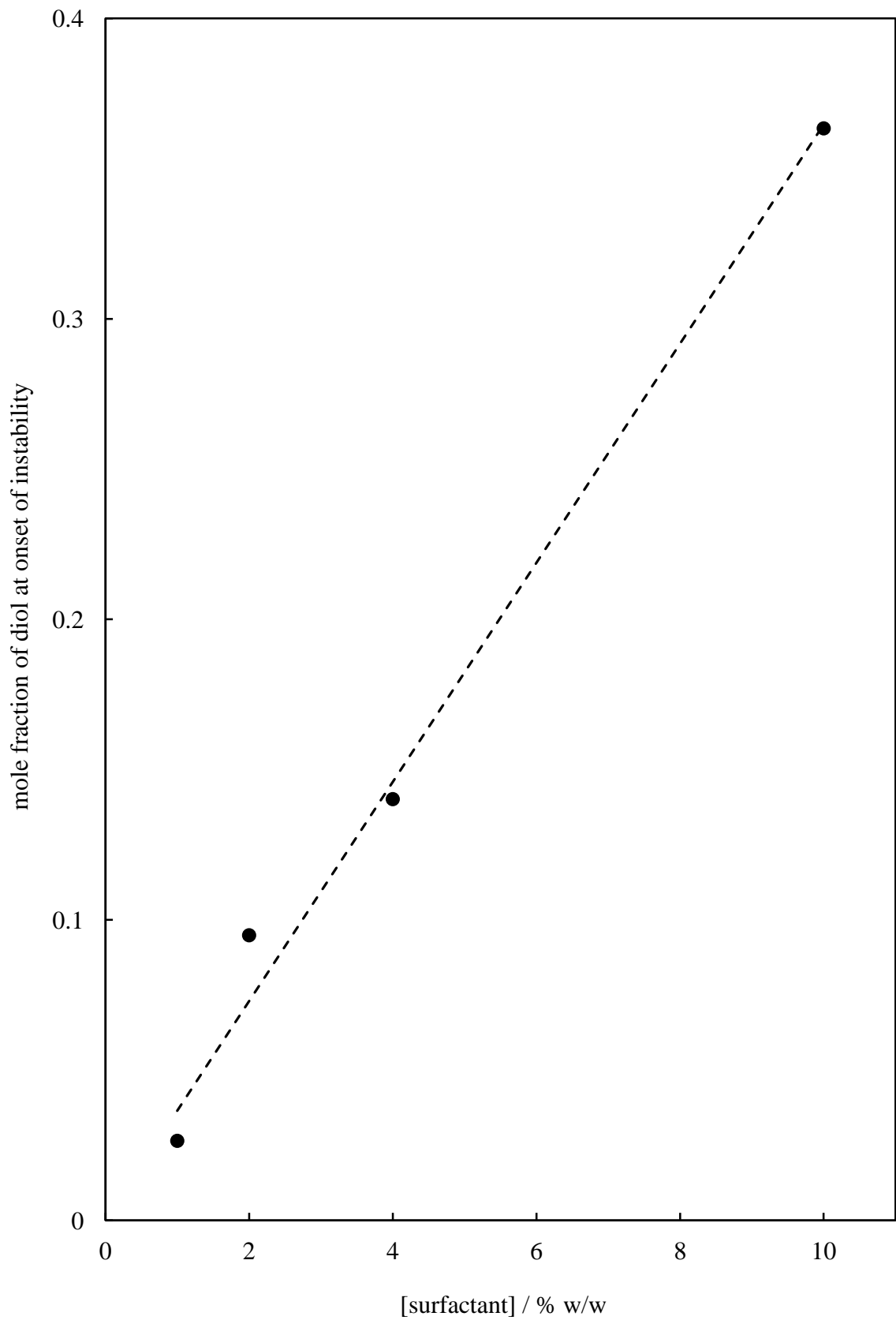


Figure 3.16. Mole fraction at the onset of the drop coalescence instability plotted versus the % w/w of surfactant.



3.6 Conclusions

The effect of diols on the phase inversion in emulsions stabilised by and containing non-ionic surfactants, water/diol and paraffin liquid has been investigated establishing principles which enable the rational formulation of emulsions containing different diols, as used in many pharmaceutical creams. The results from this chapter can be summarised as follows:

- All the diols studied do not partition to the oil phase (paraffin liquid) in emulsions to a significant extent (with a maximum of 0.47% w/w at 20 °C for pentane-1,5-diol).
- It was shown that in a system containing equal volumes of aqueous and oil phase plus non-ionic surfactant, phase inversion is strongly dependent on the addition of diol content in the replacement of the water phase. For emulsions containing no diol content and a non-ionic surfactant of low HLB, w/o emulsions are generally made. For the first time it was shown that upon increasing the diol content in the emulsions, the emulsions will phase invert from w/o to o/w. The variation of diol concentration required for emulsion phase inversion with surfactant type and with temperature is consistent with diol addition leading to increased positive preferred curvature of the adsorbed surfactant film.
- The effect of diol structure on phase inversion is well understood, with investigations showing differences between α,ω -diols, 1,2-diols and also changing the second alcohol position. In all cases the addition of a carbon atom to the diol (either α,ω - or 1,2-diols) decreased the amount of diol needed to phase invert. 1,2-diols show a larger difference, shown to be from the increased surface activity at a bare water-paraffin liquid interface. Keeping the number of carbon atoms the same and moving the position of the alcohol groups show that as the alcohol group moves further away from each other the more diol is required to phase invert, again linked to the surface activity of the diols.
- Both the stability of the emulsions and initial average droplet diameters indicate that the water-oil interfacial tension of the system is lowest at phase inversion and again

is consistent with diol addition leading to the pre-emulsified microemulsion systems passing through zero curvature.

- It is also shown that the cac of non-ionic surfactant is increased with increasing diol concentration. This yields instability with increasing diol, after the surfactant concentration is $< \text{cac}$.
- The understanding from the results indicate for the first time the possibility of using the phase inversion method for the process of making stable emulsions containing varying amounts of diol content. Key aspects to this preparation are that non-ionic surfactants with initial negative curvature are required. This is not intuitive when formulating an o/w emulsion which contains diol where a hydrophilic surfactant might be thought of as the best stabiliser. Techniques for phase inversion could include, temperature controlled emulsification and storage or dilution with the diol of interest. This would change the preferred monolayer curvature after emulsification to gain the minimum droplet diameter benefits of approximately zero curvature at emulsification and stability of coalescence from higher interfacial tension after emulsification.

3.7 References

1. R. Strickley, *Pharm. Res.*, **21**, 201 (2004).
2. B. de Spiegeleer, E. Wattyn, G. Slegers, P. Van der Meeren, K. Vlaminck and L. Van Vooren, *Pharm. Dev. Technol.*, **11**, 275 (2006).
3. A. Otto, J. W. Wiechers, C. L. Kelly, J. Hadgraft and J. du Plessis, *Skin Pharmacol. Physiol.*, **21**, 326 (2008).
4. J. Ziming Sun, M. C. E. Erickson and J. W. Parr, *Int. J. Cosmetic Sci.*, **27**, 355 (2005).
5. R. D. Hamill, F. A. Olson and R. V. Petersen, *J. Pharm. Sci.*, **54**, 537 (1965).
6. R. D. Hamill and R. V. Petersen, *J. Pharm. Sci.*, **55**, 1268 (1966).
7. R. D. Hamill and R. V. Petersen, *J. Pharm. Sci.*, **55**, 1274 (1966).
8. K. W. Reichmann and R. V. Petersen, *J. Pharm. Sci.*, **62**, 1850 (1973).
9. A. Imhof and D. J. Pine, *J. Colloid Interface Sci.*, **192**, 368 (1997).
10. K. Shinoda and H. Saito, *J. Colloid Interface Sci.*, **30**, 258 (1969).
11. B. P. Binks, *Langmuir*, **9**, 25 (1993).
12. H. Wennerström, O. Söderman, U. Olsson and B. Lindman, *Colloids Surf. A*, **123-124**, 13 (1997).

13. J.-L. Salager, L. Márquez, A. A. Peña, M. Rondón, F. Silva and E. Tyrode, *Ind. Eng. Chem. Res.*, **39**, 2665 (2000).
14. F. Harusawa, T. Saito, H. Nakajima and S. Fukushima, *J. Colloid Interface Sci.*, **74**, 435 (1980).
15. R. Aveyard, B. P. Binks, S. Clark and P. D. I. Fletcher, *J. Chem. Soc., Faraday Trans.*, **86**, 3111 (1990).
16. M. Ben Ghoulam, N. Moatadid, A. Graciaa and J. Lachaise, *Langmuir*, **18**, 4367 (2002).
17. P. A. Winsor, *Solvent properties of amphiphilic compounds*, Butterworths, London (1954).
18. R. Aveyard, B. P. Binks, T. A. Lawless and J. Mead, *J. Chem. Soc. Faraday Trans.*, **81**, 2155 (1985).
19. K. Shinoda and B. Lindman, *Langmuir*, **3**, 135 (1987).
20. M. Kahlweit, R. Strey, P. Firman, D. Haase, J. Jen and R. Schomaecker, *Langmuir*, **4**, 499 (1988).
21. R. Aveyard, B. P. Binks and P. D. I. Fletcher, *Langmuir*, **5**, 1210 (1989).
22. R. Strey, *Colloid Polym. Sci.*, **272**, 1005 (1994).
23. H. Leitao, A. M. Somoza, M. M. T. d. Gama, T. Sottmann and R. Strey, *J. Chem. Phys.*, **105**, 2875 (1996).
24. D. H. Smith, S. N. Nwosu, G. K. Johnson and K. H. Lim, *Langmuir*, **8**, 1076 (1992).
25. K.-H. Lim, W. Zhang, G. A. Smith and D. H. Smith, *Colloids Surf. A*, **264**, 43 (2005).
26. R. Aveyard, B. P. Binks, P. D. I. Fletcher, A. J. Kirk and P. Swansbury, *Langmuir*, **9**, 523 (1993).
27. M. J. Rosen, *Surfactants and Interfacial Phenomena*, John Wiley & Sons, New York (1978).
28. L. Marszall and J. W. Van Valkenburg, *Ind. Eng. Chem. Prob. Rd.*, **20**, 708 (1981).
29. L. Marszall and J. Van Valkenburg, *J. Am. Oil Chem. Soc.*, **59**, 84 (1982).

CHAPTER 4. EFFECT OF DIOL ADDITION ON PARTICLE DISPERSIONS AND PARTICLE-STABILISED EMULSIONS

4.1 Introduction

In chapter 3, immiscible mixtures of oil and water/diol were shown to be made kinetically stable by the addition of molecular emulsifier; forming emulsions in which drops of one liquid become dispersed in the continuous phase of a second liquid.[1-9] It is well documented that stable emulsions or foams can be formed from mixtures of solid particles, water and either oil or air.[9-13] The stabilisation of foams and emulsions to coalescence and disproportionation occurs through the particles ability to partially wet both bulk phases.[14]

The wettability of a particle can be quantified through the three-phase contact angle θ , which is measured through the aqueous phase. In systems containing equal volumes of oil and water, hydrophilic particles of $\theta < 90^\circ$ stabilise o/w emulsions, whereas hydrophobic particles of $\theta > 90^\circ$ stabilise w/o emulsions. The change in free energy for the desorption of a spherical particle from the oil-water interface to either bulk is given by,[15, 16]

$$\Delta E = \pi r^2 \gamma_{ow} (1 \pm \cos\theta)^2 \quad (4.1)$$

where r is the particle radius and γ_{ow} is the bare oil-water interfacial tension; the plus sign refers to desorption into oil and the minus sign refers to desorption into water. ΔE is maximum when $\theta = 90^\circ$ and corresponds to the maximum area of interface taken up by particles present at the interface. If ΔE is large (several hundred kT where k is the Boltzmann constant and T is the absolute temperature) intermediate contact angles (not close to 0 or 180°) are exhibited and emulsions stable to coalescence are produced. Equally, particles exhibiting very low or high contact angles are not held at the interface strongly (ΔE very low) and give rise to emulsions which are unstable to coalescence.[15, 17, 18] It is known that fumed silica particles of varying wettability are excellent stabilisers for a range of oil-water emulsions and that the optimum particle hydrophobicity varies depending on the oil type.[19]

Results in this chapter have been rationalised in terms of the influence of propane-1,2-diol on the contact angles of the particles at the air-polar phase or oil-polar phase interfaces. For this reason the chapter is split into two parts:

1. The immersion of fumed silica powders of varying wettability in water-propane-1,2-diol mixtures is discussed and from simple theory the contact angles of particles at the air-polar phase interface were determined. The materials formed upon aerating these samples are then described in terms of the wettability of the particles *in situ*.
2. The emulsions properties of paraffin liquid and aqueous propane-1,2-diol stabilised by silica particles are explained in terms of transitional phase inversion as a function of particle hydrophobicity for different water:propane-1,2-diol ratios, along with emulsion inversion as a function of propane-1,2-diol content demonstrated for selected particle hydrophobicities. A model used to calculate the contact angle of particles at the oil-polar phase predicted, for a given propane-1,2-diol content, the hydrophobicity of particles required for phase inversion. The calculated results from theory are then compared to the experimental findings.

4.2 Effect of diol on water-propane-1,2-diol-silica-air systems

An indication of the wettability of powders/particles at the air-water interface without measuring the contact angle was achieved by the immersion test - the time it takes for a powder floating on the surface of a liquid to completely immerse into a liquid.[20] The process of submersion of a powder has three stages; adhesion, immersion and spreading; the solid-vapour surfaces are replaced by solid-liquid interfaces. For a powder of cube side length equal to 1 cm, the total work for the overall dispersion process, W_d , is equal to $-6\gamma_{la}\cos\theta$, where γ_{la} is the tension of the liquid-air surface and θ is the contact angle between solid and liquid phases measured into the liquid. Powders which have $\theta < 90^\circ$, W_d is negative and therefore the process of dispersion is spontaneous. Powders with $\theta > 90^\circ$, W_d is positive and work must be done to bring about complete dispersion/immersion.[15] The immersion times for a fixed amount of powdered silica into water-propane-1,2-diol mixtures as a function of propane-1,2-diol content and varying silica hydrophobicities are plotted in Figure 4.1 where the majority of particles (varying wettability) displayed a progressive decrease in immersion time

when diol was added to the water, *i.e.* wetting of the particle is enhanced by diol. Enhanced wetting was also achieved at a fixed ratio of propane-1,2-diol-water and increasing % SiOH on the silica surface as can be seen in Figure 4.2 for 50:50 mixtures of propane-1,2-diol and water.

Figure 4.1. Immersion time for 25 mg of fumed silica powders with different hydrophobicity (given) into 10 cm³ propane-1,2-diol-water mixtures at room temperature. Arrows indicate times > 24 hr.

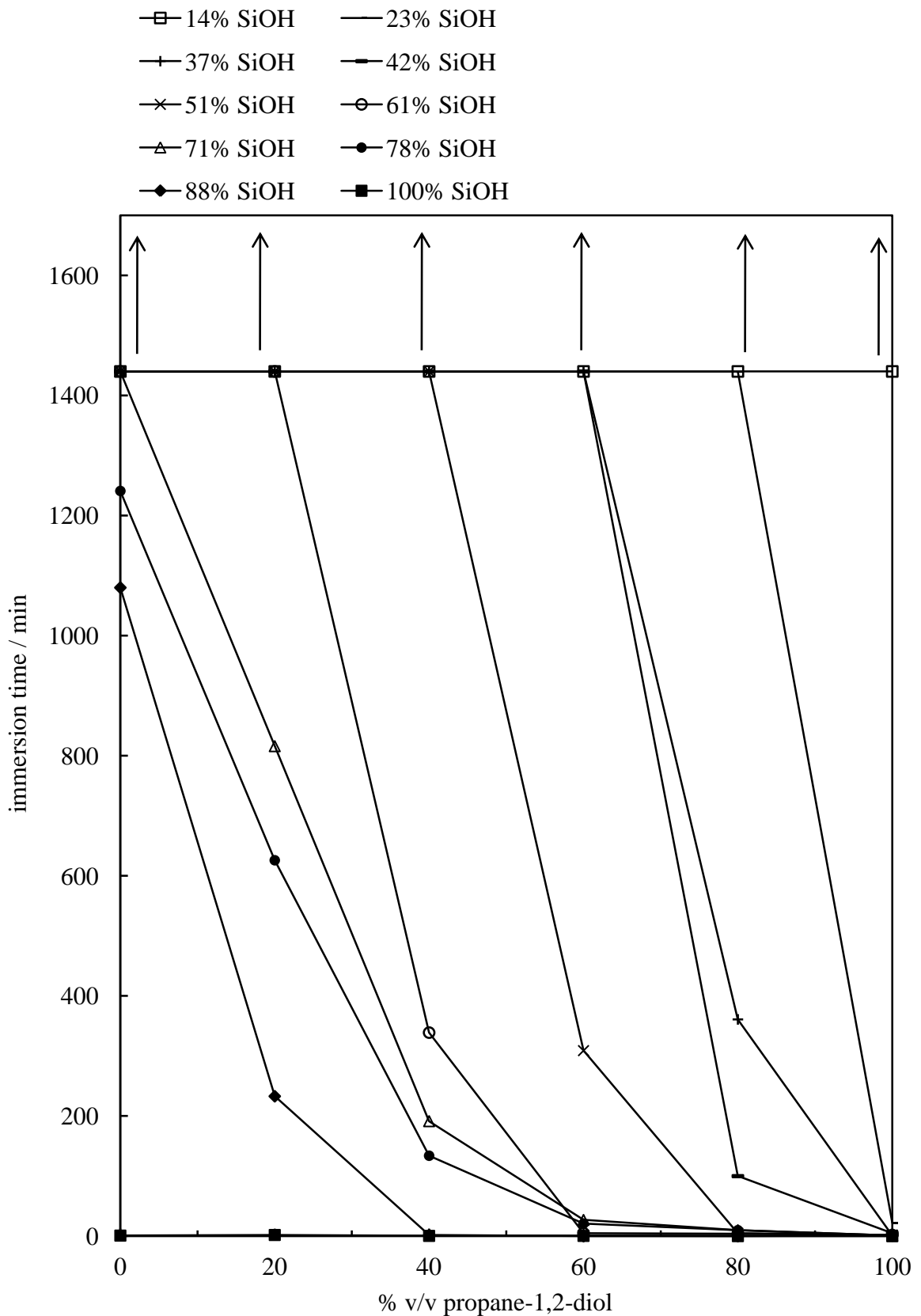
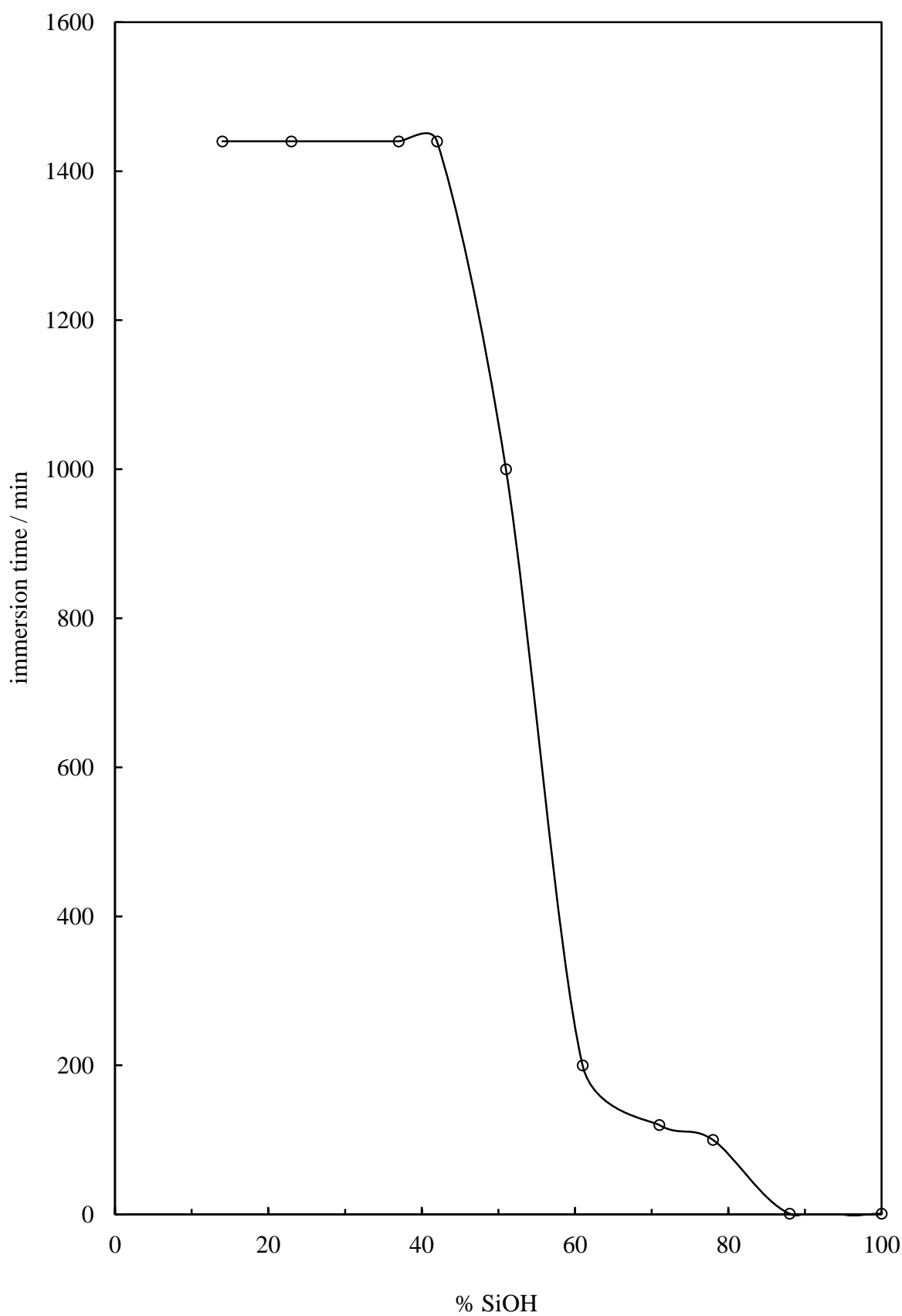


Figure 4.2. Immersion time for 25 mg of powdered fumed silica into 10 cm³ of 50% v/v mixture of propane-1,2-diol and water as a function of % SiOH on the silica particles.



To confirm the findings of immersion time with varying propane-1,2-diol-water mixtures and hydrophobicity, a model was used (based on surface energy components) to calculate the contact angle θ at the air-polar liquid surface as a function of % SiOH on the silica surfaces and the composition of the polar phase (water/propane-1,2-diol). The model assumes that no adsorption of the diol occurs on the silica surfaces. For a solid particle (s) located at the air (a)-polar liquid (l) interface, the three interfacial tensions are related to θ (measured in the polar phase) by the Young equation.

$$\cos\theta = \frac{\gamma_{sa} - \gamma_{sl}}{\gamma_{la}} \quad (4.2)$$

The surface tension between air and polar liquid, γ_{la} , can be readily measured accurately through experiment; there is no direct way to measure γ_{sa} and γ_{sl} . This is unfortunate, as it would be useful to calculate predictable contact angles θ using equation (4.2) if the two unknowns were known. Therefore if these two interfacial energies could be estimated from some other source of data calculation of contact angles would be achievable. To do this we use combining rules that allow any interfacial tension to be predicted from surface tension components and the determination of such components from the solid surfaces.

It is common practice to express any surface tension γ as a sum of components due to dispersion forces (γ^d) and polar forces (γ^p):[21]

$$\gamma = \gamma^d + \gamma^p \quad (4.3)$$

The interfacial tension between two phases is then expressed in terms of the dispersion and polar components for each phase and becomes

$$\gamma_{sl} = \gamma_{sa} + \gamma_{la} - 2\sqrt{\gamma_s^d \gamma_l^d} - 2\sqrt{\gamma_s^p \gamma_l^p} \quad (4.4)$$

for the solid-polar phase interface.[22] To determine γ_{sl} from equation (4.4), $\gamma_w^d = 21.5$ mN m⁻¹ and $\gamma_w^p = 50.7$ mN m⁻¹ at 20 °C for the contributions to the surface tension of water from literature.[23] Additionally, $\gamma_{pg}^d = 26.4$ mN m⁻¹ and $\gamma_{pg}^p = 9.0$ mN m⁻¹ for propane-1,2-diol at 20 °C.[24] To determine the remaining polar and dispersed phase components of different propane-1,2-diol-water mixtures if was assumed that a linear variation of γ_{pg}^d with γ_w^d occurred and from the calculated dispersion component the

polar component was calculated from simply subtraction. The dispersion and polar components of the solid surface energy, γ_{sa} , have been argued before, which are taken as linearly related to the percentage of silanol groups on particle surfaces.[25] For the most hydrophilic surface (100% SiOH) the polar and dispersion components are taken as that of a clean glass surface with a range of polar liquid and are $\gamma_s^d = 42.0 \text{ mN m}^{-1}$ and $\gamma_s^p = 34.0 \text{ mN m}^{-1}$. [26] For the most hydrophobic surface (0% SiOH), $\gamma_s^d = 22.0 \text{ mN m}^{-1}$ and $\gamma_s^p = 0.9 \text{ mN m}^{-1}$ which are those of a high molecular weight poly(dimethylsiloxane) fluid whose structure is chemically similar to that of the coating of DCDMS on the fumed silica particles.[26]

Using equations (4.2) - (4.4), calculated contact angles at the air-aqueous propane-1,2-diol-silica surface as a function of propane-1,2-diol content in water for surfaces of varying hydrophobicity were calculated (Table 4.1). Much like the experimental findings shown in Figure 4.1 and Figure 4.2, the contact angle θ of silica at the air-aqueous propane-1,2-diol interface decreases with increasing propane-1,2-diol in water and with increasing particle hydrophilicity, *i.e.* making systems more hydrophilic.

Table 4.1. Calculated contact angles θ at the air-aqueous propane-1,2-diol-silica surface at 20 °C as a function of propane-1,2-diol content in the water for surfaces of different hydrophobicity (given as % SiOH). Measured liquid-air surface tensions, γ_{la} , are also given ($\pm 0.1 \text{ mN m}^{-1}$).

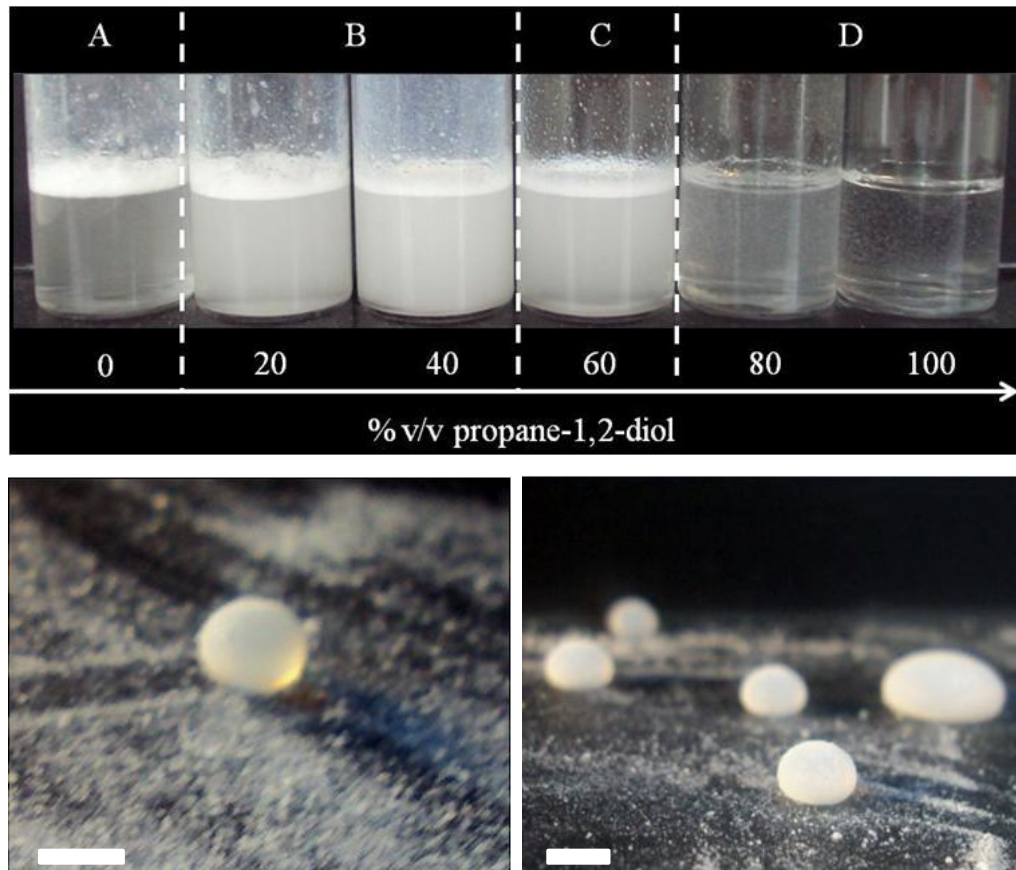
Propane-1,2-diol / % v/v	$\gamma_{la} / \text{mN m}^{-1}$	Contact angle (θ) / °		
		10% SiOH	30% SiOH	50% SiOH
0	72.2	88.0	70.8	56.6
10	63.5	81.9	63.2	46.8
20	56.8	76.0	55.8	36.3
30	51.4	70.1	47.9	22.6
40	47.2	64.6	40.1	0.0
50	44.7	60.6	34.0	0.0
60	43.6	58.4	30.6	0.0
80	41.1	53.2	20.9	0.0
100	35.4	39.6	0.0	0.0

4.2.1 Effect of aeration

In addition to the immersion investigations, the same samples (Figure 4.1 and Figure 4.2) were also used to determine the materials formed following aeration. Aerating was controlled by hand shaking at a relatively vigorous constant force and regular time (10 seconds). This approach was investigated by Binks and Murakami where in air-fumed silica-water systems it was reported that upon increasing the particle hydrophobicity (decreasing % SiOH) stable aqueous dispersions were replaced by foaming dispersions (air-in-water foams) followed by phase inversion to produce dry water (water-in-air powders).[27] The use of charged surfactants to phase invert dry water was also shown by Binks *et al.*, where the addition of surfactant caused the hydrophobic fumed silica particles to become more hydrophilic and therefore phase invert to air-in-water foams.[28] It was shown that the cause of inversion was due to tail down adsorption of the surfactant on the silica surface.

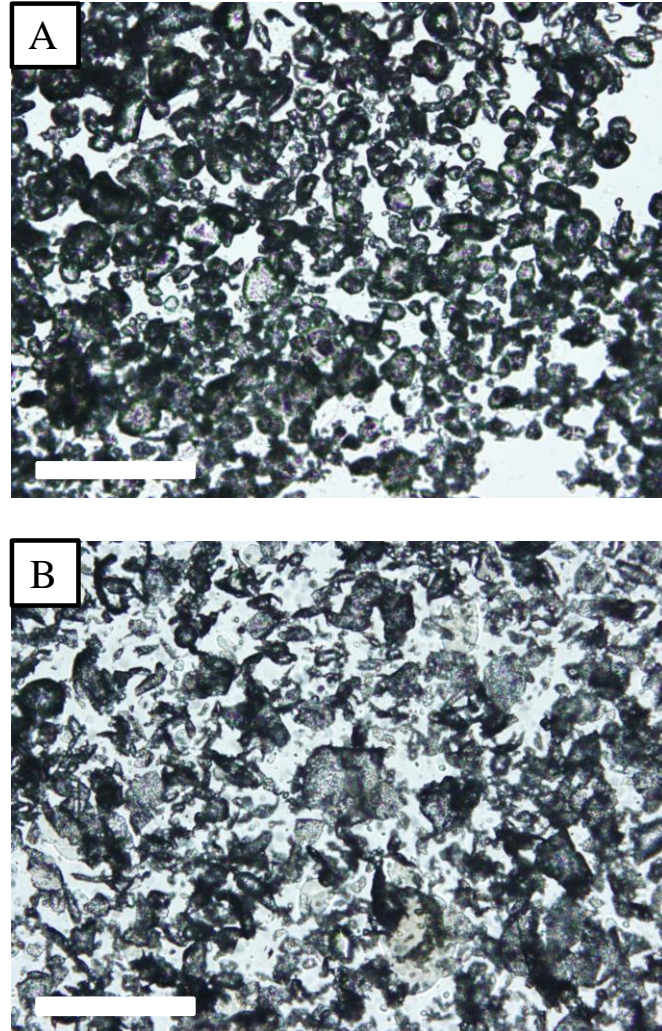
The appearance of vessels after shaking containing 51% SiOH silica are shown in the upper photograph in Figure 4.3 for different propane-1,2-diol:water ratios. (A) shows stable foam bubbles that also coalesce with the liquid surface and release particles which exert a sizeable surface pressure causing a climbing film to coat the vessel sides.[29] Upon increasing the propane-1,2-diol content in the system the behaviour of the samples follow foam + climbing film (B), stable foam (C) and aqueous dispersion (D). For extremely hydrophobic particles (14% SiOH) the formation of liquid marbles (drops in air) is shown in the lower photograph of Figure 4.3 for neat propane-1,2-diol.

Figure 4.3. Upper photograph: Photograph of vessels taken 1 min. after shaking mixtures of air, aqueous propane-1,2-diol and 25 mg of 51% SiOH fumed silica powder at room temperature (20 ± 2 °C). A represents a climbing film (powder remains on liquid surface); B represents a stable foam with climbing film; C is a stable foam and D shows an aqueous dispersion. Lower photograph: Liquid marbles of propane-1,2-diol stabilised by 14% SiOH particles. Scale bar = 1 cm.



The microscopic appearance of some of the materials is shown in Figure 4.4, where A represents stable foams, showing stable spherical and non-spherical air bubbles within a 20% v/v propane-1,2-diol aqueous continuous phase. Micrograph B shows the unstable air bubbles coalescing with the 20% v/v propane-1,2-diol aqueous continuous phase which go on to form climbing films on the sample tube glass surface, consistent with the work described by Binks *et al.* [29].

Figure 4.4. Micrographs of air-water-propane-1,2-diol-silica mixtures containing 20% v/v propane-1,2-diol in the aqueous phase after aeration by hand shaking at room temperature (20 ± 3 °C). A shows a system classified as a stable foam (51% SiOH) and B represents a system designated as stable foam + climbing film (23% SiOH). Scale bar = 100 μ m.



The materials formed from all the other air-silica-water-propane-1,2-diol mixtures are summarised in Figure 4.5. Stable foams are designated as foams that are stable for at least 1 week, and unstable foams are ones which collapse in less than 5 min. The boundaries between different materials are shown in Figure 4.6 and using the data presented in Table 4.1 it can be seen that stable foams occur in systems in which the contact angle θ is in the range $35-70^\circ$ and with particles of increased inherent hydrophobicity upon increasing the propane-1,2-diol content in water. Fletcher and Holt show similar findings for methanol-water-silica-air systems where their average contact angle for the preparation of stable foams is approx. $30-60^\circ$. [30]

Figure 4.5. Type of material formed after aeration of mixtures of aqueous propane-1,2-diol and fumed silica particles of different hydrophobicity (measured as % SiOH).

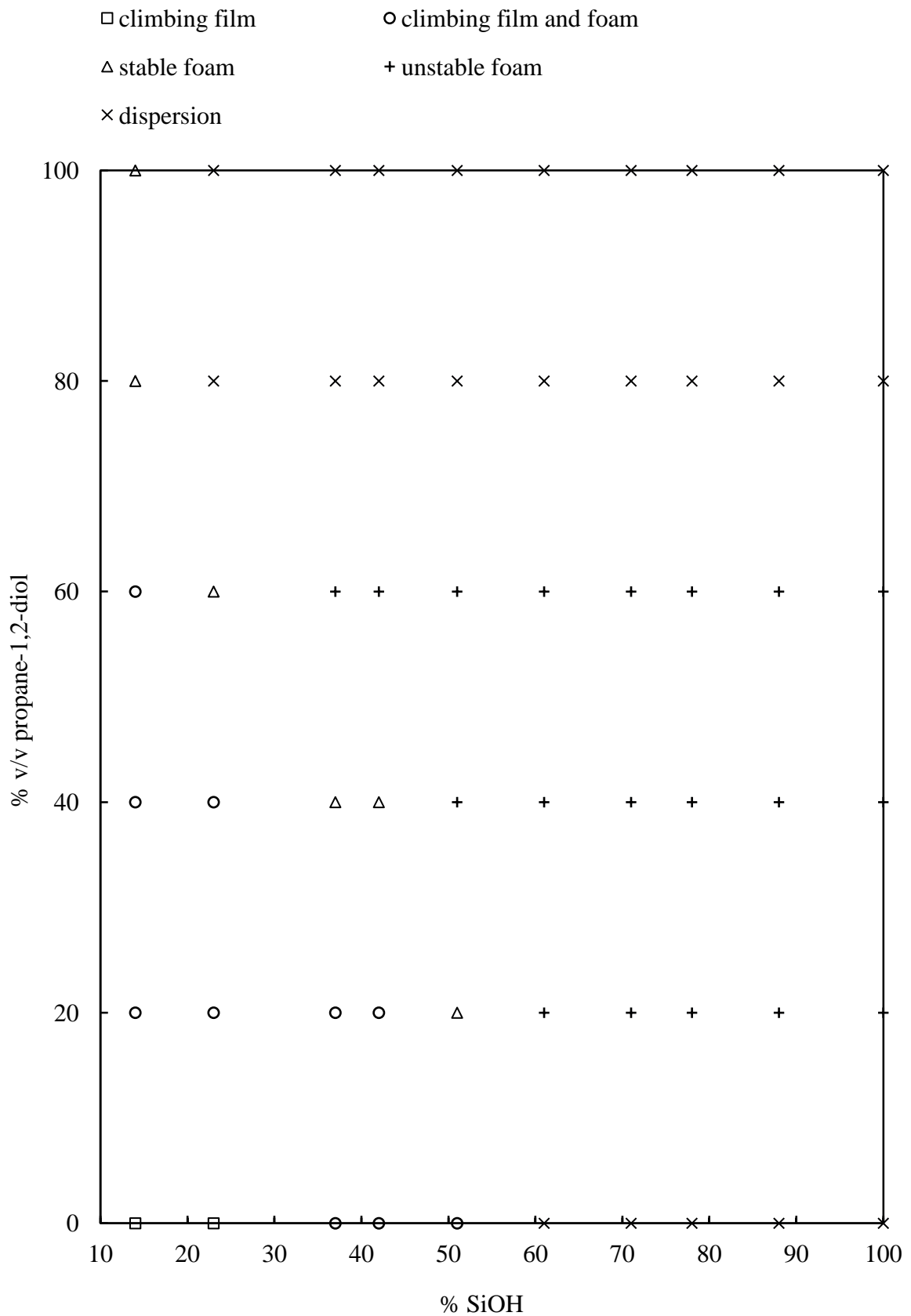
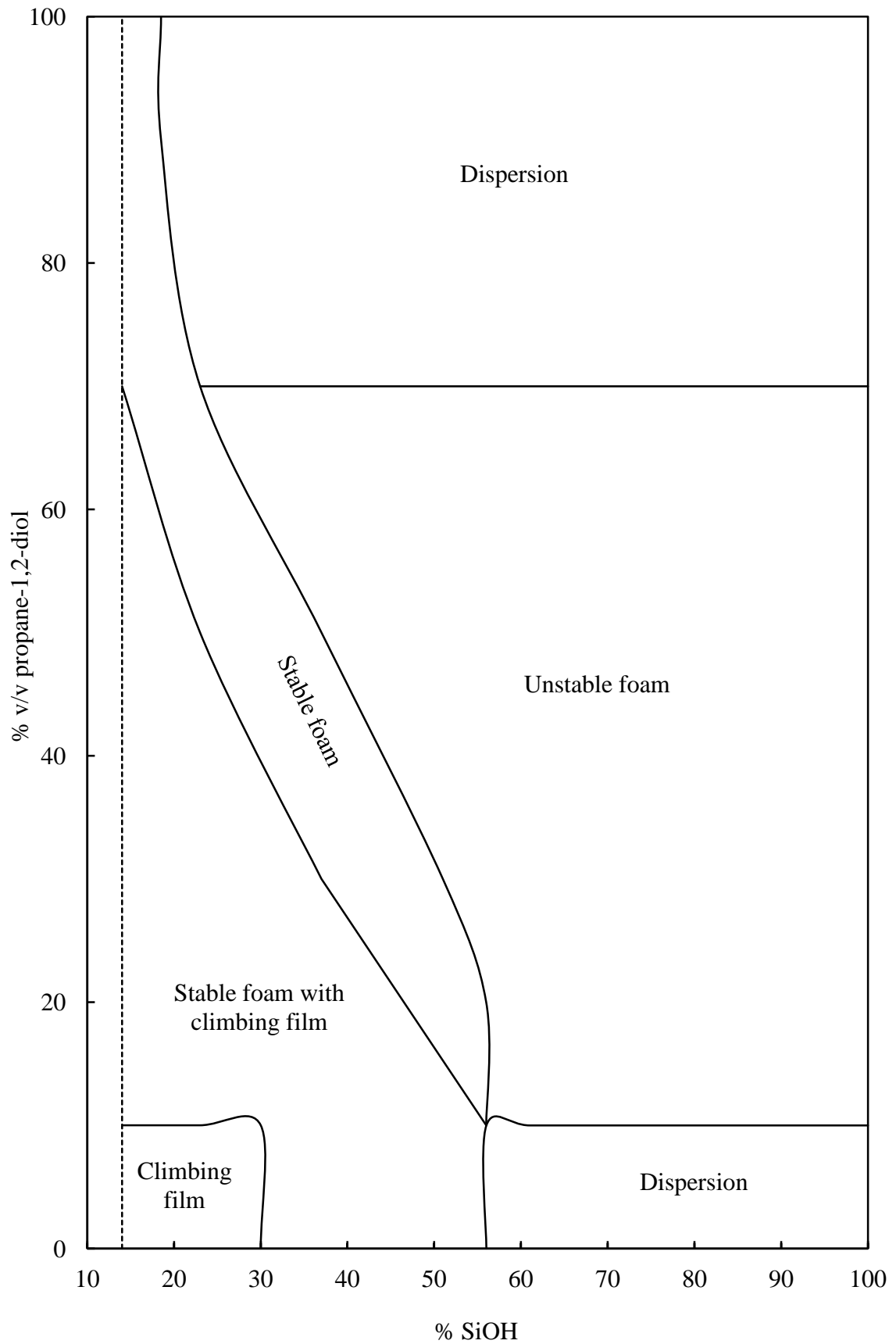


Figure 4.6. Schematic of the materials prepared from data shown in Figure 4.5. Dotted line represents the lowest % SiOH investigated (14% SiOH).



4.3 Emulsions formed in water-propane-1,2-diol-silica-paraffin liquid systems

The effect of propane-1,2-diol on systems now containing oil (paraffin liquid) will be discussed and the findings rationalised in terms of contact angle θ , much like the system with oil absent, which is discussed in section 4.2. The results will be split into two sub-sections relating to the experimental findings and theoretical analysis.

4.3.1 Experimental findings

Emulsions with constant particle concentration (1% w/w) and fixed oil:polar phase volume ratio (1:1) were investigated as a function of particle hydrophobicity for selected propane-1,2-diol:water ratios and as a function of propane-1,2-diol:water ratio for selected particle hydrophobicities. It is known from data shown in chapter 3 and ref. [1] that propane-1,2-diol is miscible in all proportions with water and has a solubility in paraffin liquid of 0.3% w/w at 20 °C. Therefore, propane-1,2-diol is expected to partition exclusively to the aqueous phase.

4.3.1.1 Increasing particle hydrophobicity (fixed aqueous phase ratio)

As the transitional phase inversion of water-paraffin liquid (in the absence of propane-1,2-diol) emulsions with varying particle hydrophobicity has not been investigated before this is discussed first. Emulsions invert from w/o to water-continuous (o/w) upon increasing the hydrophilicity of the particles. The transition from oil-continuous to water-continuous was easily detected *via* conductivity measurements of the emulsions (prepared from equal volumes of paraffin liquid and water containing 1% w/w silica particles) immediately after preparation and the drop test (Figure 4.7).

The visual appearance of emulsions from Figure 4.6 after 6 months of storage (room temperature, 23 ± 4 °C) is shown in Figure 4.8. The vessels clearly indicate that for w/o emulsions using relatively hydrophobic silica particles ($\leq 42\%$ SiOH), a large amount of water remains below the emulsion layer non-emulsified (which is present from time = 0). Figure 4.8 also revealed the most stable conditions for w/o emulsions to coalescence and sedimentation were with 51% SiOH, close to transitional phase inversion. Water-continuous emulsions formed after phase inversion were stable to coalescence but creamed over time. In addition, the most hydrophilic particles (100% SiOH) did not form stable emulsions.

Figure 4.7. Conductivity and type of emulsions prepared from equal volumes of paraffin liquid and water containing 1% w/w silica particles as a function of particle hydrophobicity.

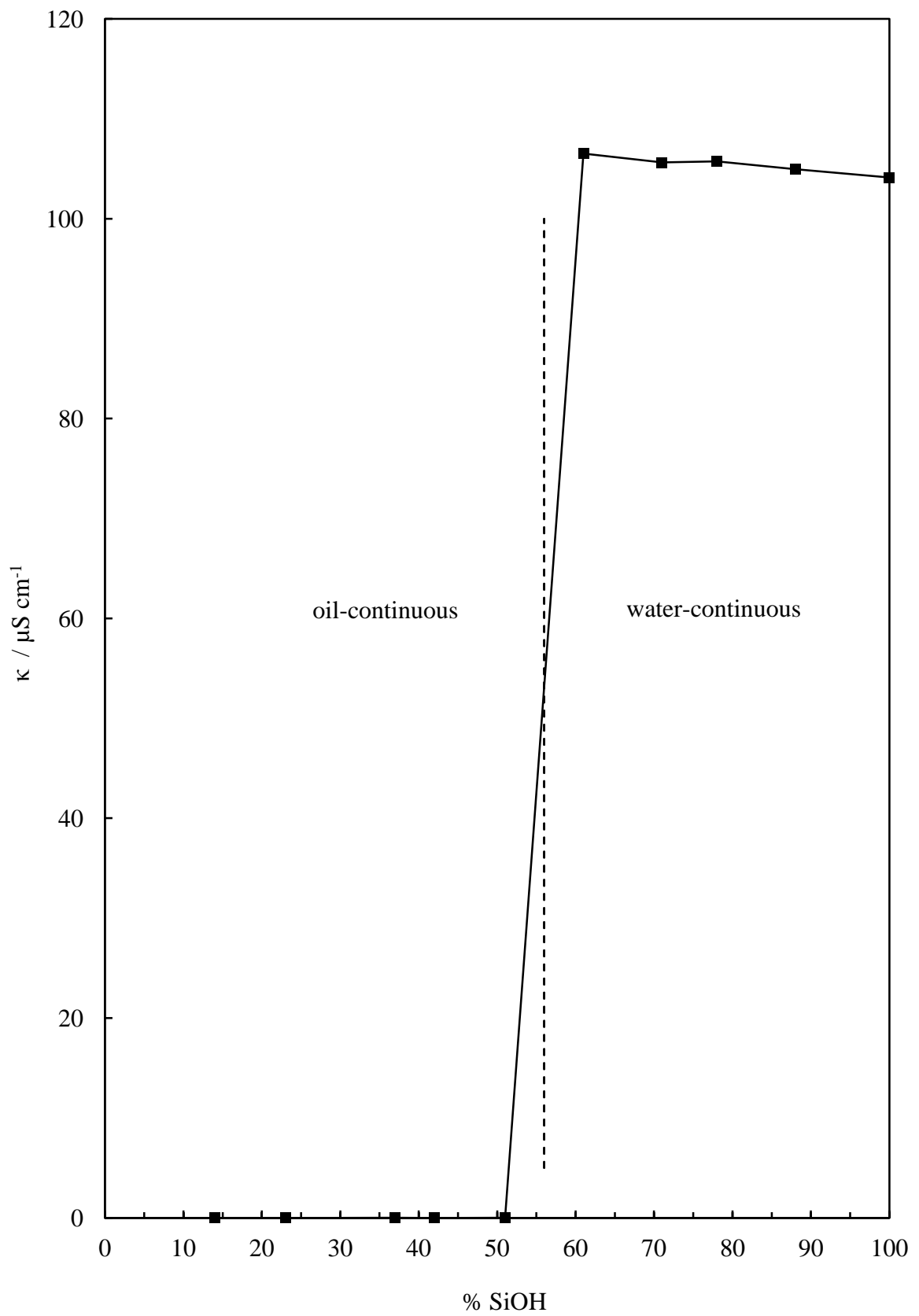
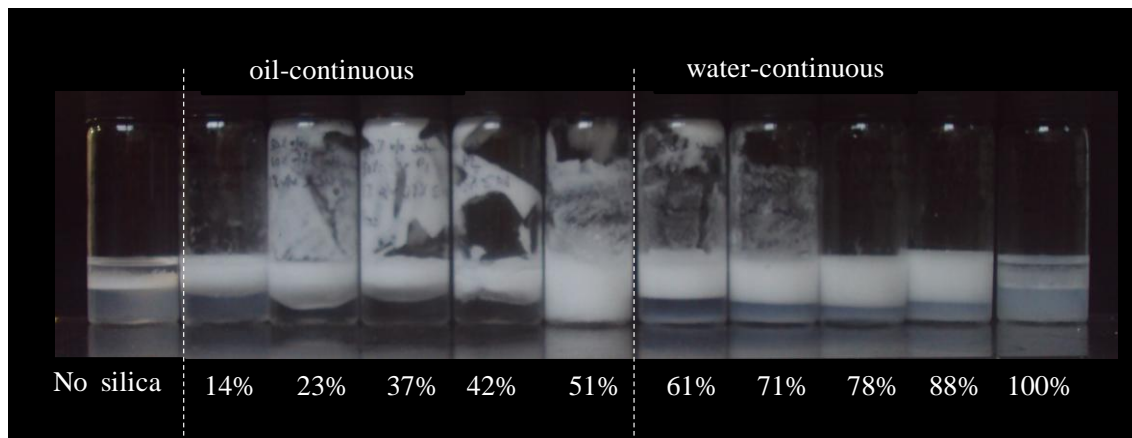


Figure 4.8. Appearance of vessels after 6 months containing emulsions prepared from equal volumes of paraffin liquid and water containing 1% w/w silica particles as a function of particle hydrophobicity (% SiOH given beneath).



Optical micrographs (Figure 4.9) of the water-paraffin liquid-silica system (no propane-1,2-diol) shows that the w/o emulsions invert to multiple water-in-oil-in-water (w/o/w) emulsions around phase inversion and then to simple emulsions of o/w. The appearance of stable multiple emulsions around phase inversion with fumed silica has been witnessed before in the case of commercial oils, *e.g.* silicone and triglycerides, in this case the commercial oil is paraffin liquid.[31, 32] The phenomenon of multiple emulsions present in systems containing commercial oils could be due to oils of different types, *e.g.* chain length, favouring both emulsion types with particles of the same hydrophobicity. The mean droplet diameter passes through a minimum value around phase inversion, Figure 4.10, alongside a maximum in stability to coalescence and either creaming (w/o/w) or sedimentation (w/o), much like what has been reported in the literature for emulsions stabilised by such particles.[15, 33]

Figure 4.9. Optical micrographs of emulsions formed in paraffin liquid-water systems for silica particles possessing different % SiOH (given) at room temperature (20 ± 3 °C) after 6 months of storage. Emulsions are w/o for 14 and 51% SiOH and water-continuous above this. Scale bars = 100 μ m.

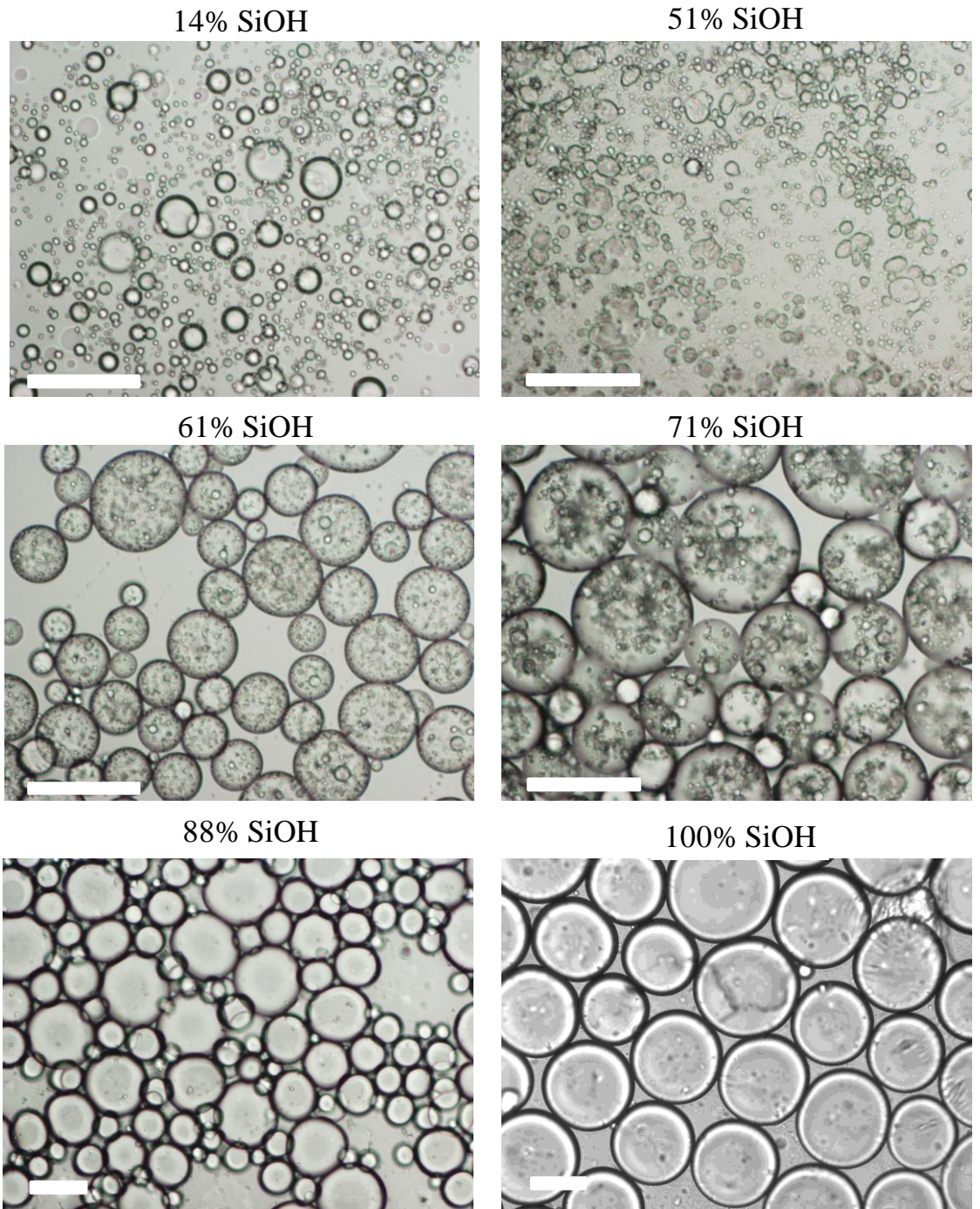
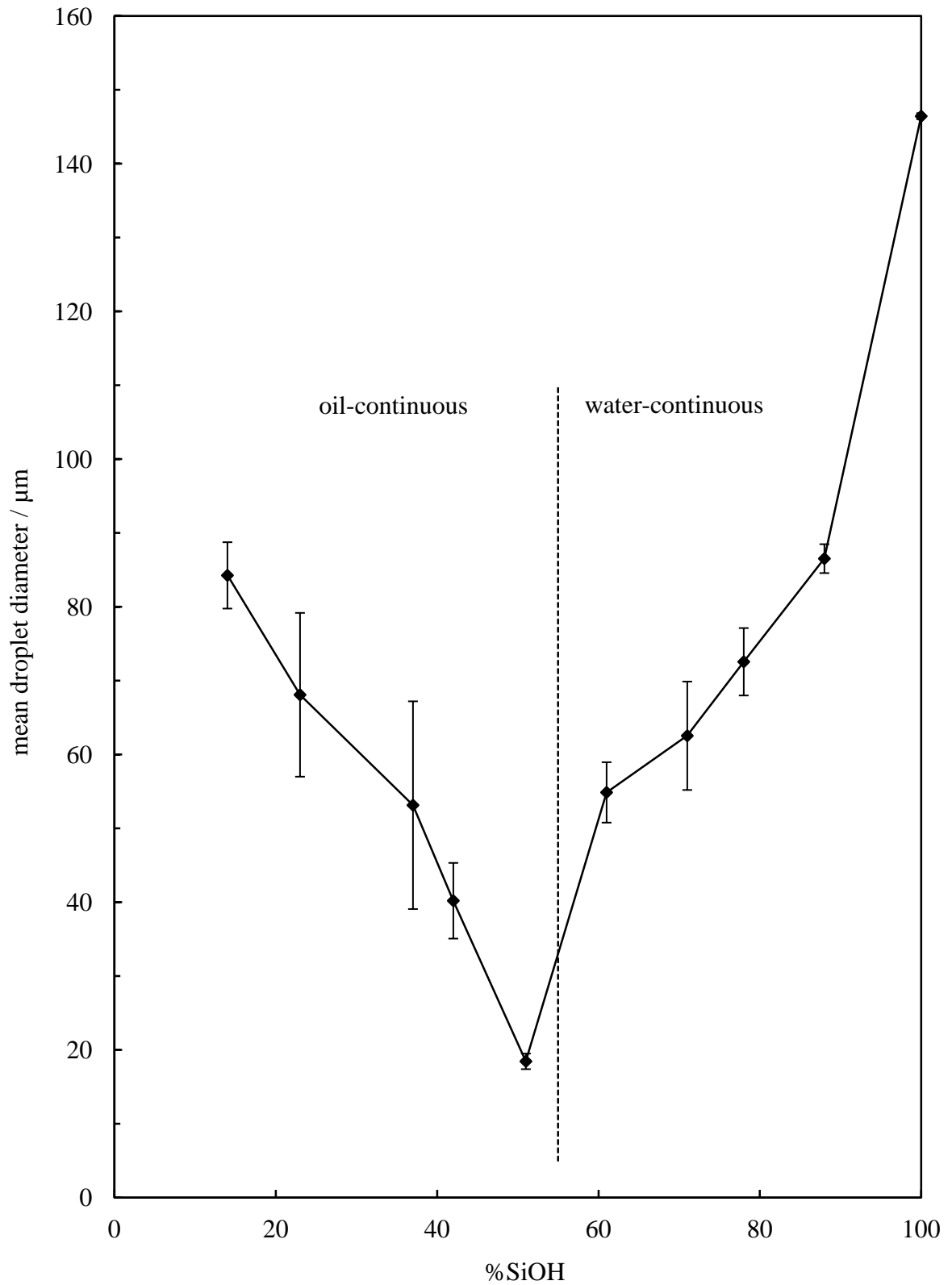


Figure 4.10. Mean droplet diameter (measured using microscope images) versus particle hydrophobicity of emulsions containing paraffin liquid-water for silica particles possessing different % SiOH at room temperature (20 ± 3 °C) after 6 months of storage. In the case of the w/o/w emulsion values refer to oil globules.



4.3.1.1.1 Addition of propane-1,2-diol to the aqueous phase

Figure 4.11 and Figure 4.12 show the appearance of emulsions of neat propane-1,2-diol and paraffin liquid emulsions stabilised by 1% w/w fumed silica of varying hydrophobicity and their conductivities as a function of the particle hydrophilicity. Compared to the water-oil-silica emulsions (Figure 4.7), phase inversion occurs at a much lower % SiOH (between 14 and 23%), *i.e.* replacement by propane-1,2-diol makes particles effectively more hydrophilic *in situ*. Again, emulsification of all the water is incomplete for particles forming w/o emulsions at initial homogenisation and afterwards. For o/w emulsions, the stability to coalescence and creaming over 6 months is very high near phase inversion but by 61% SiOH both processes are significant until above 88% SiOH complete phase separation (CPS) occurs immediately after emulsion formation.

Figure 4.11. Appearance of vessels after 6 months containing emulsions prepared from 50% v/v propane-1,2-diol and 50% v/v paraffin liquid containing 1% w/w silica particles as a function of particle hydrophobicity.

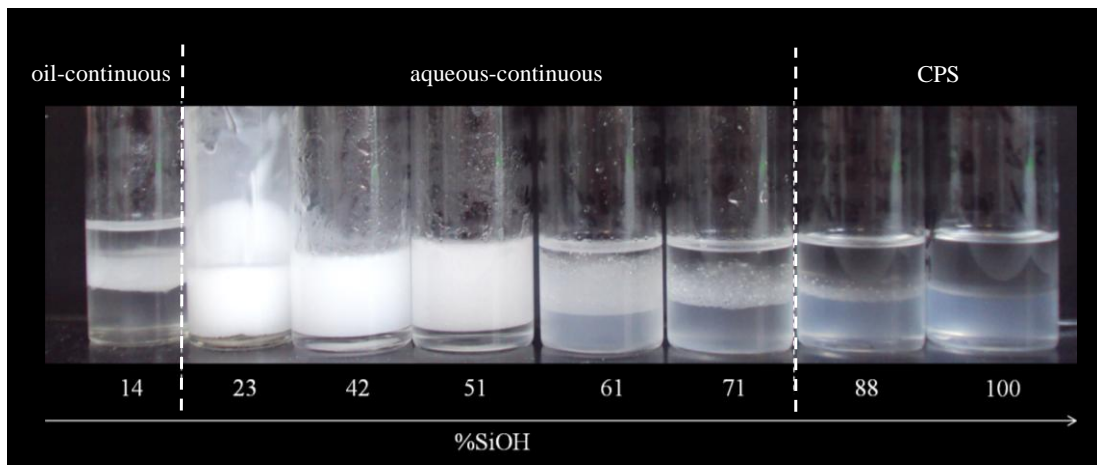
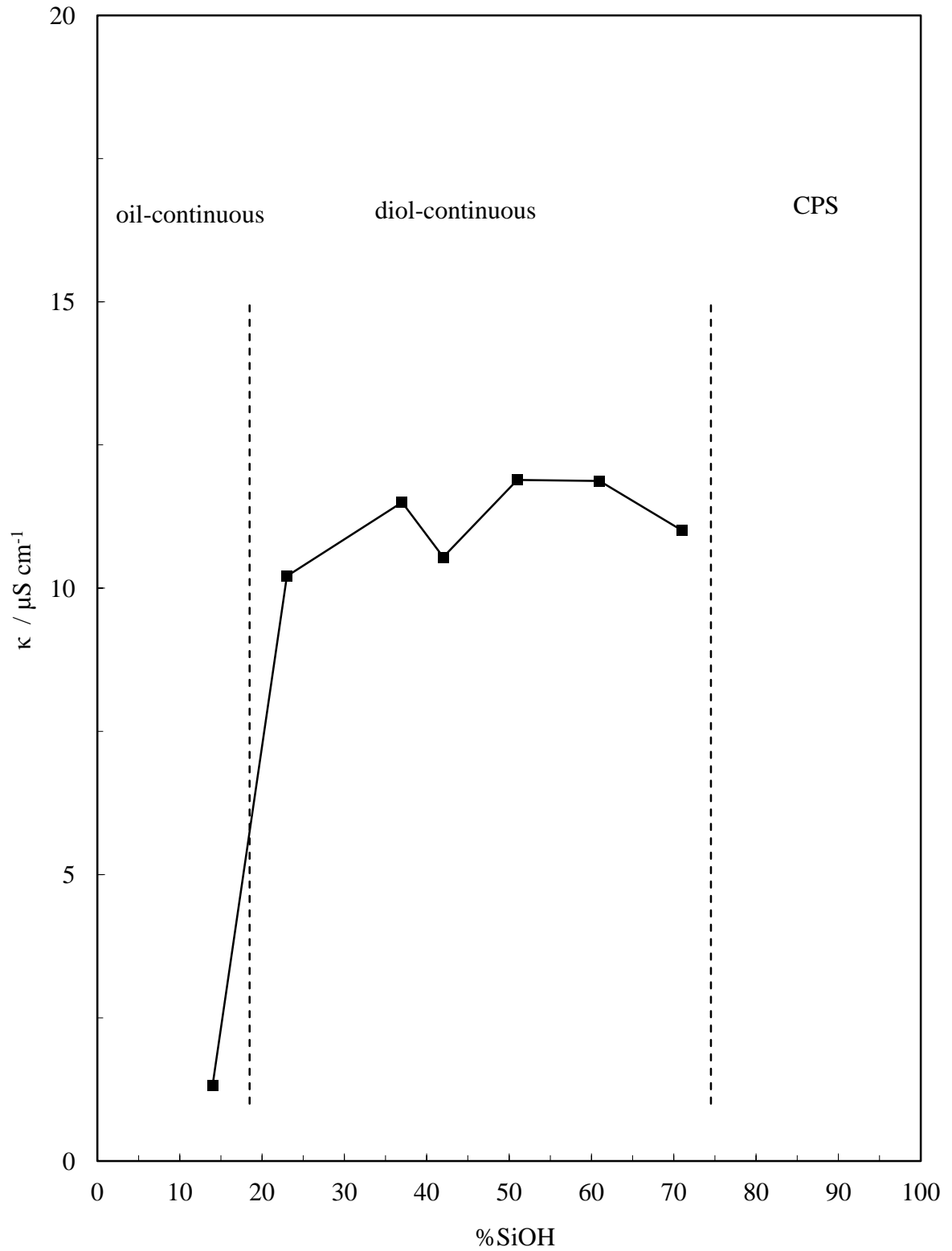


Figure 4.12. Conductivity and type of emulsions prepared from 50% v/v propane-1,2-diol and 50% v/v paraffin liquid containing 1% w/w silica particles as a function of particle hydrophobicity. For CPS systems, conductivity fluctuates between that of oil and propane-1,2-diol.



The average droplet diameter is a minimum (Figure 4.13) at phase inversion from the emulsions described in Figure 4.12 with particularly small (5 μm) oil drops in pure diol being formed for particles possessing 23% SiOH. The upper two optical micrographs shown in Figure 4.14 demonstrate the non-spherical nature of these droplets arising from jamming of the particles at interfaces preventing shape relaxation.[33]

Long term stability to coalescence was seen for an indefinite time period in sharp contrast to high diol containing emulsions stabilised by low molecular weight surfactants discussed in Chapter 3 and ref [1]. In those studies, even with 10% w/w surfactant, no stable emulsion was possible for propane-1,2-diol mole fractions (in mixtures of water) above 0.4. The same investigations were repeated in systems containing a 20:30 or 25:25 ratio of propane-1,2-diol:water and will summarised in section 4.3.1.3 on page 126.

Figure 4.13. Mean droplet diameter (measured using microscope images) versus particle hydrophobicity (varying % SiOH) for emulsions formed from paraffin liquid (50% v/v) and propane-1,2-diol (50% v/v) with 1% w/w fumed silica particles.

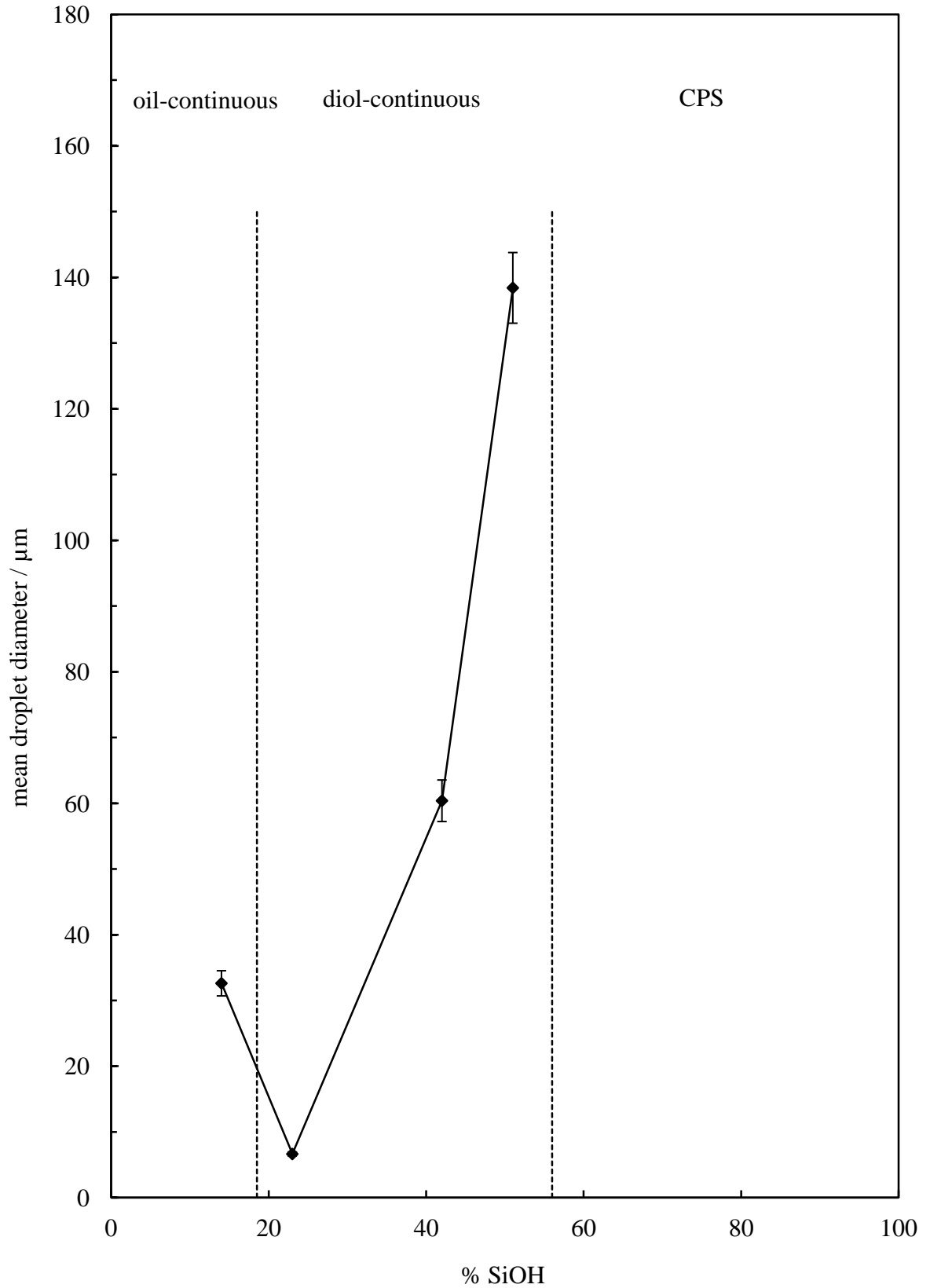
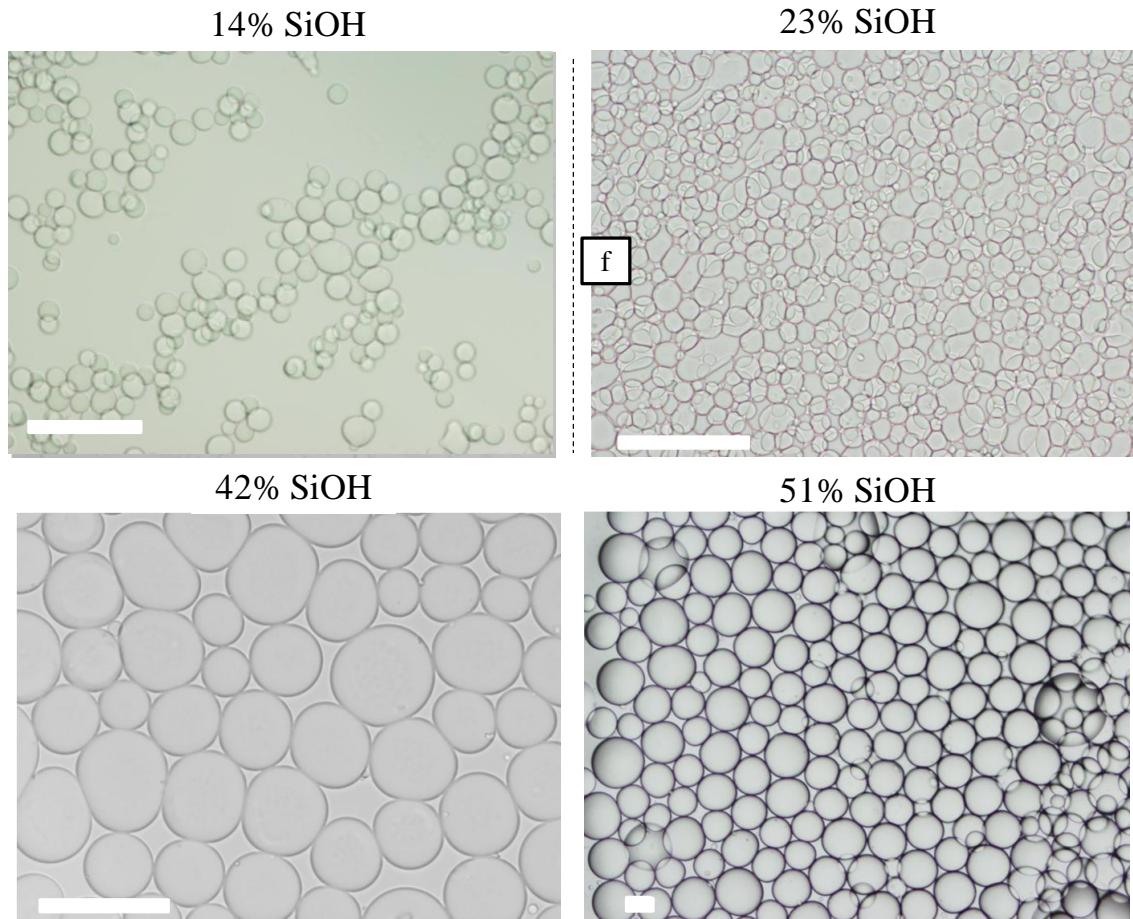


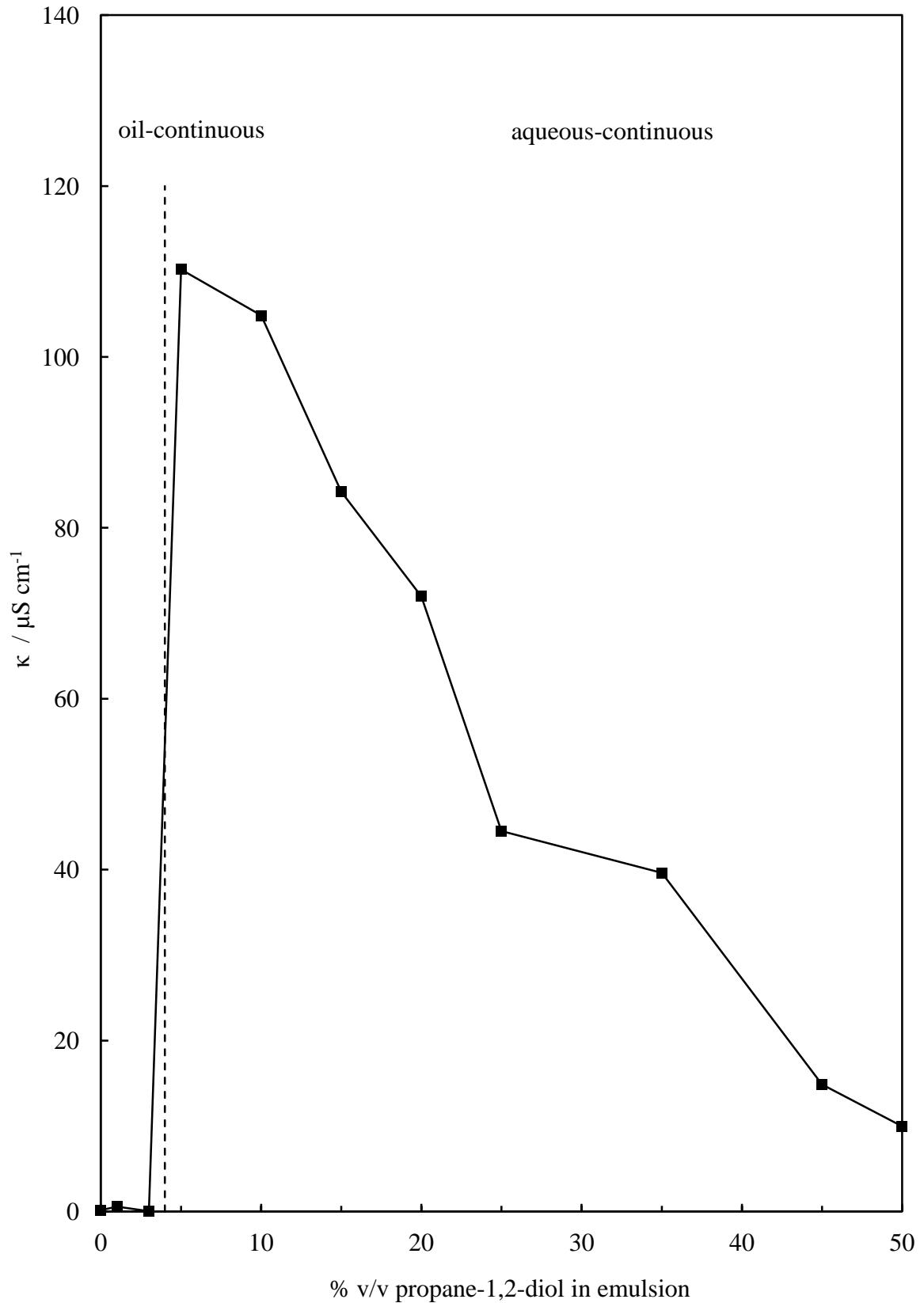
Figure 4.14. Optical micrographs of emulsions formed in paraffin liquid (50% v/v) and propane-1,2-diol (50% v/v) systems for silica particles possessing different % SiOH (given). Emulsions are oil-continuous for 14% SiOH and diol-continuous above this. Scale bars = 100 μm .



4.3.1.2 Increasing propane-1,2-diol in the emulsion (fixed particle hydrophobicity)

The characteristics of particle-stabilised emulsions prepared at fixed particle hydrophobicity (42% SiOH) with increasing propane-1,2-diol content in water are shown here to demonstrate the effect of diol addition to the aqueous phase on the particle-stabilised emulsions. Conductivity changes (Figure 4.15) indicated that phase inversion from oil-continuous to aqueous-continuous emulsions occurred around 4% v/v propane-1,2-diol in the emulsion (8% v/v in the water). The decrease in conductivity with increasing diol is a direct result of the decrease in dissociation of NaCl in propane-1,2-diol aqueous solutions.

Figure 4.15. Conductivity and type of emulsions prepared from equal volumes of paraffin liquid and aqueous propane-1,2-diol containing 1% w/w silica particles possessing 42% SiOH as a function of diol content in the emulsion. 50% v/v on the x-axis corresponds to neat diol.



The w/o emulsions from Figure 4.15 did not undergo sedimentation after 6 months but did demonstrate a small amount of coalescence (Figure 4.16); whereas the aqueous-continuous emulsions, including the emulsion containing neat propane-1,2-diol, show no coalescence after 6 months. The emulsion series (Figure 4.16) presented different trends in creaming instability compared to the series in which the hydrophobicity of the particles varied (Figure 4.10 and Figure 4.13). Here the stability to creaming increases moving away from inversion by increasing the diol content in the aqueous phase.

Figure 4.16. Appearance of vessels after 6 months containing emulsions prepared from equal volumes of paraffin liquid and aqueous propane-1,2-diol containing 1% w/w silica particles possessing 42% SiOH as a function of diol content in the emulsion.

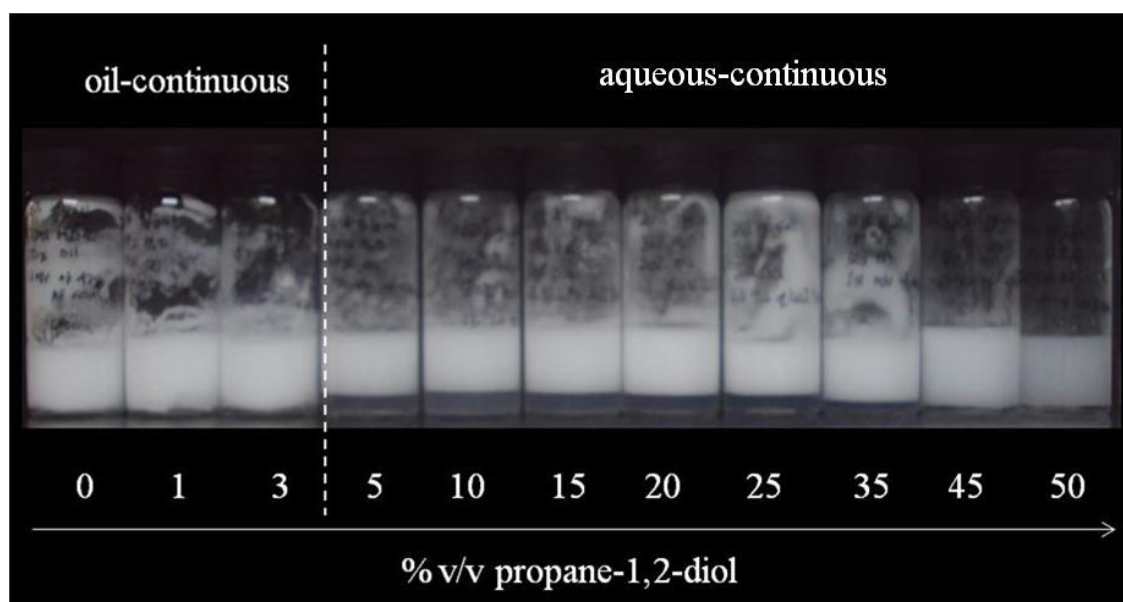


Figure 4.17 shows the variation of mean droplet diameter with increasing propane-1,2-diol in the emulsion. The smallest droplets (w/o at low diol content and o/w at high diol content) gave rise to emulsions with high stability to creaming and sedimentation, as expected. Spherical droplets were seen throughout the emulsion series, as seen in Figure 4.18 upper four images, while the lower two images show cryo-SEM images and from that the close-packed fractal nature of the fumed silica particles at the surface of a water droplet in oil (bottom left image) can be seen as well as the silica particles present at w/o/w interfaces. In addition, a stable w/o/w multiple emulsion can be visualised in Figure 4.18 (bottom right image). Supplementary investigations were conducted for emulsions stabilised with 37 and 23% SiOH fumed silica with varying propane-1,2-diol in the emulsion, summarised below.

Figure 4.17. Mean droplet diameter (measured using microscope images) - after 6 months versus propane-1,2-diol content in emulsions of paraffin liquid and aqueous propane-1,2-diol stabilised by 1% w/w of 42% SiOH silica particles. 50% v/v on the x-axis corresponds to neat diol.

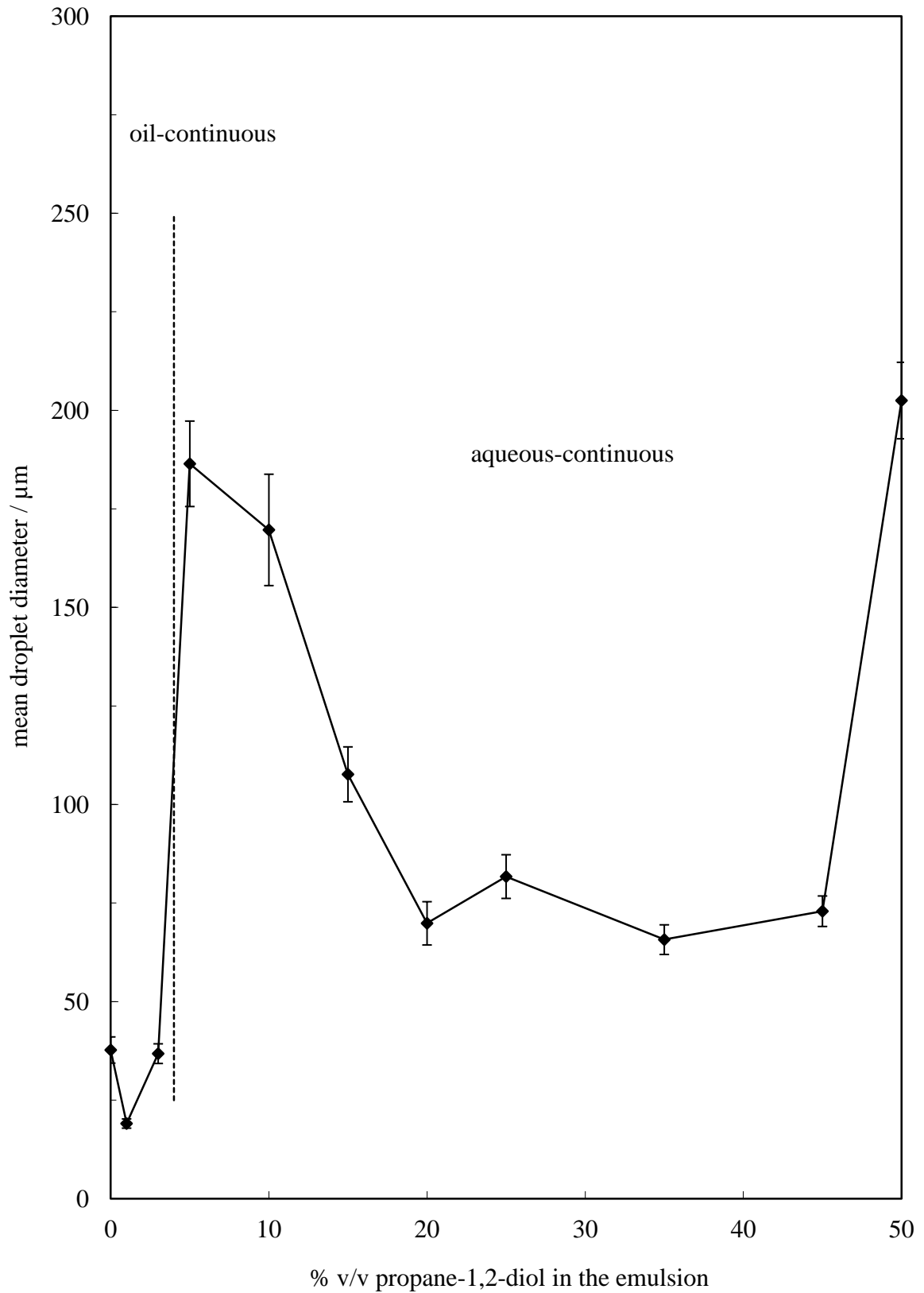
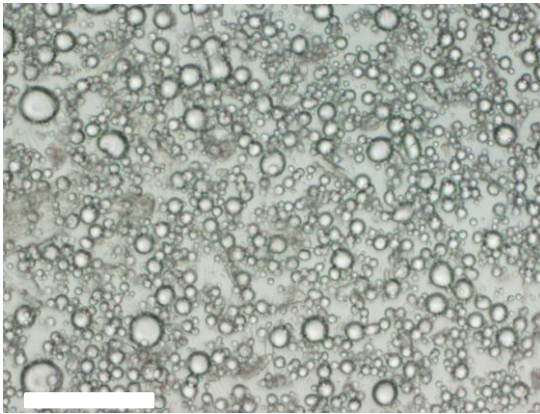
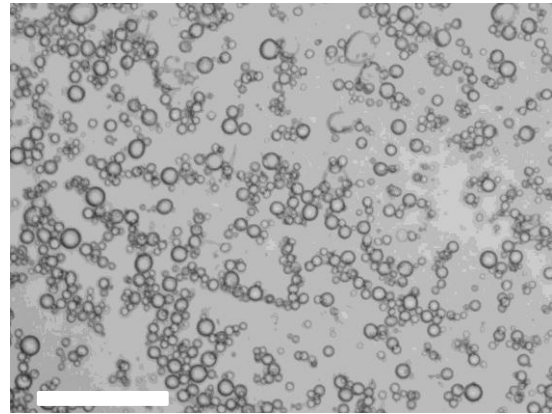


Figure 4.18. Upper four – optical micrographs of emulsions of paraffin liquid and aqueous propane-1,2-diol stabilised by 1% w/w of 42% SiOH silica particles; scale bars = 100 μ m. Lower two – cryo-SEM images of emulsions containing 2.5 (w/o) and 5% v/v (w/o/w) propane-1,2-diol in the overall emulsion.

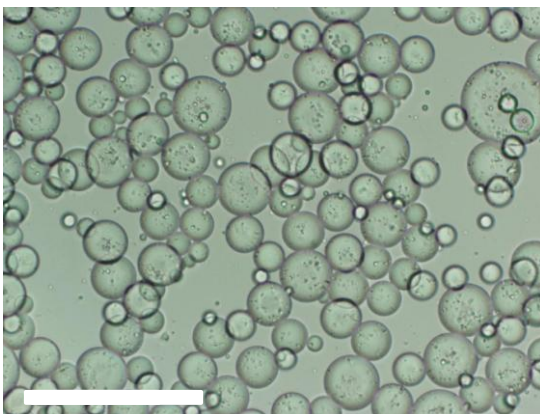
0% v/v propane-1,2-diol



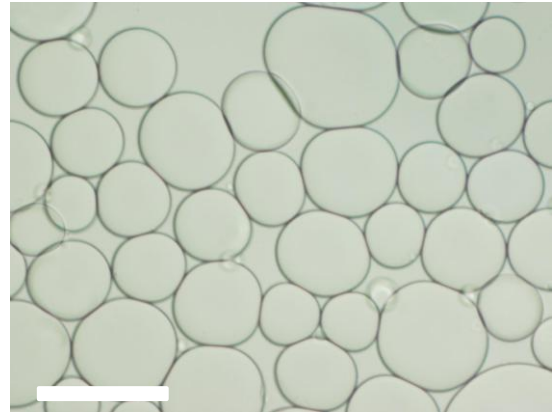
3% v/v propane-1,2-diol



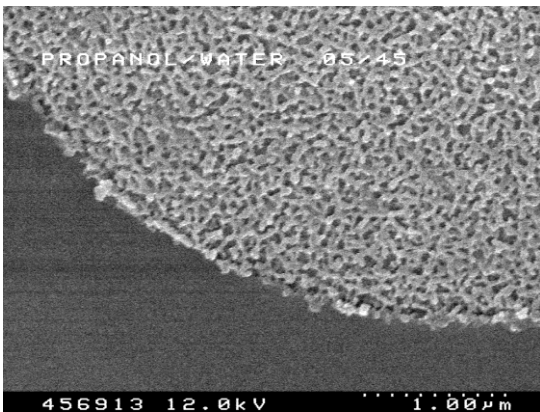
15% v/v propane-1,2-diol



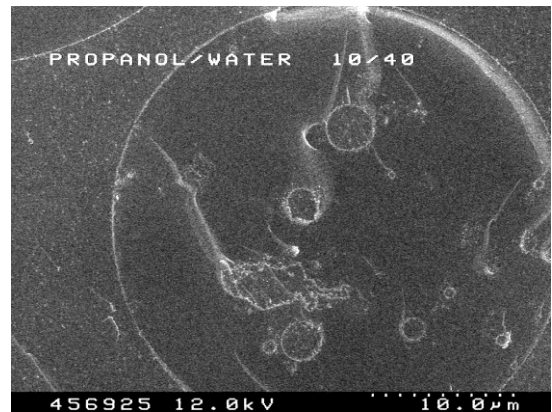
50% v/v propane-1,2-diol



2.5% v/v propane-1,2-diol



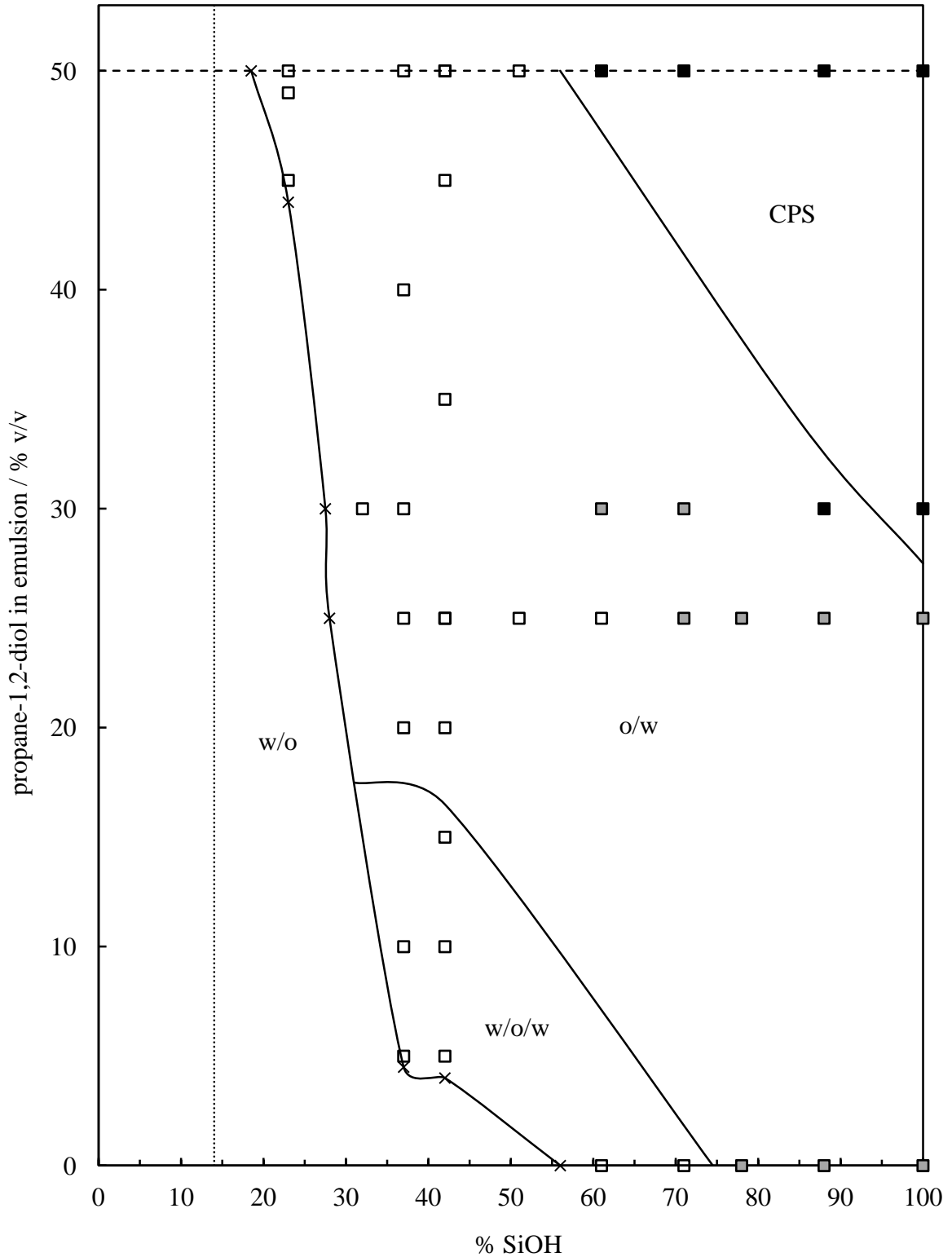
5% v/v propane-1,2-diol



4.3.1.3 Summary of quaternary silica-water-paraffin liquid-propane-1,2-diol systems

In total the results of seven series of quaternary systems of silica particles, paraffin liquid, propane-1,2-diol and water were investigated and are summarised in Figure 4.19 where the diol content in the emulsion is plotted against the % SiOH of the particles. In all emulsions studied, Figure 4.19 revealed that an increase of diol in the emulsion leads to a reduction in the hydrophilicity of the particles required to cause phase inversion from oil-continuous to water/aqueous-continuous. Thus, the region in which stable oil-continuous emulsions can be prepared is reduced. For example, at low propane-1,2-diol content in the emulsion, multiple emulsions of w/o/w are stabilised around phase inversion, while the unstable emulsions to coalescence occur at high diol content in the emulsion prepared with relatively hydrophilic particles (> 50% SiOH). However, high diol-containing emulsions (o/w) can still be stabilised to coalescence with particles of intermediate hydrophobicity including systems containing neat diol, *i.e.* no water. Figure 4.19 describes the fraction of dispersed phase F_d which is the fraction of the dispersed oil phase which has resolved over a six month time period.

Figure 4.19. Emulsion type and coalescence stability as a function of propane-1,2-diol content and % SiOH on particles (1% w/w) in paraffin liquid-propane-1,2-diol-water-silica emulsions. Solid lines indicate the boundaries between the different types of emulsions; dotted line indicates the most hydrophobic particles; dashed line indicates emulsions with pure diol. Within 6 months the fraction of the dispersed phase resolved f_d : $f_d = 0$ (unfilled squares), $f_d < 0.1$ (grey squares), $f_d > 0.1$ (black squares).



4.3.2 Theoretical approach of determining phase inversion by contact angle of fumed silica at the water/propane-1,2-diol-paraffin liquid interface

Experimental investigations of the phase inversion in water-paraffin liquid-propane-1,2-diol-silica systems clearly indicate that the addition of diol played a major role in determining the point of phase inversion. Here the influence of propane-1,2-diol within these emulsions has been theoretically calculated in terms of the apparent contact angles of the fumed silica particles at the paraffin liquid-polar phase interface. For a solid particle (s) located at the oil (o)-polar phase (l) interface, the three interfacial tensions are related to the contact angle θ (measured through the polar phase) by the equivalent Young equation (equation (4.2)), in which γ_{sa} becomes γ_{so} and γ_{la} becomes γ_{lo} .

$$\cos\theta = \frac{\gamma_{so} - \gamma_{sl}}{\gamma_{lo}} \quad (4.5)$$

Values of γ_{lo} were measured experimentally (see Table 4.2) and values of γ_{sl} for silica particle surfaces were calculated earlier in section 4.2. In order to predict values of contact angles for silica particles at the oil-polar phase interface in equation (4.5) γ_{so} needs to be determined.

Using combining rules and the methodology discussed in section 4.2, the interfacial tensions for the solid-oil and polar liquid-oil interfaces, respectively, become

$$\gamma_{so} = \gamma_{sa} + \gamma_{oa} - 2\sqrt{\gamma_s^d \gamma_o^d} - 2\sqrt{\gamma_s^p \gamma_o^p} \quad (4.6)$$

$$\gamma_{lo} = \gamma_{la} + \gamma_{oa} - 2\sqrt{\gamma_o^d \gamma_l^d} - 2\sqrt{\gamma_o^p \gamma_l^p} \quad (4.7)$$

From equation (4.6) it is apparent that estimates of γ_o^d and γ_o^p are required to determine γ_{so} . The appropriate form of equation (4.3) for the oil-air surface tension is

$$\gamma_{oa} = \gamma_o^d + \gamma_o^p \quad (4.8)$$

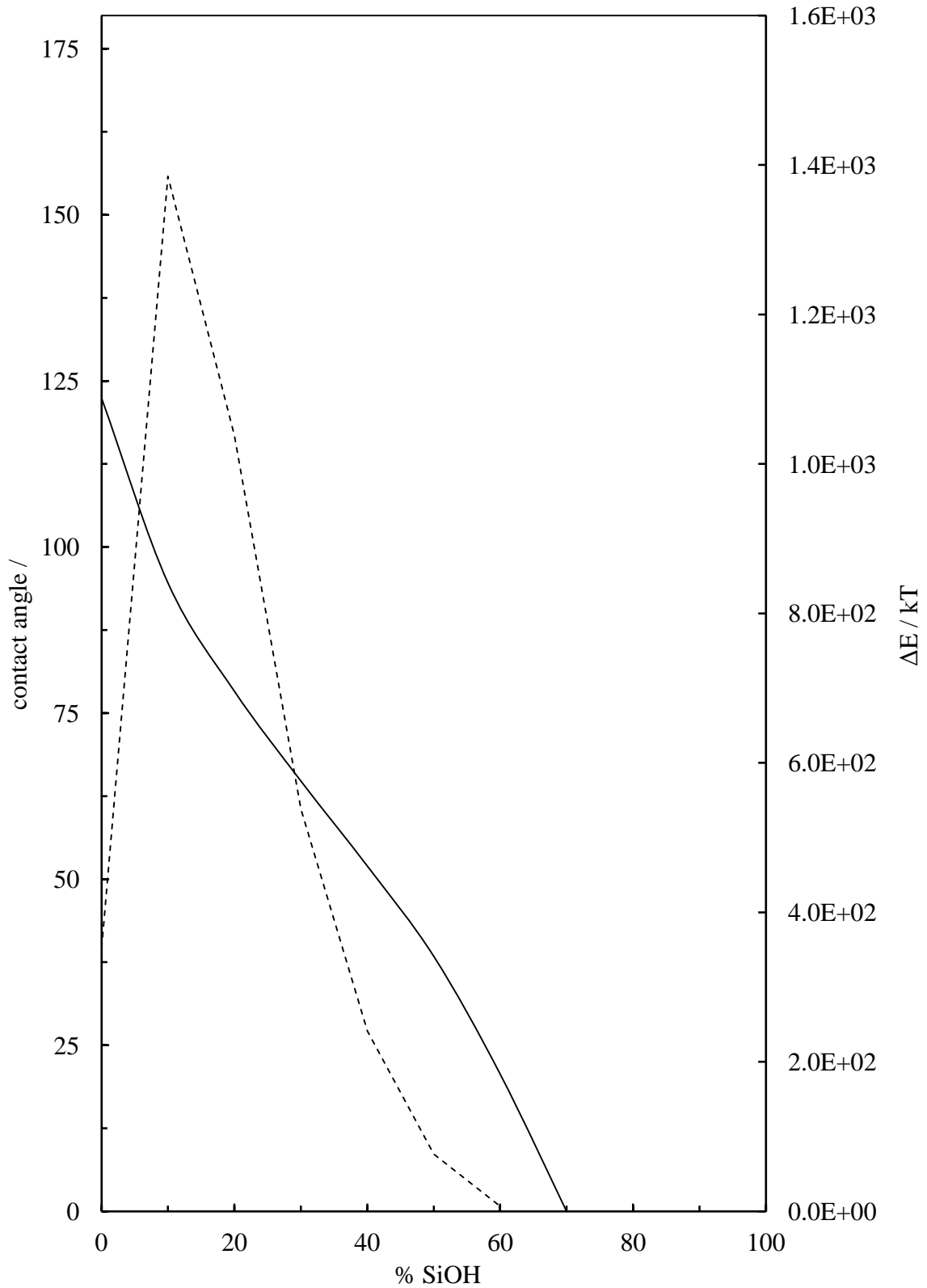
with the polar phase-oil tension γ_{lo} given by equation (4.7). Experimental data gave values for both these tensions (Table 4.2). Therefore, solution of the simultaneous equations (4.7) and (4.8) allows calculation of γ_o^d and γ_o^p (and hence γ_{so} for surfaces of different SiOH content). The values determined were 29.9 and 0 mN m⁻¹ respectively.

Table 4.2. Measured values of interfacial tension ($\pm 0.1 \text{ mN m}^{-1}$) at $20 \text{ }^\circ\text{C}$ between aqueous solutions of propane-1,2-diol and paraffin liquid. Surface tension of paraffin liquid-air = $29.9 \pm 0.1 \text{ mN m}^{-1}$.

<u>Propane-1,2-diol / % v/v</u>	<u>$\gamma_{10} / \text{mN m}^{-1}$</u>
0	44.5
2	41.9
5	38.6
10	35.8
15	32.1
20	30.0
30	26.6
40	24.2
50	21.4
60	18.9
80	15.9
100	12.1

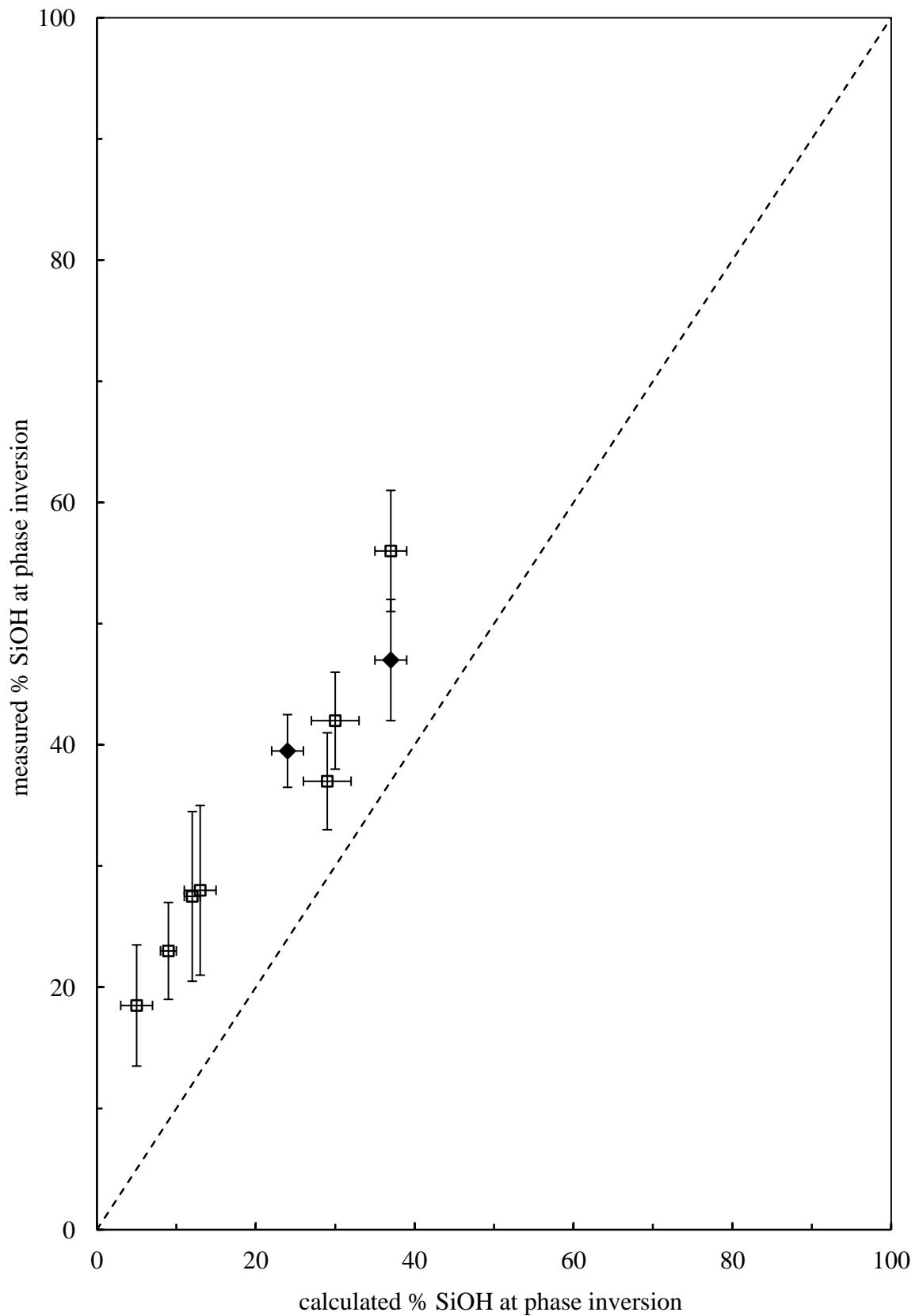
As an illustration of the use of the model described above to calculate contact angles at the oil-polar phase interface, Figure 4.20 shows the calculated contact angle θ (left-hand ordinate) at the oil-polar phase interface as a function of % SiOH on the particle surfaces in an emulsion system containing equal volumes oil and aqueous propane-1,2-diol, where the aqueous propane-1,2-diol ratio was 1:1 (25% v/v propane-1,2-diol and water in emulsion). The contact angle decreases, as expected, with increasing particle hydrophilicity and equals 90° for particles possessing 13% SiOH. Using the hypothesis that emulsions stabilised by particles are of the opposite type below and above 90° (see section 4.1), this can denote the calculated % SiOH at phase inversion for that system. The free energy change upon desorption of a single particle, ΔE , calculated using equation (4.1) was also plotted in Figure 4.20 (right-hand ordinate). A maximum occurs at 13% SiOH implying maximum emulsion stability at this condition.

Figure 4.20. Calculated oil-polar phase contact angle (filled line, left-hand ordinate) and detachment energy (dashed line, right-hand ordinate) of silica nanoparticles in equal volumes paraffin liquid and 1:1 propane-1,2-diol:water as a function of % SiOH on particle surfaces. Particle radius = 10 nm.



With the calculated % SiOH at phase inversion successfully determined, Figure 4.21 presents a comparison between the measured and calculated emulsion phase inversion points for all of the systems investigated. The agreement between the measured and calculated % SiOH at phase inversion is reasonable (within the uncertainties over a range of particle wettability), and is similar to that observed in a previous study where silica-particle stabilised emulsions of water and a range of polar oils are described.[33] However, the emulsions prepared by the powdered particle method here, with 1% w/w particles (open points), invert at a consistently higher SiOH content (more hydrophilic) than calculated. The relatively high concentration of particles, with the absence of pre-dispersion in one of phases results in particle aggregation, believed to enhance particle hydrophobicity.[34, 35] Due to this known deviation when using the powdered particle method for preparation of emulsions, two samples of lower particle concentration were prepared one containing 50% v/v water, *i.e.* no diol, the other containing 50% v/v diol. Results are indicated by the filled points in Figure 4.21, where the improvement between calculated and measured inversion only occurs in the sample containing no diol. Possible reasons for this mis-match in diol-containing emulsions could be that the interactions between the different phases (oil, polar phase and solid) are not fully accounted for and the diol may absorb to some extent on the particle surfaces for certain systems. However, both of the aforementioned ideas require further investigation in the future to establish a solid conclusion.

Figure 4.21. Comparison of calculated and measured % SiOH at phase inversion for emulsions containing water, aqueous propane-1,2-diol or neat propane-1,2-diol, paraffin liquid and silica particles. Filled and open points represent emulsions prepared with 0.1 or 1.0% w/w particles respectively. Dashed line indicates ideal.



4.4 Conclusions

The effect of adding diol (propane-1,2-diol) to aqueous dispersions of silica nanoparticles and paraffin liquid-water emulsions stabilised by the same particles have been investigated and the following conclusions made:

- Aerated propane-1,2-diol aqueous dispersions (no oil) containing fumed silica particles yields stable dispersions, aqueous foams, climbing particle films or liquid marbles. The formation of the aforementioned materials can be controlled by diol content in the dispersion and the particle hydrophobicity. An increase in diol content is associated with a more hydrophilic system. Contact angle calculations of the particles *in situ* confirm that diol addition does decrease the contact angle and therefore makes the particles effectively more hydrophilic.
- For emulsions containing aqueous diol and paraffin liquid inversion occurs from oil-continuous to aqueous-continuous with increasing particle hydrophilicity of the particles or increasing diol content in the system.
- Emulsions inverted by an increase in diol content show deviations from previous publications, *e.g.* mean droplet diameter and stability to gravitational induced instability show unfamiliar trends. However, the phase inversion results are rationalised in terms of the contact angle at the oil-polar phase interface with reasonable agreement found between the measured and calculated phase inversion conditions.

4.5 References

-
1. B. P. Binks, P. D. I. Fletcher, M. A. Thompson and R. P. Elliott, *Colloids Surf. A*, **390**, 67 (2011).
 2. R. D. Hamill and R. V. Petersen, *J. Pharm. Sci.*, **55**, 1268 (1966).
 3. R. D. Hamill and R. V. Petersen, *J. Pharm. Sci.*, **55**, 1274 (1966).
 4. A. Imhof and D. J. Pine, *J. Colloid Interface Sci.*, **192**, 368 (1997).
 5. A. Otto, J. W. Wiechers, C. L. Kelly, J. Hadgraft and J. du Plessis, *Skin Pharmacol. Physiol.*, **21**, 326 (2008).
 6. R. Strickley, *Pharm. Res.*, **21**, 201 (2004).
 7. B. de Spiegeleer, E. Wattyn, G. Slegers, P. Van der Meeren, K. Vlaminck and L. Van Vooren, *Pharm. Dev. Technol.*, **11**, 275 (2006).

8. M. Klapper, S. Nenov, R. Haschick, K. Müller and K. Müllen, *Acc. Chem. Res.*, **41**, 1190 (2008).
9. B. P. Binks and T. S. Horozov (eds.), *Colloid Particles and Liquid Interfaces*, Cambridge University Press, Cambridge (2006).
10. B. P. Binks and T. S. Horozov, *Angew. Chem. Int Ed.*, **117**, 3788 (2005).
11. I. Akartuna, A. R. Studart, E. Tervoort, U. T. Gonzenbach and L. J. Gauckler, *Langmuir*, **24**, 7161 (2008).
12. T. N. Hunter, R. J. Pugh, G. V. Franks and G. J. Jameson, *Adv. Colloid Interface Sci.*, **137**, 57 (2008).
13. F. Leal-Calderon and V. Schmitt, *Curr. Opin. Colloid Interface Sci.*, **13**, 217 (2008).
14. B. P. Binks, *Curr. Opin. Colloid Interface Sci.*, **7**, 21 (2002).
15. B. P. Binks and S. O. Lumsdon, *Langmuir*, **16**, 8622 (2000).
16. A. F. Koretsky and P. M. Kruglyakov, *Izv. Sib. Otd. Akad. Nauk USSR*, **2**, 139 (1971).
17. N. W. Yan, M. R. Gray and J. H. Masliyah, *Colloids Surf. A*, **193**, 97 (2001).
18. S. Stiller, H. Gers-Barlag, M. Lergenmueller, F. Pflücker, J. Schultz, K. P. Wittern and R. Daniels, *Colloids Surf. A*, **232**, 261 (2004).
19. B. P. Binks and S. O. Lumsdon, *Phys. Chem. Chem. Phys.*, **2**, 2959 (2000).
20. R. Benitez, S. Contreras and J. Goldfarb, *J. Colloid Interface Sci.*, **36**, 146 (1971).
21. D. K. Owens and R. C. Wendt, *J. Appl. Polym. Sci.*, **13**, 1741 (1969).
22. D. K. Owens and R. C. Wendt, *J. Appl. Polym. Sci.*, **13**, 1741 (1969).
23. J. J. Jasper, *J. Phys. Chem. Ref. Data*, **1**, 841 (1972).
24. I. Moutinho, M. Figueiredo and P. Ferreira, *Tappi J.*, **6**, 26 (2007).
25. B. P. Binks and J. H. Clint, *Langmuir*, **18**, 1270 (2002).
26. J. H. Clint and A. C. Wicks, *J. Adhes. Adhes.*, **21**, 267 (2001).
27. B. P. Binks and R. Murakami, *Nat Mater*, **5**, 865 (2006).
28. B. P. Binks, A. J. Johnson and J. A. Rodrigues, *Soft Matter*, **6**, 126 (2010).
29. B. P. Binks, J. H. Clint, P. D. I. Fletcher, T. G. J. Lees and P. Taylor, *Chem Commun*, 3531 (2006).
30. P. D. I. Fletcher and B. L. Holt, *Langmuir*, in press (2011).
31. B. P. Binks and C. P. Whitby, *Langmuir*, **20**, 1130 (2004).
32. B. P. Binks and J. A. Rodrigues, *Langmuir*, **19**, 4905 (2003).
33. B. P. Binks, P. D. I. Fletcher, B. L. Holt, J. Parker, P. Beaussoubre and K. Wong, *Phys. Chem. Chem. Phys.*, **12**, 11967 (2010).
34. B. P. Binks, P. D. I. Fletcher, B. L. Holt, P. Beaussoubre and K. Wong, *Langmuir*, **26**, 18024 (2010).
35. B. P. Binks, J. Philip and J. A. Rodrigues, *Langmuir*, **21**, 3296 (2005).

CHAPTER 5. EFFECT OF CRYSTALLISATION IN DIOL CONTAINING EMULSIONS

5.1 Introduction

The final aspect of the non-conventionality in emulsions to be discussed is the effect of crystallisation in diol containing emulsions. The system used to investigate and understand these emulsions with changing temperature is described below in Table 5.1. As the investigations are reliant on crystallisation of the emulsion components the melting points are stated for convenience. The emulsion system produces an o/w emulsion upon homogenisation and the dispersed phase (white soft paraffin and paraffin liquid composition) is thought to be semi-crystalline at room temperature as well as four surfactants (cetostearyl alcohol, Arlacel 165, sodium lauryl sulphate and Pluronic F127).

Table 5.1. Composition and concentrations of the model system used throughout the investigations.

<u>Component</u>	<u>Concentration / % w/w</u>	<u>Melting point / °C</u>
Propane-1,2-diol	40.00	-59
Water	27.50	0
White soft paraffin	11.50	30 – 35
Paraffin liquid	10.00	2 - 10
Cetostearyl alcohol	6.75	25 - 34
Arlacel 165	1.50	46
Dimethicone	1.00	-44
Pluronic F127	1.00	56
Sodium lauryl sulphate	0.75	204 – 207

An understanding of how the emulsion properties are affected by crystallisation is important in both formulation and stability of emulsions. The formation of crystals/crystal networks in either the dispersed or continuous phase of an emulsion can be advantageous for the stability of the product and the aesthetic feel and application of the product. However, the formation of crystals and their crystal networks can also lead to instability.[1, 2]

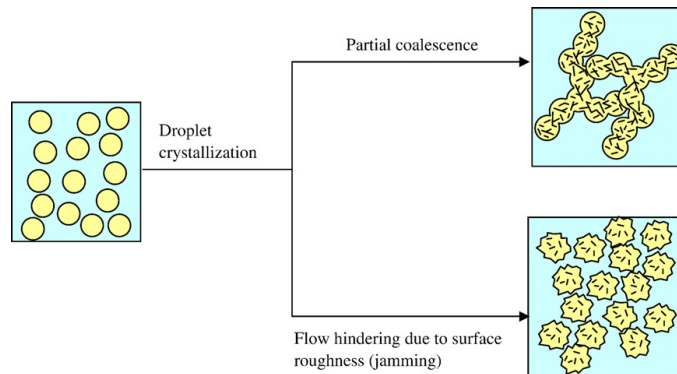
The general concept of crystallisation in conventional emulsions (oil, water, surfactant mixtures) has been studied and has a large contribution in the literature.[3-5] The literature includes investigations into the understanding of crystallisation within emulsions with varying droplet diameter and the formation of crystal networks in food products such as margarine.[4, 6-8]

One of the main understandings from the literature is that crystallisation within emulsion dispersed droplets can have a feature known as supercooling. This is where the dispersed droplets remain liquid at temperatures lower than the corresponding bulk dispersed phase melting temperature. Supercooling is hypothesised to be the result of the larger number of emulsion droplets limiting the amount of nucleation sites available to each droplet, meaning only a very small fraction of droplets will contain a nucleation site and therefore upon cooling (below the bulk dispersed phase melting temperature) supercooling of such droplets occurs.[6] The dependence of the onset of supercooling has been linked to the droplet diameter, presence of impurities and emulsifier type.[7, 9, 10] From investigations into supercooling, crystallisation in dispersed emulsion phases is known to occur in two ways; homogeneous and heterogeneously.[5] The crystallisation mechanism which occurs is dependent on the number of nucleation sites within the droplets. If the droplets contain no impurities, the crystals will form in a homogeneous way. If impurities are present, then heterogeneous crystallisation will occur. These two mechanisms can be distinguished from the onset of crystallisation, as it is known that droplets crystallising by homogeneous mechanism will occur at a lower temperature than the bulk. Alternatively heterogeneous crystallisation will occur at approximately the bulk crystallisation temperature.[11] Interestingly it has been shown by Skoda *et al.* and confirmed by Vanapalli *et al.* that in polydisperse emulsions, with droplet sizes ranging between 1 – 5 μm , crystallisation by both mechanisms can occur. Therefore two crystallisation peaks will be witnessed experimentally; one around the bulk crystallisation temperature and the other at a temperature lower than the bulk crystallisation temperature.[4, 12] The difference between homogeneous and heterogeneous crystallisation can be explained by describing the Gibbs free energy of the system.[13] Classic nucleation theory can explain the homogeneous mechanism; where crystallisation of dispersed oil droplets in water shows a release in heat, as the crystalline phase has a lower Gibbs free energy compared to the liquid (at the equilibrium freezing temperature the Gibbs free energy is equal between the liquid and

solid phases).[5] Consequently the difference in the Gibbs free energy between liquid and crystalline phases is the driving force for crystallisation. The primary stage of crystallisation is the formation of a nucleation site, which is an ordered domain within the liquid. Once this ordered domain becomes a critical size the addition of monomers will cause a decrease in the Gibbs free energy meaning that the nucleation site will grow and if such growth continues the nucleus forms a crystal.[14] For heterogeneous nucleation to occur the presence of impurities, such as dust or anything else with a size greater than the nucleus, lowers the energy requirements for the formation of a nucleus and the activation Gibbs energy for nucleation decreases.

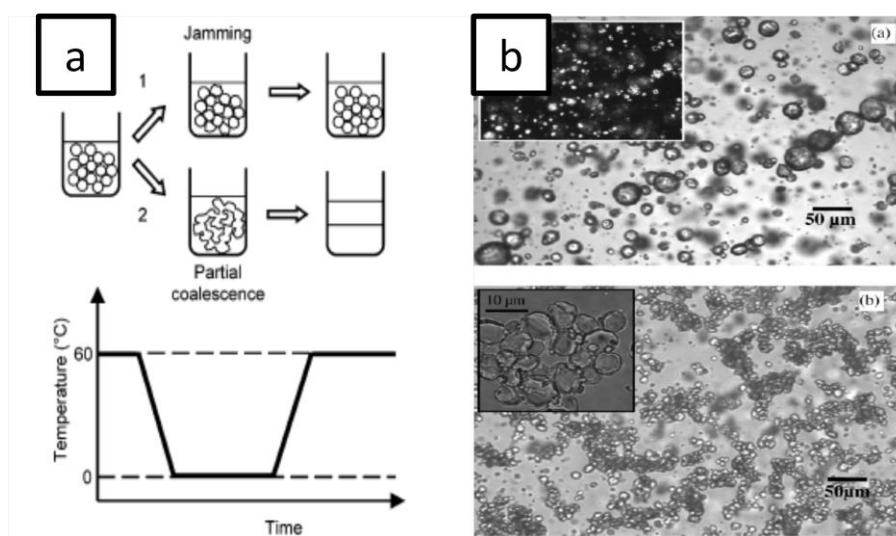
The primary cause of instability in emulsions where the dispersed phase crystallises is known as partial coalescence. Partial coalescence is where two droplets come together, one containing crystals and the other liquid; the crystals from the crystalline drop penetrates the interface of the liquid drop which is in turn crystallised. A “bridge” is now formed between the two combined crystalline droplets, here the key difference between partial and “normal” coalescence is that in the former each droplet retains its own shape to some extent, the inter-droplet interactions that cause partial coalescence then go on to give other instability problems from the increased size of joined droplets. On the other hand the instability process of partial coalescence can be used as an advantage by the formation crystal networks which aid stability. Leal-Calderon *et al.* and Golemanov *et al.* looked at the different ways in which gelling can occur in o/w emulsions from partial coalescence and came up with two mechanisms both induced by crystallisation of dispersed droplets.[15, 16] The first proposed gelling was occurring in o/w emulsions stabilised by non-ionic surfactants where partial coalescence caused a 3D network of interconnected droplets. The second proposed that the restriction of droplets from internal dynamics was caused by surface roughness and the latter is known as the “jammed state” which involves no coalescence at all. The technique used to induce both of the aforementioned gelling properties is called tempering; a thermal technique where the dispersed droplets are melted and then cooled, allowing them to re-crystallise and form gel networks. An illustrated representation is shown in Figure 5.1 of the two mechanisms which can occur with tempering/thermal cycling.

Figure 5.1. Schematic representation of the two scenarios for the formation of gel emulsions caused from crystallisation of the dispersed phase of emulsions using thermal cycling.[17]



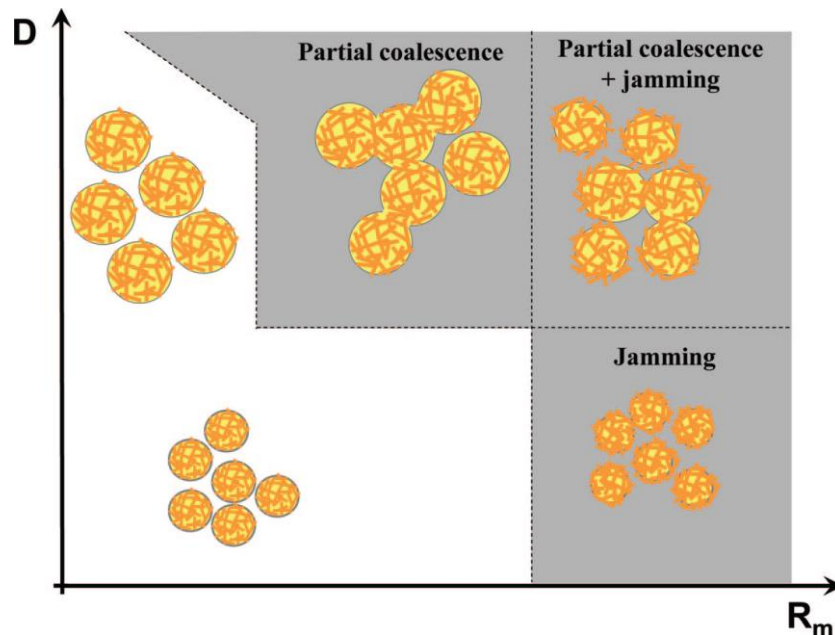
Leal-Calderon *et al.* also showed using crystallisable droplets made of alkanes or paraffin oil in a tempering cycle that o/w emulsions that form a “jamming mechanism” did not phase separate upon reheating, unlike gels formed in a partial coalescence mechanism.[16] Figure 5.2 shows Leal-Calderon’s findings with micrographs showing the two different types of gel networks discussed, jamming or partial coalescence. In the same work it was also found that jamming was more likely to occur if the dispersed droplets had a small average drop size, and partial coalescence was more likely to occur if the average drop size was large.

Figure 5.2. (a) Mechanism of gelling through a thermal cycling, (b) appearance of each gelling network when subjected to microscope after being stored at 0°C for 1 hour; top micrograph represents partial coalescence mechanism and the bottom micrograph represents the jamming mechanism.[16]



In 2008, Thivilliers *et al.* showed comparable findings with respect to the droplet size and gel network occurring in emulsions with crystalline dispersed phases and thermal cycling.[18] Using triglyceride-in-water emulsions, Thivilliers concluded that two gel networks were witnessed, correlating to the mean droplet diameter. The qualitative summary of Thivilliers findings are depicted in Figure 5.3 below, accounting for the general phenomena of gelling in emulsions, which contain partially solidified oil droplets Thivilliers results show that a small droplet diameter ($\approx 5 \mu\text{m}$) and high surfactant to protein molar ratio (more likely to crystallise) gelling caused by jamming occurs. Whereas larger drop diameters ($>15 \mu\text{m}$) form either partial coalescence or partial coalescence plus jamming states depending on the amount of crystalline dispersed phase present. Thivilliers believed that jamming occurred with small droplets as the crystal size is sufficient to cause surface roughness, but insufficient to cause film piercing. Thivilliers also reported that Figure 5.3 could account for the general phenomena of gelling in emulsions which contain partially solidified oil droplets.

Figure 5.3. Summary of different gelling mechanisms induced by thermal cycling as a function of mean droplet size (D) and surfactant to protein molar ratio (R_m) in the continuous phase for triglyceride-in-water emulsions.[18]



5.1.1 Aims

We investigated the crystallisation of droplets within an o/w model emulsion system containing high amounts of diol. To do this the following investigations will be discussed:

- The droplet size variation of the model emulsion system with changing shear rate of homogenisation and the characterisation of the system.
- Stability of the model emulsion system will be investigated with variation in the droplet size and temperature.
- The characteristic effects of the model emulsion system to crystallisation will be investigated using a range of techniques; DSC, rheology and NMR.
- Investigations of a similar, but simpler, model system will be discussed to rationalise findings from the more complex model emulsion system described above.

5.2 *Effect of homogeniser conditions on droplet diameter of model system*

5.2.1 Universal graph of droplet diameter vs. shear rate

The aim of this section is to establish a relationship between the amount of shear rate used during homogenisation and the final droplet diameter of the model emulsion system. A graph was established to show the relationship between these however certain parameters had to be fixed in order to establish a trend. The parameters fixed are:

- Model emulsion composition
- Homogenised at fixed temperature, 70 °C (*i.e.* constant interfacial tension (γ))

The model emulsion system is the same as described in the introduction section but is shown below again in Table 5.2 for convenience. Emulsions prepared from this composition always formed o/w emulsions.

Table 5.2. Composition and concentrations of the model system used throughout the investigations.

<u>Component</u>	<u>Concentration / % w/w</u>
Propane-1,2-diol	40.00
Water	27.50
White soft paraffin	11.50
Paraffin liquid	10.00
Cetostearyl alcohol	6.75
Arlacel 165	1.50
Dimethicone	1.00
Pluronic F127	1.00
Sodium lauryl sulphate	0.75

To understand the crystallisation and stability properties of emulsions containing large amounts of diol with varying droplet diameter a technique for varying droplet diameter was needed. Shear rate was used for its easy variability during homogenisation and the fact that it is a cross platform parameter for different homogenisers, *i.e.* different homogeniser and homogeniser parts can be used to vary the shear rate. Homogenisers used included Ultra-Turrax (different head sizes), Silverson and GSK plant conditions (Becomix).

Shear rate ($\dot{\gamma}$ (s^{-1})) of a homogeniser rotor stator head is calculated using the circumference of the rotor $\Pi.d$ (m), revolutions per minute rpm and the gap size between the rotor and the teeth h (m):

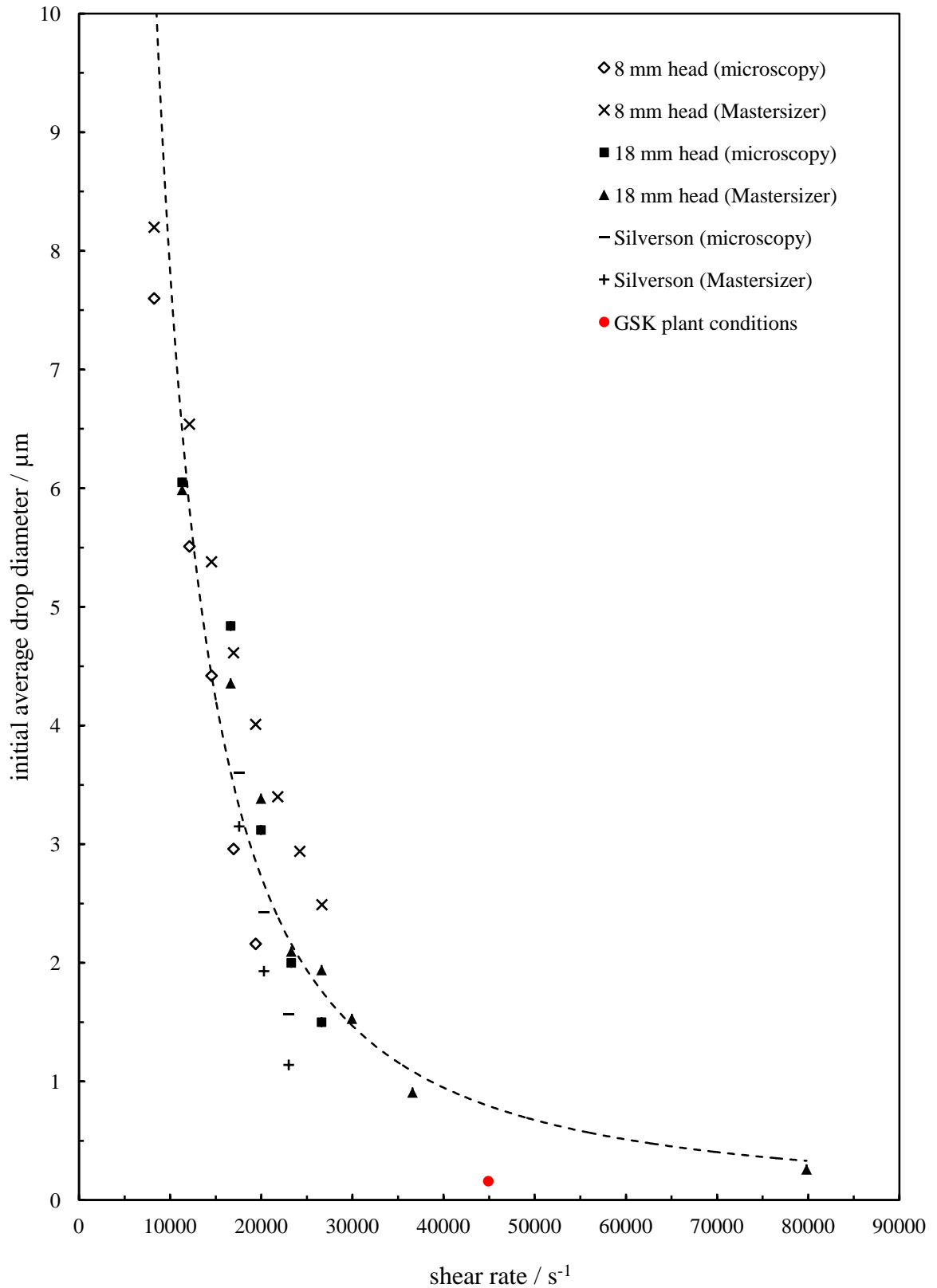
$$\dot{\gamma} = \frac{\Pi.d \text{ rpm}}{h.60} \quad (5.1)$$

Table 5.3. Homogeniser parameters including outer rotor diameters, gap sizes, max and min rpm, and max and min shear rate.

<u>Homogeniser engine</u>	<u>Outer diameter of rotor (mm)</u>	<u>Gap (mm)</u>	<u>Rpm range (max – min)</u>	<u>$\dot{\gamma}$ range (s⁻¹) (max – min)</u>
Ultra-Turrax T25	6.5	0.14	3400 - 24000	8200 - 58100
Ultra-Turrax T25	12.7	0.20	3400 – 24000	11300 - 79800
Silverson	31.2	0.39	4200 - 5500	17500 - 23000
Becomix	143.0	0.50	3000	45000

Ultra-Turrax prepared emulsions contained 10 ml of sample and were homogenised for 10 seconds (18 mm head) or 20 seconds (8 mm head) at varying homogenisation speed. The larger head size of the Silverson homogeniser caused an increase of sample volume to 100 ml and a homogenisation time of 10 seconds. Becomix values were calculated from measurements given by industry. Figure 5.4 shows that the universal graph of droplet diameter versus shear rate and indicates that a relationship is witnessed between the two parameters and therefore it is a successful method for calculating the initial average droplet diameter of the model emulsion system. Two measurement techniques were also implemented to determine droplet diameter; microscopy and Mastersizer (see experimental chapter). The results of both measuring techniques are plotted in Figure 5.4 for comparison; no significant difference was noted between the two methods of measurements within error.

Figure 5.4. Universal graph of droplet diameter vs. shear rate for the model emulsion system with varying homogenisation conditions, such as head size and type. Also shown are different measurement techniques, microscopy and Mastersizer. Power trend line fitted, all emulsified at 70 °C for 10 seconds (18 mm head and Silverson) and 20 seconds (8 mm head).



5.2.2 Droplet diameter versus shear rate⁻¹

Investigations were continued to further understand the droplet diameter measurements with varying shear rate by applying the capillary number equation. The equation considers the shear induced rupture of droplets and shear rate where capillary number C_a , droplet radius r , continuous phase viscosity η_c , interfacial tension γ and shear rate $\dot{\gamma}$ are linked:[19]

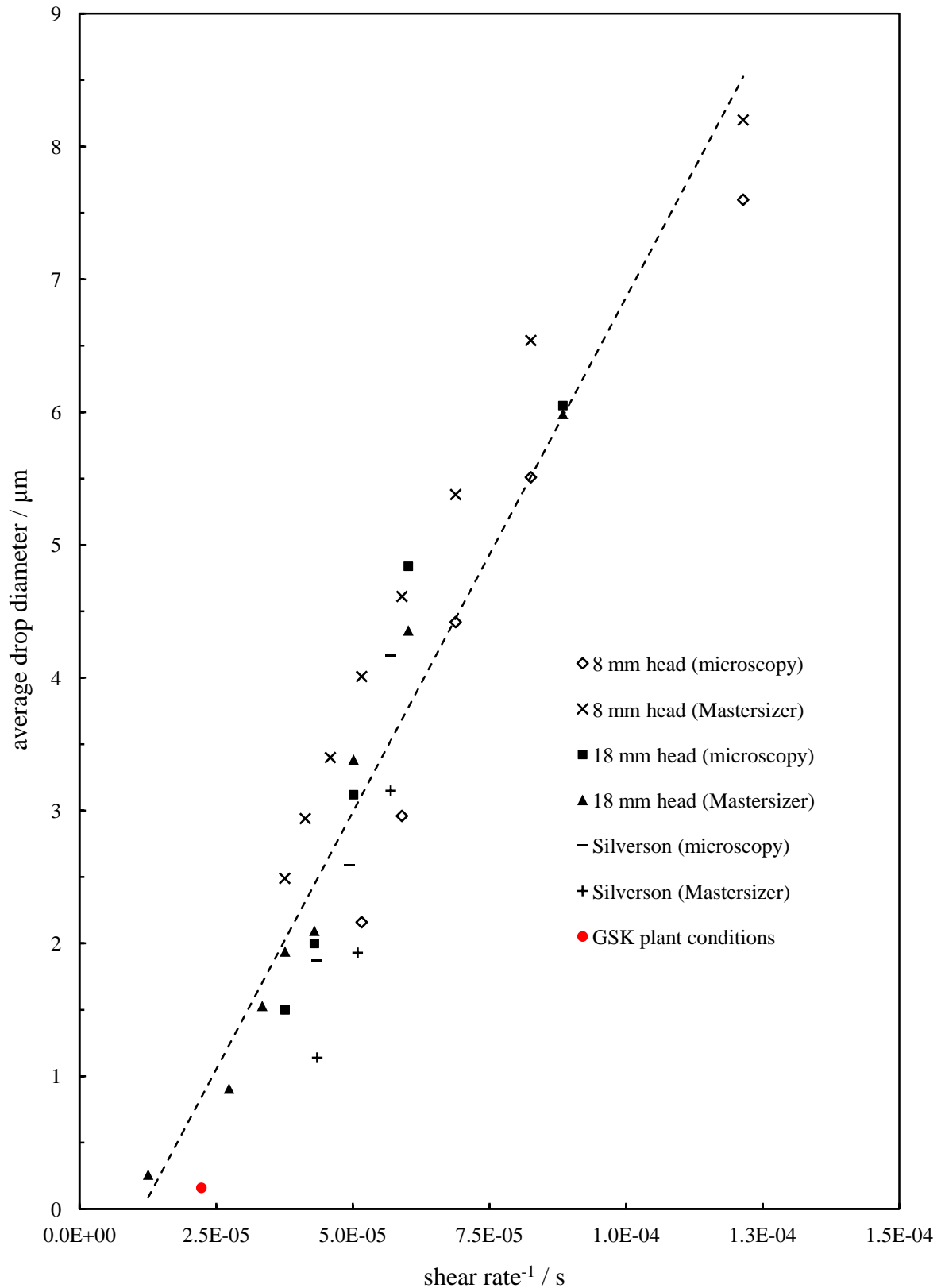
$$C_a = \frac{\eta_c \cdot \dot{\gamma} \cdot r}{\gamma} \quad (5.2)$$

If η_c and γ are kept constant, as in this investigation, and $C_a = 1$;

$$r \propto \frac{1}{\dot{\gamma}} \quad (5.3)$$

Figure 5.4 shows the relationship between lab and industrial (GSK) droplet diameters and shear rate to follow a power trend. Here, in Figure 5.5 the results indicate that when applying the theory of droplet rupture, using the capillary number equation, a plot of droplet radius (or droplet diameter) versus $1/\dot{\gamma}$ produces a linear trend as predicted.

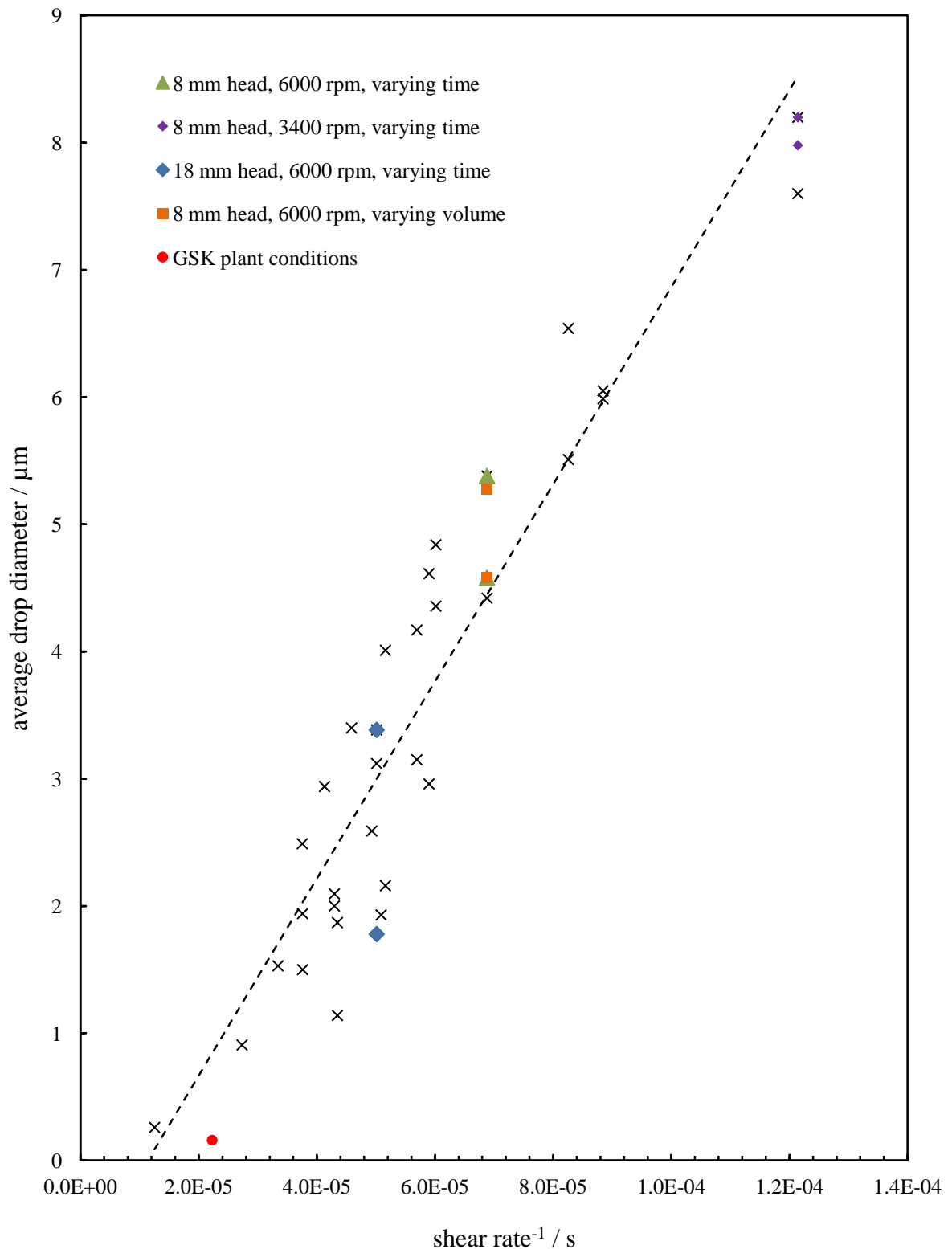
Figure 5.5. Universal graph of droplet diameter vs. 1/shear rate with varying homogenisation conditions, such as head size and type. Model emulsion system at fixed emulsification temperature (70 °C) for 10 seconds (18 mm head and Silverson) and 20 seconds (8 mm head), therefore constant interfacial tension and continuous phase viscosity. Data points are indicated in the legend.



5.2.3 Varying homogenisation time and volume

It can be argued that the as droplet diameter vs. $1/\text{shear rate}$ (Figure 5.5) had a clear power trend (as expected from the capillary theory) the droplet diameter must have reached a plateau with regards to the homogenisation time. To fully understand the effect of homogenisation time and sample volume on the trend presented in Figure 5.4 and Figure 5.5, samples were homogenised for a longer time period, 5 minutes, compared to the 10 or 20 seconds in the original figure with the volumes increased from 10 ml to 100 ml. These investigations would indicate if the process of using shear rate to predict droplet diameter is a robust process, *i.e.* changing homogenisation time and sample volume. Figure 5.6 shows the results determined and indicate that a good correlation of droplet diameter with varying homogenisation time and volume is gained. Hence, droplet diameters of the model emulsion system with varying homogenisation time and volume (<100 ml) must have reached a plateau after the first 10 or 20 seconds independent of head size. The plateau reached would indicate that if the emulsion is homogenised for a longer time period the droplet diameter relating to the shear rate will be reproduced, *i.e.* regardless of sample volume the droplet diameter achieved is dependent solely on the shear rate. Therefore all emulsions prepared for these investigations were homogenised using the $1/\text{shear rate}$ plot (Figure 5.5) with additional investigations Figure 5.6 proving the robustness of the procedure.

Figure 5.6. Average droplet diameter versus 1/shear rate for model emulsion formulation at fixed emulsification temperature (70 °C), therefore constant interfacial tension and continuous phase viscosity. Red circle indicates GSK plant conditions, remaining paired coloured points indicate varying homogenisation time, from 10 or 20 seconds to 5 minutes, and varying volume, from 10 ml to 100 ml, with fixed shear rate of emulsification. Measurements taken using Mastersizer.



5.3 *Stability with varying droplet diameter*

Instability of the model emulsion system has been witnessed in industry where storage (over varying time period but generally around weeks) at low temperature ($\approx 5\text{ }^{\circ}\text{C}$) gave rise to oiling out (resolved oil). Here, the effects of instability during storage are investigated using varying droplet diameter with changing shear rate (section 5.2). The production of varying droplet diameters was established using a controlled shear rate throughout the homogenisation procedure. An Ultra-Turrax (18 mm head) with changeable speed (Table 5.4) at fixed temperature of $70\text{ }^{\circ}\text{C}$. Following homogenisation the samples were stored at varying temperatures, 5, 15 and $30\text{ }^{\circ}\text{C}$ for a period of 1 month. The cooling of sample was at approximately $1\text{ }^{\circ}\text{C min}^{-1}$. The range of homogenisation speed produced varying droplet diameters and any link between droplet diameter and the corresponding instability were measured using micrographs and monitoring the amount of oil/aqueous phase resolved over selected time periods as described in the experimental chapter. The homogenisation and shear rate parameters chosen for the samples used in the stability analysis of the model emulsion system are shown in Table 5.4, together with the predicted and actual droplet diameters of the oil within the o/w emulsions.

Table 5.4 confirms that the droplet diameter does decrease with an increase in homogenisation speed. Therefore again showing that droplet diameter versus shear rate fits the established trend and has good correlation to Figure 5.5.

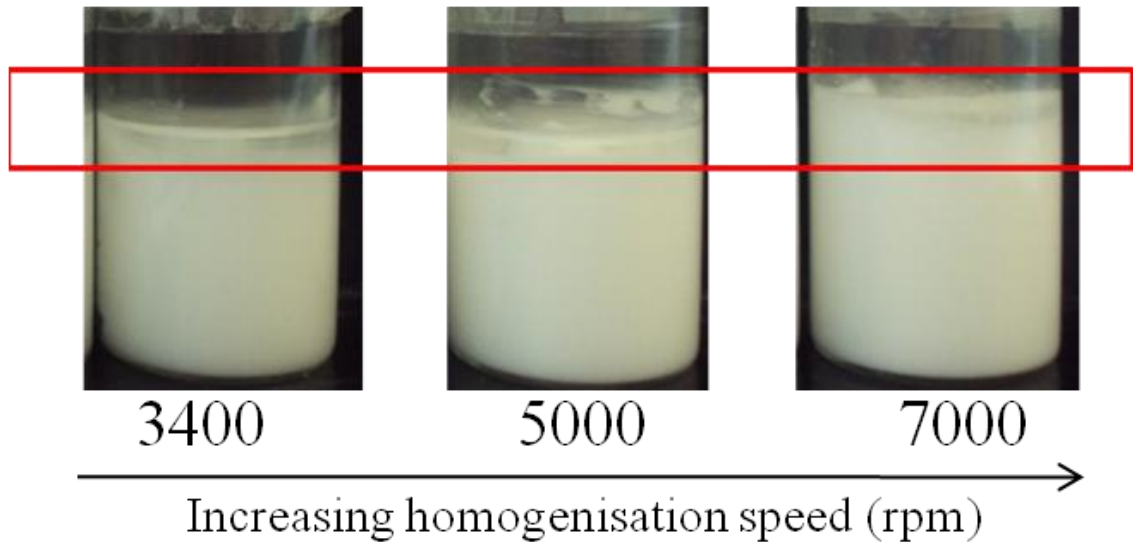
Table 5.4. Droplet diameter with changing homogenisation speed, and hence changing shear rate, when using 18 mm head for 5 minutes at 70 °C for the model emulsion system. Predicted droplet diameters calculated from linear trend in droplet diameter versus shear rate⁻¹ (Figure 5.6). Actual droplet diameters are averages of three emulsions, with each of the 3 emulsions stored at different temperatures. Droplet diameter was determined using Mastersizer. Error in droplet diameters represents standard deviation.

<u>Sample number</u>	<u>Homogenisation speed (rpm)</u>	<u>Shear rate (s⁻¹)</u>	<u>Shear rate⁻¹ (s)</u>	<u>Predicted droplet diameter (µm)</u>	<u>Initial droplet diameter (µm)</u>
1	3400	11300	8.84 x 10 ⁻⁵	5.97	5.58 ± 1.99
2	5000	16600	6.01 x 10 ⁻⁵	3.77	3.48 ± 1.39
3	7000	23300	4.30 x 10 ⁻⁵	2.45	1.83 ± 0.66
4	11000	36600	2.73 x 10 ⁻⁵	1.23	0.73 ± 0.25

Figure 5.7 shows oiling out of samples 1, 2 and 3 from Table 5.4, the oiling oil is clearly seen on the top of the bulk emulsion phase (red box). The results from Figure 5.7 are presented with respect of fraction of oil resolved against initial droplet diameter in Figure 5.8.

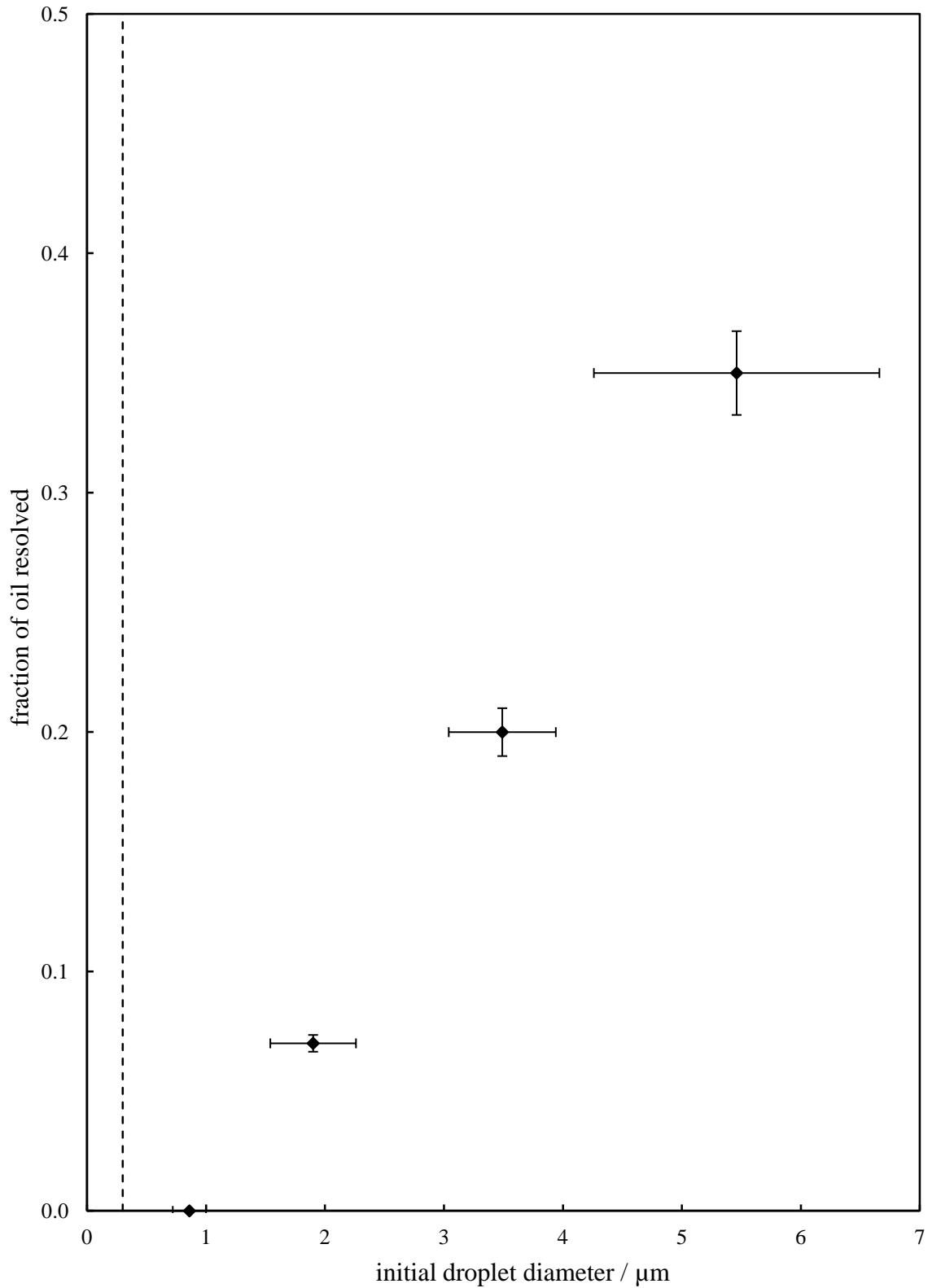
Figure 5.7 and Figure 5.8 clearly demonstrate that the model emulsion system with large droplet diameters stored at low temperatures (5 °C) have an increased instability to oiling out.

Figure 5.7. Photograph showing oil resolved (red square) in model emulsion system against homogenisation speed, at a fixed storage temperature of 5 °C, after a time of 21 days storage. Homogenisation speed was used to vary initial droplet diameter using different homogenisation speed. Pictures taken at storage temperature (5 ± 2 °C).



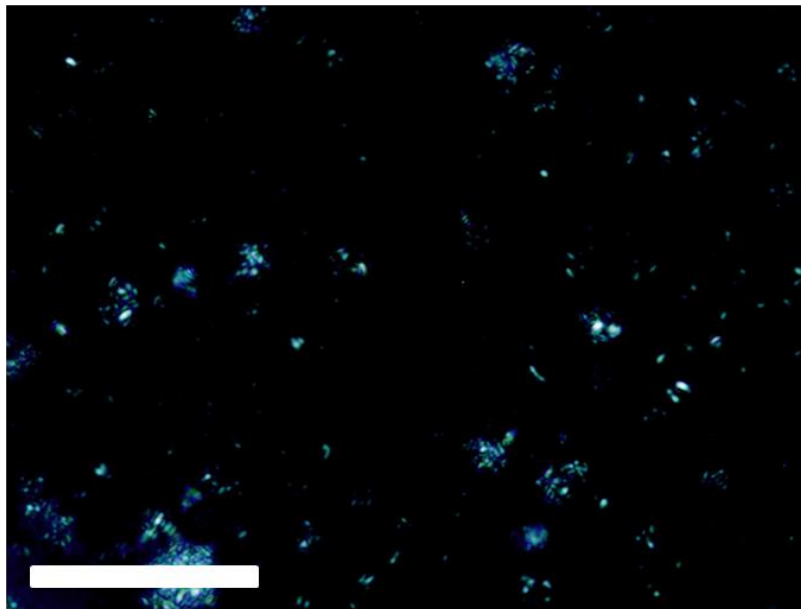
Resolved oil is normally attributed to coalescence of the oil drops within an o/w emulsion. Therefore, the results presented in Figure 5.6 and Figure 5.7 suggests that at a storage temperature of 5 °C instability due to coalescence is seen with increasing droplet diameter. No instability is seen in the emulsions stored at the two higher temperatures of 15 and 30 °C. The instability results at lower storage temperature and larger initial droplet diameters could indicate the cause of instability to be from partial coalescence in accordance to the investigations of Leal-Calderon *et al.*[20] Whereas the higher storage temperatures and smaller initial droplet diameters may be stable due to jamming of the semi-solid droplets.

Figure 5.8. Stability of the model emulsion system by fraction of oil phase resolved against initial droplet diameter, at a fixed storage temperature of 5 °C, after a fixed time period of 21 days. Initial droplet diameter was varied using different homogenisation speed and measured using Mastersizer. Dotted line represents initial average droplet diameter in industrial prepared model emulsion system.



The solid content of the dispersed phase from some of the samples of the model emulsion system can be viewed using cross polar microscopy. Only in sample 1 (Table 5.4) was crystals observable within the oil dispersed phase under light microscopy (Figure 5.9). Sample 1 had the highest initial droplet diameter of $\approx 5.58 \mu\text{m}$ and was stored at 5°C for 21 days, suggesting that crystallisation occurs in emulsions stored at lower temperatures (5°C or lower) and large droplet diameters. Microscopy also indicates that the oil droplets which are larger tend to flocculate.

Figure 5.9. Cross polarised micrograph of model emulsion system, homogenised at 3400 rpm using 18 mm head in an Ultra-Turrax T25 homogeniser for 10 seconds. Initial droplet diameter $\approx 5.58 \mu\text{m}$. Magnification = x50, scale bar = $50 \mu\text{m}$. Micrograph taken at storage temperature ($5 \pm 1^\circ\text{C}$).



5.4 Crystallisation with varying droplet diameter

As the droplet diameter of the model emulsion system continues to decrease, theory suggests that crystallisation of the dispersed phase will reduce due to the lack of nucleation sites present in the drop.[5] However, cross polarisation (Figure 5.9) does not have the capability to detect such small changes in solid content. Other techniques such as differential scanning calorimetry (DSC), rheology and nuclear magnetic resonance (NMR) will be used in this section to determine the accurate crystallisation point and possible indication of solid content. The additional information gathered with these techniques aims to identify a reason for instability with varying droplet diameter in the model emulsion system, as well as establishing whether the unconventional

addition of diol in the emulsion leads to "conventional" theory of emulsions being reached. To do this, the model emulsion system was studied with the two extremes of droplet diameters established by varying shear rate (Table 5.5).

Table 5.5. Experimental parameters used to vary the average emulsion droplet diameters of the model emulsion system. Data shown represents the extremes of shear rate and average initial droplet diameter achievable. All systems were homogenised at 70 °C.

	<u>Large droplet diameter</u>	<u>Small droplet diameter</u>
Ultra Turrax head size (mm)	18	18
Ultra Turrax speed (rpm)	3200	24000
Homogenisation time (min)	10	10
Shear rate (s^{-1})	≈ 10000	≈ 80000
Shear rate $^{-1}$ (s)	9.40E-05	1.25E-05
Expected droplet diameter (μm)	6.40	0.10

5.4.1 Differential scanning calorimetry

Differential scanning calorimetry (DSC) is a thermoanalytical technique in which the difference in the amount of heat required to increase the temperature of a sample and reference is measured as a function of temperature. This can help identify thermal changes within samples and in this case has been used to establish the crystallisation point of the oil dispersed phase in the model emulsion system.

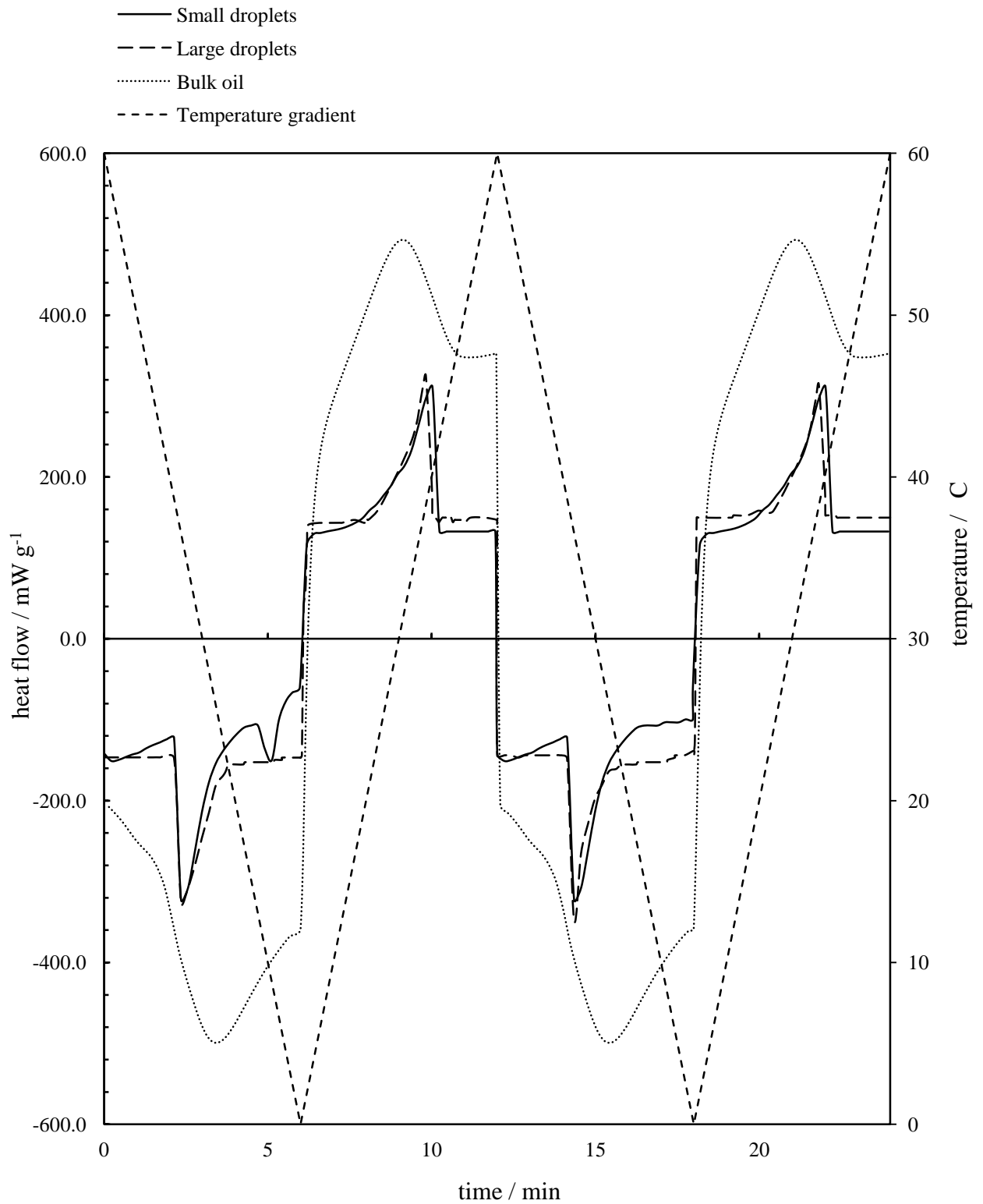
Figure 5.10 shows the difference in heat flow between the model emulsion system with initial small droplet diameter and initial large droplet diameter. The small droplet emulsion shows two crystallisation peaks upon the first cooling cycle, one at the same temperature that the crystallisation peak of the bulk oil occurs (≈ 30 °C) and one at a much lower temperature of 8 – 9 °C. The second peak witnessed in the small droplet emulsion is contributed to supercooling of emulsion droplets within that emulsion, *i.e.* a portion of the emulsion droplets are undergoing homogeneous crystallisation and heterogeneous crystallisation. Vanapalli *et al.* witnessed two crystallisation peaks and concluded that in poly dispersed emulsions, a range of small droplets which do not contain a nucleation site crystallise via a homogeneous mechanism lower than the known bulk crystallisation temperature, whereas the remaining droplets contain a nucleation site and crystallise via a heterogeneous route at a similar temperature of the

bulk sample.[4] In contrast the large droplet diameter emulsion consists of one crystallisation peak within the first cooling cycle occurring at a similar temperature to the bulk oil. The crystallisation behaviour of the large droplets is also consistent with Skoda *et al.*, who states that as the average droplet diameter increases homogeneous crystallisation stops.[12]

Interestingly, the crystallisation mechanisms present in the first thermal cycle are absent in the 2nd thermal cycle. Here, both the small and large droplet emulsions have crystallisation peaks similar to that occurring in the bulk sample; indicating heterogeneous crystallisation only, *i.e.* no supercooling. As discussed by Leal-Calderon *et al.*, upon thermal cycling of emulsions the droplet diameter change due to partial coalescence followed by coalescence upon heating then heterogeneous crystallisation is more likely to occur.[17] To access the aforementioned theory the initial droplet diameters were measured after the investigation of 2 thermal cycles. The small droplet emulsion increased from 0.18 to 2.64 μm , whereas the large droplet diameter emulsion increased from 3.70 to 5.21 μm . The observed increase in droplet diameter concludes that thermal cycling increases in droplet diameter and that the emulsion droplets in the small droplet emulsion have enlarged to the extent that only heterogeneous crystallisation occurs rather than a mixture of both heterogeneous and homogeneous.

The coalescence witnessed with thermal cycling is especially important for work presented in this thesis as it showed that the stability of this diol containing model emulsion system fluctuates with changing temperature and droplet diameter, much like that shown in the stability analysis discussed earlier (section 5.3). To validate the results the temperature cycling rate was investigated, these investigations were to ensure that the experimental parameters of DSC do not play a major role in the results observed. Results show that no change is observed when temperature ramping is performed at varying rates between 0.1 – 10 $^{\circ}\text{C min}^{-1}$.

Figure 5.10. DSC profiles of the emulsion model, with varying initial droplet diameters, and the bulk oil used as the dispersed phase within the emulsions (white soft paraffin and paraffin liquid). Initial droplet diameters of small droplets = 0.18 μm and large droplets = 3.70 μm . Legend indicates each series, where the temperature gradient ($10\text{ }^{\circ}\text{C min}^{-1}$) is read off the secondary y-axis and the DSC profiles is read off the primary y-axis. Data shows two thermal cycles for each sample.



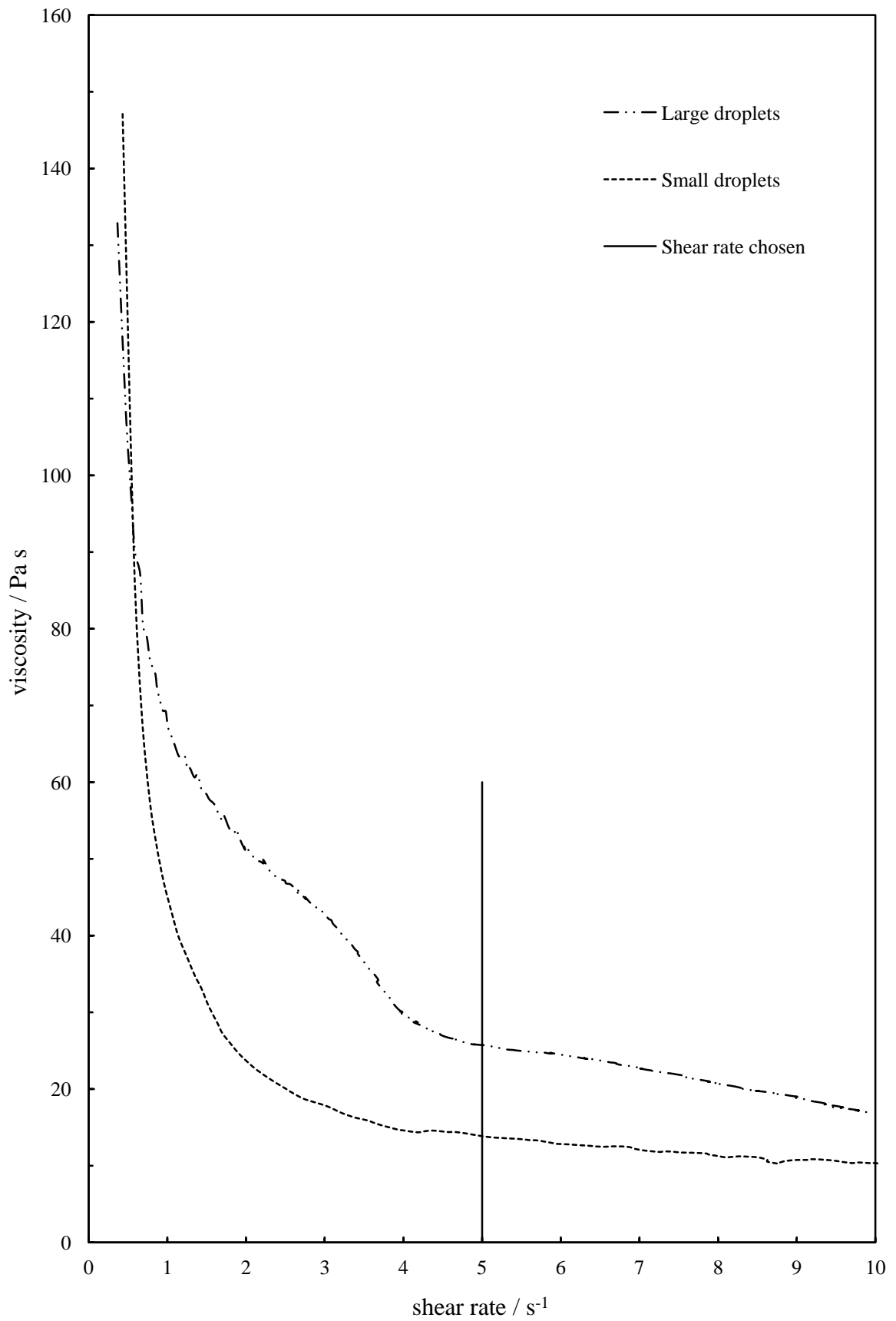
5.4.2 Rheology

Rheology is the study of the flow of matter and in the investigations presented in this thesis changes in emulsion viscosity with varying temperature were investigated. Rheology of a model emulsion system with varying droplet diameter (Table 5.5) were investigated, in all cases they are described as small and larger droplets. The aim of these investigations was to establish if rheology was a sensitive technique to distinguish crystallisation properties of the model emulsion system with varying droplet diameters. Viscosity measurements using the cone and plate method were used, with experimental factors such as shear rate, thermal cycles, experimental temperature range and cooling rates investigated.

5.4.2.1 Shear rate

The shear rate required for experimental conditions had to be determined by performing a viscosity versus shear rate scan. Viscosity versus shear rate showed the plateau regions of viscosity for the two emulsions and was used to identify the experimental shear rate used in the investigations to reduce error in viscosity measurements. Figure 5.11 shows the scans of viscosity versus shear rate for both emulsions. Shear thinning can be seen as the major characteristic with a dramatic decrease between $0.5 - 3.0 \text{ s}^{-1}$ and it also indicates the optimum shear rate to use was above 3.0 s^{-1} , where a plateau region is witnessed. The shear chosen for further experiments was 5.0 s^{-1} as it was well within the plateau region observed. Interestingly, emulsions with large initial droplet diameters show a higher viscosity when compared to the smaller droplet diameter emulsions; the opposite to what is expected usually where emulsions of the same composition produce higher viscosity for smaller droplet diameters than the larger droplet diameter counterparts, the latter thought to be an affect from greater interactions of small droplets within the emulsion from flocculation and aggregation.[21] However, from theory already discussed, the likelihood of crystalline droplets is higher in the larger droplets within the model emulsion system through partial coalescence thereby enhancing the chance of crystal networks which would increase the viscosity when compared to an emulsion with small droplets with potentially less crystals and no crystal network.[4]

Figure 5.11. Viscosity versus shear rate for both the large and small droplet diameters of the model emulsion system at 25 °C.



5.4.2.2 Pre-shear and temperature cycle

Pre-shear conditions were applied to each sample to assess if the viscosity of the samples changed over time, independent of other fixed parameters, *i.e.* shear rate, sample, and sample volume. Here, the viscosity of a sample was expected to decrease with increasing time as the sample structure breaks down under shear.[21] In addition the temperature range in which the investigation was performed was also analysed to ensure the temperature range was not affecting the samples results.

The emulsions of interest were prepared at 70 °C, because of this the ideal temperature cycle for investigations would start at the same temperature (70 °C) followed by cooling to the lowest temperature before the solidification of water affected the results, *i.e.* ≈ 0 °C, therefore allowing the temperature cycle to give a good indication of the rheology of the emulsion as it cools *in situ*. However, as the temperature cycle started at 70 °C with pre-shear applied, the structural stability of the emulsions to both temperature and pre-shear was a concern. Therefore, microscopy, Mastersizer and viscosity versus shear rate measurements were taken before and after the emulsion had been heated to 70 °C and pre-sheared at 5 s^{-1} for 10 minutes; providing information on emulsion stability, prior to and following thermal cycling.

5.4.2.2.1 Thermal cycling (small droplets)

Figure 5.12 and Figure 5.13 show the Mastersizer and viscosity versus shear rate measurements taken of the model emulsion system with small droplets (0.18 μm) before and after pre-shear at emulsification temperature (70 °C) for 30 minutes.

Figure 5.12. Mastersizer of model emulsion system prepared to have small average droplet diameter (0.18 μm). Both results taken at room temperature ($\approx 22\text{ }^\circ\text{C}$), using the usual methods. Red line indicates emulsion before pre-shear, green line represents emulsion after pre-shear.

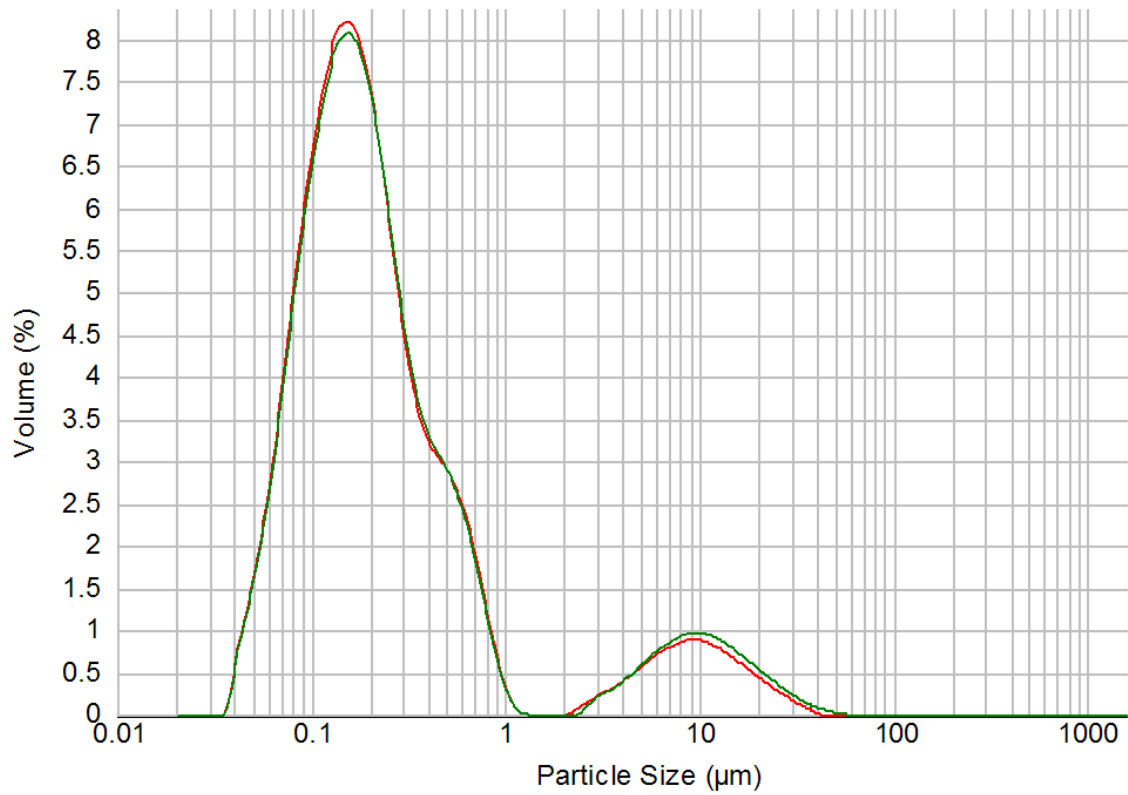
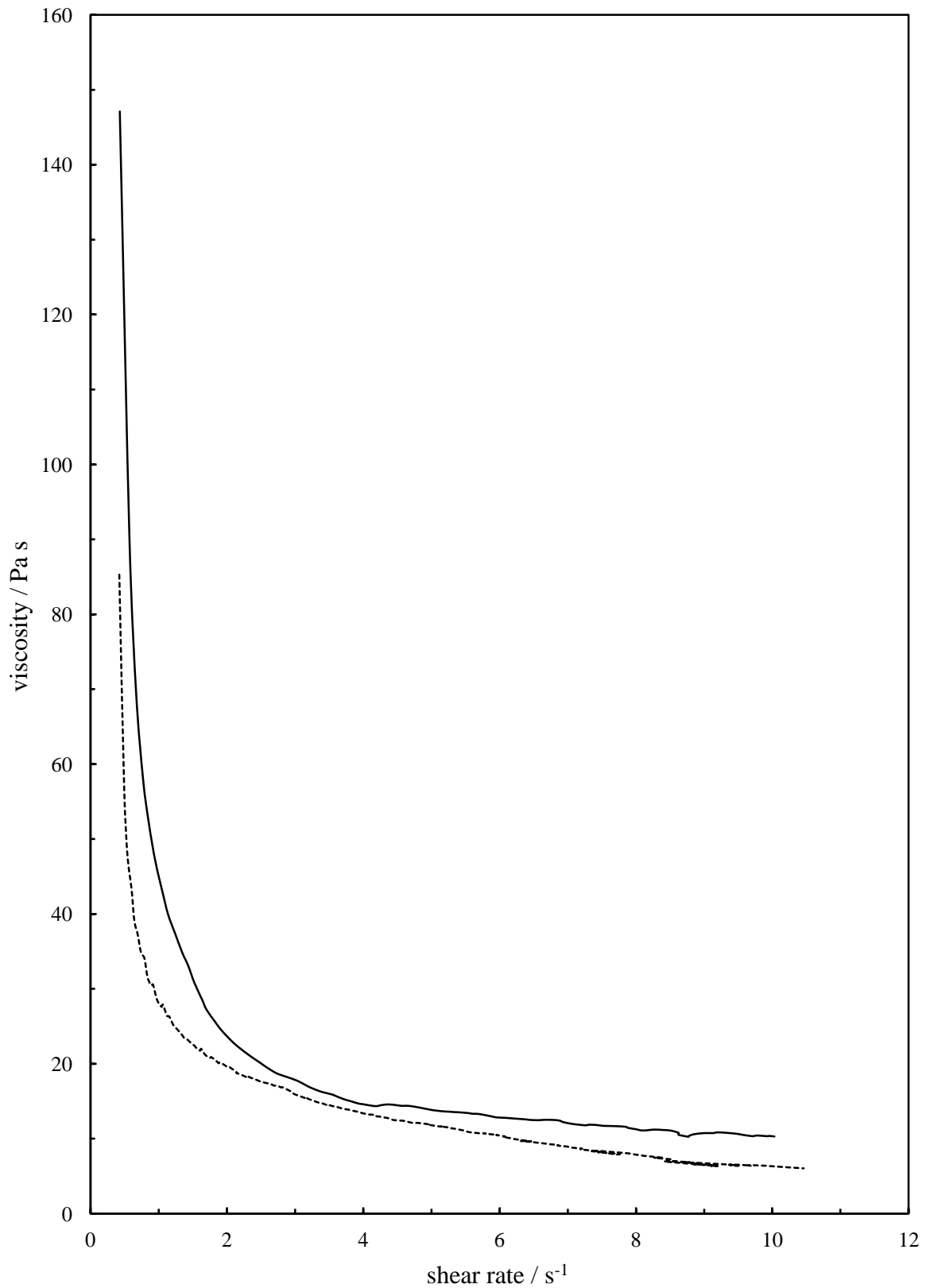


Figure 5.13. Viscosity versus shear rate before (solid black line) and after (dotted black line) pre-shear for 10 minutes at 70 °C at shear rate = 5 s⁻¹. Model emulsion system of small droplet diameter (0.18 μm), measurements taken after cooling to 25 °C.



The Mastersizer and rheology results are very similar before and after pre-shear in the model emulsion system with small droplets. Therefore, the model emulsion system with an initial average droplet diameter of 0.18 μm can withstand a temperature cycle up to 70 $^{\circ}\text{C}$, with pre-shear applied. A very small change in viscosity versus shear rate was witnessed before and after the cycle. Microscopy of the sample before and after the thermal cycle show little difference (results not shown). However, due to the small droplet sizes it is quite difficult to establish detailed enough micrographs for analysis therefore the Mastersizer results were used as the primary evidence for emulsion instability with thermal cycling.

5.4.2.2.2 Thermal cycling (large droplets)

Again, microscopy, Mastersizer and viscosity versus shear rate measurements were taken of the model emulsion system with large droplets (3.70 μm), Figure 5.14 -Figure 5.16.

Figure 5.14. Mastersizer results before (red line) and after (green line) pre-shear for 10 minutes at 70 $^{\circ}\text{C}$ at shear rate = 5 s^{-1} of the model emulsion system with initial average droplet diameter of 3.70 μm . Measurements taken after cooling to 25 $^{\circ}\text{C}$.

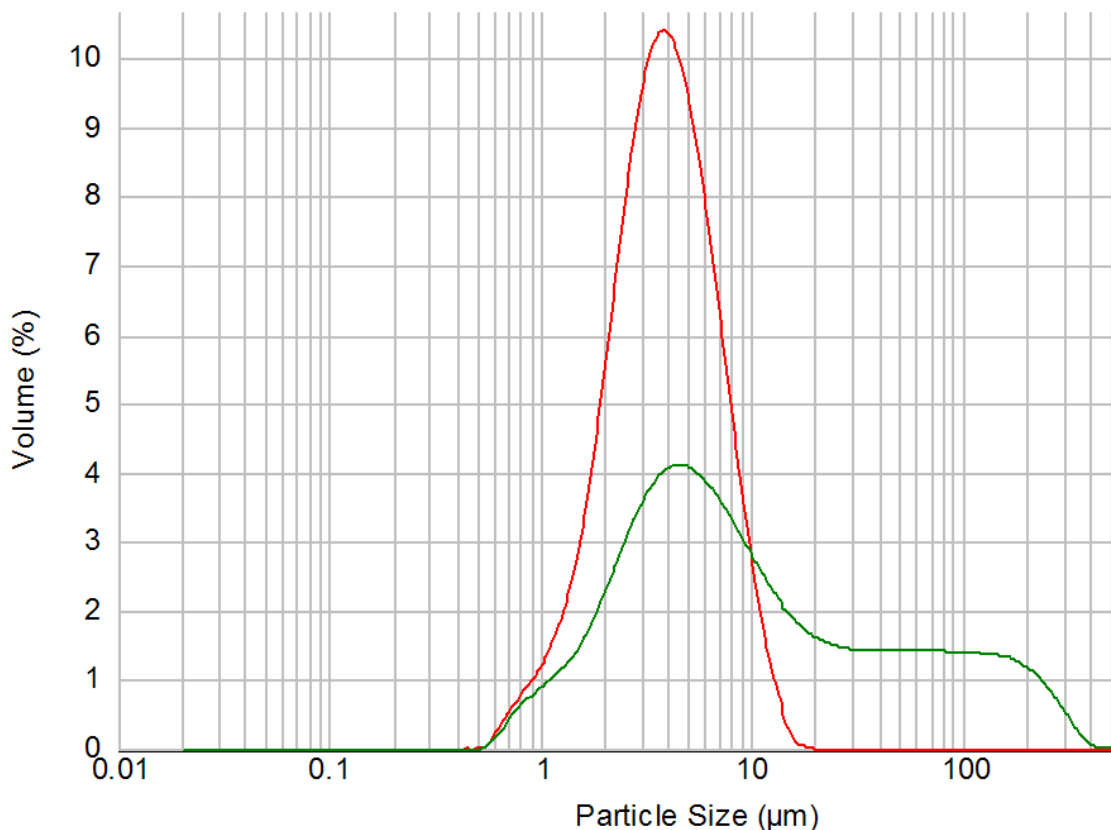


Figure 5.15. Viscosity versus shear rate before (solid black line) and after (dotted black line) pre-shear for 10 minutes at 70 °C at shear rate = 5 s⁻¹ of model emulsion system with initial average droplet diameter of 3.70 μm. Measurements taken after cooling to 25 °C.

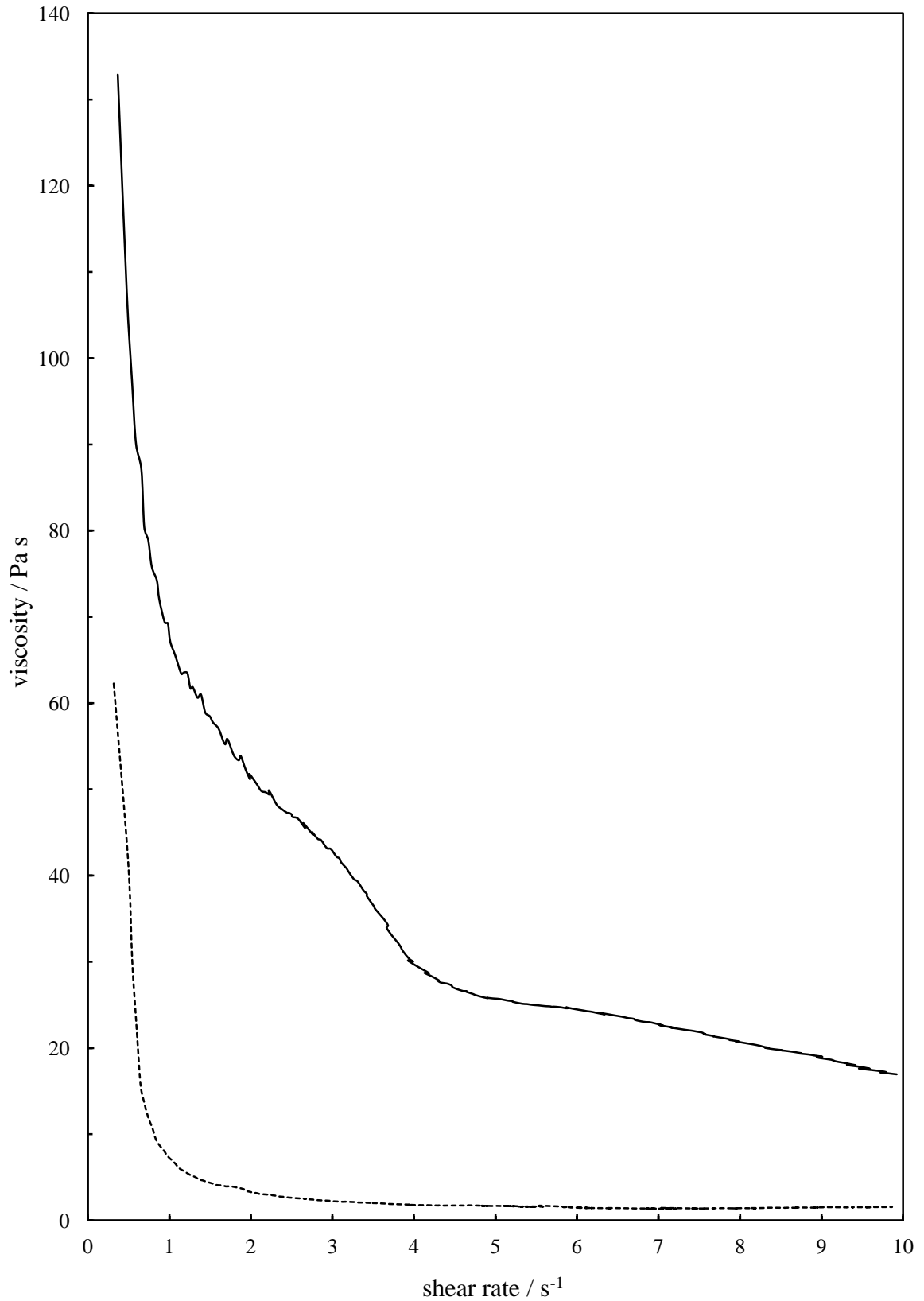
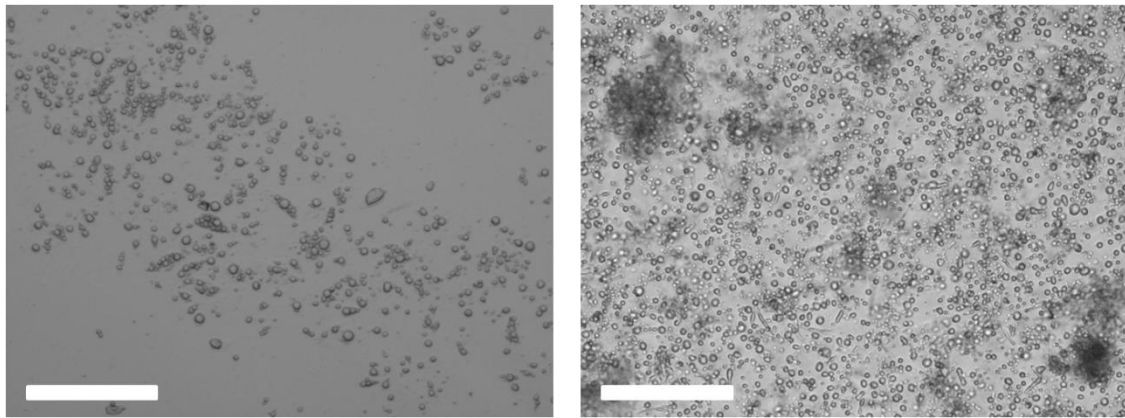


Figure 5.16. Brightfield microscopy before (left) and after (right) pre-shear for 10 minutes at 70 °C at shear rate = 5 s⁻¹ of model emulsion system with initial average droplet diameter of 3.70 μm. Measurements taken after cooling to 25 °C. Scale bar = 50 μm.



All three characterisation techniques (Mastersizer, rheology and micrographs) applied to the large droplet emulsion show differences in the emulsion properties before and after pre-shear at 70 °C. Mastersizer and microscopy show an increased in both aggregates and average droplet diameter after the thermal cycle. Also, the viscosity is drastically different at all shear rates tested after the cycle. The original viscosity before thermal cycle at 25 °C with a shear rate of 5 s⁻¹ was ≈ 25 Pa s and after the viscosity dropped to ≈ 2 Pa s at the same shear rate. The change in viscosity highlights a major difference in the rheology after one pre-shear at high temperature. Therefore direct comparison of the large droplet emulsion with the small droplet emulsion was not possible at the 70 °C starting temperature.

The visual appearance of the emulsion was also very different with oil droplets > 1 mm coming out of the emulsion. The hypothesis for the large droplet diameter emulsion characteristics demonstrated here is that the high temperature and pre-shear of the emulsion causes instability from droplet coalescence of the oil; giving partially broken emulsion, *i.e.* oil outing. As higher temperature investigations were not comparable for small and large droplet emulsions the rheology investigations versus temperature for both emulsions were started at a reduced temperature of 30 °C or lower where the emulsion showed no sign of breaking.

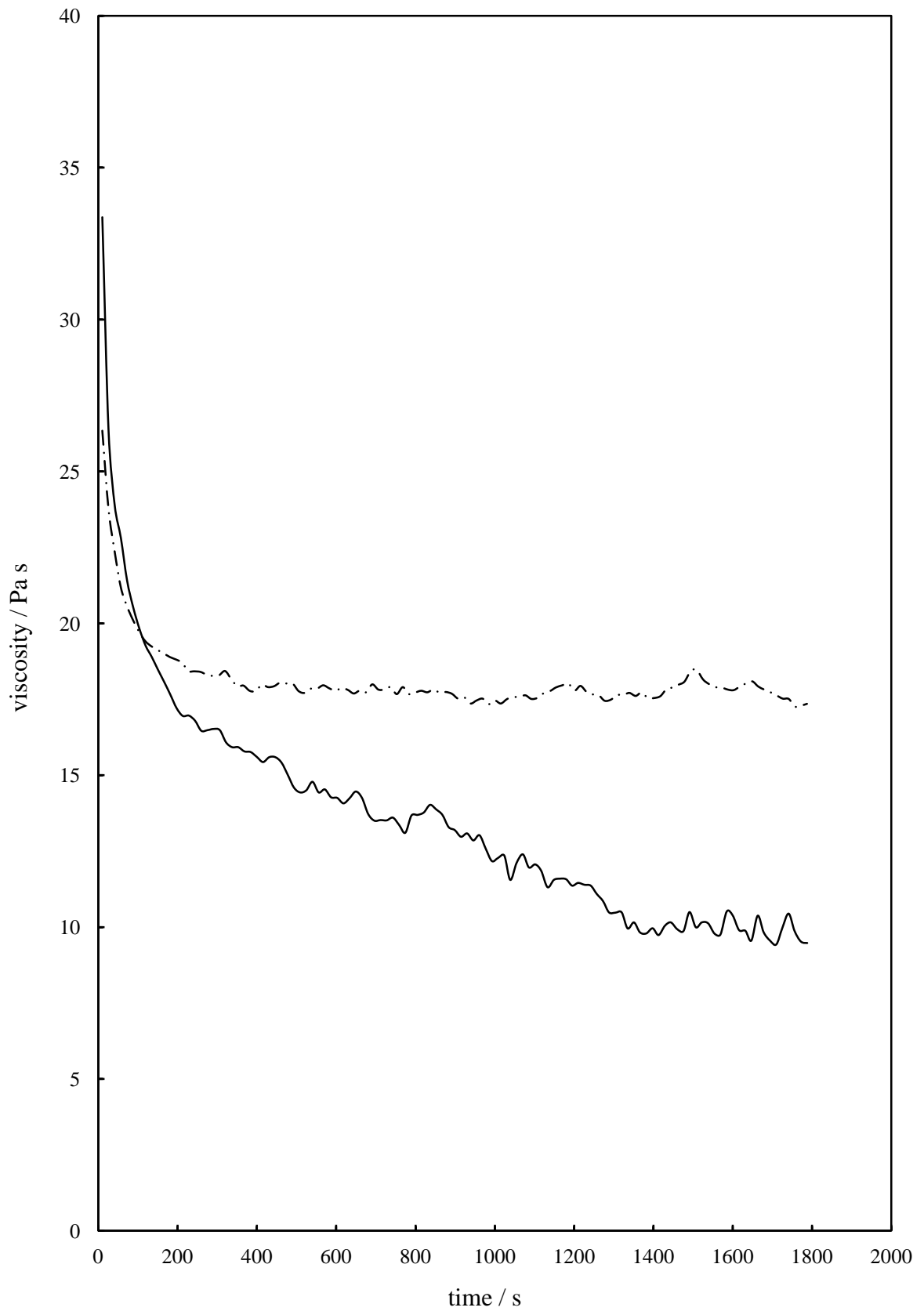
5.4.2.2.3 Pre-shear time

The model emulsion system with large droplet diameters had structural and rheological differences upon heating and re-cooling (section 5.4.2.2.2), therefore the optimised condition for rheology investigations was from a lower starting temperature, *i.e.* room temperature, 25 °C. Pre-shear time (the time viscosity plateaus at the start temperature) was re-investigated for optimisation. The viscosity versus time was examined for both small and large droplet diameter emulsions at 25 °C, shown in Figure 5.17. The results indicate that a pre-shear time of 30 min. (1800 s) gives a plateau point for both emulsion droplet diameters and decrease in viscosity due to structure re-organisation that will not affect the initial viscosity measurements after a pre-shear application of 30 min.

5.4.2.3 Cooling rates

Fast temperature changes upon cooling produced inconsistent results as the rheometer was unable to detect any changes in the viscosity with different model emulsion samples (small and large droplet diameter). Therefore samples were cooled at a slower rate of 0.1 °C min⁻¹ while rheology investigations were being performed.

Figure 5.17. Viscosity versus time at 25 °C for the model emulsion system with small initial droplet diameter (solid black line = 0.18 μm) and large initial droplet diameter (dotted black line = 3.70 μm) at a shear rate of 5 s^{-1} .



5.4.2.4 Comparison between large and small droplet diameters

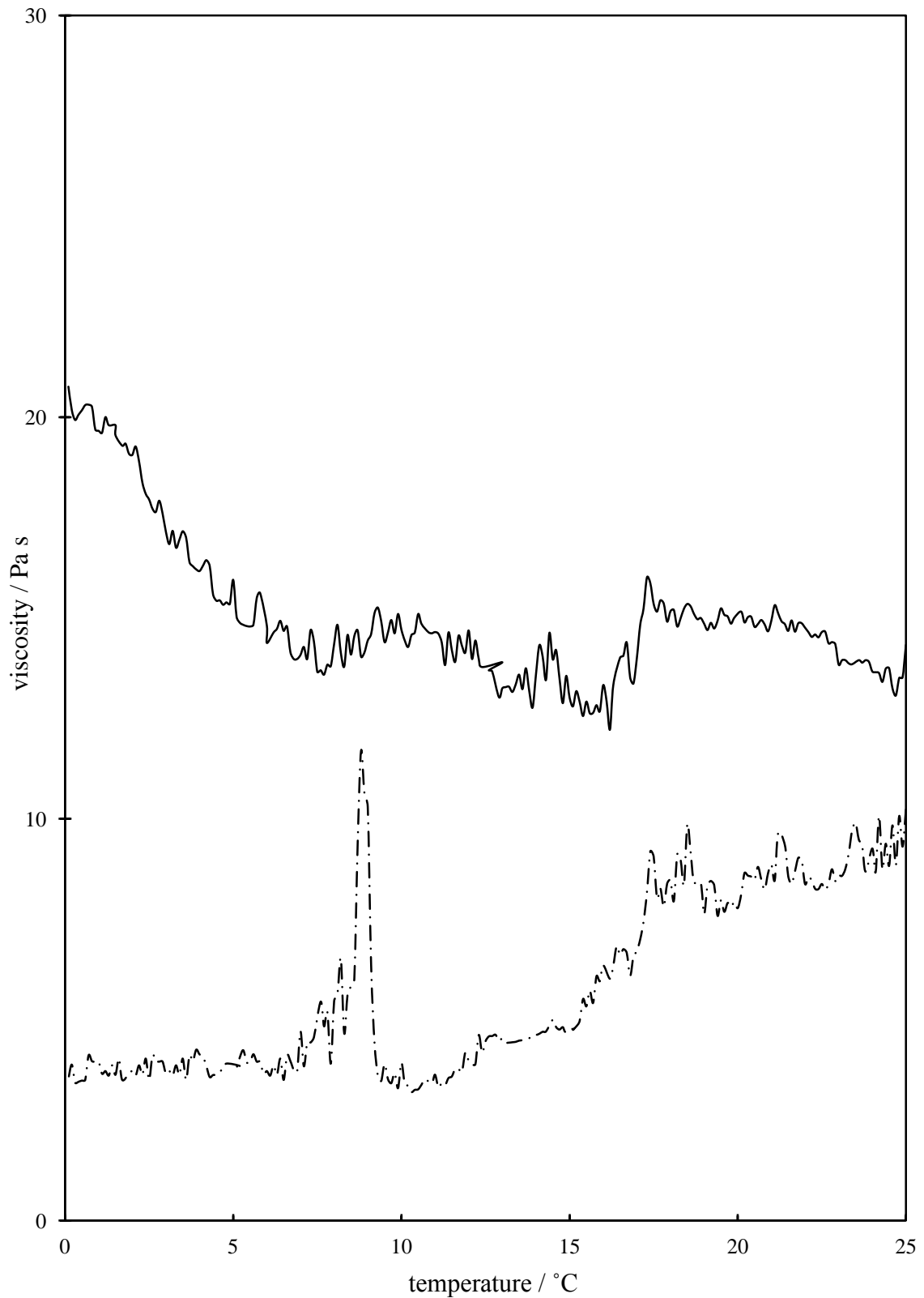
Experimental parameters to investigate the rheology difference between the two emulsions with varying droplet diameter and temperature were successfully established in detail and are as follows:

- Starting temperature of 25 °C.
- Pre-shear for 30 min. at a shear rate of 5 s⁻¹.
- Thermal cycle from 25 – 0 – 25 °C at a rate of 0.1 °C min⁻¹ at a fixed shear rate of 5 s⁻¹.

A direct comparison between the two could be examined and is shown in Figure 5.18. Comparison of the rheological data sets for the two emulsions under decreasing temperature show that the model emulsion system presented shows no abrupt change in the viscosity when the average droplet diameter is large ($\approx 3 \mu\text{m}$), unlike the small droplet diameter emulsion which shows a rapid change in viscosity between 7 – 8 °C. The two results from Figure 5.18 support the results from the DSC investigations discussed earlier (section 5.4.1) along with the theory of smaller emulsion droplets causing a supercooling effect.[5]

The additional aspect that the larger droplet model emulsion system gave an increased viscosity compared to the smaller droplets again indicates that the larger droplet does contain structurally integrity likely caused from crystals or a crystal network. This is an additional indication that larger droplets have a higher amount of aggregation than the small droplet diameter emulsion and that the possible crystal network caused from partial coalescence returns an emulsion with higher viscosity. In addition, the increase in viscosity in the model emulsion system with the smaller droplet diameter around 7 – 8 °C goes on to decrease; hypothesised to arise from structural reorganisation after the homogeneous crystallisation, the same effect is observed in pre-shear and therefore indicates the possibility of a “jammed” state in the small droplet emulsion which can be structurally reorganised. Furthermore, results are reproducible with only slight variations seen when additional measurements are taken.

Figure 5.18. Viscosity with changing temperature when cooling from 25 – 0 °C, at 0.1 °C min⁻¹, of the model emulsion system with two different initial droplet diameters (0.18 μm – dotted black line and 3.70 μm – solid black line), at a fixed shear rate of 5 s⁻¹. Measurements taken after pre-shear conditions of shear rate = 5 s⁻¹ for 30 min. at 25 °C.



5.4.3 Nuclear magnetic resonance

DSC and rheology investigations in the crystallisation characteristics of the model emulsion system both give an indication that there is a difference with varying droplet diameter. NMR was used here with the aim to understand the process in more detail by examining the individual components mobility, therefore their solid nature and crystallisation, with varying temperature and droplet size of the model emulsion system. Investigations involved collecting H^1 NMR spectra at varying temperatures, from 70 – 0 °C, for the two samples of the model emulsion system, 0.18 and 3.70 μm (Table 5.5). The spectra of these samples was then used to determine the extent of liquid like and solid like regions within the system, where the former would give a sharp NMR peak and the latter would give a broad peak due to lack of mobility.[22] A plot of full width at half height (FWHH), of a certain peak, with changing temperature would give an indication of the solid content/characteristics.

The process of using FWHH as an indication of molecule mobility has been used for example in the detection of liquid water in glass to the diffusion of Aluminium (Al) in Al/Al-oxide nanophase composite. [23, 24] However, to the authors' knowledge it has never been used for estimating solid transitions/solid content in emulsions. Crystallisation/solid content in emulsions is generally measured using the van Putte and van den Enden pulse NMR method; where the whole sample is excited by a strong and very short NMR pulse followed by measuring the relaxation of the sample. The relaxation time of the sample produces two distinct regions, fast and slow, corresponding to the liquid and solid part respectively. The ratio of the fast and slow measurements are used to estimate the solid content of the sample.[25] However, the aim of the investigations presented here are to examine individual peaks represented by different molecules, *i.e.* diol and oil. “wide-line” NMR was used, applying a continuous relatively small radio frequency to measure the absorption of all nuclei in the sample. Thus all part of the NMR spectrum can be used in analysis.

Figure 5.19 shows the typical spectrum obtained from the model emulsion system; droplet diameter 0.18 μm at 60 °C. Independent of the temperature and initial droplet diameter, all spectra remain “simple” and are available for analysis. Table 5.6 shows the assignment of peaks within the spectra to the components of the model emulsion

system. Assignments were determined from individual spectra of each component at 60 °C (results not shown) and NMR chemical shift theory.

NMR spectra versus temperature were obtained for the two different emulsions with varying initial droplet diameter. It was important to identify if the experimental procedure changed the emulsion properties, *e.g.* droplet diameter and oil/water resolved. Microscopy and physical appearance of the emulsion after a thermal cycle, 60 – 2 – 25 °C at approximately 1 °C min⁻¹ were analysed to establish any change in emulsion properties; the changes observed were deemed insignificant (*i.e.* droplet diameters remained the same within standard deviation); unlike the rheology investigation discussed in section 5.4.2. However, there was a lack of pre-shear in the NMR investigations postulated to be the potential cause of instability in rheology the investigations.

Figure 5.19. ¹H NMR spectrum of the model emulsion system at 60 °C with initial droplet diameter of 0.18 μm. Labels indicate the ppm of the peaks.

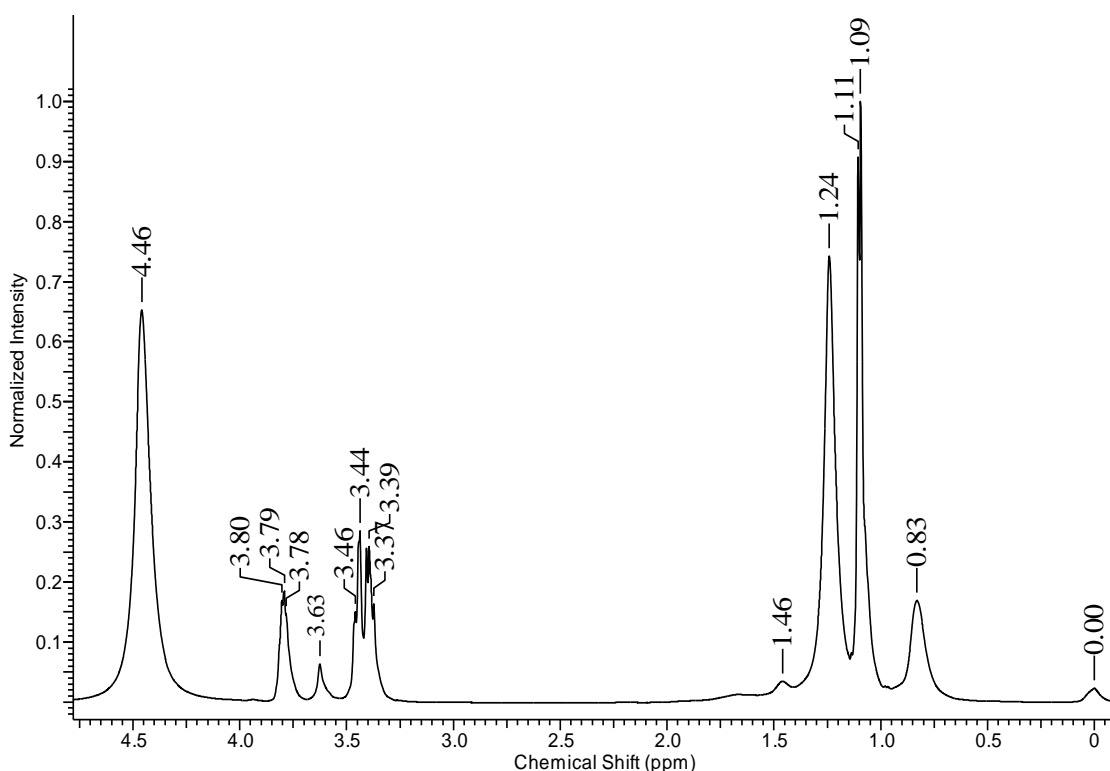


Table 5.6. Assignment of H¹ NMR peaks for the model emulsion system at 60 °C for emulsions with both 0.18 and 3.70 μm initial droplet diameter. Assignment determined from individual spectra of each component and NMR chemical shift theory.

<u>Chemical shift (ppm)</u>	<u>Component assignment</u>	<u>Component chemical region</u>
0.00	Dimethicone	Si(CH ₃) ₃ and Si(CH ₃) ₂
0.83	Propane-1,2-diol, SDS, cetostearyl alcohol, Arlcel 165, paraffin liquid and white soft paraffin	CH ₃ (end of alkyl chain)
1.09 and 1.11	Propane-1,2-diol	CH ₂
1.24	Arlcel 165, paraffin liquid, white soft paraffin, cetostearyl alcohol and SDS	CH ₂
1.46	SDS	CH ₂ (next to electronegative oxygen)
3.37 to 3.80	Propane-1,2-diol, cetostearyl alcohol and Arlcel 165	OH groups
4.46	Water	H ₂ O

Figure 5.20 shows the H¹ NMR spectra of both the model emulsions (varying droplet diameter) with decreasing temperature. The results from this data are as follows:

- No dramatic difference in the overall spectra peaks observed with decreasing temperature; allowing for analysis of individual peaks.
- The exception to the above finding is the change in the water peak with decreasing temperature. The water peak splits into two peaks and shifts to a greater ppm. The splitting is thought to be an exchange process between the water and propane-1,2-diol in the system. The exchange process between the two decreases as temperature decreases; approximately the same as the NMR measurement time scales, meaning that two peaks are witnessed for both the water with and without the exchanged hydrogen. A similar phenomenon has been witnessed in water alcohol mixtures.[26-

29] The additional shifting of the water peak to a higher ppm is a well known effect with changing temperature.[30]

- As expected, peaks which are assigned to alkyl chains of oil and surfactant broaden with decreasing temperature, and the resolution of these peaks indicates that the 0.18 μm emulsion still has a high amount of mobility at the lowest temperature in comparison to the 3.70 μm model emulsion system. For example, the spectrum of the 0.18 μm model emulsion system has 4 defined peaks between the assigned propane-1,2-diol range $\approx 3.3 - 3.5$ ppm at the lowest temperature, whereas the model emulsion with an initial droplet diameter of 3.70 μm only has 2 defined peaks in the same region.

Broadening of assigned alkyl chain peaks belonging to the oil and surfactants tails was investigated further by using ACD/LABS NMR processor software to determine the full width at half height (FWHH) for the peaks of interest. Modelling parameters of Gauss-Lorentz in the software were used in the calculation. Figure 5.20 shows the resulting full width at half height versus temperature plots for the two main peaks that represent the bulk oil of the emulsion in the spectra, 0.82 and 1.22 ppm. The peak at 0.82 ppm is assigned to CH_3 terminal groups on the alkyl chains, whereas the 1.22 is assigned to the CH_2 groups within the alkyl chains. The results of FWHH versus temperature for the two assigned alkyl peaks show that both emulsions have a sharp increase in line width at the known crystallisation onset of the bulk oil (35 – 40 $^\circ\text{C}$, see section 5.4.1), with the 0.18 μm emulsion shows another abrupt increase at 8 – 10 $^\circ\text{C}$. Again the resulting increase witnessed between 8 – 10 $^\circ\text{C}$ is in conjunction with the DSC and rheology investigations discussed earlier. Together the NMR/rheology and DSC results show that the model emulsion system has very different crystallisation properties with changing droplet diameter.

Figure 5.20. Upper plot: H^1 NMR spectra of model emulsion system with $0.18 \mu\text{m}$ initial droplet diameter. Spectra of decreasing temperature from 60, 55, 50, 45, 40, 35, 30, 25, 20, 15, 10, 8, 6, 4 and 2°C . Lower plot: Same as upper plot with initial droplet diameter = $3.70 \mu\text{m}$.

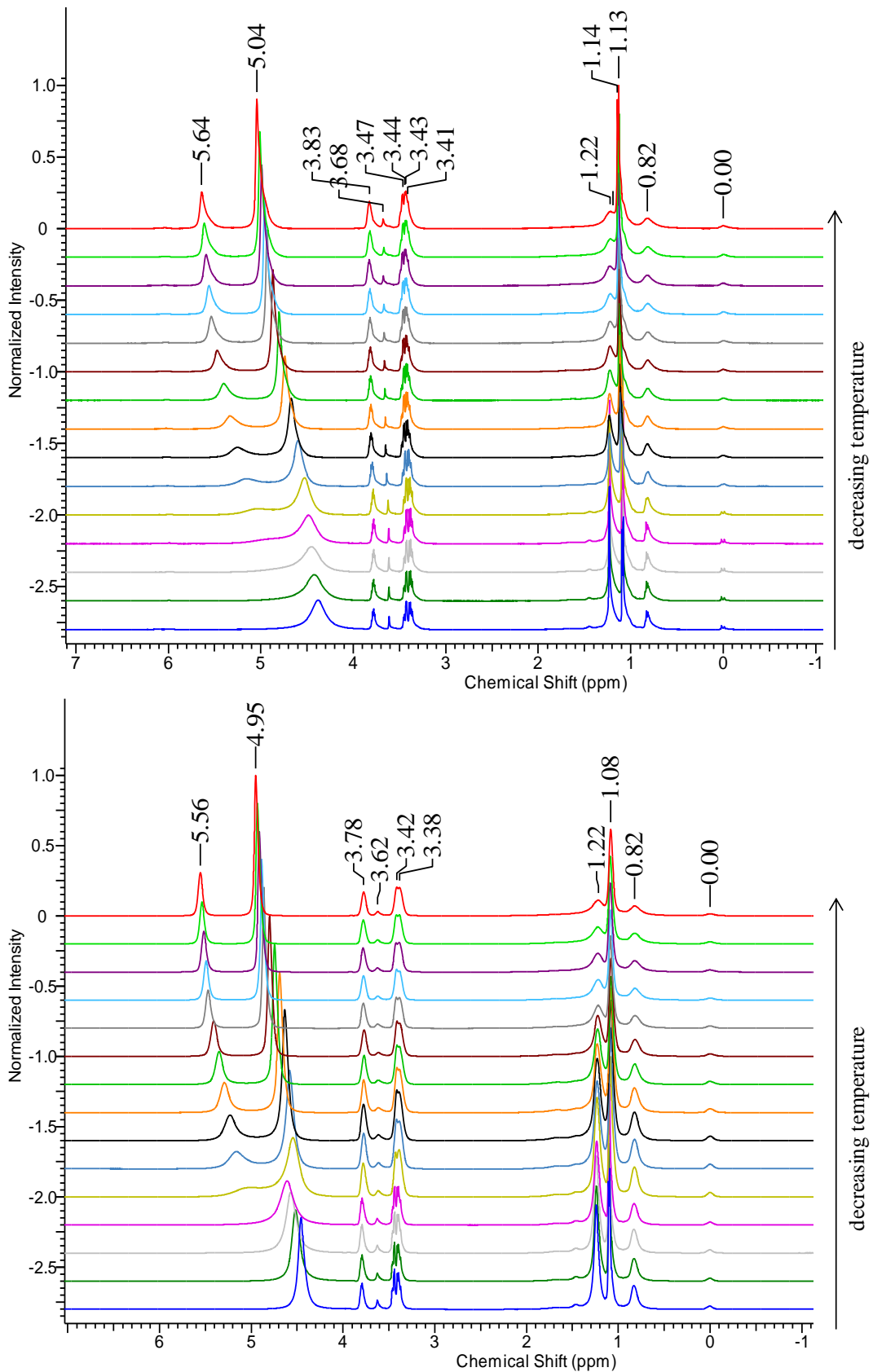


Figure 5.21. Full width at half height for H^1 NMR peaks at 1.22 (upper plot) and 0.82 ppm (lower plot) versus temperature for two initial droplet diameters of the model emulsion. Peaks represent CH_2 and CH_3 from oil phase and surfactant alkyl chains. In all cases the temperature was reduced, *i.e.* from hot to cold.

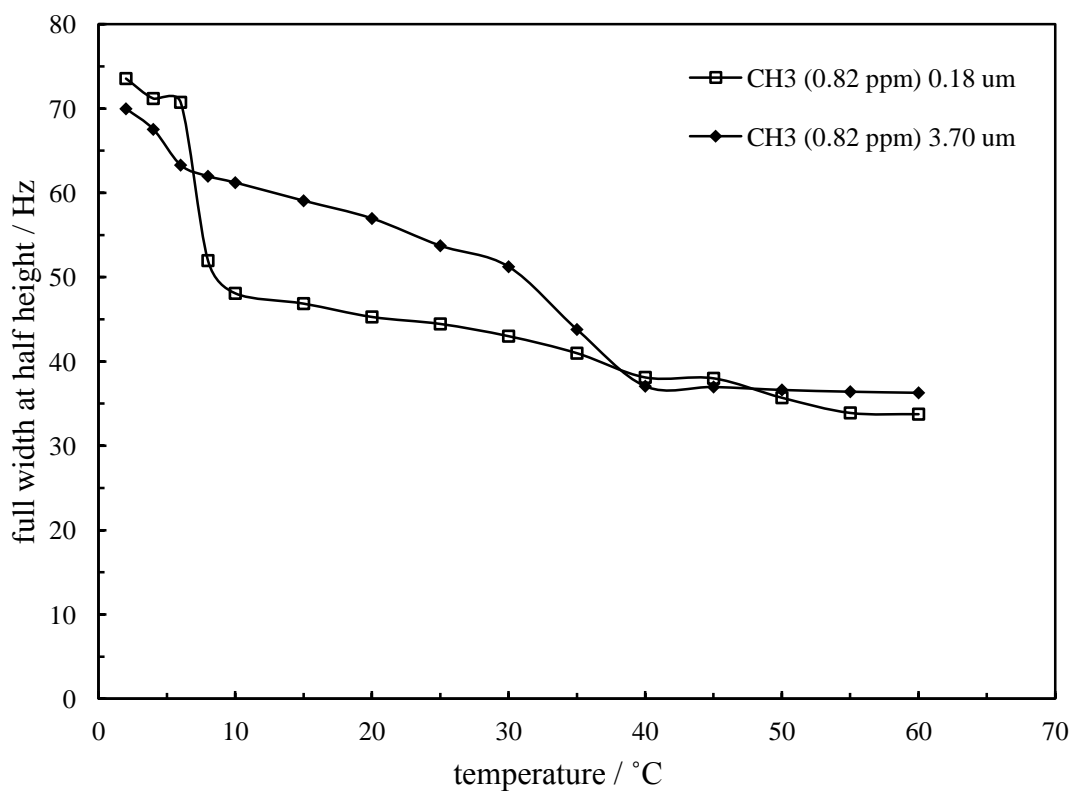
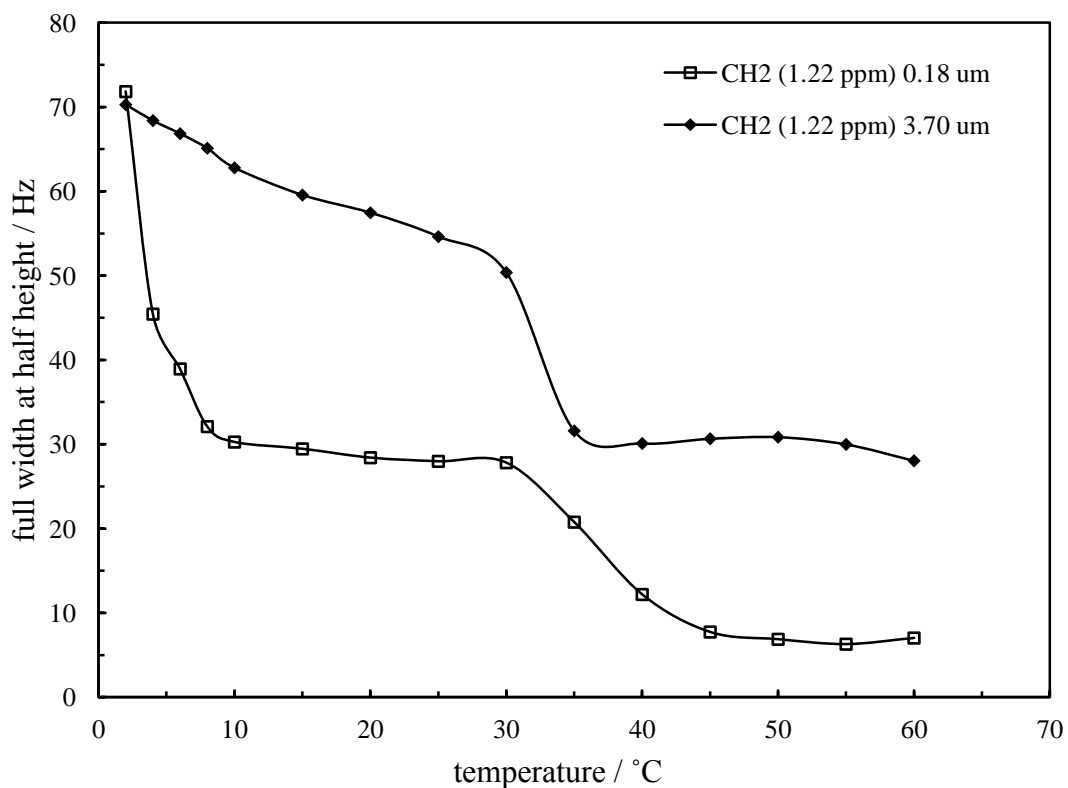
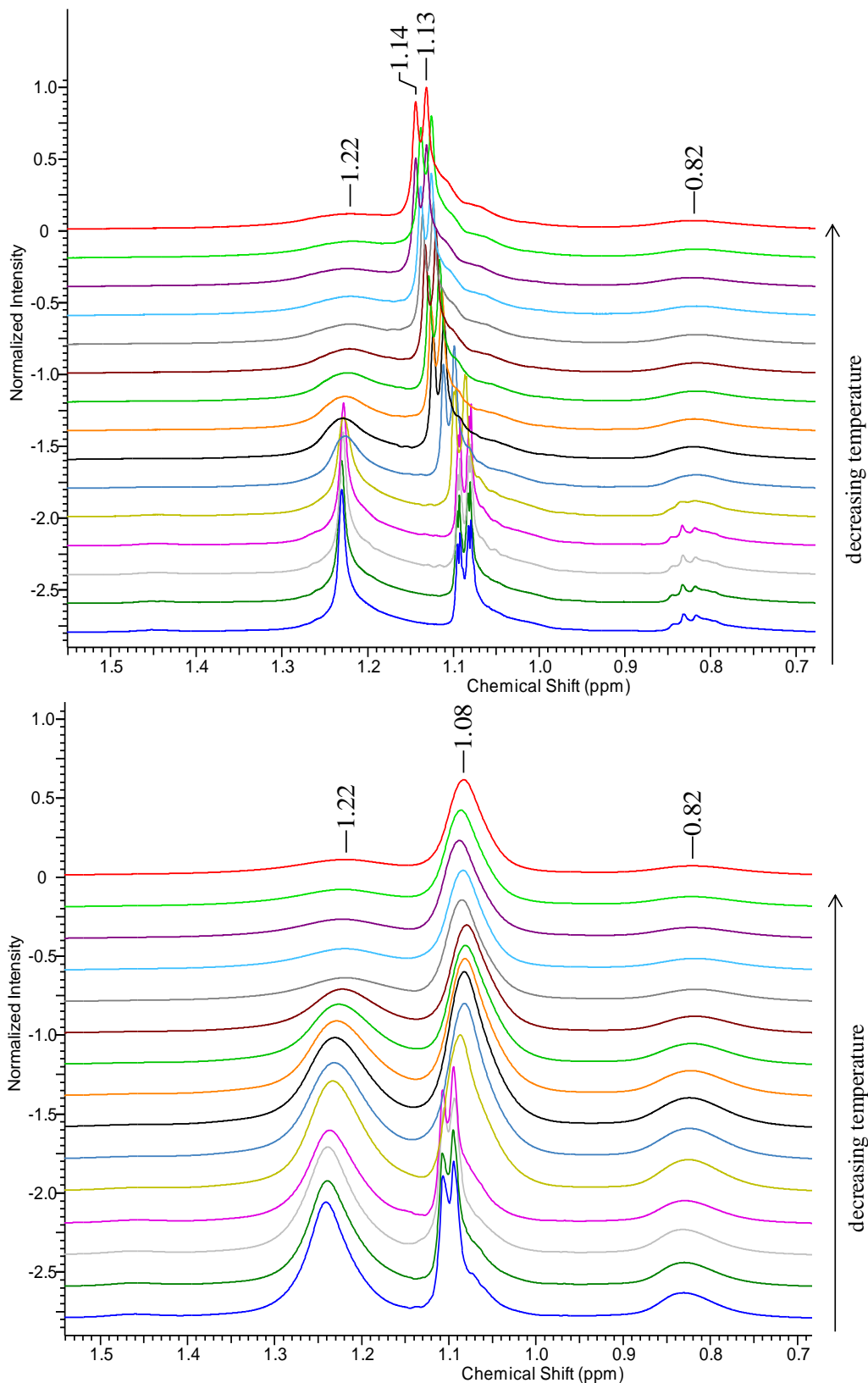


Figure 5.22. Expanded ^1H NMR of model emulsion system between 0.7 – 1.5 ppm showing peaks assigned to CH_3 from oil (0.82), CH_2 from oil (1.22) and CH_2 from propane-1,2-diol (1.13 – 1.14) with decreasing temperature from 60, 55, 50, 45, 40, 35, 30, 25, 20, 15, 10, 8, 6, 4 and 2 $^\circ\text{C}$. Upper plot shows emulsion with initial droplet diameter of 0.18 μm , lower plot = 3.70 μm .



As the spectra have peaks individual to propane-1,2-diol (for example see Figure 5.22), the mobility and liquid like nature of the diol can be investigated *in situ*. The two areas of interest, diol peaks at ≈ 1.0 to 1.1 and 3.3 to 3.5 ppm, show high resolution at all temperatures for the $0.18 \mu\text{m}$ model emulsion system, but low resolution of peaks in the $3.70 \mu\text{m}$ model emulsion system with decreasing temperature. Interestingly the loss of resolution in the $3.70 \mu\text{m}$ model emulsion is witnessed at exactly the same temperature as the oil phase is known to start crystallising; thus it is hypothesised that the solidification of the oil in the model emulsion system hinders the mobility of diol. A reasonable explanation for the loss of diol mobility at oil crystallisation temperature is that the diol is somehow interacting with/or near the oil when it crystallises, thereby immobilising the diol. As such the immobilised diol would add credence to the argument of diol addition on the effect of preferred curvature of the surfactant monolayer discussed in detail in chapter 3.[31]

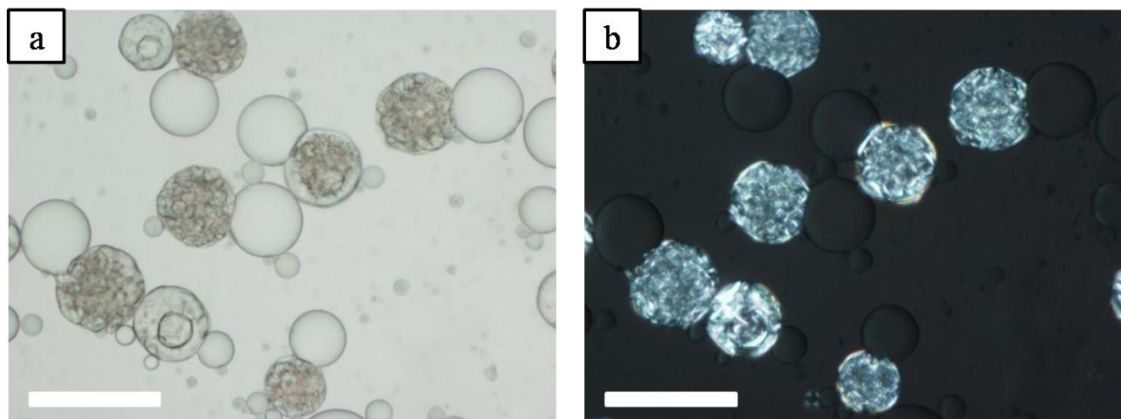
5.5 Possible mechanism of instability in diol containing emulsions – dumbbell droplets

The instability of the model emulsion system at low temperatures is thought to be linked to solidification of the dispersed phase with varying droplet diameter. Crystallisation of the model emulsion system with varying droplet diameter has been investigated using various techniques including DSC, rheology and NMR. The findings show, like theory suggests, that as the droplet diameter decreases in the emulsion a larger portion of the droplets crystallise homogeneously at temperatures lower than the bulk freezing temperature.[5] To establish any link between the observed crystallisation effect and the instability results discussed in section 5.3, investigations from another model system are presented here to further assess the mechanism of the instability witnessed in diol containing emulsions.

In the preliminary investigation of phase inversion with changing propane-1,2-diol in surfactant-oil-water systems discussed in chapter 3 (results not shown in chapter 3), another model emulsion system containing cetostearyl alcohol and equal volumes oil and aqueous phase (water/propane-1,2-diol and paraffin liquid) showed interesting droplet behaviour. The emulsion system contained 6.75% w/w cetostearyl alcohol, 25% v/v propane-1,2-diol, 25% v/v water and 50% v/v paraffin liquid and micrographs

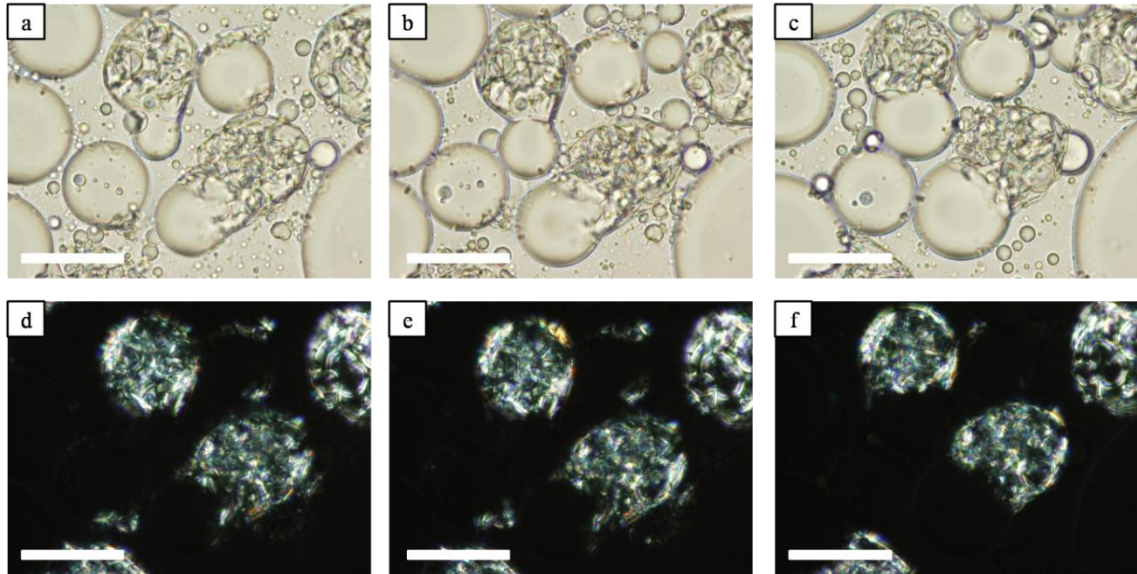
showed many oil droplets which were partially coalesced, in pairs, with one of the pairs containing crystals and the other immiscible liquid oil (Figure 5.23).

Figure 5.23. (a) bright microscopy, (b) cross polarised microscopy, of 6.75% w/w cetostearyl alcohol, 25% v/v propane-1,2-diol, 25% v/v water, and 50% v/v paraffin liquid. Emulsified at 70 °C, cooled to room temperature at ≈ 1 °C min⁻¹. Magnification = x20, scale bar = 100 μ m.



The appearance of these droplets, termed “dumbbells”, shows two droplets connected together with one containing liquid/crystals and other just liquid. The formation of the dumbbells was of great interest for two reasons; first the dumbbells were only witnessed when high amounts of propane-1,2-diol were present in the emulsion continuous phase, secondly the presence of dumbbells could be a contributing factor to instability if present in an emulsion sample. Microscopy investigations showed that the dumbbells formed rapidly and images of their formation were difficult to obtain. Further microscopy investigations showed that the liquid part of the droplet increases over a time period of up to 1 hr (Figure 5.24), until it became approximately the size of its counterpart.

Figure 5.24. Microscopy over time 30 minutes of an o/w emulsion containing 6.75% w/w cetostearyl alcohol, 25% v/v propane-1,2-diol, 25% v/v water, and 50% v/v paraffin liquid, emulsified at 70 °C. Micrographs taken at room temp, (a-c) bright field, (d-f) cross polarised. (a and d) t = 0, (b and e) t = 30 min., and (c and f) t = 3 hrs. Magnification = x50, scale bar = 50 µm.



As the liquid section of the dumbbell grew over time (30 min.) it was hypothesised that the crystallised droplet was excluding the excess paraffin liquid. For this reason, an observational investigation into the solidification of a mixture of only the oil (paraffin liquid) and surfactant (cetostearyl alcohol) was conducted. If these oil/surfactant mixtures gave crystal networks, would paraffin liquid be excluded in a similar way to that observed in the dumbbells? If so, this could explain the observations within the emulsion droplets shortly after emulsification. Mixtures of paraffin liquid and the appropriate amounts of cetostearyl alcohol (0 -10% w/w), spanning the concentration in the model emulsion system (Table 5.7), were investigated. The samples were heated in a Grant thermostat bath set to the emulsification temperature of the pervious emulsion samples (70 °C for 30 minutes). The heated samples were placed on a magnetic stirrer plate (VARIOMAG Electronicrührer POLY 15) at room temperature, and cooled while stirring at ≈ 960 rpm for approximately 1 hour. Without the additional step of stirring the binary mixtures did not form a crystal network throughout the whole bulk solution. The samples were observed over time and recorded by photography (Sony Cyber-Shot DSC-S950).

Table 5.7 shows the compositions of samples investigated describing simple binary mixtures of paraffin liquid and cetostearyl alcohol.

Table 5.7. Composition of cetostearyl alcohol/paraffin liquid binary mixtures.

<u>Sample Number</u>	<u>Paraffin liquid (% w/w)</u>	<u>Cetostearyl alcohol (% w/w)</u>
1	100	0
2	98	2
3	96	4
4	94	6
5	92	8
6	90	10

Figure 5.25 and Figure 5.26 show the appearance of the samples described in Table 5.7 and three main results were observed:

- The concentration range of cetostearyl alcohol investigated is shown to be completely miscible at the investigation temperature of 70 °C.
- Cooled samples 4 – 6 formed crystals network structures which did not flow under the force of gravity.
- All samples containing cetostearyl showed phase separation between crystals and liquid over time (2 weeks). Separation in samples 2 and 3 was contributed to gravitational affects, as the samples still remained liquid like after cooling. Samples 4 – 6 separation was contributed to exclusion of the liquid from the solid due to the crystal network structure witnessed.

Figure 5.25. Samples of paraffin liquid/cetostearyl alcohol before thermostated to 70 °C and immediately after heating. Compositions correspond to Table 5.7 above. Pictures taken at room temperature, 23 ± 3 °C.

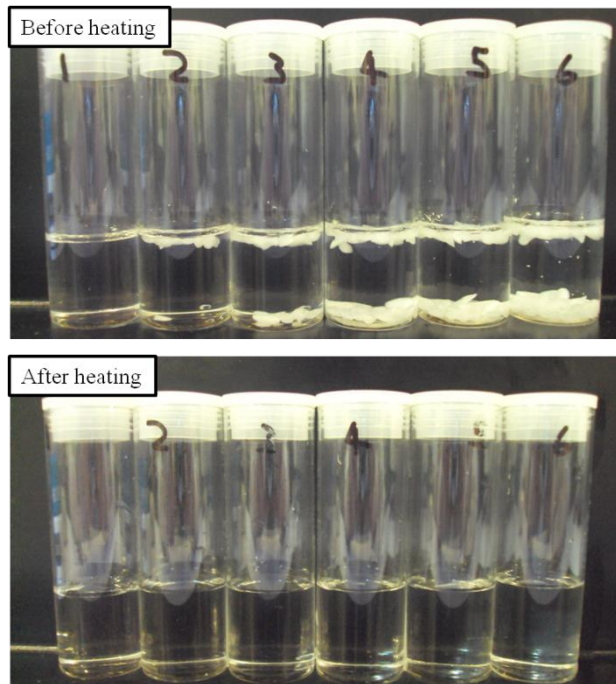
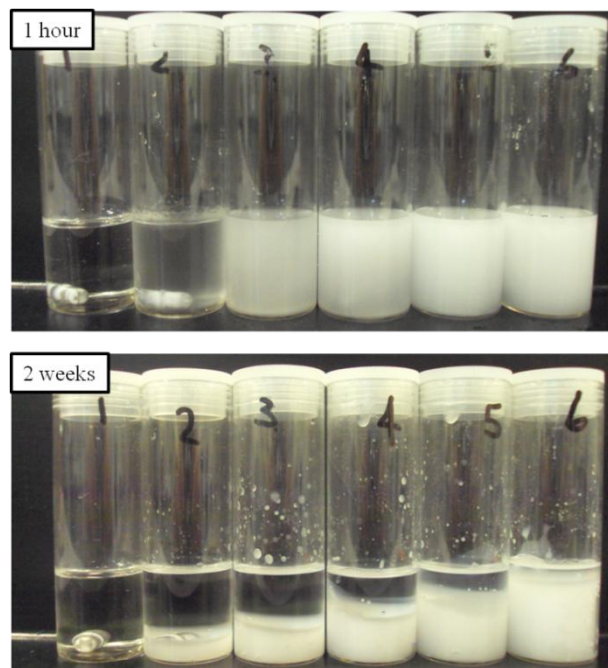


Figure 5.26. Samples of paraffin liquid/cetostearyl alcohol after 1 hour of cooling at room temperature while stirring, and after 2 weeks of storage at room temperature. Compositions correspond to Table 5.7 shown above. Pictures taken at room temperature, 23 ± 3 °C.



Paraffin exclusion investigations and micrographs of the dumbbell droplets over time (2 weeks and 30 min. respectively) suggest that paraffin liquid is expelled out of the crystal network upon cooling from oil/surfactant droplets or samples. The working hypothesis for the dumbbell droplets is that the crystal network restricts the volume of the bulk; hence, the paraffin liquid is expelled due to lack of space. The dumbbell droplets have only been witnessed in the paraffin liquid, water/propane-1,2-diol, and cetostearyl alcohol emulsions shown above. Importantly, dumbbells are only seen when propane-1,2-diol is present in the system. Further work is required to establish the unknown factors as to why dumbbells only form in the presence of propane-1,2-diol. However, the discovery that dumbbell droplets are formed, and only in diol containing systems to date, could give insight to a link between instability and crystallisation in diol emulsions, as the formation of dumbbell droplets seems to be connected to crystallisation.

The dumbbell phenomenon has not been witnessed in the first model emulsion system although this could be attributed to the smaller droplet sizes of 0.18 and 3.70 μm , making observations of dumbbells difficult. In contrast dumbbells are easy to see and investigate in the second model emulsion (paraffin liquid, water/propane-1,2-diol and cetostearyl alcohol) due to the large droplet diameter. It is possible however, that dumbbells are being formed in the first model emulsion system with their formation causing the oil resolved witnessed in such emulsions.

A good understanding of how the dumbbell droplets behaviour under changing conditions has also been achieved with varying temperature and electrolyte concentration (results not shown). It was found that if the second model emulsion system contained a small concentration of sodium chloride (0.1 mM), dumbbells were still formed, but upon heating the droplets coalesced to form multiple emulsions of w/o/w. If the emulsions did not contain salt, upon heating the emulsion would form simple emulsions, o/w. However, further work is again needed to establish a better understanding of the formation of dumbbells and their possible links to emulsion instability in diol containing emulsions.

5.6 Conclusions

The crystallisation of an o/w model emulsion system containing high amounts of diol has been investigated and the following conclusions have been reached:

- The effect of shear rate on initial droplet diameter has been demonstrated and linked to theory; showing that the model emulsion system containing non-conventional aspects can be manipulated using known “conventional” theory.
- Stability of the model emulsion system has shown that the amount of oil resolved over a storage time of 21 days is both linked to the initial droplet diameter and the storage temperature. Results indicate that the larger the initial droplet diameter and the lower the storage temperature (5 °C) the more oil resolved witnessed.
- DSC, rheology and NMR have been used to determine changes in viscosity, crystallisation and effects of crystallisation in the model emulsion system with changing droplet diameter. These measurements have shown the difference in crystallisation of the model emulsion system with varying droplet diameter; that droplet sizes as low as 0.18 μm show heterogeneous and homogenous crystallisation, whereas 3.70 μm emulsion droplets only have heterogeneous crystallisation. In addition the rheology results indicate the presence of crystal networks in the large droplet diameter system (3.70 μm), thought to be from partial coalescence. Unlike the smaller droplet diameter system (0.18 μm), where a smaller portion of droplets are crystalline, therefore the possibility of a “jamming” state is hypothesised.
- Stability and crystallisation investigations into dispersed oil droplets have shown that a change in droplet diameter of the model emulsion system causes instability at low temperatures. The instability at low temperatures is hypothesised to occur from the formation of the crystalline droplets with changing emulsion droplet diameter. Within another high containing diol model emulsion the generation of so called “dumbbell droplets” was shown, and provides a possible explanation of the process involved in the instability of high diol content emulsions.

- A good understanding of so called “dumbbell droplets” has been gained. It is known that expulsion of paraffin liquid from within the semi-solid emulsion drop is the probable cause of the dumbbells. Secondly the liquid part of the dumbbells grows to a specific size which is possibly controlled by the initial droplet diameter of the semi-solid droplet. Future work is needed to fully understand this possible connection. Finally, with increasing temperature the dumbbells form a single coalesced droplet of liquid content, or a multiple emulsion droplet of unknown composition in the absences or presents of electrolyte respectively.

5.7 References

1. H. D. Goff, *J. Dairy Sci.*, **80**, 2620 (1997).
2. N. M. Barford and N. Krog, *J. Amer. Oil Chemists Soc.*, **64**, 112 (1987).
3. D. Rousseau, *Food Research International*, **33**, 3 (2000).
4. S. A. Vanapalli, J. Palanuwech and J. N. Coupland, *Colloids Surf. A*, **204**, 227 (2002).
5. J. N. Coupland, *Curr. Opin. Colloid Interface Sci.*, **7**, 445 (2002).
6. E. Dickinson, D. J. McClements and M. J. W. Povey, *J. Colloid Interface Sci.*, **142**, 103 (1991).
7. N. Kaneko, T. Horie, S. Ueno, J. Yano, T. Katsuragi and K. Sato, *J. Cryst. Growth*, **197**, 263 (1999).
8. D. J. McClements, S. R. Dungan, J. B. German, C. Simoneau and J. E. Kinsella, *J. Food Sci.*, **58**, 1148 (1993).
9. D. J. McClements, S. R. Dungan, J. B. German, C. Simoneau and J. E. Kinsella, *J. Food Sci.*, **58**, 1148 (1993).
10. R. J. Davey, A. M. Hilton, J. Garside, M. d. I. Fuente, E. Edmondson and P. Rainsford, *J. Chem. Soc. Faraday Trans.*, **92**, 1927 (1996).
11. R. Montenegro, M. Antonietti, Y. Mastai and K. Landfester, *The Journal of Physical Chemistry B*, **107**, 5088 (2003).
12. W. Skoda and M. v. d. Tempel, *J. Coll. Sci.*, **18**, 568 (1963).
13. E. Dickinson, *An Introduction to Food Colloids*, Oxford University Press, Oxford (1992).
14. S. Hindle, M. J. W. Povey and K. Smith, *J. Colloid Interface Sci.*, **232**, 370 (2000).
15. K. Golemanov, S. Tcholakova, N. D. Denkov and T. Gurkov, *Langmuir*, **22**, 3560 (2006).
16. J. Giermanska, F. Thivilliers, R. Backov, V. Schmitt, N. Drelon and F. Leal-Calderon, *Langmuir*, **23**, 4792 (2007).
17. F. Leal-Calderon, F. Thivilliers and V. Schmitt, *Curr. Opin. Colloid Interface Sci.*, **12**, 206 (2007).
18. F. Thivilliers, E. Laurichesse, H. Saadaoui, F. Leal-Calderon and V. Schmitt, *Langmuir*, **24**, 13364 (2008).

19. B. P. Binks, in *Modern Aspects of Emulsion Science*, Ch.1, B. P. Binks (ed.), The Royal Society of Chemistry, Cambridge (1998).
20. F. Leal-Calderon and V. Schmitt, *Curr. Opin. Colloid Interface Sci.*, **13**, 217 (2008).
21. R. Pal, *AIChE J.*, **42**, 3181 (1996).
22. E. Andrew, *J. Chem. Phys.*, **18**, 607 (1950).
23. J. Rault, R. Neffati and P. Judeinstein, *Eur. Phys. J. B*, **36**, 627 (2003).
24. P. Apte and B. H. Suits, *NanoStruct. Mater.*, **10**, 917 (1998).
25. K. Van Putte and J. Van Den Enden, *J. Am. Oil Chem. Soc.*, **51**, 316 (1974).
26. G. A. Manley and D. Rovnyak, *Application Note - Manley and Rovnyak* (2006).
27. W. G. Paterson, *Can. J. Chem.*, **41**, 714 (1963).
28. K. C. Tewari and N. C. Li, *Can. J. Chem.*, **48**, 1616 (1970).
29. W. G. Paterson, *Can. J. Chem.*, **41**, 2472 (1963).
30. P. J. Hore, *Nuclear Magnetic Resonance*, Oxford University Press, Oxford (1995).
31. B. P. Binks, P. D. I. Fletcher, M. A. Thompson and R. P. Elliott, *Colloids Surf. A*, **390**, 67 (2011).

SUMMARY AND CONCLUSIONS

Surface and colloidal properties of various systems containing oil + water + diol and surfactant/particle stabilisers have been investigated with the effect of diol addition been analysed in terms of emulsion properties and phase inversion. Crystallisation of emulsions containing high amounts of diol, oil, water and surfactant has also been studied in terms of bulk emulsion properties. The results obtained are summarised below and are conveniently discussed in chapter numbers:

3. In systems containing oil (paraffin liquid), water and non-ionic surfactant, phase inversion by addition of various diols (ranging from ethane-1,2-diol to pentane-1,5-diol) has been shown. Surface tension measurements of aqueous diol systems are used to calculate the relative Gibbs free energy of adsorption to the polar-air interface for the various diols. From these the induced phase inversion from w/o emulsions (low diol content) to o/w emulsions (high diol content) is explained in terms of changing preferred surfactant monolayer curvature, being that preferred curvature changes from negative to positive with addition of diol. To collaborate this finding, known traits of phase inversion from “simple” oil + water + surfactant systems (containing no diol) induced from changing preferred surfactant monolayer curvature are examined including average droplet diameter, stability, surfactant structure/type and emulsification temperature. It is also shown that the cac of non-ionic surfactant is increased with increasing diol concentration. This yields instability with increasing diol after the surfactant concentration is < cac.
4. The effect of adding diol (propane-1,2-diol) to aqueous dispersion of silica nanoparticles and paraffin liquid-water emulsions stabilised by the same particles has been investigated. Aerated propane-1,2-diol aqueous dispersions (no oil) containing fumed silica particles yields stable dispersions, aqueous foams, climbing particle films or liquid marbles. The formation of each material can be controlled by the diol content in the dispersion and the particle hydrophobicity, where increasing diol creates the materials associated with more hydrophilic system, thus particles become more hydrophilic. Contact angle calculations of the particles *in situ* indicate that diol does decrease the contact angle and

therefore makes the system progressively more hydrophilic. For the first time systems containing aqueous diol in the presence of oil show particle-stabilised emulsions to invert from oil-continuous to water/aqueous-continuous with increasing particle hydrophilicity of the particles or increasing diol content in the system. Emulsion characterisation indicates trends witnessed in similar systems containing various different oils and water stabilised by the same particles. Emulsions inverted by the increase in diol show deviations from known findings, *e.g.* mean droplet diameter and stability to gravitational induced instability show familiar trends. The phase inversion results are rationalised in terms of the contact angle at the oil-polar phase interface with reasonable agreement found between the measured and calculated phase inversion conditions.

5. Crystallisation of an o/w model emulsion system containing high amounts of diol has been investigated; the effect of shear rate on initial droplet diameter has been shown and linked to theory indicating that the model formulation containing non-conventional aspects can be manipulated using known “conventional” emulsion breakdown theory. Rheology, DSC and NMR have been used to determine changes in viscosity, crystallisation points and effects of crystallisation in the model formation with changing droplet diameter, results show that droplet sizes as low as 0.18 μm show heterogeneous and homogenous crystallisation, whereas droplet sizes of 3.70 μm only have heterogeneous crystallisation. Rheology results indicate the presence of crystal networks in the large droplet diameter system (3.70 μm), thought to be from partial coalescence by increased viscosity, unlike the smaller droplet diameter system (0.18 μm), which results suggest a smaller portion of droplets is crystalline therefore the possibility of a “jamming” state is hypothesised. A change in droplet diameter of the model formulation causes instability at low temperatures and is hypothesised this is from the formation of the crystalline droplets with changing emulsion droplet diameter. Within another high containing diol model emulsion the generation of so called “dumbbell droplets” has been shown, and is given as a possible explanation of the process involved in the instability witnessed in the original model system. A good understanding of so called “dumbbell droplets” has been gained with expulsion of paraffin liquid from within the semi-solid emulsion drop as the probable cause of the formation of dumbbells. Secondly the liquid part of the

dumbbells grows to a specific size which is possibly controlled by the initial droplet diameter of the semi-solid droplet. Finally, with increasing temperature the dumbbells will form a single coalesced droplet, or a multiple emulsion droplet of unknown composition in the absences or presents of electrolyte respectively.

FUTURE WORK

The following ideas are suggested as future work to contribute further to the work described in this thesis:

Chapter 3 investigated in detail the effect of diol addition on systems containing water, oil and non-ionic surfactants. It is proposed the effect that diol has on systems containing different types of surfactant, *i.e.* with different head groups, is to be investigated to determine if similar findings are obtained. This would include surfactants with ionic head groups, where the interest would lie on whether diols have such a big effect on the preferred surfactant monolayer curvature. In addition, the effect of diol on anionic surfactant stabilised systems could be looked at.

Again, future work following on from Chapter 4 would be similar to the detailed work discussed in Chapter 3, *i.e.* more diols would be investigated to understand the effect of each and with individual diols behaviour tested via the model already described in Chapter 4. Investigations into diol adsorption on to silica particles could also be studied in order to adapt the model described in Chapter 4. These investigations could lead to a better understanding of diol interactions on the silica surfaces as well as a more accurate model for determining phase inversion with varying particle wettability and diol addition. The method could then be used to make extremely stable emulsions to coalesce within a predictive manner. Many other investigations could include using different oils, particles and most interestingly different additives to induce phase inversion rather than diols, including alcohols and glycerols. This would open the findings to be used in a wider range of industrial/commercial products.

Chapter 5 shows the formation of “dumbbells” in diol containing emulsions and their possible link to instability within crystallising emulsion oil drops. Future work for this section of work should include a detailed investigation into the reason for the formation of these dumbbells. In addition the use of NMR in the detection of emulsion bulk properties should be investigated in more detail. The use of such a technique has been shown, at a very primary level, in Chapter 5 and indicates the possibilities at which this technology can be used in emulsion/colloidal science. For example the ability to calculate solid content and position of components (using NOSTY) within the system would be advantageous. In the aspect of non-convention emulsions Chapter 5 has given a starting point to understanding the crystallisation in a diol (propane-1,2-diol)

containing emulsion with surfactants, this should be expended to other diols, with a more systematic look at varying surfactant types. Most interestingly, the solidification in emulsions stabilised by solid particles should be investigated and compared to “conventional emulsions”.

One of the major gains from the conclusions discussed throughout this thesis and the future work described in this section can be the use of the knowledge gained in the optimisation and development of current and new products containing all the non-conventional aspects investigated. The ability to make extremely stable “waterless” emulsions with alternative polar phases and solid particles is of great interest and additionally the knowledge of the effects diols can have on different o/w emulsions including the change in preferred surfactant curvature and the possibility of the formation of dumbbells which could lead to oil separation are of great interest.